ISSN 1316-7081
ISSN Electrónico 2244-8780

CIENCIA e INGENIERÍA

Vicerrectorado Administrativo y
Académico
Mérida, Venezuela

UNIVERSIDAD DE LOS ANDES
(ULA)
Facultad de Ingeniería
Núcleo Universitario
«Pedro Rincón Gutiérrez»
Mérida - Venezuela

Vol. 47 **Abril -Julio 2026** **No 2**

Artículo de Investigación. Revista Ciencia e Ingeniería. Vol. 47, No. 2 pp. 107-116, abril-julio, 2026.
ISSN 1316-7081. ISSN Elect. 2244-8780 Universidad de los Andes (ULA)

A review of Max-Plus Algebra approach and some extensions to discrete event systems

Una revisión del Álgebra Max-Plus y algunas extensiones a sistemas de eventos discretos

Ferrer-Guillén, María Dolores[1]; Mantilla-Morales, Gisella[2]*; Bastidas Chalán, Rodrígo Vladimir[3]; Rentería Torres, Aníbal Vicente[3]; Mata-Díaz, Guelvis[4]
[1]Engineering Faculty, Calculus Department, University of Andes, Venezuela.
[2]Technical University of Manabí, Ecuador.
[3]Universidad de las Fuerzas Armadas ESPE, Ecuador.
[4]Faculty of Sciences, Department of Mathematics, University of Andes, Venezuela.
*gisella.mantilla@utm.edu.ec

Abstract

The basic form of the systems we will study is $x_i(k+1) = max\{a_{i1} + x_1(k), a_{i2} + x_2(k), \dots, a_{in} + x_n(k)\} = \max_j\{a_{ij} + x_j(k)\}$, $i = 1,2,\dots,n$. *It is common in practice to change the notation somewhat. Addition* $+$ *will be written as* $\otimes$ *and max will be written as* $\oplus$. *This change of notation makes the resemblance with conventional linear difference systems visible:* $x_i(k+1) = \oplus_j \{a_{ij} \otimes x_j(k)\}$, $i = 1,2,\dots,n$, *which in vector notation will be written as* $x(k+1) = A \otimes x(k)$. *Of the latter equation one speaks as a linear (difference) equation in the max-plus algebra, this in clear analogy with linear difference equations in the conventional, 'plus-times', algebra. We will briefly mention the following specializations and/or extensions: axiomatic foundations, minimal realizations, stochastic discrete event systems, min-max-plus systems and nonexpansive mappings, numerical procedures, 'continuous' discrete event systems and the Fenchel transform.*

Keywords: discrete event systems, max-plus algebra, γ −transform, extensions, the Fenchel transform.

Resumen

La forma básica de los sistemas que estudiaremos es $x_i(k+1) = max\{a_{i1} + x_1(k), a_{i2} + x_2(k), \dots, a_{in} + x_n(k)\} = \max_j\{a_{ij} + x_j(k)\}, i = 1,2,\dots,n.$ *En la práctica es común cambiar la notación. Además,* $+$ *será denotada por* $\otimes$, *y* max *será escrito como* $\oplus$.*Este cambio de notación se hace en términos de los sistemas de diferencia lineales convencionales visibles:* $x_i(k+1) = \oplus_j \{a_{ij} \otimes x_j(k)\}$, $i = 1,2,\dots,n$, *en los cuales, la notación vectorial se escribirá como* $x(k+1) = A \otimes x(k)$. *En la última ecuación uno se refiere a una ecuación (en diferencias) lineal en el algebra max-plus, lo cual es una clara analogía con las ecuaciones lineales en diferencias en el algebra 'max-plus'. Mencionaremos brevemente las siguientes especializaciones y/o extensions: fundamentaciones axiomáticas, realizaciones minimales, sistemas de eventos discretos estocásticos, sistemas min-max-plus y mapeos no expansivos, procedimientos numéricos, sistemas de eventos discretos 'continuos' y la transformada de Fenchel.*

Palabras clave: sistemas de eventos discretos, algebra max-plus, γ −transformada, extensions, transformada de Fenchel.

1 Introduction

The discrete event systems (DES) is a research area of current vitality. The development of this is largely stimulated by discovering general principles which are useful to a wide range of application domains. In particular, manufacturing systems, communication networks, and logistic systems. There are two key features that characterize these systems:

- Their dynamics are event-driven, i.e., the behavior of a DES is governed only by occurrences of different types of events overtimes rather than by ticks of a clock;

- At least some of the natural variables required to describe a DES are discrete (see Branicky, 1995). The theory of DES encompasses a variety of classes of problems and of modelling approaches (see Murata, 1989). In this paper, one will discover the max-plus algebra approach (Coen et al., 1999), in which, in addition to the precise ordering of the events, the timing of the events plays an essential role (see Anderson, 2002).

From a formal point of view, a DES can be thought of as a dynamical system (see Baccelli et al., 2001), with a state space and a state-transition mechanism. The event-driven nature of a DES forces us to seek new mathematical frameworks for modelling and analysis (see Komenda et al., 2018), since differential or differential equations no longer provide an adequate setting.

Finally, we include some extensions; namely, axiomatic foundations, minimal realizations, stochastic discrete event systems, min-max-plus systems (see De Schutter and Van Den Boom, 2008) and nonexpansive mapping, numerical procedures, 'continuous' discrete event systems and the Fenchel transform.

2 Motivation and Petri net

It is assumed that the reader is familiar with the basic properties of Petri net. It will be shown that the max-plus algebra is extremely suitable in describing the timed behavior of tokens in so-called event graphs, which form a subclass of Petri nets. In order to set the notation and the stage, we do start with some formal definitions.

A Petri net is a pair $(\boldsymbol{G}, \boldsymbol{b})$, where $\boldsymbol{G} = (\boldsymbol{E}, \boldsymbol{V})$ is a bipartite graph with a finite number of nodes $(\boldsymbol{V})$ which are partitioned into the disjoint sets $\boldsymbol{P}$ and $\boldsymbol{Q}$; $\boldsymbol{E}$ consist of pairs of the form $(\boldsymbol{P_i}, \boldsymbol{q_j})$, and $(\boldsymbol{q_j}, \boldsymbol{P_i})$ with $\boldsymbol{P_i} \in \boldsymbol{P}$ and $\boldsymbol{q_j} \in \boldsymbol{Q}$. The initial marking $\boldsymbol{b}$ is an m-vector, with m being the number of elements in P, of nonnegative integers. The elements of P are called places, those of Q are called transitions. The number of elements in these sets are m and n respectively. The elements of the vector b denote the number of tokens in the respective places. One talks about a timed Petri net if time durations are associated with places and transitions.

A (timed) Petri net is called a (timed) event graph if each place has exactly one upstream and one downstream transition.

A (timed) Petri net is called a (timed) state graph if each transition has exactly one upstream and one downstream place.

Note that the definitions of event graph and state graph are dual one to the other. In these definitions it was tacitly assumed that the networks are 'closed', i.e., all places (transitions) do have an upstream and a downstream transition (place). The definitions can be extended in the obvious way to include imput transitions (places), so-called sources, which do not have upstream places (transitions) and output transitions (places), so-called sinks, which do not have downstream places (transitions).

A transition can fire (or can start firing if there is a positive firing time) if all its (directly) upstream places contain at least one token (which must be 'enabled'). After the firing these tokens are removed and one token is added to each of the (directly) downstream places.

The firing time of a transition is the time that elapses between the starting and the completion of the firing of the transition. The holding time of a place is the time a token must spend in the place before it can contribute to the enabling of the downstream transitions.

An event graph with both firing times and holding times is equivalent to an event graph with only holding times (i.e., the firing time are zero). This equivalence means that the time instants at which the transitions fire are the same in both event graphs.

The number of tokens in any circuit of an event graph is constant. (*)

From now on we will only consider event graphs with firing times which are zero. Each place connects precisely one transition with precisely one (possibly different) transition. One says in such a situation that the upstream transition, say $\boldsymbol{q_j}$, is a predecessor of the downstream transition, say $\boldsymbol{q_i}$. Equivalently one can say that $\boldsymbol{q_i}$ is a successor of $\boldsymbol{q_j}$. One writes in such a case $\boldsymbol{j} \in \boldsymbol{\pi}^{-}(\boldsymbol{i})$ and $\boldsymbol{i} \in \boldsymbol{\pi}^{+}(\boldsymbol{j})$.

We make the explicit assumption that if a place connects two transitions such as just has been described, there is no other place with does exactly the same. In general, event graphs there can be more 'parallel' places in between two transitions of which one is the successor of the other. The reason for this restriction is purely a notational issue. The theory to be given can handle the more general situation routinely. We also make the assumption that the underlying network is strongly connected.

If a place exists between the transition $\boldsymbol{q_j}$ and $\boldsymbol{q_i}$ and $\boldsymbol{q_j}$ is upstream with regard to this place and $\boldsymbol{q_i}$ downstream, then the holding time of this place is indicated by $\boldsymbol{a_{ij}}$. The holding times are nonnegative real numbers. The number of tokens in this place is indicated by $\boldsymbol{b_{ij}}$. In the course of time, $\boldsymbol{b_{ij}}$ may change of course, but what is meant here, and also in the formulas to come,

$$\boldsymbol{\tau_i(x) = \max_{j\in\pi^-(i)}\{a_{ij} + \tau_j(x - b_{ij})\},\ i = 1, 2, \dots, n,}$$

where $\boldsymbol{\tau_i(x)}$ denotes the earliest time instant at which transition $\boldsymbol{q_i}$ has fired $\boldsymbol{x}$ times, and

$$\boldsymbol{x_i(t) = \min_{j\in\pi^-(i)}\{b_{ij} + x_j(t - a_{ij})\}, i = 1, 2, \dots, n,} \quad (**)$$

where $\boldsymbol{x_i(t)}$ denotes the number of firings of transition $\boldsymbol{q_i, i = 1, 2, \dots, n}$, which have taken place up to, and including, time t.

Rather than having used the conventional notation x for the state, we now used the symbol $\boldsymbol{\tau}$. The equations above describe the same underlying system and one equation is called the dual of the other. Note that x and $\boldsymbol{x_i}$ are integer-valued. The functions $\boldsymbol{x_i(t)}$ and $\boldsymbol{\tau_i(x)}$ are each other inverse in a way.

If in the original event graph there would have been a positive firing time, then the equations above do not exclude the possibility that a transition 'works' simultaneously on two or more tokens. If one wants to exclude this, a loop, including one place with one token, around the transition concerned should be added. The holding time of this new place is defined to be equal to the original firing time of this transition. This loop now takes care of the fact that in the equivalent event graph with only zero firing times, the transition cannot work on two or more tokens simultaneously anymore.

In a metropolitan area there are two railway stations, S_1 and S_2, which are interconnected by a railway system as indicated in Figure 1. This railway system consists of an inner circle and of two outer circles. The trains on these outer circles deliver and pick up passengers in the suburbs. The stations in the suburbs have not been drawn since they do not play any role in the model to be formulated.

Suppose there are four trains (two at each station) and the leave the stations at time 0, one along each track. They reach the other (or the same) station after a certain time which is indicated in the figure. The arriving trains at a station have to wait for each other such as to allow the passengers to change trains.

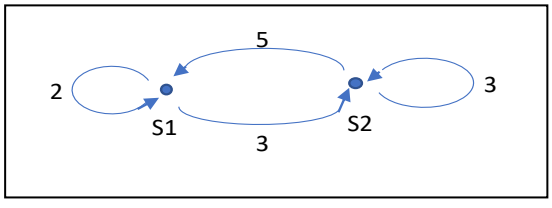

Fig. 1. The two stations example

Figure 1 can easily be redrawn as an event graph. The two stations are transitions and in the four railway tracks one can put a place. If a train is running along a track, one puts a token in the place corresponding to this track.

Suppose that there is not time table and that the trains leave directly after the change over of the passengers at the stations and that the time needed for change overs has been incorporated in the travelling time. This 'travelling time' was called 'holding time' in the theory of Petri nets. If this process of departing and arriving trains is continued, the departure time $\boldsymbol{x_i(k+1)}$ for the $\boldsymbol{(k+1)}$ −st departure at station $\boldsymbol{S_i}$ satisfies:

$$\begin{aligned} \boldsymbol{x_1(k+1)} &= \boldsymbol{\max\{x_1(k) + 2, x_2(k) + 5\}} \\ \boldsymbol{x_2(k+1)} &= \boldsymbol{\max\{x_1(k) + 3, x_2(k) + 3\}} \end{aligned} \quad (1)$$

for k = 0, 1, 2, …., with $\boldsymbol{x_1 = 0, x_2 = 0}$, the evolution of equations (1) becomes

$$\underset{x(0)}{\begin{pmatrix}0\\0\end{pmatrix}} \to \underset{x(1)}{\begin{pmatrix}5\\3\end{pmatrix}} \to \underset{x(2)}{\begin{pmatrix}8\\8\end{pmatrix}} \to \underset{x(3)}{\begin{pmatrix}13\\11\end{pmatrix}} \to \underset{x(4)}{\begin{pmatrix}16\\16\end{pmatrix}} \to \cdots$$

This pattern of departure times shows a periodic solution superimposed on a linear drift, the 'period' equals 2 and the average time between two subsequent departures is 4. From a time's table point of view, it is better to start with the initial departures $\boldsymbol{x_1 = 1, x_2 = 0}$, since then the evolution becomes

$$\underset{x(0)}{\begin{pmatrix}1\\0\end{pmatrix}} \to \underset{x(1)}{\begin{pmatrix}5\\4\end{pmatrix}} \to \underset{x(2)}{\begin{pmatrix}9\\8\end{pmatrix}} \to \underset{x(3)}{\begin{pmatrix}13\\12\end{pmatrix}} \to \cdots$$

where the interdeparture time is now exactly 4 at each station and thus the departure times are very regular (they have period 1). By trial and error, it turns out that, whatever the initial condition, after possibly a short transient period of time, a periodic behavior of either period 1 or 2 is obtained with (average) interdeparture times 4. A solution with an (average) departure time smaller than 4 is not possible, since for a train to go around in the inner circle costs 3+5=8 times units. There are two trains on the inner circle and therefore the (average) interdeparture time is limited from below by 8/2=4.

With the above sketched railway system and trains, it is not possible to design a time table with interdeparture times smaller than 4. If one wants a faster time table, one must change the problem. To this end, let us add a train on the inner circle, such that three trains will run along this circle all the time. Suppose that initially this extra train is situated at station $\boldsymbol{S_1}$. The equations for the departure times now become

$$\boldsymbol{x_1(k+1) = \max\{x_1(k) + 2, x_2(k) + 5\},} \quad (2)$$
$$\boldsymbol{x_2(k+1) = \max\{x_1(k-1) + 3, x_2(k) + 3\},} \quad (3)$$

which can be rewritten as a set of first order equations as

$$\begin{aligned} x_1(k+1) &= \max\{x_1(k)+2, x_2(k)+5\}, \\ x_2(k+1) &= \max\{x_3(k)+3, x_2(k)+3\} \\ x_3(k+1) &= x_1(k) \end{aligned} \quad (4)$$

with the initial condition $x_1 = 0, x_2 = 0, x_3 = 0$. The evolution of the latter set of equations becomes

$$\underset{x(0)}{\begin{pmatrix}0\\0\\0\end{pmatrix}} \to \underset{x(1)}{\begin{pmatrix}5\\3\\0\end{pmatrix}} \to \underset{x(2)}{\begin{pmatrix}8\\6\\5\end{pmatrix}} \to \underset{x(3)}{\begin{pmatrix}11\\9\\8\end{pmatrix}} \to \underset{x(4)}{\begin{pmatrix}14\\12\\11\end{pmatrix}} \to \cdots$$

which shows, after a transient part, a regular behavior of 'period' 1, with interdeparture times 3. This interdepartures time is caused by the outer loop at station S_2; on this loop there is one train which needs 3 times units to travel around. The inner loop is not the bottleneck anymore this inner loop itself would lead to a lower limit of 8/3 (travelling time of the loop divided by the number of trains on this loop). In order to lower the interdeparture times even more, one should add the next extra train to the outer loop of S_2. If we do so, the equations for the departure times become

$$\begin{aligned} x_1(k+1) &= \max\{x_1(k)+2, x_2(k)+5\}, \\ x_2(k+1) &= \max\{x_3(k)+3, x_2(k-1)+3\} \\ x_3(k+1) &= x_1(k) \end{aligned} \quad (5)$$

which can be rewritten as a set of first order equations as

$$\begin{aligned} x_1(k+1) &= \max\{x_1(k)+2, x_2(k)+5\}, \\ x_2(k+1) &= \max\{x_3(k)+3, x_4(k)+3\} \\ x_3(k+1) &= x_1(k) \\ x_4(k+1) &= x_2(k) \end{aligned} \quad (6)$$

If we start again with zero initial conditions, the solution become

$$\ldots \to \underset{x(3)}{\begin{pmatrix}10\\8\\8\\3\end{pmatrix}} \to \underset{x(4)}{\begin{pmatrix}13\\11\\10\\8\end{pmatrix}} \to \underset{x(5)}{\begin{pmatrix}16\\13\\13\\11\end{pmatrix}} \to \underset{x(6)}{\begin{pmatrix}18\\16\\16\\13\end{pmatrix}} \to \underset{x(7)}{\begin{pmatrix}21\\19\\18\\16\end{pmatrix}} \to \ldots \quad (7)$$

This solution has a 'period' 3 ($x_i(k+3) = x(k) + 8, k \geq 4$) and the average interdeparture time is 8/3, which is caused by the inner circle. Another solution results, with the same interdeparture time but with period 1, if one start with the initial condition $x_1(0) = 5, x_2(0) = \frac{8}{3}, x_3(0) = \frac{7}{3}, x_4(0) = 0$. One then has $x_i(k+1) = x_i(k) + \frac{8}{3}, i = 1, 2, 3, 4$, and k = 0, 1, 2, ….

3 Structure

Consider the systems

$$\begin{aligned} x_i(k+1) &= \max_j\{a_{i1} + x_1(k), a_{i2} + x_2(k), \ldots, a_{in} \\ &\quad + x_n(k)\} \\ &= \max_j\{a_{ij} + x_j(k)\}, i = 1, 2, \ldots, n \end{aligned} \quad (8)$$

Equivalent,

$$x_i(k+1) = \bigoplus \{a_{ij} \otimes x_j(k)\}, i = 1, 2, \ldots, n, \quad (9)$$

with addition + be written as $\otimes$ and **max** be written as $\oplus$, which in vector notation will be written as

$$x(k+1) = A \otimes x(k). \quad (10)$$

If it is clear from the context that the underlying algebra is the max-plus one, one even writes $x(k+1) = Ax(k)$, for (10). If the initial condition for (10) is $x(0) = x_0$, then

$$\begin{aligned} x(1) &= A \otimes x_0, \\ x(2) = A \otimes x(1) &= A \otimes (A \otimes x_0) = (A \otimes A) \otimes x_0 \\ &= A^2 \otimes x_0. \end{aligned}$$

It can be shown that indeed $A \otimes (A \otimes x_0) = (A \otimes A) \otimes x_0$. For the example given in Section 2, it is easy to check this by hand. Instead of $A \otimes A$, we simply write A^2. We get, for the general case,

$$x(k) = \left(\underbrace{A \otimes A \otimes \ldots \otimes A}_{k\ times}\right) \otimes x_0 = A^k \otimes x_0.$$

The matrices $A^2, A^3, \ldots$ can be calculated directly. Let us consider the $A-$ matrix of (1), $A = \begin{pmatrix}2 & 5\\3 & 3\end{pmatrix}$, then

$$\begin{aligned} A^2 &= \begin{pmatrix}\max\{2+2, 5+3\} & \max\{2+5, 5+3\}\\ \max\{3+2, 3+3\} & \max\{3+5, 3+3\}\end{pmatrix} \\ &= \begin{pmatrix}8 & 8\\6 & 8\end{pmatrix}. \end{aligned}$$

In general,

$$(A^2)_{ij} = \bigoplus_l a_{il} \otimes a_{lj} = \max_l\{a_{il} + a_{lj}\}. \quad (11)$$

In terms of the railway example, the quantity $(A^2)_{ij}$ can be interpreted as the máximum (with respect to l) of all connections from station S_j, via station S_l to station S_i. One speaks of paths of length two between the stations S_j and S_i. In graph-theory terminology, the stations are called nodes and the tracks between stations are called arcs. More generally, $(A^k)_{ij}$ denotes the maximum of all paths of length k, starting at node j and ending at node i.

In many networks such as a railway net there will not be an

arc from each node to each other node. If there is not arc from node S_j to node S_i then the behavior of node S_i is not directly influenced by that of node S_j. In such situation it is useful to consider the element a_{ij} to be equal to $-\infty$. In (8) a term $-\infty + x_j(k)$ does not directly influence $x_i(k+1)$ as long as $x_j(k)$ is finite. The number $-\infty$ will occur frequently in the sequel and it will be indicated by ε.

Linear systems in the max-plus algebra with inputs and outputs are given by

$$\begin{cases} x(k+1) = Ax(k) \oplus Bu(k) \\ y(k) = Cx(k) \end{cases} \quad (12)$$

which is short-hand notation for

$$x_i(k+1) = \max\{a_{i1} + x_1(k), \dots, a_{in} + x_n(k), b_{i1} + u_1(k), \dots, b_{im} + u_m(k)\}, i = 1, 2, \dots, n;$$
$$y_i(k) = \max\{c_{i1} + x_1(k), \dots, c_{in} + x_n(k)\}, i = 1, 2, \dots, p.$$

A seeming generalization of (10) is

$$x(k+1) = A_0x(k+1) \oplus A_1x(k) \oplus \dots \oplus A_{l+1}x(k-1), \quad (13)$$

which is implicit in $x(k+1)$ and which has extra delays. By repeated substitution of the whole right-hand side of (13) for the term $x(k+1)$ in this right-hand side, one gets

$$x(k+1) = A_0^*A_1x(k) \oplus \dots \oplus A_0^*A_{l+1}x(k-1) \quad (14)$$

where $A_0^* = I \oplus A_0 \oplus A_0^2 \oplus A_0^3$ .... The notation I refers to the identity matrix in the max-plus algebra: it has zeros on the main diagonal and ε's elsewhere. Equation (14) only makes sense if A_0^* is well defined (its elements are finite or ε). This is for instance the case if the precedence graph of A does not contain circuits, because then $A^k = \varepsilon$ for $k \geq n$. Equation (14) can be rewritten as a first order difference equation by augmenting the state space. This is a standard trick in system theory and has already been used in section 2.

4 Behavior

Given a square matrix A, we consider the problema of existence of eigenvalues and eigenvectors in the max-plus algebra, that is, the existence of λ and $v \neq \varepsilon$ such that

$$Av = \lambda v. \quad (15)$$

This equation has to be interpreted in the max-plus algebra sense; the expresión λv means that one adds λ to each component of v. We already have seem examples of eigenvalues and eigenvectors in section 2; v correspond to an initial state resulting in a solution with 'period' 1 and λ is the interdeparture time.

Before formulating a theorem about eigenvalues, some graph theory must be recapitulated. In the following definition the starting point is a square matrix, the entries of which may again assume the 'value' ε.

Definition 1 (Precedence graph). The precedence graph of an $n \times n$ matrix A is a weighted digraph with n nodes and an arc (j, i) if $a_{ij} \neq \varepsilon$, in which case the weight of this arc receives the numerical value of a_{ij}. The precedence graph is denoted by $G(A)$.

It is not difficult to see that any weighted digraph $G = (V, E)$, with V being the set of nodes and E being the set of arcs, is the precedence graph of an appropriately defined square matrix. The weight a_{ij} of the arc from node j to node i is defined as the $ij-th$ entry of a matrix A. If an arc does not exist, the corresponding entry of A becomes ε. The matrix A thus defined has G as its precedence graph.

As we have seen before, the element (i, j) of $A^k = A \otimes A \otimes \dots A \otimes A$, considered within the max-plus algebra denotes the maximum weight with respect to all paths of length k, which go from node j to node i. If no such path exists, then $(A^k)_{ij} = \varepsilon$. The weight of a path ρ is denoted $|\rho|_w$ and its length is denoted $|\rho|_l$.

Definition 2. The mean weight of a path is defined as the sum of the weights of the individual arcs of this path, divided by the length of this path. If the path is denoted by ρ, then the mean weight equals $\frac{|\rho|_w}{|\rho|_l}$. If such a path is a circuit one talks about the mean weight of the circuit, or simply the cycle mean.

We are interested in the maximum of these cycle means, where the maximum is taken over all circuits in the graph. This number will be called the maximum cycle mean. If the cycle mean of a circuit equals the maximum cycle mean, then the circuit is called critical. The graph consisting of all critical circuits (if there happen to be more than one) is called the critical graph and denoted by G^c. In the following theorem the notion 'strongly connected' digraph is used. A graph is called strongly connected if there exist a path from any node to any other node. The matrix corresponding to a strongly connected graph is called irreducible.

Theorem 1. We are given a square matrix A. If $G(A)$ is strongly connected, then there exist one an only one eigenvalue and at least one eigenvector. The eigenvalue is equal to the maximum cycle mean of the graph: $\lambda = \max_{\chi} \frac{|\chi|_w}{|\chi|_l}$, where χ ranges over the set of circuits of $G(A)$.

Definition 3 (Cyclicity of a graph). Given a strongly connected graph, its cyclicity equals the greatest common divisor of the lengths of all its circuits. The cyclicity of an arbitrary graph (which may consist of several strongly connected subgraphs) equals the least common multiple of the cyclicities of all its maximal strongly connected subgraphs.

Definition 4 (Cyclicity of a matrix). A matrix $\boldsymbol{A}$ is said to be cyclic, if there exist scalars $\boldsymbol{M}, \boldsymbol{\lambda}$ and d, such that for all $\boldsymbol{m} \geq \boldsymbol{M}, \boldsymbol{A^{m+d}} = \boldsymbol{\lambda^d A^m}$. The least such d is called the cyclicity of A. The quantity $\boldsymbol{\lambda}$ equals the maximun cycle mean of A.

The expression $\boldsymbol{A^{m+d}} = \boldsymbol{\lambda^d A^m}$ in the definition above must be interpreted in the max-plus algebra sense of course. Thus $\boldsymbol{\lambda^d}$ in the max-plus algebra means $\boldsymbol{d\lambda}$ in the conventional algebra and $\boldsymbol{\lambda^d A^m}$ refers to the addition of $\boldsymbol{\lambda^d}$ to each element of $\boldsymbol{A^m}$.

Theorem 2. Any irreducible matrix is cyclic. The cyclicity of the irreducible matrix A equals the cyclicity of $\boldsymbol{G^c(A)}$, being the critical graph corresponding to matrix A.

Example 1. Consider the A-matrix of (6):

$$\boldsymbol{A} = \begin{pmatrix} \mathbf{2} & \mathbf{5} & \boldsymbol{\varepsilon} & \boldsymbol{\varepsilon} \\ \boldsymbol{\varepsilon} & \boldsymbol{\varepsilon} & \mathbf{3} & \mathbf{3} \\ \mathbf{0} & \boldsymbol{\varepsilon} & \boldsymbol{\varepsilon} & \boldsymbol{\varepsilon} \\ \boldsymbol{\varepsilon} & \mathbf{0} & \boldsymbol{\varepsilon} & \boldsymbol{\varepsilon} \end{pmatrix}.$$

The corresponding precedence graph has three circuits, viz from node 1 to node 1 with cycle mean 2/1=2; from node 1 to 3 to 2 to 1 with cycle mean (0+3+5)/3=8/3; from node 2 to 4 to 2 with cycle mean (0+3)/2=3/2 (it is tacitly assumed here that node i corresponds to $\boldsymbol{x_i}$). The maximum cycle means equals 8/3. There is only one critical circuit. The cyclicity of the critical graph (which equal the critical circuit) equal 3. The quantities of definition 4 are M=5, $\boldsymbol{\lambda = 8/3}$ and d=3;

$$\boldsymbol{A^8} = \begin{pmatrix} \mathbf{20} & \mathbf{23} & \mathbf{24} & \mathbf{24} \\ \mathbf{19} & \mathbf{20} & \mathbf{21} & \mathbf{21} \\ \mathbf{18} & \mathbf{21} & \mathbf{20} & \mathbf{20} \\ \mathbf{15} & \mathbf{18} & \mathbf{19} & \mathbf{19} \end{pmatrix} = \left(\frac{\mathbf{8}}{\mathbf{3}}\right)^{\mathbf{3}} \boldsymbol{A^5}$$
$$= \mathbf{8}\begin{pmatrix} \mathbf{12} & \mathbf{15} & \mathbf{16} & \mathbf{16} \\ \mathbf{11} & \mathbf{12} & \mathbf{13} & \mathbf{13} \\ \mathbf{10} & \mathbf{13} & \mathbf{12} & \mathbf{12} \\ \mathbf{7} & \mathbf{10} & \mathbf{11} & \mathbf{11} \end{pmatrix}.$$

5 The $\boldsymbol{\gamma}$ −Transform

Conventional linear systems with inputs and outputs are of the form (12), though (12) itself has the max-plus algebra interpretation. This equation, now considered in the conventional way, is a representation of a linear system in the time domain. Its representation in the Z-domain equals

$$\boldsymbol{Y(Z) = C(ZI - A)^{-1}BU(Z)},$$

where $\boldsymbol{Y(Z)}, \boldsymbol{U(Z)}$ are defined by

$$\boldsymbol{Y(Z) = \sum_{i=0}^{\infty} y(i)Z^{-1}},\ \boldsymbol{U(Z) = \sum_{i=0}^{\infty} U(i)Z^{-1}},$$

where it is tacitly assumed that the system was at rest for $\boldsymbol{t \leq 0}$ and where I refer to the unit matrix in the conventional algebra. The matrix $\boldsymbol{H(Z) = C\,(ZI - A)^{-1}B}$ is called the transfer matrix of the system.

In the max-plus algebra context, the Z-transform also exists, but here it is customary to refer to it as the $\boldsymbol{\gamma}$ −transform where $\boldsymbol{\gamma}$ operates as $\boldsymbol{Z^{-1}}$ and is assumed to be real-valued. For instance, the $\boldsymbol{\gamma}$ −transform of u is defined as

$$\boldsymbol{U(\gamma)} = \oplus_{\boldsymbol{i=0}}^{\boldsymbol{\infty}}\, \boldsymbol{u(i) \otimes \gamma^i} \qquad (\mathbf{16})$$

and $\boldsymbol{Y(\gamma)}$ and $\boldsymbol{X(\gamma)}$ are defined likewise. Multiplication of (12) by $\boldsymbol{\gamma^k}$ yields

$$\begin{cases} \boldsymbol{\gamma^{-1}x(k+1)\gamma^{k+1} = A \otimes x(k)\gamma^k \oplus B \otimes u(k)\gamma^k} \\ \boldsymbol{y(k)\gamma^k = C \otimes x(k)\gamma^k} \end{cases} \qquad (\mathbf{17})$$

If these equations are summed with respect to $\boldsymbol{k = 0, 1}$, ..., and if we add $\boldsymbol{\gamma^{-1}x_0}$ to both sides of the first equation thus obtained, then we obtain

$$\begin{cases} \boldsymbol{\gamma^{-1}X(\gamma) = A \otimes X(\gamma) \oplus B \otimes U(\gamma) \oplus \gamma^{-1}x_0} \\ \boldsymbol{Y(\gamma) = C \otimes X(\gamma)}. \end{cases} \qquad (\mathbf{18})$$

The first of these equations can be solved be first multiplying (max-plus algebra), equivalently adding (conventional), left and right-hand side by $\boldsymbol{\gamma}$ and then repeatedly substituting the right-hand side for $\boldsymbol{X(\gamma)}$ within this right-hand side. This results in

$$\boldsymbol{X(\gamma) = (\gamma A)^*(\gamma BU(\gamma) \oplus x_0)}.$$

Thus, we obtain $\boldsymbol{Y(\gamma) = H(\gamma)U(\gamma)}$, provided that $\boldsymbol{x_0 = \varepsilon}$, and where the transfer matrix $\boldsymbol{H(\gamma)}$ is defined by

$$\boldsymbol{H(\gamma) = C \otimes (\gamma A)^* \otimes \gamma \otimes B}$$
$$\boldsymbol{= \gamma CB \oplus \gamma^2 CAB \oplus \gamma^3 CA^2 B \oplus \ldots} \quad (\mathbf{19})$$

The expression $\boldsymbol{Y(\gamma) = H(\gamma)U(\gamma)}$ is the max-plus algebra equivalent of $\boldsymbol{Y(Z) = H(Z)U(Z)}$ in the conventional system theory. If one writes

$$\boldsymbol{H(z) = C(zI - A)^{-1}B = C\left(\frac{1}{\gamma}I - A\right)^{-1}B}$$
$$\boldsymbol{= \gamma C(I - \gamma A)^{-1}B}$$
$$\boldsymbol{= \gamma C(I + \gamma A + \gamma^2 A^2 + \cdots)B},$$

one has obtained the equivalence of (19) in the conventional

sense.

The transfer matrix (19) is defined by means of an infinite series and the convergence depends on the value of $\boldsymbol{\gamma}$. If the series is convergent for $\boldsymbol{\gamma} = \boldsymbol{\gamma}'$, then it is also convergent for all $\boldsymbol{\gamma}'\boldsymbol{s}$ which are smaller than $\boldsymbol{\gamma}'$. If the series does not converge, it still has a meaning as a formal series.

Exactly as in conventional system theory, the transfer matrix is especially useful when subsystems are combined to build larger systems, by means of parallel, series and feedback connections. For instance, the product of two transfer matrices (of which it is tacitly assumed that the sizes of these matrices are such that the multiplication is possible), is a new transfer matrix which refers to a system which consists of the original systems put into a series connection.

Suppose that $\boldsymbol{H}(\boldsymbol{\gamma})$ is a scalar function, i.e., the system has one input and one output. The term $\boldsymbol{\gamma^k C A^{k-1} B}$ in (19) can be written in conventional algebra as $\boldsymbol{C_{k-1} + k\gamma}$ (where $\boldsymbol{C_{k-1}}$ represents the coefficient $\boldsymbol{CA^{k-1}B}$) which is a straight line with slope k. The transfer function can be viewed as the maximum (of an infinite number) of such lines and hence is a continuous, piecewise linear and convex function of the variable $\boldsymbol{\gamma}$.

6 Some Extensions

6.1 Axiomatic foundations

The operations $\oplus$ and $\otimes$ defined on the set R can also be defined with respect to a more general set of elements D. One then speaks of a dioid (sometimes also referred to as a semiring).

Definition 5. A dioid is a set D endowed with two operations denoted $\oplus$ and $\otimes$ (called 'sum' or 'addition', and 'product' or 'multiplication') obeying the following axioms:

1. For all $a, b, c \in D, (a \oplus b) \oplus c = a \oplus (b \oplus c)$;
2. For all $a, b \in D, a \oplus b = b \oplus a$;
3. For all $a, b, c \in D, (a \otimes b) \otimes c = a \otimes (b \otimes c)$;
4. For all $a, b, c \in D$, $(a \oplus b) \otimes c = (a \otimes c) \oplus (b \otimes c), c \otimes (a \oplus b) = (c \otimes a) \oplus (c \otimes b)$.

This is right, respectively left, distributivity of multiplication jwith respect to addition. One statement does not follow from the other since multiplication is not assumed to be commutative.

5. Exist $\varepsilon \in D: \forall a \in D, a \oplus \varepsilon = a$;
6. $\forall a \in D, a \otimes \varepsilon = \varepsilon \otimes a = \varepsilon$;
7. Exist $e \in D: \forall a \in D, a \otimes e = e \otimes a = a$;
8. $\forall a \in D, a \oplus a = a$.

Definition 6. A dioid is commutative if multiplication is commutative.

With the noticeable exception of axiom 8, most the axioms of dioids are required for rings too. Indeed, axiom 8 is the most distinguishing feature of dioids. Because of this axiom, addition can not be cancellative, that is, $\boldsymbol{a \oplus b = a \oplus c}$ does not imply b=c in general. Multiplication is not necessarily cancellative either (of course, because of axiom 6, cancellation would anyway only apply to elements different from $\boldsymbol{\varepsilon}$). For an example in which multiplication is not cancellative take $\boldsymbol{D} = \mathbb{R} \cup \{-\infty\} \cup \{+\infty\}$ and define $\oplus$ as max and $\otimes$ as min.

It is easily shown that in dioids the distributivity with respect to matrices also holds, i.e., $\boldsymbol{A \otimes (B \otimes C) = (A \otimes B) \otimes C}$, where these multiplilcations only make sense if the matrices have appropriate dimensions.

6.2 Minimal realizations

In Section 5 it was shown how to derive the transfer matrix of a system if the representation of the system in the 'event domain' is given. This event domain representation is characterized by the matrices A, B and C. Now one could pose the opposite question; how to obtain an event domain representation, or equivalently, how to find A, B and C if the transfer matrix is given. In the conventional linear system theory, the corresponding theory is known as the realization theory and one speaks of a minimal realization if the sizes of A, B and C are as small as possible.

The simplest formulation of the (minimal) realization problem in the max-plus algebra is probably as follows. Let G be a sequence of real numbers $\{\boldsymbol{g_l}\}_{\boldsymbol{l=0}}^{\boldsymbol{\infty}}$ and let $\boldsymbol{A} \in \boldsymbol{R^{n\times m}}, \boldsymbol{x_0} \in \boldsymbol{R^{n\times 1}}, \boldsymbol{C} \in \boldsymbol{R^{1\times n}}$ be such that $\boldsymbol{g_j = C \otimes A^j \otimes x_0}, \boldsymbol{j = 0, 1}, ...,$ then G is said to be reproduced by the discrete event system $\boldsymbol{x(k+1) = A \otimes x(k), x(0) = x_0}$ and $\boldsymbol{y(k) = C \otimes x(k)}$. Given a sequence produced in this way, finds its realization of the smallest dimension. This realization problem has attracted a lot of attention recently, but for the moment it remains unclear whether an exact algorithmic procedure of polynomial complexity can be found for the general case.

In most approaches the theorem of Cayley-Hamilton, suitably adapted to the max-plus algebra plays a crucial role.

6.3 Stochastic Discrete Event Systems

The evolution equation studied in this part is

$$\boldsymbol{x(k+1) = A(k) \otimes x(k), \qquad k = 0, 1, 2, ...} \qquad (\boldsymbol{20})$$

with some initial condition $\boldsymbol{x(0)}$. Some (or all) entries of $\boldsymbol{A(k)}$ are stochastic. We assume that:

- The underlying distribution functions do not depend on k.
- The stochastic entries can assume only a finite number of different values. It will also be assumed that

these values are finite, though the method to be described can be generalized to the case that $-\infty$ is also allowed as a value.
- A(k) and A(n) are independent stochastic matrices for $k \neq n$ (extensions exist for problems where A(k) and A(k+1) are correlated).
- No correlation between stochastic entries of exists, though such correlations can be treated rather routinely.
- G(A(k)) is strongly connected (if this assumption is true for one k, it automatically is true for all k due to the second assumption above).

The quantity of central interest is

$$\lim_{k\to\infty} E\left(\frac{\boldsymbol{x_i(k)}}{\boldsymbol{k}}\right), \qquad (\mathbf{21})$$

For an arbitrary i, being the average cycle time for component i. This quantity is a kind of 'average cycle time'; it can be proved that this average cycle time is independent of i.

6.4 Min-max-plus systems and nonexpansive mappings

Referring to the right-hand side of (8), one can define a max-plus expression as a (finite) set of $\boldsymbol{x_i + a_{ij}}$ terms, connected by the max operator. Similarly, one defines a min-max-plus expression as a (finite) set of $\boldsymbol{x_i + a_{ij}}$ term, connected by both the max and min operators. An example of such an expression is

$$\mathbf{max}\{\boldsymbol{x_1+7}, \mathbf{min}\{\boldsymbol{x_2-4}, \boldsymbol{x_3+1}, \mathbf{max}\{\boldsymbol{x_1}, \boldsymbol{x_4+2}\}\}\}.$$

With respect to the operator, we introduced the neutral element $-\infty$. Since we now also deal with the min operator, it is convenient to introduce its neutral element $+\infty$ also. Exactly as one can define a max-plus system by means of max-plus expressions, as (8) can be viewed, one can define a min-max-plus system. Such systems are nonlinear in the max-plus algebra (because of the presence of the min operator) and also nonlinear in the min-plus algebra (because of the presence of the max operator). Not with standing this higher complexity, various results about min-max plus systems are known. Specifically necessary and sufficient conditions are known under which the evolution of (subclasses of) minx-max-plus systems show a regular pattern as the evolution of max-plus systems does.

Min-max-plus systems are quite naturally imbedded in the class of so-called nonexpansive mappings, which also are know to have the possibility of periodic behavior. For more information on such mappings, we end this subsection by the definition of nonexpansive mappings.

Definition 7. A mapping f, which maps $\boldsymbol{R^n}$ into $\boldsymbol{R^n}$ is called nonexpansive, if $\left|\left|\boldsymbol{f(z)-f(\xi)}\right|\right| \leq \left|\left|\boldsymbol{z-\xi}\right|\right|$, $(\mathbf{22})$ for arbitrary $\boldsymbol{z, \xi \in R^n}$, and where the norm is an arbitrary $\left|\left|.\right|\right|_{\boldsymbol{p}}$ norm, with $\mathbf{1} \leq \boldsymbol{p} \leq \infty$.

6.5 Numerical procedures

In this subsection we will confine ourselves to numerical procedures which yield the eigenvalue and eigenvector of a matrix A, as expressed by (15).

Theorem 3. Given is an $\boldsymbol{n \times n}$ matrix A, with corresponding precedence graph $\boldsymbol{G = (V, E)}$. The maximum cycle mean is given by

$$\boldsymbol{\lambda} = \max_{\boldsymbol{i=1,\ldots,n}} \min_{\boldsymbol{k=0,1,\ldots,n-1}} \frac{(\boldsymbol{A^n})_{\boldsymbol{ij}} - \left(\boldsymbol{A^k}\right)_{\boldsymbol{ij}}}{\boldsymbol{n-k}}, \forall \boldsymbol{j}. \qquad (\mathbf{23})$$

In this equation, $\boldsymbol{A^n}$ and $\boldsymbol{A^k}$ are to be evaluated in the max-plus algebra; the other operations (subtraction and division) are conventional ones. This theorem is known as Karp's theorem. This theorem yields the eigenvalue but does not give information about the eigenvectors. For that purpose construct the matrix B by subtracting $\boldsymbol{\lambda}$, obtained by Karp's theorem, from all elements of A. The máximum circuit weight of $\boldsymbol{G(B)}$ equals 0. Hence $\boldsymbol{B^* = I \oplus B \oplus B^2 \oplus}$ ... and $\boldsymbol{B^+ = BB^*}$ exist. Matrix $\boldsymbol{B^+}$ has some columns with diagonal elements equal to zero. To prove this, pick a node k of a circuit $\boldsymbol{x}$, such that $\boldsymbol{x \in \arg_\xi \frac{|\xi|_w}{|\xi|_l}}$. The maximum weight of paths from node k to k is 0. Therefore $\boldsymbol{B_k^+ = 0}$. Let $\boldsymbol{B_k}$ denote the k-th column of B. Then, since $\boldsymbol{B^+ = BB^*}$ and $\boldsymbol{B^* = I \oplus B^+}$ (I is the identity matrix), for that k, $\boldsymbol{B_k^+ = B_k^*}$ imply $\boldsymbol{BB_k^* = B_k^+ = B_k^*}$ imply $\boldsymbol{AB_k^* = \lambda B_k^*}$. Hence, $\boldsymbol{V = B_k^+ = B_k^*}$ is an eigenvector of A, corresponding to the eigenvalue $\boldsymbol{\lambda}$.

A few other numerical approaches exist which calculate the eigenvalue and/or eigenvector:
- Study of the zero (s) of the characteristic equation in the max-plus algebra yields the eigenvalue.
- By means of linear programming techniques.
- Consider (7). Calculate $x(k), k = 0,1, \ldots$, starting from an arbitrary initial condition, until a state becomes linearly dependent on a state already calculated ($x(7) = 8 \otimes x(4)$). Now 8/7-4 equals the eigenvalue and $\frac{(x(4)+x(5)+x(6))}{7} - 4$.

6.6 'Continuous' Discrete event systems and the Fenchel transform

The central equations of this part are (1) and (2). It is assumed now that in addition to t and $\boldsymbol{\tau_i}$, also x and $\boldsymbol{x_i}$ are real-valued, and so are the quantities $\boldsymbol{b_{ij}}$. The interpretation of these equations is still a (strongly connected) network with n transitions (also called nodes now). These nodes can now fire continuously. The intensity of this firing is indicated by $\boldsymbol{v_i(t)}$. Quantity $\boldsymbol{x_i(t)}$ denotes again the total amount produced by node i up to (and including) time t. As initial condition it is assumed

that $\boldsymbol{x_i(0) = 0}$. The production of a continuously firing transition in sent with unit speed along the outgoing arcs to the downstream transitions. Thus along an arc there is a continuous flow. The intensity of this flow is $\boldsymbol{\varphi_i(t, l)}$, where l is the parameter indicating the exact location along the arc; l=0 coincides with the beginning of the arc, l= coincides with the end of the arc, where it is assumed that the downstream transition is $\boldsymbol{q_j}$. As long as the parameters lie in appropriate intervals, we have $\boldsymbol{\varphi_i(t, l) = \varphi_i(t + s, l + s)}$. Moreover, $\boldsymbol{\varphi_i(t, l) = \varphi_i(t - l, 0) = v_i(t - l)}$.

At time t, the total amount of material along the arc from $\boldsymbol{q_i}$ to $\boldsymbol{q_j}$ equals

$$\int_{\boldsymbol{l=0}}^{\boldsymbol{l=a_{ji}}} \boldsymbol{\varphi_i(t, s)ds}\,. \qquad (\mathbf{24})$$

The quantities $\boldsymbol{b_{ij}}$ satisfy $\boldsymbol{b_{ij} = \int_0^{a_{ij}} \varphi(0, l)dl}$. The integrand and the integral in (24) must be considered with some care. It is quite well possible that the integrand will contain $\boldsymbol{\delta}$ −functions. This will particularly happen at the end of an arc, when material must wait there to be processed by the downstream transition because the other incoming arcs to the same transition have brought in less material sofar. If $\boldsymbol{q_k}$ is a downstream transition to both $\boldsymbol{q_i}$ and $\boldsymbol{q_j}$ and if $\boldsymbol{x_i(t) < x_j(t)}$, then $\boldsymbol{\varphi_{kj}}$ will start to build a $\boldsymbol{\delta}$ −function at $\boldsymbol{l = a_{kj}}$, from t onwards. Of course this $\boldsymbol{\delta}$ −function can disappear again later on if $\boldsymbol{x_i(s) > x_j(s)}$ for an $\boldsymbol{s}$ −value with $\boldsymbol{s > t}$. The total amount of material along an arc, as expressed by (24), will in general be time dependent. Many standard results of Section 4 on periodic behavior remain valid for this continuous version of flow on networks.

Theorem 4. Along a circuit the total amount of material is constant. In formula, if the circuit x is characterized by the transition $\boldsymbol{\{q_{i1}, q_{i2}, \dots, q_{i(k+1)} = q_{i1}\}}$,
then

$$\sum_{\boldsymbol{l=1}}^{\boldsymbol{k}} \int_{\boldsymbol{0}}^{\boldsymbol{a_{il+1,il}}} \boldsymbol{\varphi_{il}(t, s)ds}$$

is constant (it does not depend on time).

This is the 'continuous event' analogue of (*). Note that the total amount of material in the network is not necessarily constant.

Definition 8. Given a circuit

$$\boldsymbol{\tau = \{q_{i1}, q_{i2}, \dots, q_{i(k+1)} = q_{i1}\}},$$

its cycle mean is defined as $\frac{|\tau|_w}{|\tau|_l}$, where the weight $\boldsymbol{|\tau|_w}$ and the length $\boldsymbol{|\tau|_l}$ (assumed to be positive) are defined as

$$\boldsymbol{|\tau|_w = \sum_{l=1,\dots,k} a_{i(l+1),i_l}}\,, \qquad \boldsymbol{|\tau|_l = \sum_{i=1,\dots,k} b_{i(l+1),i_l}}.$$

Definition 9. The circuits which have the maximum cycle mean are called critical. The corresponding cycle mean is indicated by $\boldsymbol{\lambda}$.

Theorem 5. Equations (**) has a solution $\boldsymbol{x_i(t) = \frac{1}{\lambda} t + d_i}$, with appropriately chosen constants $\boldsymbol{d_i}$.

Just as there are linear difference equations versus Z-transforms, and similarly, linear differential equations versus Laplace transforms, we have in the max-plus algebra setting their counterparts. For the discrete event systems we had the max-plus algebra systems versus the $\boldsymbol{\gamma}$ transform. Fort he continuous flow variation we have the description above versus a slight variation of the Fenchel transform, called Fenchel* transform. This Fenchel* transform turns out to be the max-plus algebra variant of Laplace transform. The Fenchel transform of a function is also referred to as the conjugate function. We conclude with its definition.

Definiton 10. The Fenchel transform $\boldsymbol{J(f)}$ of a function f in a Hilbert space $\boldsymbol{H}$ is a function in the dual space $\boldsymbol{H^*}$;

$$\boldsymbol{\forall c \in H^*: [J^*(f)](c) = \sup_{z \in H}\{\langle c, z\rangle + f(z)\}}. \qquad (\mathbf{25})$$

Usually one confines the definition to convex functions f. Note the resemblance between (16) and (25).

References

Andersen, H. (2002). *Max-plus algebra: Properties and Applications*.

Baccelli, F, and Cohen, G. and Olsder, G. and Quadrat, J. (2001). *Synchronization an linearity. An algebra for discrete event systems*. Inria. France.

Branicky, M. (1995). *Studies in hybrid systems: Modeling, analysis and control*. Doctoral dissertation, Massachusetts Institute of Technology.

De Schutter, B. and Van Den Boom, T. *(2008). Max-plus algebra and max-plus linear discrete event systems: An introduction*. Proceedings of the 9th International Workshop on Discrete Event Systems (WODES'08), *Göteborg, Sweden, pp. 36–42.*

Komenda, J and Lahaye, S. and Boimond, J.-L. and Van Den Boom, T. (2018) *Max-plus algebra in the history of discrete event systems*, Annual Reviews in Control. Volume 45, pp. 240-249

Murata, T. (1989). *Petri nets: Properties, analysis and aplications*. Proceedings of the IEEE, Vol. 77(4).

Coen, G. and Gaubert, S. and Quadrat, J. (1999) *Max-plus algebra and system theory: where we are*

and where to go now. Annual Reviews in Control. *Vol. 23, pp. 207-219.*

Received: *november 12, 2026*

Accepted: *february 23,2026*

Ferrer-Guillén, María Dolores. *Master's degree in Computing. Active Full Professor. Department of Calculation, Faculty of Engineering, ULA. Research area: analysis and control in dynamic systems.*
E-mail: mariadfg@gmail.com
https://orcid.org/0009-0002-8162-233X

Mantilla-Morales, Gisella: *Engineer in Electronics and Telecommunications, Master's degree in Mathematics; full-time professor at the Technical University of Manabí.*
https://orcid.org/0000-0002-0826-7741

Bastidas Chalán, Rodrigo Vladimir: *Engineer in Electronics and Control; full-time professor at the University of the Armed Forces, ESPE.*
E-mail: rvbastidas@espe.edu.ec
https://orcid.org/0000-0002-2811-1672

Rentería Torres, Aníbal Vicente: *Electrical Engineer; full-time professor at the University of the Armed Forces, ESPE.*
E-mail: avrenteria@espe.edu.ec
https://orcid.org/0009-0002-9057-4536

Mata-Díaz, Guelvis E.*: Graduate in Mathematics. Master of Sciences in Mathematics. PhD in Applied Sciences. Active Full Professor. Faculty of Sciences, ULA. Department of Mathematics. Research area: analysis and control in discrete-event Dynamic systems.*
E-mail: gematad2017@gmail.com
https://orcid.org/0000-0001-7147-1422

Artículo de Investigación. Revista Ciencia e Ingeniería. Vol. 47, No. 2 pp. 117-128, abril-julio, 2026.
ISSN 1316-7081. ISSN Elect. 2244-8780 Universidad de los Andes (ULA)

Antibacterial potential of the ethanolic extract of pericarp of cacao (*Theobroma cacao* L.) on *Staphylococcus aureus* and *Escherichia coli*

Potencial antibacteriano del extracto etanólico de pericarpio de cacao (*Theobroma cacao* L.) sobre *Staphylococcus aureus* y *Escherichia coli*

María Ocanto[1]; Guillermo, Centeno-Bordones[2,3]; Ana, Ramos-Villarroel[1,2*]
[1]Universidad de Oriente, Nucleo de Monagas, Venezuela.
[2]Instituto Venezolano de Investigaciones Científicas (IVIC), Caracas, Venezuela.
[3]Universidad de Carabobo, Valencia, Venezuela
*ay2170@gmail.com

Abstract

Cocoa pericarp is a waste product in the cocoa industry, but it contains a large amount of bioactive compounds with high antibacterial potential. The objective of this research was to evaluate the antibacterial potential of the ethanolic extract of cocoa pericarp (*Theobroma cacao* L.) on *Staphylococcus aureus* and *Escherichia coli*. The ethanolic extraction was carried out by digestion was performed (Soto Hernández et al., 2019). Four (4) concentrations (25 mg/mL, 50 mg/mL, 75 mg/mL, and 100 mg/mL) and a negative control (sterilized distilled water) were established. The agar well diffusion method was used (Balouiri et al., 2016). The results showed that *S. aureus* bacteria were much more sensitive to cocoa pericarp ethanolic extract (CPE) than *E. coli*, yielding average inhibition zones of 10.8 and 13.53 mm at concentrations of 50 mg/mL and 75 mg/mL, unlike E. coli, which had averages of 9.88 and 9.46 mm at the same concentrations. The concentration with the greatest inhibitory power on both bacteria was 100 mg/mL, yielding average inhibition halo values of 14.84 and 17.68 mm on *E. coli* and *S. aureus*, respectively. These results demonstrate that EPC has high antibacterial power on Gram-positive and Gram-negative bacteria, with the former being more susceptible to this natural antimicrobial. In view of the antibacterial properties observed, EPC has the potential to be developed as a natural antimicrobial agent in food preservation.

Keywords: ethanolic extraction, cocoa pericarp, natural antibacterial.

Resumen

El pericarpio de cacao constituye un producto de desecho en la industria del cacao, sin embargo, éste posee una gran cantidad de compuestos bioactivos de alto potencial antibacteriano. El objetivo de esta investigación fue evaluar el potencial antibacteriano del extracto etanólico del pericarpio de cacao (Theobroma cacao L.) sobre Staphylococcus aureus y Escherichia coli. La extracción etanólica se realizó por digestión (Soto Hernández et al., 2019). Se establecieron cuatro (4) concentraciones (25 mg/mL, 50 mg/mL, 75 mg/mL, y 100 mg/mL) y un control negativo (agua destilada esterilizada). Se utilizó el método de pocillo o Agar well diffusion method (Balouiri et al., 2016). Los resultados mostraron que la bacteria S. aureus fue mucho más sensible al extracto etanólico de pericarpio de cacao (EPC) que E. coli, arrojando promedios de halos de inhibición de 10,8 y 13,53 mm a la concentración de 50 mg/mL y 75 mg/ml, a diferencia de E. coli con promedios de 9,88 y 9,46 mm a las mismas concentraciones. La concentración con mayor poder inhibitorio sobre ambas bacterias fue aquella de 100 mg/mL, arrojando valores promedios de halos de inhibición de 14,84 y 17,68 mm sobre E. coli y S. aureus respectivamente. Estos resultados demuestran que el EPC posee un alto poder antibacteriano sobre bacterias Gram positivas y Gram negativas, siendo las primeras más susceptibles a este antimicrobiano natural. En vista de las propiedades antibacterianas observadas, el EPC tiene el potencial de desarrollarse como un agente antimicrobiano natural en la conservación de alimentos.

Palabras clave: *extracción etanólica, pericarpio de cacao, antibacteriano natural.*

1 Introduction

Part of the stability and safety of food products is based primarily on preservation through the addition of natural antimicrobial agents. This is because the use of synthetic antimicrobial agents has caused problems in humans (allergic reactions, migraines, degenerative diseases, various types of cancer, among others). which is why there is a need to find preservation alternatives that offer the same antimicrobial properties and food compatibility (Kumar et al., 2025; El Sayed et al., 2022; Rodríguez and Nereyda, 2011).

Some natural antimicrobials are obtained mainly from herbs, plants, and spices, which have been used for decades to increase the shelf life of food. There are several reports in the literature on the antimicrobial activity of spices, herbs, and plants or their extracts (Khan et al., 2025; Guerrero et al., 2021; Solis, 2011; López et al., 2013; Ludy et al., 2013). Among the main bioactive compounds extracted from plants and seeds are terpenes, glucosinolates, and phenolic compounds. These, such as flavonols, typically found in fruits and green tea, have antibacterial activity.

Cocoa beans are also a rich source of polyphenols. The total polyphenol content of cocoa is significantly higher than that of acai berries, blueberries, and pomegranates, meaning that its antioxidant activity is much greater than that of other fruits (Crozier et al., 2011). Cocoa is scientifically known as Theobroma cacao L., where the term cocoa comes from the Nahuatl word 'cacahualt'. The name of the genus comes from the Greek 'theos' (God) and 'broma' (food) and means 'food of the gods' (Orwa et al., 2009). The different parts of the fruit (Figure 1) include the seed, mucilage, tegument, shell, endosperm, cotyledons, and pericarp or husk. The latter is the part of the fruit that covers the seed and is obtained by shelling it. This material represents approximately 12% of the seed's weight and is obtained after the roasting process. It is dry, crunchy, and brown in color (Kalvatchev et al., 1998).

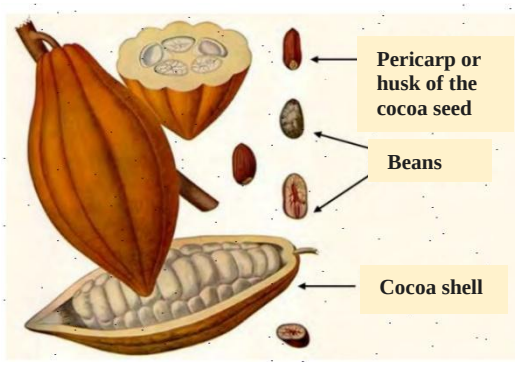

Figure 1. Parts of the cacao fruit (Beckett, 2008).

The cacao bean is a potential source of antibacterial agents and has been used since ancient times by the Aztecs to treat intestinal diseases (Dillinger et al., 2000). The husk or pericarp is usually treated as a food source for animals due to its dietary fiber content, but its alkaloid content restricts its use. Currently, there has been an increase in studies related to this type of waste and its possible use, as it represents an important component of agricultural and agroindustrial waste worldwide, constituting a good source of renewable resources and energy. Internationally, possible uses for cocoa husks are being developed, such as a source of soil fertilizers (Rojo-Poveda et al., 2020; Ayeni, 2010), animal feed for poultry and other animals (Leiva et al. 2022; Alemawor et al., 2009), and a source of pectins and gums (Ortiz et al., 2023; Barazarte et al., 2008). However, there are few studies related to its use as a natural antimicrobial agent, and most of the work refers to other parts of the fruit.

Various studies have evaluated the antimicrobial activity of cocoa on different microorganisms, including *Salmonella*, *Listeria* sp., *Staphylococcus aureus*, and *Escherichia coli*. The latter are highly implicated in foodborne illnesses (FBIs). *Staphylococcus aureus* consists of Gram-positive cocci and is an important bacterium not only because it causes infections in various parts of the human body, but also because it causes foodborne toxic infections (Goudsmit et al., 2021; Borraz, 2006). With regard to poisoning caused by *S. aureus*, it is known that most outbreaks are caused by coagulase-positive *S. aureus*, as very few coagulase-negative strains are capable of producing enterotoxins (staphylococcal food poisoning, SFP). Therefore, it is important to mention that staphylococcal enterotoxins are among the few bacterial toxins of a protein nature that are heat-resistant (Perdomo and Meléndez, 2004). On the other hand, *Escherichia coli* belongs to the Enterobacteriaceae family, the representatives of this species are Gram-negative and oxidase-negative bacilli. Among the pathogenic strains of *E. coli* is *E. coli* O157:H7. This is an enterohemorrhagic strain that causes food poisoning due to the production of verotoxin (Welinder-Olsson and Kaijser, 2005). This bacterium is considered the indicator microorganism par excellence for fecal contamination (Edberg et al., 2000). For this reason, the quantification of *E. coli* in water bodies and food in tropical environments as the main representative of the thermotolerant coliform group has gained importance in the last decade (Romeu et al., 2012).

There are several studies associated with the extraction of bioactive compounds present in plants and fruits, as well as cocoa beans and shells, which have an antimicrobial effect on different microorganisms such as *E. coli*, *Shigella dysenteriae*, *Bacillus cereus*, and *S. aureus* (Llerena et al., 2023; Ariza et al., 2013; Wulandari et al., 2012; Nsor-

Atindana et al., 2012). Most studies used extraction methods with organic solvents or hydroalcoholic extraction, which are fundamental techniques for the analysis of secondary metabolites and polyphenols.

In this regard, given that the pericarp is a waste by-product of the cocoa industry, and in accordance with the antimicrobial precedents of the fruit seed, this study set out to evaluate the antibacterial potential of the ethanolic extract of cocoa pericarp (*Theobroma cacao* L.) on strains of *Staphylococcus aureus* and *Escherichia coli*.

2 Materials and Methods

The study was conducted in the Food Technology Laboratory of the Departmen t of Food Technology, and microbiological analyses were performed in the Microbiology Laboratory of the Department of Biology and Animal Health. Both departments belong to the School of Agricultural and Environmental Sciences of the Universidad de Oriente, Maturín Municipality, Monagas State, Venezuela.

2.1 Obtaining the ethanolic extract

2.1.1 Obtaining the sample

Samples of dry Criollo cocoa pericarp were used, donated by the cocoa processing company CHOCOLATERA VILLROS C.A., located in the municipality of Caripito, Monagas State, Venezuela. These samples comprise a waste by-product of the company.

2.1.2 Sample preparation

Three hundred grams (300g) of pericarp were weighed and ground to a particle size of 0.5 mm (Ariza et al., 2013) using Thomas-Wiley equipment (Model Arthur H., Philadelphia, PA, USA). The sample obtained was weighed and hermetically sealed until the extraction process.

2.2 Preparation of the ethanolic extract

Moisture and fat content were previously determined according to AOAC (1990) to ascertain the characteristics of the pericarp sample. With the help of these results and the bibliographies consulted, the extraction method used in this study was established, which was the digestion extraction method following the methodology described by Soto Hernández et al. (2019). In this case, approximately 15 g of sample (ground pericarp) was first weighed using an Adventuer analytical balance (TM AR2140, NJ), then placed in a 250 mL distillation flask and 60 mL of ethanol was added, at a ratio of 1:4 in relation to the mass of the sample. A water-circulating condenser or Allihn cooling tube was then attached to the top of the flask. The system was then mounted on a CORNING heating plate (Stirrer PC 920, USA) with constant magnetic stirring, and extraction was performed by vacuum filtration in triplicate for approximately 6 hours. After the extraction time had elapsed, filtration was carried out using a porcelain funnel with Whatman No. 1 filter paper and a Gast Manodacturing Inc. vacuum pump (8 DAA-VGSIS-ED. USA.).

2.2.1 Solvent distillation

The filtered extract obtained was placed in a Rotaevaporator flask (R-210, Switzerland) with a Heating Bath (B-491, Switzerland). This flask was weighed once washed and dried to determine the yield of the extract, and the solvent was evaporated at 70°C at a vacuum pressure of 600 mmHg using a vacuum pump (BOECO R-300, Germany). A water chiller was used to regulate the temperature, following the methodology described by Soto Hernández et al. (2019). Once the solvent had been separated from the extract, the flask was weighed and the extract obtained was placed in an amber bottle, which was stored in a freezer at -6°C until use.

2.3 Preparation of concentrations

Once distillation was complete, the different concentrations to be used in the test were determined. Taking into account the research consulted (Wulandari et al., 2012; Sucuzhañay, 2015) and previous experimental tests using cocoa beans and shells, solutions at concentrations of 25 mg/mL, 50 mg/mL, 75 mg/mL, and 100 mg/mL were used as criteria for this study, and distilled water was used as a negative treatment, respectively. The negative control, being an inert solvent, will have no inactivating effect on them.

Four 25 mL volumetric flasks were identified corresponding to each solution of the extract at concentrations of 25 mg/mL, 50 mg/mL, 75 mg/mL, and 100 mg/mL. To do this, a stock solution of cocoa pericarp extract (CPE) with a concentration of 3000 mg/mL was prepared in advance, and from this, the different dilutions were prepared using sterile distilled water as a solvent until the respective concentrations of 25 mg/mL, 50 mg/mL, 75 mg/mL, and 100 mg/mL. The volumes of each flask were then measured with sterile distilled water (as a solvent) using a 10 mL volumetric pipette up to the calibration line.

2.3.1 Determination of concentration (C) by Spectrophotometry

To chemically determine that the dilutions were correct, the mathematical relationship of the straight line and Lambert-

Beer's law (equation 1) were used. For this purpose, a calibration curve was made for the cocoa pericarp extract in ethanol solution, with its respective blank of pure solvent. Once this preliminary step was completed, the samples were passed through the Thermo Electron Corporation Evolucion 300 spectrophotometer at a wavelength of 750 nm (Ordoñez et al., 2019; Iglesias-Guevara et al., 2022). In order to obtain the respective absorbances for the concentration, m was cleared. The concentration data will be shown in Table 2.

$$y = mx + b$$

Where:

y: Is the absorbance measured by the equipment.

x: Is the concentration (what we want to verify).

m: Is the slope (sensitivity of the method).

b: Is the intercept (the "noise" of the target).

2.4 Determination of the Effectiveness of EPC on the Inactivation of S. aureus and E. coli in vitro.

2.4.1 Microbiological Analysis (bacterial inactivation based on the concentrations used in the study)

Microbiological analyses were performed in triplicate for each of the concentrations.

2.4.2 Preparation of the inoculum

The *E. coli* and *S. aureus* strains were obtained from the culture collection of the Microbiology Laboratory of the School of Agricultural and Environmental Sciences of the Universidad de Oriente (UDO), Monagas state, Venezuela. These were kept in slanted tubes with soy trypticase agar (HIMEDIA) at a temperature of 5 °C until use. The inocula were obtained by reactivating the strains in nutrient broth at 37 °C for 24 hours (Ramos et al., 2012).

2.4.3 Preparation of culture medium

A total of 36 nutrient agar plates were prepared and labeled as follows: 18 for *E. coli* and 18 for *S. aureus*. The culture medium was prepared based on the total number of plates to be used, following the methodology described by the COVENIN standard (1292-89), for which approximately 11.76 g of nutrient agar was weighed and diluted in 360 mL of distilled water and sterilized in an autoclave. Once the medium was sterilized, it was tempered to 45°C and added at a rate of 15 mL per plate. Finally, it was left to solidify for use.

2.4.4 Determination of antibacterial potential

The determination of antibacterial activity and comparison of the degree of inhibition of the extract on different bacteria was performed using the well diffusion method proposed by Balouiri et al. (2016), which is widely used to evaluate the antimicrobial activity of plants or microbial extracts (Magaldi et al., 2004).

First, the microorganism was seeded using the streak method on the surface of the previously prepared plate (Ramos et al., 2012). Next, using a sterile punch, three 5 mm diameter holes were made per plate (Figure 2) and a volume of 1 µl of the concentrations of each treatment described in Table 8 was added to each well using an automatic micropipette. The plates were placed in the incubator without inversion for a period of 24 hours at 37°C.

Table 1. Proposed treatments to determine antibacterial potential against *E. coli* and *S. aureus*.

Treatment	**Characteristics**
T_1	Sterilized distilled water
T_2	Ethanolic extract 25 mg/mL
T_3	Ethanolic extract 50 mg/mL
T_4	Ethanolic extract 75 mg/mL
T_5	Ethanolic extract 100 mg/mL

2.4.5 Determination of zones of inhibition

After 24 hours, the zones of inhibition in each well were measured (mm) using a vernier caliper.

2.4.6. Comparison of the degree of inhibition obtained using EPC on the respective bacteria

To compare the inhibitory degree of T5 (100 mg/mL) on *E. coli* and *S. aureus*, a Student's t-test for means with n=18 was used. The best concentration of the ethanolic extract obtained from the previous objective was used.

Figure 2. Representation of the agar plate with the respective wells for measuring inhibition zones.

2.5 Experimental design

A completely randomized design was used with five treatments distributed in distilled water as a negative control, 25 mg/mL, 50 mg/mL, 75 mg/mL, and 100 mg/mL (Table 1). To study the inhibition of the different treatments evaluated, the analyses were performed in triplicate with three replicates for each treatment, for a total of 45 observations per microorganism.

2.5.1 Statistical analysis

The results were analyzed using analysis of variance (ANOVA) to determine significant differences between treatments. P-values were calculated using Tukey's test with a significance level of 5%. The InfoStaf statistical package version 2016 was used for data analysis (Di Rienzo et al., 2017). A comparison of the inhibitory degree of T5 on each microorganism was also performed using a Student's t-test, where the null hypothesis (Ho) established that there is no significant difference in the inhibitory degree of the microorganisms studied, and the alternative hypothesis (Hi) stated that there is a significant difference between them. An n=18 and a significance level of 5% were used.

3 Results and Discussion

3.1 Determination of concentration (C) by Spectrophotometry

When analyzing the experimental data obtained at 750 nm, compliance with Beer-Lambert's Law was observed, evidencing a linear relationship between the concentration of EPC and its respective absorbance (Table 2). When comparing the values, it is noteworthy that the instrumental response factor of absorbance units per ppm indicated good preparation of the dilutions and excellent sensitivity of the spectrophotometer at the selected wavelength. This validates the stability of the ethanolic extract of the pericarp and ensures that the readings are within the linear dynamic range of the equipment, allowing reliable analytical quantification without detector saturation effects.

The values obtained for polyphenol concentration are consistent with the results obtained by Ordoñez et al. (2019), Iglesias-Guevara et al. (2022), and Monroy et al. (2023), who at these wavelengths were able to validate the concentrations obtained from the polar soluble extracts of cocoa seed pericarp, such as epicatechins, catechins, tannins, phenolic acids, anthocyanins, theobromine, and caffeine.Para determinar la efectividad de la luz ultravioleta sobre microorganismos como *Escherichia coli* y *Listeria innocua* inoculados a un nivel de 10^9 y 10^7 UFC/100g, respectivamente en la piña fresca cortada, las piezas fueron tratadas con luz ultravioleta durante 5 min a una distancia de 15 y 8 cm (dosis de 1.479 y 2.064 kJ/m2 para cada tratamiento).

Table 2. Concentration of EPC dilutions by UV-Visible spectrophotometry.

Absorbance (750 nm)	Concentrations
0.176	25 ppm
0.355	50 ppm
0.528	75 ppm
0.702	100 ppm

3.2 Determination of the antimicrobial effect of EPC at different concentrations on the growth of S. aureus and E. coli.

The analysis of variance showed significant differences ($p<0.05$) for treatments T1 (sterilized distilled water), T2 (25 mg/mL), and T5 (100 mg/mL) applied to *E. coli*. Table 3 shows the inhibition halos (mm) obtained with the different treatments used in vitro on *E. coli* and *S. aureus* bacteria. The concentrations of the treatments are 25 mg/mL (T2); 50 mg/mL (T3); 75 mg/mL (T4); 100 mg/mL (T5) and the control (T1). The results for *E. coli* in the case of T1 (control with sterilized distilled water), T2 (25 mg/mL), and T5 (100 mg/mL) showed significant differences ($p<0.05$) between each other, while T3 and T4 with concentrations of 50 mg/mL and 75 mg/mL, respectively, did not show significant differences between their values, yielding inhibition halos of 9.46 mm and 9.88 mm, respectively. Finally, in this case, T5 showed greater effectiveness compared to the other treatments, yielding inhibition halos with a mean of 14.84 mm (Figure 4). On the other hand, T2 showed lower effectiveness, registering an average inhibition halo value of 5.06 mm (Figure 3). This indicated that the inhibition zones increased in diameter over the *E. coli* population as the EPC concentration increased; therefore, the higher the EPC concentration, the greater the inhibition of the bacteria.

In the case of *S. aureus* (Table 3), statistical analysis showed significant differences ($p<0.05$) for the treatments. Inhibition zones began to form with T2 at a concentration of 25 mg/mL with an average diameter of 4.6 mm (Figure 5). Concentrations T3 and T4 showed values of 10.80 mm and 13.53 mm, respectively; however, at the highest concentration of 100 mg/mL (T5), an average diameter of 17.68 mm was obtained (Figure 6). The negative control with sterile distilled water (T1) did not show an inhibition zone. This means that EPC had an antibacterial effect against the growth of this bacterium. In turn, it can be seen that the higher the concentration of EPC, the greater the antibacterial effect, where a larger diameter of the inhibition zone was achieved. It should

be noted that *S. aureus* showed greater sensitivity to the polyphenolic compounds of EPC compared to *E. coli.*

Table 3. The zones of inhibition (mm) obtained with the different treatments used in vitro on *E. coli* and *S. aureus* bacteria (averages ± standard deviation).

	Treatments	*E. coli*	*S. aureus*
T_1	Sterilized distilled water	0,00 ^{d}	0,00 ^{e}
T_2	25 mg/mL	5,06±1,70 ^{c}	4,6±1,22 ^{d}
T_3	50 mg/mL	9,46±1,1 ^{b}	10,8±2,42 ^{c}
T_4	75 mg/mL	9,88±1,79 ^{b}	13,53±2,06 ^{b}
T_5	100 mg/mL	14,84±1,32 ^{a}	17,68±2,20 ^{a}

*Different letters indicate significant differences ($p<0.05$)

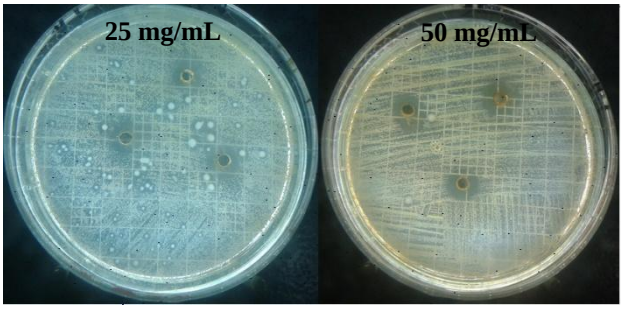

Figure 3. Zones of inhibition (measured in millimeters) of EPC at concentrations of 25 mg/mL and 50 mg/mL using the well diffusion method on *E. coli*.

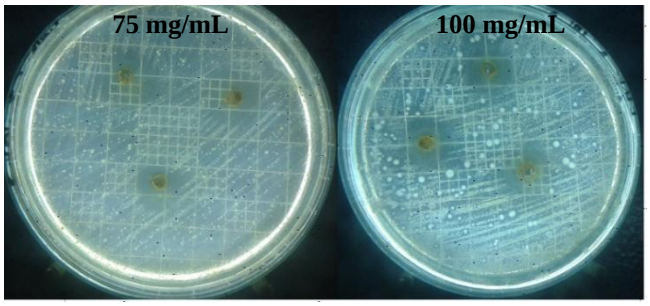

Figure 4. Zones of inhibition of EPC at concentrations of 75 mg/mL and 100 mg/mL using the well diffusion method on *E. coli.*

Larger inhibition halos were observed in *S. aureus* (Gram-positive) than in *E. coli* (Gram-negative) from T3 onwards, showing that *S. aureus* is more sensitive to EPC. This may be due to structural differences in the cell walls of the two bacteria. Gram-positive bacteria have a thick layer of peptidoglycan in their cell wall, while Gram-negative bacteria have a thin layer of peptidoglycan, but one that is much more complex because, in addition to the peptidoglycan layer, it also has an outer lipopolysaccharide membrane (Willey et al., 2023).

In this sense, the antimicrobial effect of EPC is due to the ability of phenolic compounds to penetrate the cell wall, especially in Gram-positive bacteria, because it has a simple structure consisting of an easily hydrolyzable monocomplex, whose cell wall is rigid, unselective, and lacking barrier properties, unlike the thin, multilaminar cell wall of Gram-negative bacteria, which confers a higher degree of resistance (especially due to the outer membrane component at the cell wall level) to antimicrobial agents (Gutierrez et al., 2024; Arlorio et al., 2005).

The antimicrobial capacity of cocoa pericarp extracts lies in a multifunctional chemical offensive led by polyphenols, especially epicatechin and condensed tannins. These compounds act by disrupting the cytoplasmic membrane, where their aromatic rings insert themselves into the lipid bilayer, altering its permeability and causing the loss of vital ions. Simultaneously, the hydroxyl groups of flavonoids exert a chelating effect, sequestering essential metals such as iron (Fe^{+3}) that bacteria require for their enzymatic processes and replication (Ali et al. 2022). In addition, the high affinity of these metabolites for proteins allows the formation of complexes that inactivate extracellular enzymes and transport proteins, collapsing the pathogen's energy metabolism. Together, this molecular attack not only stops cell division (bacteriostatic effect), but at high concentrations such as 100 ppm, it triggers definitive cell lysis, triggering a bactericidal effect.

The antibacterial properties of the ethanolic extract of *Theobroma cacao* L. are attributed to the polyphenols in its composition, including flavonoids, quinones, tannins, catechins, and saponins, which are believed to be responsible for its antibacterial activity. This is because flavonoids, having a variable number of phenolic hydroxyl groups in their chemical structure, easily penetrate the bacterial cell membrane, combine with and precipitate protoplasmic proteins, denaturing them and acting as protoplasmic poisons (Hemeg et al., 2020; Puupponen et al., 2001). Similarly, quinones have a wide range of action, possibly acting on adhesins exposed on the surface of bacteria, as well as on cell wall polypeptides and membrane-bound enzymes. These mechanisms reflect how different natural compounds act on the surface or essential metabolic functions of bacteria to eliminate them. Likewise, tannins can inhibit extracellular microbial enzymes, causing bacterial inactivation through cell adhesion to the surface of cells and enzymes bound to cell membranes and cell wall polypeptides, damaging the cell wall and causing the cell contents to

be emptied, leading to cell death (Arlorio et al., 2005; Akiyama et al., 2001). Catechins can damage the cytoplasmic membrane, causing leaks of important metabolites that inactivate the bacterial enzyme system (Ratnawulan et al., 2025; Volk and Wheeler, 1993). On the other hand, saponins are a group of glycosidic substances that dissolve in water and have the property of forming foam when the solution is shaken.

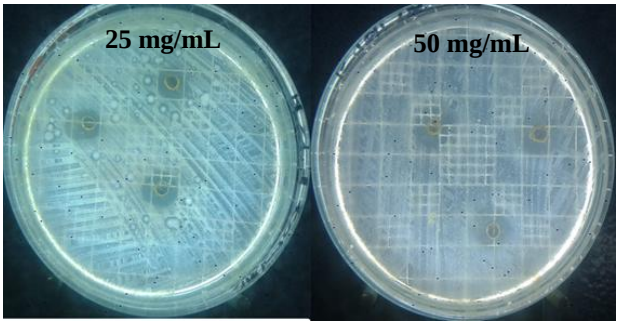

Figure 5. Zones of inhibition (measured in millimeters) of EPC at concentrations of 25 mg/mL and 50 mg/mL using the well diffusion method on *S. aureus*.

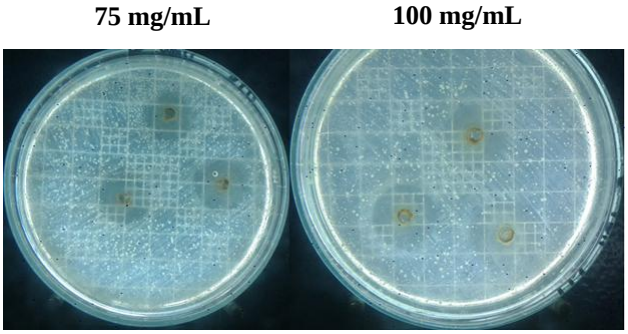

Figure 6. Zones of inhibition (measured in millimeters) of EPC at concentrations of 75 mg/mL and 100 mg/mL using the well diffusion method on *S. aureus*.

All of the above indicates that the compounds present in the extract, the type of microorganism, and the differences in the permeability of bacterial cell walls are the main factors causing microbial inhibition between the two bacteria, explaining why the inhibitory effect is greater in *S. aureus* populations than in *E. coli*.

The results obtained in this study were higher than those achieved by Ariza et al. (2013), who studied the in vitro antibacterial activity of ethanolic extract of cocoa (*Theobroma cacao* L.) against *Escherichia coli*, obtaining zones of inhibition of 1.9 mm with concentrations of 62.5 mg/mL of ethanolic extract of cocoa. For their part, Nsor-atindana et al. (2012) studied the quantification of the total polyphenolic content and antimicrobial activity of cocoa bean shells and reported inhibition halos of 10.98 mm for *S. aureus* at a concentration of 100 mg/mL of ethanolic extract of cocoa husk or pericarp (EPC).

Finally, it should be noted that the bacteriostatic and bactericidal activity of EPC is carried out in several modes of action, including alteration of bacterial cell metabolism, inhibition of cell wall synthesis, alteration of cell membrane permeability, and interference with gene and nucleic acid expression (Percival et al., 2006).

3.3 Comparison of the degree of inhibition obtained using the most effective concentration of EPC on the respective bacteria

Once the treatment with the T5 concentration (100 mg/mL) that caused the greatest inhibitory effect on both microorganisms was obtained, this section finally studied the comparison of the antibacterial effect on each microorganism. When comparing the degree of inhibition of the 100 mg/mL treatment on the *E. coli* and *S. aureus* populations, it was observed that this concentration of EPC is more effective on the latter pathogen, as it reached inhibition halos of 18 mm. The Student's t-test (Table 4) revealed significant differences ($p<0.05$) between the bacteria studied.

S. aureus is a Gram-positive bacterium whose cell wall structure is approximately 25-30 µm thick, single-layered, and consists mainly of peptidoglycan, with a low lipid content (1-4%). These groups of bacteria tend to be more susceptible to the activity of antibacterial components, such as phenolic compounds and penicillin. The simple cell wall structures cause antibacterial compounds to easily enter the cells and find the targets to function (Hemeg et al., 2020; Hawley, 2003). The antibacterial potential of EPC derives from the presence of antibacterial compounds such as tannins and flavonoids (Gutierrez et al., 2024; Volk and Wheeler, 1993). Flavonoids have antibacterial activity through the barrier function of bacterial DNA gyrase, affecting bacterial replication and translation capacity (Gunawan, 2009).

The results reported in this study are higher than those recorded by Sucuzhañay (2015), who studied the antimicrobial effect of aqueous extracts of cocoa shells and seeds (*Theobroma cacao* L.) on strains of *Streptococcus mutans* and reported inhibition halos of 8 to 10 mm using 12.5% and 20% aqueous extracts of cocoa shells on *Streptococcus mutans*. Similarly, Mariani et al. (2010) studied the bacteriostatic effect of cocoa seed extract on the growth of *Streptococcus mutans* in vitro. The authors recorded halos of 6 mm at cocoa concentrations of 0.01% and 8 mm at concentrations of 5%, 15%, and 17.5% against *S. mutans* in aqueous

cocoa seed extracts. Antimicrobial activity may vary depending on the type of microorganism and the content of phenolic compounds present in the extracts, such as polyphenols, flavonoids, epicatechin, and catechin (Percival et al., 2006), associating them with antimicrobial activity as they act specifically against the wall of Gram-positive bacteria, resulting in the loss of cell structure and cell death, altering their structural integrity through hydrophobic and electrostatic interactions with the phospholipid bilayer and porins. This causes membrane stiffening, permeabilization, ATPase inhibition, and efflux pump dysfunction, ultimately leading to cell lysis (Yan et al., 2024; Koech *et al*., 2014).

Table 4. Comparison of susceptibility levels between the bacteria studied (*E. coli* and *S. aureus*).

Microorganisms	Averages (mm)	P
E. coli	17,68	0,0045
	2,83	
S. aureus	14,84	
	1,02	

In the case of *E. coli*, being a Gram-negative bacterium, its resistance to EPC is probably due to the fact that it has a thinner cell wall structure than *S. aureus*. However, it is multilaminar, approximately 10-15 microns thick, with a component that no other group of bacteria currently has. This component is the outer membrane, which is additional to the usual peptidoglycan layer found in most bacteria. It is composed of unique structures called lipopolysaccharides (LPS) that function as endotoxins. It also has an exclusive transport system that is more complex than that found in all cytoplasmic membranes of living beings. This structure provides resistance to detergents, antibiotics (such as penicillin), and toxic agents, serving as a fundamental defensive barrier. The outer membrane consists of three layers: the outer membrane, a thin layer of peptidoglycan on the inside with a high lipid content (11-21%), and the inner membrane. The outer layer consists of two layers of lipopolysaccharide and lipoprotein (Yu et al., 2024; Hawley, 2003). It is possible that the bioactive compounds present in EPC at low concentrations cannot easily penetrate the outer membrane, resulting in less growth inhibition.

Rodríguez et al. (2009) and Alberto et al. (2006) reported in their studies that polyphenolic extracts inhibit Gram-positive bacteria more than Gram-negative bacteria due to the sensitivity of the former to spices and plant extracts. The authors concluded that the greater sensitivity in the case of *Staphylococcus aureus* can be attributed to the structure of its cell wall, which allows antibacterial substances to easily ccess and destroy it, resulting in the release of the cytoplasm.

On the other hand, Sotelo et al. (2010) studied Borojó (*Borojo apatinoi*), a source of polyphenols with antimicrobial activity, and indicated that Borojó extracts exhibited greater inhibition halos for *S. aureus* (Gram-positive) than for *E. coli* (Gram-negative), results that coincide with those obtained by Alberto et al. (2006). These researchers highlight a greater inhibition of extracts with polyphenols in Gram-positive bacteria than in Gram-negative bacteria, due to the sensitivity of Gram-positive bacteria to spices and extracts from herbs, plants, and fruits. Therefore, the greater sensitivity to the antimicrobial effect can be attributed, in the case of *S. aureus*, to the structure of its cell wall (as mentioned above), which allows antibacterial substances to easily destroy the cell membrane, causing the cytoplasm to leak out (Kuwano et al., 2005). The resistance of *E. coli* to antibacterial substances is related to the hydrophilic surface of its outer membrane. This membrane, rich in lipopolysaccharide molecules, acts as a barrier against the penetration of numerous antibiotic molecules and is also associated with enzymes in the periplasmic space, which are capable of breaking down molecules introduced from outside (Yu et al., 2024).

Artiza et al. (2013) reported that ethanol extracts of cocoa (EEC) applied to *E. coli* after a 24-hour exposure period caused cell elongation in the bacteria. At the lowest concentration of 7.8 mg/mL, *E. coli* elongated to 4.286 µm. Cell extension showed cell elongation of 6.859 µm at 15.6 mg/mL, and elongation led to broken cells, indicating permanent disruption and failure to maintain filamentation. This study confirmed that polyphenol causes elongation of *E. coli* cells, as found by Hemaiswarya et al. (2011) and Cui et al. (2012). In turn, they proposed that polyphenols in EEC suppressed the polymerization of ftsZ proteins in the bacterial cytoskeleton, a key role of the protein in septum formation. Inhibition of ftsZ protein activity slows cell division, thereby preventing the bacteria from reproducing by binary fission, and the cell dies.

In general, the response of each microorganism to different concentrations of the extract may be influenced by structural differences between Gram-negative and Gram-positive bacteria, specifically differences in cell wall composition associated with resistance patterns, as well as being affected by variations in the concentrations of phytochemical compounds present in the cocoa pericarp (Gunawan, 2009).

4 Conclusions

Cocoa pericarp, traditionally considered a waste by-product

of the cocoa industry, acted through different mechanisms depending on the structure of the bacterial wall. This study verified the inhibitory differences when faced with *E. coli* and *S. aureus*. T5 (100 mg/mL) showed the greatest antibacterial potential against *S. aureus*, resulting in average inhibition halos of 17.68 mm. This could be attributed mainly to the structural characteristics of the cell wall of this bacterium. The inhibition halos increased in diameter over the population of both bacteria as the concentration of the EPC extract increased.

The satisfactory results obtained in both bacteria confirmed that the extract has a broad-spectrum antimicrobial profile. Its integration as a natural preservative in the food industry can be justified by its multimodal preservation mechanism. Unlike synthetic preservatives, which often have a single target, the bioactive compounds in cocoa can act synergistically. Not only can they inhibit bacterial proliferation by rupturing membranes, but they can also act as powerful antioxidants. This allows for a dual function of microbiological safety and sensory stability. Overcoming the barrier of Gram-negative bacteria is particularly relevant. This expands its use to meat, dairy, and fresh vegetable products, where these pathogens are prevalent. The use of this extract transforms agro-industrial waste into a high-value functional ingredient. As a by-product of the chocolate industry, it is inexpensive to obtain and widely available, meeting circular economy standards. In addition, its natural origin responds to current consumer demand for products free of chemical additives (such as nitrites or sorbates).

5 References

Akiyama, H., Fuj, K., Yamasaki, O., Oono, T., Iwatsuki, K. (2001). Antibacterial action of several tannins against *Staphylococcus aureus*. Journal of Antimicrobial Chemotherapy, 48(2), 487-491. https://pubmed.ncbi.nlm.nih.gov/11581226/

Alberto, M., Rinsdahl, M., Manca, M. (2006). Antimicrobial effect of polyphenols from apple skins on human bacterial pathogens. Electronic Journal of Biotechnology, 9(3), 1-5. https://www.scielo.cl/scielo.php?script=sci_arttext&pid=S0717-34582006000300006

Alemawor, F., Dzogbefia, V., Eok, O., Oldham, J. (2009). Effect of *Pleurotus ostreatus* fermentation on cocoa pod husk composition: Influence of fermentation period and Mn^{2+} supplementation on the fermentation process. African Journal of Biotechnology, 8(9), 1950-1958.

Ali, A., Parisi, A., Normanno, G. (2022). Polyphenols as emerging antimicrobial agents. In Emerging modalities in mitigation of antimicrobial resistance. Cham: Springer International Publishing. https://www.ajol.info/index.php/ajb/article/view/60454

AOAC. 1990. Official methods of analysis of the AOAC, 15TH ed. Association of official analytical chemists. Arlington, VA, USA.

Ariza B, Mufida D, Fatima N, Hendrayati T, Wahyudi T, Misnawi H. (2013). In vitro antibacterial activity of cocoa ethanolic extract against *Escherichia coli*. Food Research International Journal, 21(3), 935-940. https://www.researchgate.net/publication/267033415_In_vitro_antibacterial_activity_of_cocoa_ethanolic_extract_against_Escherichia_coli

Arlorio, M., Coisson, J., Travaglia, F., Varsaldi, F., Miglio, G., Lombardi, G. (2005). Antioxidant and biological activity of phenolic pigments from Theobroma cacao hulls extracted with supercritical CO_2. Food Research International. 38(8), 1009-1014.Food Research International, 38(8), 1009-1014. https://www.researchgate.net/publication/222687611_Antioxidant_and_biological_activity_of_phenolic_pigments_from_Theobroma_cacao_hulls_extracted_with_supercritical_CO2

Ayeni, L. (2010). Effect of Combined Cocoa Pod Ash and NPK Fertilizer on Soil Properties, Nutrient Uptake and Yield of Maize (*Zea mays*). Journal of American Science, 6, 79-84. https://www.jofamericanscience.org/journals/amsci/am0603/11_2069_Ayeni_am0603_79_84.pdf

Balouiri, M., Sadiki, M., Ibnsouda, K., (2016). Methods for *in vitro* evaluating antimicrobial activity: A review. Journal of Pharmaceutical Analysis, 6(2), 71-79. https://www.sciencedirect.com/science/article/pii/S2095177915300150

Barazarte, H., Sangronis, E., Unai, E. (2008). Cocoa shell (*Theobroma cacao* L.): a possible commercial source of pectins. Latin American Nutrition Archives (ALAN), 58(1), 12-14. https://www.alanrevista.org/ediciones/2008/1/art-9/

Beckett, S. (2008). *The science of chocolate*. 2nd ed. Cambridge Yorkshire, Inglaterra: The Royal Society of chemistry.

Borraz, O. (2006). Epidemiology of methicillin resistance in *Staphylococcus aureus* strains isolated in Spanish Hospitals. University of Barcelona. Barcelona Faculty of Medicine. Barcelona, España.

Crozier, J., Preston G, Hurst J, Payne M, Mann J, Hainly L, Miller D. 2011. Cacao seeds are a "Super Fruit": A comparative analysis of various fruit powders and products. Chemistry Central Journal, 5(1), 5.

Cuellar, O., Guerrero G., (2012). Antibacterial activity of cocoa shell, *Theobroma cacao* L. Journal MVZ Córdoba,17(3): 123-129. http://www.scielo.org.co/scielo.php?pid=S0122-02682012000300012&script=sci_abstract&tlng=es

Cui, Y., Kim, S., Kim, H., Yeom, J., Ko, K., Park, W., Park,

S. (2012). AFM Probing the mechanism of synergistic effects of the green tea polyphenol (−)-epigallocatechin-3-gallate (EGCG) with cefotaxime against Extended-Spectrum BetaLactamase (ESBL)-producing *Escherichia coli*. Pub. Lib. of Science, 7(11), 1-6. https://journals.plos.org/plosone/article/file?id=10.1371/journal.pone.0048880&type=printable

Díaz, L. (2009). Molecular interactions between plants and microorganisms: saponins as chemical defenses of plants and their tolerance to microorganisms. Journal of Transdisciplinary Studies, 1(2), 32-55. https://www.redalyc.org/pdf/1792/179214945004.pdf

Dillinger, T., Barriga, P., Escárcega, S., Jimenez, J., Salazar, L., Grivettiet, L. (2000). Food of the gods: cure for humanity? A cultural history of the medicinal and ritual use of chocolate. The Journal of Nutrition, 130(8), 2057-2058. https://pubmed.ncbi.nlm.nih.gov/10917925/

Di Rienzo, J., Casanovas, F., Balrarini, M., Gonzales, L., Tablada, M., Robledo, C. (2017). InfoStaf versión 2016. Grupo InfoS.taf.

Edberg, S., Rice, E., Karlin, R., Allen, M. (2000). *Escherichia coli*: the best biological drinking water indicator for public health protection. Symposium Series Society for Applied Microbiology, 29, 106-116. https://pubmed.ncbi.nlm.nih.gov/10880185/

El Sayed, H., Magdy, S., Hanan, R., Nahed, M., Maha, A., Nisreen, K., Maha, A., Haitham, S., Mamduth D., Ehab E., (2022). Antimicrobial Activity of Some Plant Extracts and Their Applications in Homemade Tomato Paste and Pasteurized Cow Milk as Natural Preservatives Fermentation, 8(9), 428-437 https://doi.org/10.3390/fermentation8090428

Goudsmit, A., Markowicz, S., Eddine, S., Cherifi, S., (2021). Food poisoning due to a TSST1-producing *Staphylococcus aureus*. ID Cases, 26: e01272. https://doi.org/10.1016/j.idcr.2021.e01272

Guerrero, R., Risco, G., Cevallos, O., Villamar, R., y Peñaherrera, S. (2021). Plant extracts: an alternative for disease control in cocoa cultivation (*Theobroma cacao*). Engineering and Innovation, *8*(1). 110-116. https://doi.org/10.21897/23460466.2326

Gutierrez, E. (2024). Determination of the antagonistic effect of the ethanolic extract of the "cocoa" shell *Theobroma cacao* Linnaeus against pathogenic microorganisms. Undergraduate Thesis. Lima, Peru. Ricardo Palma University. https://repositorio.urp.edu.pe/entities/publication/3905af99-00a8-4187-a01f-aa722aac1354

Hawley, L. (2003). Intisari Mikrobiologi dan Penyakit Infeksi. Alih Bahasa: Brahm U. Pendit. Jakarta, Hipokrates.

Hemaiswarya, S., Soudaminikkutty, R., Doble, M. (2011). Phenylpropanoids inhibit protofilament formation of *Echerichia coli* cell division protein Ftsz. Journal of Medical Microbiology, 60, 1317-1352. https://pubmed.ncbi.nlm.nih.gov/21474608/

Hemeg, H., Moussa, I., Ibrahim S., Dawoud, T., Alhaji J., Mubarak A., Kabli S., Alsubki R., Tawfik, A., Marouf S., (2020). Antimicrobial effect of different herbaceous plant extracts against different microbial populations. Saudi Journal of Biological Sciences. 27(12), 3221-3227. https://pubmed.ncbi.nlm.nih.gov/33304127/

Iglesias Guevara, D., Morejón Ramos, B., Ruiz Karell, B., Pérez Santana, D. (2022). Optimization of the process of obtaining an aqueous extract of cocoa husk. CENIC Journal Chemical Sciences, 53(1), 60-71. https://www.redalyc.org/journal/1816/181671261004/

Kalvatchev, Z., Garzaro, D., Guerra, C. (1998). *Theobroma cacao* L.: A new approach to nutrition and health. Journal Agroalimentaria, 6, 23-25. https://www.researchgate.net/publication/44813334_Theobroma_cacao_L_Un_nuevo_enfoque_para_nutricion_y_salud

Khan, J, Gill R., Husain, F., Gahtori, B., Ahmad, I., Neyaz, L., Bazaid, F., Albarakaty, F., Elbanna, K., Tolesa, L., Abulreesh, H., (2025). Plant-Derived Antimicrobials against Foodborne Pathogenic Bacteria. Microbioloy and Biotechnology Letters, 53(1), 1-21. https://doi.org/10.48022/mbl.2408.08006

Koech, R., Wachira, N., Ngure, R., Orina, I., Wanyoko, J., Bii, C., Karori, S. (2014). Antifungal activity of crude tea extracts. African Journal of Agricultural Research, 8(19), 2087-2089. https://www.researchgate.net/publication/293104114_Antifungal_activity_of_crude_tea_extracts

Kumar, A., Das, S., Ali, S., Ganesh, S., Rabbani, A., Ehsanur, S., Chelliah, R., Deog-Hwan O., Liu, S., Wei, S. (2025). Mechanisms, applications and challenges of natural antimicrobials in food system. Food Bioscience, 74,107864. https://doi.org/10.1016/j.fbio.2025.107864

Kuwano, K., Tanxaka, N., Shimizu, T., Nagatoshi, K., Nou, S., Sonomoto, K. (2005). Dual antibacterial mechanisms of nisin Z against Gram-positive and Gram-negative bacteria. International Journal of Antimicroboial Agents, 26(5), 396-402. https://pubmed.ncbi.nlm.nih.gov/16226432/

Leiva, Y., Salvador-Tasayco, E., Yoplac, I., Zamora-Huamán, S., (2022). Effect of feeding with cocoa bean byproducts (*Theobroma cacao* L.) on the productive parameters and meat quality of improved Creole chickens. Livestock Research for Rural Development, 34 (10), 113-119. https://www.lrrd.org/lrrd34/10/3493yoan.html

Llerena, W., Samaniego, I., Vallejo, C., Arreaga, A., Zhunio, B., Coronel, Z., Quiroz, J., Angós, I., Carrillo, W., (2023). Profile of Bioactive Components of Cocoa (*Theobroma cacao* L.) By-Products from Ecuador and Evaluation of Their Antioxidant Activity. Foods, 12(13), 2583. https://doi.org/10.3390/foods12132583

López, L., Castaño, H., Mejía, C. (2013). Antimicrobial effect of Salvia officinalis L. essential oil on foodborne pathogenic microorganisms. Biological News, 35(98), 77-83. https://www.researchgate.net/publication/366844264_Efecto_antimicrobiano_del_aceite_esencia_de_Salvia_officinalis_L_sobre_microorganismos_patogenos_transmitidos_por_alimentos

Ludy, C., Pabón, B., Vanegas, J., Rendón, F., Santos, A, Hernández, R. (2013). Antioxidant and antibacterial activity of leaf extracts from four agroforestry species from the Colombian Orinoco. Cuban Journal of Medicinal Plants, 18(1), 57-70. http://scielo.sld.cu/scielo.php?script=sci_arttext&pid=S1028-47962013000100008

Magaldi, S., Mata-Essayag, S., Capriles, H., Perez, C., Colella, M., OLaizola, C., Ontiveros, Y. (2004). Well diffusion for antifungal susceptibility testing. International Journal of Infectious Diseases, 8, 39-45. https://pubmed.ncbi.nlm.nih.gov/14690779/

Mariani, M., Jaimes, G., Fernández-Da Silva, R. (2010). Bacteriostatic effect of cocoa seed extract (*Theobroma cacao* L.) on the growth of *Streptococcus mutans* in vitro. ODOUS Scientific, 11(1), 15-22. https://servicio.bc.uc.edu.ve/odontologia/revista/vol11-n1/art2.pdf

Monroy, R., Montaño, F., Salinas, N., Velásquez, I., Velásquez, J., Velazco, E., Pereira, J. (2023). Characterization and spectroscopic quantification of flavonoids and catechins from Venezuelan cocoa to be considered in cosmetic formulations. Journal of the University of Zulia, 14(40), 185-204. https://www.researchgate.net/publication/362152219_Evaluation_of_flavonoids_and_catechins_of_Venezuelan_cocoa_spectroscopic_characterization_and_quantification

Nsor-Atindana, J., Zhong, F., Kebitsamang, J., Mohamed, L., Camel, L. (2012). Quantification of Total Polyphenolic Content and Antimicrobial Activity of Cocoa *(Theobroma cacao L.)* Bean Shells. Pakistan Journal of Nuttrition, 11(7), 574-579. https://www.researchgate.net/publication/268203327_Quantification_of_Total_Polyphenolic_Content_and_Antimicrobial_Activity_of_Cocoa_Theobroma_cacao_L_Bean_Shells

Ordoñez, Elizabeth S, Leon-Arevalo, Aurelia, Rivera-Rojas, Humberto, & Vargas, Evil (2019). Quantification of total polyphenols and antioxidant capacity in cocoa shell and seed (Theobroma cacao L.), prickly pear (*Opuntia ficus indica* Mill), grape (*Vitis vinifera*) and uvilla (*Pourouma cecropiifolia*). Agricultural Scientia, 10(2), 175-183. https://doi.org/10.17268/sci.agropecu.2019.02.02

Ortiz, K., Villagran, R., Latorre, H., Borja, R., Villa, C., (2023). A commercial source of pectin from cocoa shells. Reciena, 3 (2), 45-52. https://reciena.espoch.edu.ec/index.php/reciena/index

Orwa, C., Mutua, A., Kindt, R., Jamnadass, R., Anthony, S. (2009). Agroforestree Database: a tree reference and selection guide version 4.0. World Agroforestry Centre, Kenya.

Perdomo, I., Meléndez, P. (2004). Determination and isolation of enterotoxigenic *Staphylococcus aureus* and *Clostridium perfringens* from foods. Agricultural and Food Sciences, 33(1), 59-69. https://www.semanticscholar.org/paper/Determinaci%C3%B3n-y-aislamiento-de-Staphylococcus-y-a-Perdomo-Mel%C3%A9ndez/225e5ab98e15161d0bac43918b5b84b439710b3d

Percival, R., Devine, D., Duggal, M., Chartron, S., Marsh, P. (2006). The effect of cocoa polyphenols on the growth, metabolism, and biofilm formation by *Streptococcus mutans* and *Streptococcus sanguinis*. European Journal of Oral Sciences, 2, 10-15. https://pubmed.ncbi.nlm.nih.gov/16911106/

Puupponen, P., Nohynek, L., Meier, C., Kähkönen, M., Heinonen, M., Hopia, A., Oksman, M. (2001). Antimicrobial properties of phenolic compounds from berries. Journal of Applied Microbiology, 90(4), 494-507. https://pubmed.ncbi.nlm.nih.gov/11309059/

Ratnawulan, S., Muhtar, N., Fitri, S., Sriwidodo, S., Hendrawan, R., (2025). Catechins as Antimicrobial Agents and Their Contribution to Cosmetics. Cosmetics, 12(1),11 https://doi.org/10.3390/cosmetics12010011

Ramos-Villarroel, A., Aron, M., Martin-Belloso, O., (2012). Influence of inactivation and quality spectral distribution on bacterial changes in fresh cut watermelon treated with intense light pulses. Postharvest Biology and Technology, 69, 32-39. https://www.sciencedirect.com/science/article/abs/pii/S0925521412000518

Rodríguez, S., Nereyda, E. (2011). Use of Natural Antimicrobial Agents in the Preservation of Fruits and Vegetables. Ra Ximhai Journal, 7(1): 153-170. https://www.redalyc.org/pdf/461/46116742014.pdf

Rodríguez, M., Tomassini, L., Manca, M., Strasser, A. (2009). Antioxidant capacity and antibacterial activity of phenolic compounds from Argentinean herbs infusions. Food Control, 21(5), 779-85.

https://www.researchgate.net/publication/222368109_Antioxidant_capacity_and_antibacterial_activity_of_phenolic_compounds_from_argentinean_herbs_infusions

Rojo-Poveda, O., Barbosa-Pereira, L., Zeppa, G., Stévigny, C. (2020). Cocoa bean shell: a by-product with nutritional properties and biofunctional potential. Nutrients, 12 (4), 1123. https://doi.org/10.3390/nu12041123

Romeu, A., Salazar, J., Lugo, M., Rojas, H., Eslava, C. (2012). Antimicrobial susceptibility of *Escherichia coli* isolates from freshwater ecosystems. Cuban Journal of Tropical Medicine, 64(2), 7. http://scielo.sld.cu/scielo.php?script=sci_arttext&pid=S0375-07602012000200003

Solis, P. (2011). Evaluation of the antimicrobial activity of the essential oils of oregano (*Origanum vulgare* L.) and thyme (*Thymus vulgaris* L.) as potential biopreservatives in chicken meat. Riobamba, Ecuador. Chimborazo Polytechnic Higher School. Faculty of Sciences. Degree Thesis. Chimborazo, Ecuador.

Sotelo, D., Casas F., Camelo M. (2010). Borojó (*Borojoa patinoi*): source of polyphenols with antimicrobial activity. Vitae. Journal of the Faculty of Chemistry, 17(3), 329-336. https://www.redalyc.org/pdf/1698/169815641011.pdf

Soto Hernández, RM., Palma Tenango, M., San Miguel Chavez, R. (2019). Experimental phytochemistry. 1st edition. Postgraduate College Editorial, City of Mexico. Mexico.

Sucuzhañay, M. (2015). Efecto Antimicrobial Effect of Aqueous Extracts of Cocoa Shell and Seeds (*Theobroma cacao* L.) on *Streptococcus mutans* strain, in vitro study. Quito, Ecuador. Central University of Ecuador. Faculty of Dentistry. Research Unit. Degree thesis. Ecuador.

Willey, J., Sandman, K., Wood, D. (2023). *Prescott Microbiology*. 12ª edition Nueva York: McGraw-Hill. https://lib-cat.iitd.ac.in/bib/244220#:~:text=TextPublication%20details:%20New%20York,9781265123031

Volk, W., y Wheeler, M. (1993). Mikrobiologi Dasar. Alih Bahasa. Markham. Penerbit PT Gelora Aksara Pratama, Jakarta.

Yu, Y., Xuexue, X., Aiman, F., Li, Z., Ganjun, Y., Fengxian, L., Yu, W. (2024). Antibacterial Activity and Mechanisms of Plant Flavonoids against Gram-Negative Bacteria Based on the Antibacterial Statistical Model. Pharmaceuticals, 17 (3), 292. https://www.mdpi.com/1424-8247/17/3/292

Welinder-Olsson, C., Kaijser, B. (2005). Enterohemorrhagic *Escherichia coli* (EHEC). Scandinavian Journal. of Infectious Diseases, 37(6-7): 405-16. https://pubmed.ncbi.nlm.nih.gov/16011999/

Wulandari, P., Suswati, E., Misnawi, M., Rinu, A. (2012). Antibacterial Effect of Ethanol Extract Cocoa Beans (*Theobroma cacao* L.) on growth *in vitro* by *Shigella dysentriae*. Jurnal5Medika Planta, 1(5), 3-9. https://www.neliti.com/publications/245650/antibacterial-effect-of-ethanol-extract-cocoa-beans-theobroma-cacao-on-growth-in

Received: *January 18, 2026*

Accepted: *March 10, 2026*

María Ocanto, *Graduate in Food Technology from the Universidad de Oriente, monagas nucleus, Maturín Venezuela. Email: mocanto3@gmail.com*
https://orcid.org/0009-0008-1333-3441

Guillermo Centeno, *Doctor in Technological Chemistry from the University of Carabobo, Valencia, Venezuela. Researcher at the Center for Oceanology and Antarctic Studies. Venezuelan Institute of Scientific Research. Email: gcenteno1@uc.edu.ve*
https://orcid.org/0000-0003-1436-4764

Ana Ramos*, PhD in Agricultural and Food Sciences and Technology from the University of Lleida, Lleida, Spain. Researcher at the Center for Oceanology and Antarctic Studies. Venezuelan Institute of Scientific Research. Retired professor from the Universidad de Oriente, Monagas nucleus, Maturín, Venezuela.*
https://orcid.org/0000-0003-4587-7327

Artículo de Investigación. Revista Ciencia e Ingeniería. Vol. 47, No. 2 pp. 129-142, abril-julio, 2026.
ISSN 1316-7081. ISSN Elect. 2244-8780 Universidad de los Andes (ULA)

Gestión eficiente y sostenible en la industria: Manual de evaluación de sistemas de mantenimiento

Efficient and sustainable management in industry: A Framework for assessing maintenance systems

Márquez, Vanessa [1]; Salas, Pedro[1,2*]; León, Francisco[1]
[1]Universidad de Los Andes, Mérida, Venezuela.
[2]Universidad Internacional de Valencia, VIU, España.
* pedrosalas@ula.ve

Abstract

In today's industrial landscape, competitiveness and operational efficiency rely heavily on robust production systems, where maintenance plays a critical role in ensuring asset reliability and safety. Despite its importance, the literature reveals a lack of standardized guidelines for assessing the effectiveness of these systems. In Venezuela and other Latin American countries, the COVENIN 2500-93 standard has long served as a key reference, yet its outdated framework limits its relevance considering modern technologies and management practices. This study addresses that gap by developing an evaluation manual aligned with current international standards. The methodology combined a comprehensive review of COVENIN 2500-93 and its application in academic and industrial context, with expert surveys to identify outdated procedures and gaps related to global benchmarks. Findings underscore the urgent need to update the standard, particularly in areas such as technology integration, sustainability, energy efficiency, asset management, occupational safety, and documentation process. The proposed manual incorporates the Deming Cycle (PDCA) and an organizational maturity model, structured around twelve key areas. Its implementation enhances maintenance practices, reduces operational costs, and strengthens business competitiveness through a more proactive, efficient, and sustainable approach.

Keywords: Asset management, maintenance system, Industry 4.0, organizational maturity, Deming cycle (PDCA), maintenance sustainability, energy efficiency, occupational safety, evaluation manual.

Resumen

En el contexto industrial actual, la competitividad y la eficiencia operativa dependen de sistemas productivos sólidos, donde el mantenimiento industrial desempeña un rol esencial para garantizar el rendimiento seguro y eficiente de activos. No obstante, la revisión del estado del arte evidencia una carencia de manuales estandarizados para evaluar la eficacia de estos sistemas. En Venezuela y otros países latinoamericanos, la norma COVENIN 2500-93 ha sido una referencia clave, pero su desactualización limita su aplicabilidad frente a los avances tecnológicos y metodologías contemporáneas. Este artículo propone un manual de evaluación de sistemas de mantenimiento alineado con estándares internacionales, basado en una revisión exhaustiva de la norma COVENIN 2500-93 y su aplicación en proyectos académicos e industriales, complementada con encuestas a expertos del sector. Los resultados destacan la necesidad urgente de actualizar la norma incorporando enfoques tecnológicos, sostenibilidad, eficiencia energética, gestión integral de activos, seguridad laboral y modernización documental. El manual propuesto integra el ciclo Deming (PHVA) y un modelo de madurez organizacional, estructurado en doce áreas clave. Su adopción permite optimizar procesos, reducir costos y mejorar la competitividad empresarial mediante una gestión de mantenimiento más proactiva, eficiente y sostenible.

Palabra clave: Gestión de activos, sistema de mantenimiento, Industria 4.0, madurez organizacional, ciclo Deming (PHVA), sostenibilidad del mantenimiento, eficiencia energética, seguridad laboral, manual de evaluación.

1 Introducción

La competitividad y eficiencia operativa en el sector industrial contemporáneo dependen, en gran medida, de la solidez de los sistemas productivos y de una gestión de mantenimiento eficaz, la cual es esencial para garantizar el rendimiento óptimo y la continuidad operativa de los activos. No obstante, la acelerada evolución tecnológica y las crecientes exigencias del entorno industrial han dejado obsoletos muchas de las estructuras de evaluación actualmente vigentes. En la era de la Industria 4.0, que impulsa la digitalización avanzada y el uso de datos, así como la adopción de tecnologías emergentes, las normativas de mantenimiento requieren una profunda actualización. La norma venezolana COVENIN 2500-93, aunque ha constituido una referencia fundamental desde su publicación en 1993 para la evaluación de sistemas de mantenimiento en Venezuela y otros países de América Latina, presenta limitaciones significativas frente a los avances tecnológicos y a las metodologías de gestión modernas.

La revisión del estado del arte evidencia una carencia de manuales estandarizados y actualizados que permitan evaluar de manera efectiva la eficiencia de los sistemas de mantenimiento industrial, una situación reconocida por la literatura especializada (Parida et al., 2015). Este vacío resalta la necesidad de integrar aspectos cruciales como la gestión de activos (alineada con estándares como la norma ISO 55000), la sostenibilidad y eficiencia energética (promovidos por la norma ISO 14000), la seguridad y salud ocupacional (según la norma ISO 45001), y la modernización de los procedimientos documentales. La naturaleza generalista de muchas normas internacionales y la protección intelectual de metodologías internas (desarrolladas por empresas consultoras) han contribuido a esta falta de herramientas prácticas. Por ello, se hace necesario el desarrollo de una herramienta práctica, moderna y contextualizada que permita a las organizaciones diagnosticar y optimizar sus sistemas de mantenimiento.

Este artículo responde a dicha necesidad mediante la presentación del proceso de desarrollo de un manual de evaluación de sistemas de mantenimiento, concebido bajo un enfoque actualizado y alineado con los estándares internacionales vigentes. La metodología de investigación se fundamenta en una exhaustiva revisión documental de la norma COVENIN 2500-93 y su aplicación en diversos proyectos académicos e industriales, complementada con encuestas dirigidas a expertos del sector. Este enfoque permitió la identificación y el análisis de los factores y procedimientos de la norma COVENIN 2500-93 que requieren actualización o presentan vacíos frente a las mejores prácticas internacionales.

Como resultado, se propone un manual que incorpora principios fundamentales como el ciclo Deming (PHVA) y un modelo de madurez organizacional, ofreciendo una estructura integral para la evaluación de doce áreas clave. Estas áreas abarcan desde la gestión organizacional y estratégica hasta dimensiones contemporáneas esenciales para la Industria 4.0, como la sostenibilidad, la eficiencia energética la seguridad y salud ocupacional, y los sistemas de información. La adopción de este manual no solo permite optimizar los procesos de mantenimiento y reducir los costos operativos, sino que también fortalece la competitividad empresarial al alinearse con estándares internacionales, promoviendo una gestión más proactiva, eficiente y sostenible.

Debido a su extensión, el contenido de este manual se presenta como un documento separado a este artículo. Para su acceso, se indica un enlace electrónico proporcionado en el apartado *5.1 Estructura del manual*.

2 Marco Teórico

El presente marco teórico sienta las bases conceptuales y normativas esenciales para comprender la evolución y las exigencias actuales de la gestión del mantenimiento industrial. En un entorno impulsado por la Industria 4.0 y la creciente demanda de eficiencia y sostenibilidad, es imperativo que las prácticas de mantenimiento se adapten a los avances tecnológicos y a los estándares internacionales más recientes. Esta sección aborda definiciones clave, los tipos de mantenimiento más relevantes, el papel de las normas internacionales y las metodologías que sustentan la propuesta de un manual de evaluación actualizado.

2.1 La industria 4.0 y el mantenimiento

La industria 4.0 representa una transformación fundamental en la manufactura y la gestión operativa, caracterizadas por la digitalización avanzada, la interconectividad y el uso intensivo de datos. Esta nueva era integra tecnologías emergentes para crear entornos productivos inteligentes y autónomos (IBM, s.f.). En el contexto del mantenimiento, la Industria 4.0 habilita una transición de enfoques reactivos o preventivos basados en tiempo, hacia modelos predictivos y prescriptivos (ESingeniería, s.f.). Esto implica el monitoreo constante de la condición de los activos en tiempo real, el análisis avanzado de grandes volúmenes de datos (Big Data) para anticipar fallas y optimizar las intervenciones, y la toma de decisiones informadas para maximizar la vida útil y la eficiencia de los equipos. La adopción de estas tecnologías es crucial para que las empresas logren una gestión de mantenimiento más proactiva, eficiente y sostenible (Indestan, s.f.).

2.2 La industria 4.0 y el mantenimiento

Un sistema de mantenimiento es un conjunto de procesos, procedimientos y recursos, organizados y estructurados, que se implementan para gestionar el mantenimiento de los activos físicos de una organización. Para Mora (2010), un sistema de mantenimiento eficiente requiere de dos aspectos básicos que definen la función de mantenimiento en la in-

dustria: la gestión (manejo de recursos) y la operación (realización física del servicio).

Estos sistemas son cada vez más digitalizados y basados en datos, integrando tecnologías para una mayor eficiencia y proactividad

2.3 Gestión de mantenimiento

La gestión de mantenimiento es un conjunto de actividades planificadas y sistemáticas destinadas a asegurar el buen funcionamiento de los activos físicos de una empresa, como maquinaria, equipos, instalaciones y edificios. Según la norma UNE-EN 13306:2018 (Asociación Española de Normalización y Certificación, 2018a), estas actividades incluyen la determinación de requisitos, objetivos, estrategias y responsabilidades del mantenimiento. Su implementación se realiza a través de la planificación, organización, dirección y control, garantizando que los activos físicos se mantengan en condiciones óptimas de funcionamiento al menor costo económico posible.

En el contexto actual, la gestión de mantenimiento se percibe como una inversión estratégica para la confiabilidad y la eficiencia de los activos, buscando no solo el buen funcionamiento, sino también la creación de valor a lo largo de todo su ciclo de vida.

2.4 Tipos de mantenimiento

La norma UNE-EN 13306:2018 (Asociación Española de Normalización y Certificación, 2018a) establece varios tipos de mantenimiento, entre los cuales se destacan la definición de los siguientes para el desarrollo de esta investigación:

- Mantenimiento Preventivo: es un conjunto de actividades programadas que se realizan para evaluar y/o mitigar la degradación, reduciendo la probabilidad de falla de un elemento. Estas actividades incluyen inspecciones regulares, ajustes, limpieza, lubricación, calibración y reemplazo de piezas desgastadas. Aunque el mantenimiento preventivo es esencial para la industria, su enfoque programado puede no siempre optimizar los tiempos de intervención o el estado real del activo, lo que ha llevado al desarrollo de enfoques avanzados como el mantenimiento predictivo y el mantenimiento basado en condición de los activos.
- Mantenimiento Predictivo: consiste en un conjunto de actividades relacionadas con el mantenimiento basado en condición, pero siguiendo una predicción obtenida del análisis repetido o de características conocidas y de la evaluación de los parámetros significativos de la degradación del elemento. Se basa en el monitoreo continuo del estado de los equipos mediante técnicas de diagnóstico y pronóstico como el análisis de vibraciones, termografía, análisis de aceite, entre otras. Estas técnicas permiten analizar datos para predecir fallas antes de que ocurran y realizar intervenciones en el momento óptimo, asegurando el funcionamiento eficiente y prolongando la vida útil de los equipos.
- Mantenimiento Basado en Condición (CBM): consiste en un conjunto de actividades que se realizan en función del estado de un elemento, determinado a partir de datos de monitoreo en tiempo real. A diferencia del mantenimiento predictivo, que busca pronosticar una falla, el CBM se centra en evaluar la condición actual para programar intervenciones solo cuando es necesario, optimizando el uso de recursos y extendiendo la vida útil de los activos. Este enfoque es fundamental en la Industria 4.0, ya que se apoya en el uso de sensores IoT y análisis de datos para una toma de decisiones más precisa.
- Mantenimiento Correctivo: es el conjunto de acciones que se realizan después del reconocimiento de una avería, con el objetivo de restaurar un elemento a un estado en que pueda cumplir con una función requerida. Estas acciones pueden no realizarse de inmediato, sino que puedan retrasarse según reglas establecidas (mantenimiento correctivo diferido) o llevarse a cabo sin demora tras la detección de la avería para evitar consecuencias inaceptables (mantenimiento correctivo inmediato). La norma UNE acota que el mantenimiento correctivo diferido puede planificarse y ejecutarse de manera programada.

2.5 Normas Internacionales (ISO) aplicadas al mantenimiento industrial

Las normas internacionales relacionadas con el mantenimiento industrial proporcionan un marco de referencia para la gestión de activos, calidad y medio ambiente. Algunas de las normas más relevantes son

- Norma ISO series 55001 (Gestión de activos): conjunto de estándares que proporcionan directrices para la gestión eficiente de los activos físicos de una organización, asegurando su valor a lo largo de su ciclo de vida (International Organization for Standardization, 2024). Esta norma redefine el mantenimiento como una función estratégica para maximizar el valor de los activos físicos, alineándolo con los objetivos empresariales globales. En su úlima actualización (2024) introduce aspectos como gobernanza, decisión basada en valor, datos y cambio climático.
- Norma ISO series 9000 (Gestión de calidad): normas que establecen las directrices para un sistema de gestión de calidad, con el objetivo de asegurar que una organización pueda cumplir consistentemente con los requisitos del cliente y mejorar continuamente (International Organization for Standardization, 2015a). Esta norma asegura la mejora continua en los procesos de mantenimiento, contribuyendo directamente a la confiabilidad de los activos y la satisfacción del cliente interno.

- Norma ISO series 14000 (Gestión ambiental): normas que especifican las directrices para un sistema de gestión ambiental, ayudando a las organizaciones a mejorar su desempeño ambiental y cumplir con las regulaciones legales y otros requisitos (International Organization for Standardization, 2015b). Esta norma es fundamental para la sostenibilidad del mantenimiento, al proporcionar directrices para minimizar el impacto ambiental de las operaciones, incluyendo la eficiencia energética, la gestión de residuos y la reducción de la huella de carbono.
- Norma ISO 45001 (Seguridad y salud en el trabajo): norma que establece los requisitos para un sistema de gestión de seguridad y salud de los empleados en el lugar de trabajo, reduciendo los riesgos y creando condiciones laborales más seguras (International Organization for Standardization, 2018). La norma es un pilar esencial para cualquier organización responsable que promueva un entorno laboral seguro.

2.6 Norma COVENIN 2500-93

La norma COVENIN 2500-93 es una normativa venezolana que establece los procedimientos y criterios para evaluar la gestión de mantenimiento en la industria (Comisión Venezolana de Normas Industriales, 1993a). Desde su implementación en el año 1993, ha sido una referencia esencial en el sector manufacturero en Latinoamérica. Proporciona directrices claras y prácticas para la evaluación y mejora de los sistemas de mantenimiento, contribuyendo significativamente a la eficiencia operativa y a la reducción de costos. Su aplicabilidad también ha sido ampliamente reconocida y utilizada en diversos proyectos académicos, incluyendo pasantías industriales, trabajos de grado, tesis de maestrías y doctorales. Sin embargo, a pesar de su valor histórico, su desactualización limita severamente su aplicabilidad frente a los rápidos avances tecnológicos, la emergencia de la industria 4.0 y las metodologías de gestión contemporáneas.

2.7 Ciclo Deming

El ciclo Deming, también conocido como ciclo de mejora continua, es una herramienta fundamental en la gestión de procesos para la mejora continua (Asociación Española de Normalización y Certificación, 2004). Este ciclo consta de cuatro etapas (Planificar, Hacer, Verificar y Actuar), las cuales permiten a las organizaciones optimizar sus operaciones y adaptarse a las exigencias del entorno industrial. La aplicación efectiva del ciclo Deming en la gestión de mantenimiento es relevante porque permite un enfoque estructurado y sistemático para la optimización de sus procesos. En el manual propuesto el ciclo Deming (PHVA) es una metodología fundamental para la mejora continua dentro de cada una de las doce áreas de evaluación.

2.8 Modelo de madurez organizacional

El modelo de madurez organizacional es una metodología esencial para evaluar el nivel de desarrollo y la capacidad de una organización en la gestión de mantenimiento (Asociación Española de Normalización y Certificación, 2018b). se fundamenta en que las organizaciones evolucionan a través de diferentes niveles, cada uno reflejando un mayor grado de sofisticación, eficacia y eficiencia en sus procesos de mantenimiento. La relevancia de este modelo radica en su capacidad para proporcionar un diagnóstico claro del estado actual del sistema de mantenimiento. Esto permite a las organizaciones comprender sus fortalezas y debilidades, así como establecer un plan de acción para su mejora continua, definiendo objetivos específicos para escalar hacia niveles superiores de madurez.
Este modelo es esencial para el manual de evaluación, ya que no solo proporciona un diagnóstico claro del estado actual del sistema de mantenimiento, sino que también quía el establecimiento de objetivos y planes de acción para escalar hacia niveles superiores de eficiencia y sofisticación, alineando las mejoras con la estrategia organizacional.

2.9 Sostenibilidad del mantenimiento

La sostenibilidad del mantenimiento es un pilar cada vez más crítico en la gestión industrial moderna. Se define como la capacidad de una organización para mantener sus operaciones de mantenimiento de forma continua y eficiente, considerando factores ambientales, sociales y económicos a largo plazo (Asociación Española de Normalización y Certificación, 2018a). Esto implica minimizar el impacto ambiental (reducción del consumo energético, gestión de residuos, disminución de emisiones de carbono), pero también asegurar la viabilidad económica y el bienestar social, lo que contribuye directamente a la competitividad y reputación empresarial.

2 Metodología

El desarrollo de la presente investigación se fundamenta en un enfoque metodológico de carácter documental y descriptivo conforme a lo establecido por Hernández-Sampieri & Mendoza (2018). Este enfoque fue seleccionado por la naturaleza exploratoria del estudio, cuyo objetivo principal es actualizar y mejorar la norma COVENIN 2500-93 mediante una comparación sistemática con estándares internacionales vigentes y la recopilación de percepciones de expertos en el campo del mantenimiento industrial. Este proceso permitió obtener una comprensión profunda y detallada de las deficiencias y oportunidades existentes en la gestión de mantenimiento. Para lograr esto, la metodología se estructuró en las siguientes etapas interrelacionadas para la recolección, procesamiento y análisis de datos.

3.1 Recolección de datos

En este estudio, se emplearon dos técnicas para la recolección de datos: la revisión documental y la aplicación de encuestas (Hernández-Sampieri & Mendoza, 2018). Ambas técnicas fueron seleccionadas por su capacidad para proporcionar información relevante y de alto valor sobre la norma COVENIN 2500-93 y el estado actual de la gestión de mantenimiento, en cumplimiento con el objetivo de la investigación.

3.1.1 Revisión documental

La revisión documental consistió en una búsqueda exhaustiva en base de datos académicas y bibliotecas digitales de acceso libre para analizar la aplicabilidad de la norma COVENIN 2500-93 en proyectos recientes. Esta revisión permitió identificar los sectores industriales donde se ha utilizado (como manufactura, minería, construcción y transporte), su alcance geográfico (principalmente Venezuela y también en países como Costa Rica, Ecuador, Perú y Colombia), y los distintos propósitos de su aplicación, evidenciando su versatilidad como herramienta metodológica y marco de referencia en diversos contextos industriales. Se analizaron tanto proyectos académicos (Márquez, 2024; Vargas, 2024; Mendoza, 2023; Morales, 2023; Olmos & Morón, 2018; Solano, 2020; Olivo, 2019) como proyectos de investigación (Salas et al., 2024; Mota, 2021; Díaz et al. 2019; Cárdenas et al., 2018; Parida et al., 2015; Ortiz et al., 2013; Castillo, 2011) que han aplicado la norma.

3.1.2 Aplicación de la encuesta

La encuesta fue diseñada en formato digital, utilizando Google Forms®, con el propósito de complementar la información documental con la percepción directa de expertos en gestión de mantenimiento. Se seleccionaron 33 profesionales, provenientes del sector industrial y académico, con al menos 5 años de experiencia en el área, mediante un muestreo intencional no probabilístico, una técnica apropiada para estudios cualitativos y de expertos, donde el objetivo es obtener información rica y profunda de individuos con conocimiento específico, en lugar de una representatividad estadística de una población más amplia (Ruiz, 2012).

El número de 33 participantes se consideró adecuado dentro del dominio de la gestión de mantenimiento, asegurando la saturación de categorías de información y la validez de los resultados al incluir profesionales tanto en el ámbito industrial como académico. Esto permitió una evaluación multifacética de las limitaciones y oportunidades de la norma frente a las prácticas modernas.

El cuestionario estuvo compuesto por preguntas cerradas y abiertas, abordando aspectos clave relacionados con la norma COVENIN 2500-93, tanto como su nivel de conocimiento y uso, la precepción de su utilidad y relevancia en el contexto industrial actual, la necesidad actualización y su comparación con otras normas internaciones del sector.

Adicionalmente, se reconoce que el uso de un muestreo intencional no probabilístico puede introducir un potencial sesgo de autoselección. Esto implica que los participantes que decidieron responder la encuesta podrían tener un interés particular en el tema de la gestión de mantenimiento o en la norma COVENIN 2500-93, lo podría influir en sus percepciones. Aunque se buscó la diversidad en la experiencia (sectorial y geográfica) y en el rol (industrial y académico) de los 33 profesionales para mitigar este efecto, los resultados reflejan primariamente las perspectivas de un grupo de expertos motivados y conocedores, y no son directamente generalizables a la totalidad de la población de profesionales del mantenimiento en Latinoamérica.

3.2 Procesamiento y análisis de datos

3.2.1 Análisis comparativo documental

Los datos obtenidos de la revisión documental fueron organizados y sintetizados para identificar patrones, limitaciones y áreas de obsolescencia de la norma COVENIN 2500-93. Se realizó un análisis comparativo sistemático entre los factores clave de la norma venezolana (como la organización de la empresa, la organización de la función de mantenimiento, la planificación, programación y control de actividades, y la competencia del personal), y los requisitos y directrices establecidos por normas internacionales vigentes. Específicamente, se comparó con los estándares de gestión de activos (ISO 55000), gestión de calidad (ISO 9000), gestión ambiental (ISO 14000) y seguridad y salud en el trabajo (ISO 45001), así como con la terminología de mantenimiento (UNE-EN 13306:2018). Este análisis permitió identificar explícitamente los vacíos y procedimientos obsoletos de la norma COVENIN 2500-93 en relación con las tendencias y mejores prácticas actuales de la industria.

3.2.2 Análisis de resultados de la encuesta

Las respuestas de la encuesta fueron procesadas mediante análisis descriptivo para cuantificar las percepciones y opiniones de los expertos, calculando porcentajes de uso, conocimiento y opiniones sobre la adecuación de la norma COVENIN 2500-93. Las respuestas a las preguntas abiertas fueron sometidas a un análisis cualitativo temático para identificar las razones subyacentes a las percepciones expresadas, particularmente en relación con la necesidad de modernización y las características específicas de la norma que requieren atención urgente.

4 Resultados

Esta sección presenta los hallazgos clave derivados de la revisión documental exhaustiva de la norma COVENIN 2500-93 y de la aplicación de encuestas a expertos en gestión de mantenimiento. A partir de este diagnóstico se detalla, en la siguiente sección, la propuesta del manual de evaluación de sistemas de mantenimiento, diseñado para abordar las necesidades actuales de la industria y alineare con los estándares internacionales.

4.1 Análisis y diagnóstico de la gestión de mantenimiento

Los datos recolectados mediante la revisión documental y las encuestas revelan la necesidad de abordar dos aspectos fundamentales para el diseño de un manual actualizado para la evaluación de los sistemas de mantenimiento industrial. Estos incluyen la revisión de los factores de la norma COVENIN 2500-93 que inciden en la capacidad de gestión de mantenimiento, evaluando su pertenencia y posibles áreas de mejora, así como el análisis de procedimientos actuales de la norma para identificar vacíos, determinar los elementos que requieren actualización e incorporar los avances tecnológicos.

4.1.1 Percepción de expertos sobre la norma COVENIN 2500-93

La aplicación de la encuesta a profesionales del sector industrial y académico complementó la información documental. De acuerdo con los resultados, 21 de 33 encuestados (63,6%) nunca han utilizado la norma COVENIN 2500-93 para evaluar los sistemas de mantenimiento, mientras que 12 de 33 (36,4%) si la han utilizado en algún momento. Este hallazgo indica que, aunque la norma existe y está disponible, su adopción práctica en la industria es limitada.

Quienes si han utilizado la norma, 10 de 12 (83,3%) destacaron la necesidad de modernizarla, señalando su estructura compleja, obsolescencia tecnológica y falta de incorporación de otros sistemas de gestión. Este resultado confirma que la norma no incorpora adecuadamente los avances tecnológicos recientes, afectando su aplicabilidad en el contexto actual.

Estos hallazgos empíricos, que revelan un bajo uso y una percepción generalizada de la desactualización de la norma, confirman las limitaciones teóricas de la COVENIN 2500-93 ya destacadas en la introducción del presente estudio. La falta de adaptación al contexto industrial actual, mencionada por la gran mayoría de los encuestados, subraya la necesidad de una herramienta de evaluación que integre los avances tecnológicos y las metodologías contemporáneas, como se propone en este artículo para una gestión más proactiva, eficiente y sostenible.

4.1.2 Revisión de factores de la norma COVENIN 2500-93 que influyen en la capacidad de gestión de mantenimiento

La norma venezolana COVENIN 2500-93 ha sido una guía fundamental, pero su última actualización en 1993 hace necesaria la revisión de sus factores clave para una gestión efectiva frente a los desafíos y tecnologías actuales. La revisión comparativa con estándares internacionales vigentes permitió identificar las siguientes áreas:

- Organización de la empresa. La norma COVENIN 2500-93 reconoce la importancia de la estructura organizativa. Sin embargo, se requiere que el manual de evaluación actualice la necesidad de estructuras organizacionales flexibles que promuevan la agilidad y la rápida toma de decisiones, alineadas con normas internacionales como la ISO 9000, que fomenta una cultura de calidad y mejora continua.
- Organización de la función de mantenimiento. La norma COVENIN 2500-93 establece que la función de mantenimiento debe estar claramente organizada con roles y responsabilidades específicas. No obstante, la gestión de activos ha ganado mayor relevancia con normas como la ISO 55000, que conciben el mantenimiento como una inversión estratégica para la confiabilidad y eficiencia. Por lo tanto, el manual propuesto debe integrar los principios de gestión de activos para maximizar el valor de éstos en función de la estrategia global de la empresa.
- Planificación, programación y control de las actividades de mantenimiento. La norma COVENIN 2500-93 enfatiza la importancia de la planificación, programación y control para reducir fallas imprevistas y optimizar tiempos. Sin embargo, se enfoca principalmente en el mantenimiento preventivo y correctivo, omitiendo enfoques modernos como el mantenimiento basado en condición y el mantenimiento predictivo, que utilizan datos en tiempo real. La inclusión de estos métodos y el uso de sistemas de gestión de mantenimiento computarizados (CMMS) son importantes para una gestión más efectiva y basada en datos.
- Competencia del personal. La norma COVENIN 2500-93 establece requisitos mínimos de capacitación, pero estos son insuficientes ante la rápida evolución tecnológica. Es imperativo incluir requisitos de capacitación continua para operar equipos avanzados, utilizar herramientas de diagnóstico modernas y desarrollar habilidades de gestión para una planificación y administración eficiente de recursos, incluyendo el uso de *CMMS* y análisis de indicadores clave de desempeño (KPIs).

4.1.3 Procedimientos de la norma COVENIN 2500-93. Áreas de mejora

La norma COVENIN 2500-93 establece procedimientos para la planificación, programación, ejecución, registro

y documentación de actividades de mantenimiento preventivo y correctivo. La revisión de estos procedimientos permite identificar áreas de obsolescencia, inadecuación y vacíos en relación con las tendencias actuales.

- Aspectos que requieren de actualización inmediata:
  - Enfoque de aplicabilidad. La norma se fundamenta en el tiempo o en el uso de los equipos, sin considerar el estado real de los activos (mantenimiento basado en condición y predictivo).
  - Análisis de fallas. No se establece procedimientos para el análisis de fallas, limitando la identificación y mitigación de causas raíz.
  - Indicadores clave de desempeño (KPIs). No se considera la evaluación de la efectividad de las actividades, el control de su desempeño y la identificación de áreas de mejora.
  - Documentación. Los procedimientos son básicos y manuales, dificultando el análisis de tendencias y el seguimiento de indicadores.
- Vacíos identificados:
  - Gestión de activos. La norma no incorpora un enfoque de gestión de activos a lo largo de su ciclo de vida, esencial en normas como la ISO 55000.
  - Sostenibilidad y eficiencia energética. Ausencia de procedimientos relacionados con aspectos promovidos por la norma ISO 14000, que buscan minimizar el consumo energético y reducir las emisiones de carbono.
  - Seguridad y salud laboral. Ausencia de medición de riesgos en el lugar de trabajo contemplados en la norma ISO 45001 para garantizar un entorno de trabajo seguro y saludable
- Incorporación de avances tecnológicos. La norma COVENIN 2500-93 fue desarrollada en un contexto previo a la digitalización avanzada y el uso intensivo de datos. La falta de integración de estas tecnologías emergentes limita su efectividad. Es necesario una estructura más adaptable y eficiente para la gestión de mantenimiento, que incluya estas tecnologías para mejorar la competitividad.

Las limitaciones y vacíos identificados en los procedimientos de la norma COVENIN 2500-93 particularmente en la ausencia de un enfoque integral de gestión de activos, sostenibilidad y eficiencia energética, seguridad y salud laboral, y la incorporación de avances tecnológicos, corroboran la argumentación inicial del estudio sobre la necesidad de actualización. Estos hallazgos empíricos refuerzan la urgencia de adoptar un enfoque metodológico que se alinee con los estándares internacionales vigentes como la ISO 55000 para la gestión de activos, ISO 14000 para la gestión ambiental y la ISO 45001 para la seguridad y salud en el trabajo. La brecha entre la norma existente y las mejores prácticas internacionales evidencia que su marco es insuficiente para garantizar una gestión proactiva, eficiente y sostenible en el contexto industrial moderno.

5 Diseño del manual de evaluación de sistemas de mantenimiento

El manual propuesto, cuyo diseño busca modernizar los procedimientos de mantenimiento establecidos en la norma COVENIN 2500-93, se alinea con los estándares internaciones y las mejores prácticas actuales. Este manual ofrece una guía práctica y detallada para la implementación de un sistema de mantenimiento eficiente y sostenible en el entorno industrial, reformulando procedimientos obsoletos, incorporando nuevos factores y desarrollando una estructura práctica.

5.1 Estructura del manual

El manual está organizado en varias secciones clave que facilitan su comprensión y aplicación:

- Introducción. Expone el propósito del manual, antecedentes y normativas de referencia, relevantes para la gestión de mantenimiento.
- Terminología y definiciones. Proporciona los fundamentos teóricos y conceptuales.
- Metodología de evaluación. Detalla los métodos empleados, destacando el uso del ciclo Deming y el modelo de madurez organizacional.
- Áreas de evaluación del sistema de mantenimiento. Establece las 12 áreas clave a considerar, que incluyen: gestión organizacional y estratégica; estructura y gestión de la función de mantenimiento; planeación y programación de actividades; mantenimiento correctivo, preventivo y predictivo; desarrollo de competencias y capacitación continua; control y evaluación de actividades; sostenibilidad y eficiencia energética; seguridad y salud ocupacional; sistemas de información; y apoyo logístico.
- Procedimientos de evaluación. Describe las etapas del proceso, que comprenden la revisión y auditoría inicial, la evaluación del sistema, el análisis del nivel de madurez, la definición de los objetivos de mejora, la elaboración del plan de acción y la redacción del informe de auditoría.
- Modelo de ficha de evaluación. Presenta una herramienta práctica para una evaluación estructurada.

Cabe destacar que, debido a su extensión, el contenido completo del manual ha sido redactado de manera separada de este artículo, bajo el nombre de *Sostenibilidad y eficiencia energética en la industria. Metodología para evaluar sistemas de mantenimiento* (Salas et al, 2026), y puede consultarse digitalmente en la siguiente página web del Sello Editorial Publicaciones del Vicerrectorado Académico de la Universidad de Los Andes (ULA):

http://bdigital2.ula.ve:8080/xmlui/654321/24086

5.2 Aplicación y funcionalidad del manual

El manual integra los principios del ciclo Deming (PHVA) y del modelo de madurez organizacional. El ciclo Deming, que incluye las etapas de planificar, hacer, verificar y actuar, es fundamental para la mejora continua en la gestión de mantenimiento. El modelo de madurez organizacional evalúa el nivel de desarrollo de una organización en la gestión de mantenimiento, dividiendo el progreso en cinco niveles: nivel 0 (deficiente), nivel 1 (básico), nivel 2 (estándar), nivel 3 (avanzado) y nivel 4 (óptimo).

La estructura del manual permite una evaluación integral de las áreas clave del sistema de mantenimiento, organizadas en torno a cuatro dimensiones fundamentales del PHVA:

- Planificación efectiva de las actividades de mantenimiento, alineadas con los objetivos operativos.
- Programación eficiente de las tareas para optimizar recursos y tiempos.
- Ejecución adecuada de las actividades mediante procedimientos estandarizados y mejores prácticas.
- Control de las actividades y evaluación del desempeño del sistema, facilitando la toma de decisiones y la mejora continua.

5.3 Impacto en la competitividad de las empresas

El uso del manual de evaluación propuesto genera un impacto significativo en la competitividad de las empresas, especialmente en la gestión de mantenimiento industrial. Su implementación contribuye a:

- Mejora en la eficiencia operativa. Moderniza procedimientos, optimiza planificación y ejecución de las actividades, reduce tiempos de inactividad y mejora el uso de recursos.
- Reducción de costos. La incorporación de tecnologías avanzadas permite la detección temprana de fallas, disminuyendo errores, interrupciones y costos asociados a reparaciones imprevistas. El enfoque en mantenimiento predictivo y preventivo prolonga la vida útil de los equipos, reduciendo costos por acciones correctivas.
- Estandarización y calidad. Alineado con normas internacionales como ISO 55000, ISO 9000, ISO 14000, ISO 45001 e ISO 31000, garantiza la consistencia y calidad de las operaciones, simplifica la formación del personal y fomenta la mejora continua.
- Sostenibilidad y eficiencia energética. La integración de estos criterios minimiza el impacto ambiental y reduce los costos operativos relacionados con el consumo de energía.
- Simplificación de la documentación. Reduce la carga administrativa, permitiendo a las empresas enfocarse en actividades de mayor valor estratégico.
- Acceso a nuevos mercados y reputación. El cumplimiento de estándares internacionales abre oportunidades comerciales y fortalece la percepción de confiabilidad y compromiso con la calidad y sostenibilidad.

Innovación y adaptabilidad. Fomenta la adopción de nuevas tecnologías y la agilidad para adaptarse a los cambios del entorno, manteniendo la competitividad a largo plazo.

5.4 Limitaciones y recomendaciones para la validación del manual

Este estudio se centró en el diseño conceptual del manual y su ficha de evaluación para sistemas de mantenimiento industrial, integrando criterios de las normas COVENIN, UNE e ISO. Sin embargo, no se ejecutó una prueba piloto que permitiera estimar métricas estadísticas de validez y confiabilidad del instrumento, lo cual constituye una limitación metodológica por atender en futuras investigaciones (Hernández, Fernández & Baptista, 2014; Creswell, 2017).

Para garantizar la robustez del instrumento, se sugiere aplicar procedimientos de validación ampliamente usados en ingeniería y gestión:

a. Validez de contenido (CVR de Lawshe). Evalúa si cada ítem es esencial para el constructo. Su cálculo requiere de un panel de expertos que clasifique cada ítem como esencial, útil o no necesario. El coeficiente de validez de contenido se determina según la siguiente ecuación:

$$CVR = \frac{n_e - N_2}{N/2} \quad (1)$$

donde n_e es el número de expertos que consideran el ítem esencial y N el total de expertos (Lawshe, 1975).

b. Consistencia interna (α de Cronbach). Mide la homogeneidad de los ítems. El coeficiente se obtiene mediante:

$$\alpha = \frac{k}{k-1}\left(1 - \frac{\sum \sigma_i^2}{\sigma_t^2}\right) \quad (2)$$

donde k es el número de ítems, σ_i^2 la varianza de cada ítem y σ_t^2 la varianza total (Cronbach, 1951). El valor de α indicará el tipo de consistencia entre los ítems.

c. Confiabilidad interevaluador (Kappa/ICC). Evalúa el acuerdo entre evaluadores independientes que aplican la ficha. Se recomienda usar el coeficiente kappa para variables categóricas y usar el coeficiente de correlación intraclase (ICC), para puntuaciones continuas. Si se aplica el ICC, debe indicarse el modelo, número de evaluadores y el número de unidades evaluadas (Creswell, 2017). Por ejemplo, si se considera que los evaluadores son representativos de una población de posibles jueces, se sugiere usar el ICC con un modelo de dos vías aleatorio (ICC (2,1)):

$$ICC\ (2,1) = \frac{MS_R - MS_E}{MS_R + (k-1)MS_E + \frac{k(MS_C - MS_E)}{n}} \quad (3)$$

donde *k* es el número de áreas y *n* la varianza total (Cronbach, 1951; citado en Hernández et al., 2014).

5.4.1 Ejemplo ilustrativo (worked-out)

Aunque este trabajo no incluye datos empíricos para calcular dichos indicadores, se presenta a continuación un ejemplo ilustrativo (*worked-out*) de cómo se aplicaría la ficha en una empresa (Véase tabla 1) con puntajes hipotéticos por área y nivel de madurez. Además, muestra cómo se calculan los indicadores descritos anteriormente. Este ejemplo solo tiene fines demostrativos (no sustituye datos reales) y busca facilitar la comprensión del procedimiento proporcionando datos en la ficha de evaluación del manual propuesto (Ver tabla 2).

Los indicadores mostrados en la tabla 2 permiten inferir lo siguiente para el ejemplo ilustrativo:

- Nivel de madurez global estimado. Con un puntaje total global de 118, el sistema de mantenimiento se encuentra en un nivel 3 (avanzado). Este valor se encuentra en el rango de puntaje establecido en el manual propuesto (97-144). También debe tenerse en cuenta que se puede determinar el nivel de madurez por área de evaluación del sistema.
- Validez de contenido de un ítem (área clave del sistema de mantenimiento). Para un panel de 6 expertos, de los cuales 5 han considerado el área como esencial, el valor CVR ≥ 0,62, por lo cual se considera aceptable.
- Consistencia interna de los ítems. El valor de α de Cronbach da como resultado 0,827 (consistencia buena), considerando las doce áreas como observaciones y los cuatro dominios PHVA como ítems. Esto quiere decir que los cuatros dominios PHVA se comportan de manera suficientemente coherente como escala técnica para diagnóstico (Cronbach, 1951).
- Confiabilidad interevaluador. El valor de ICC se determina usando un modelo [2.1] entre dos evaluaciones (con una segunda evaluación sintética para ilustrar el cálculo, no se muestra) y aplicando ANOVA de dos vías de manera aleatoria. El resultado de este indicador es de 0,939 que implica un acuerdo excelente.

Tabla 1. Ejemplo de aplicación de datos usando la ficha de evaluación del manual propuesto.

Área de evaluación	Planificar	Hacer	Verificar	Actuar	Puntaje Área
Gestión organizacional y estratégica	3	3	2	3	11
Estructura y gestión de la función de mantenimiento	3	3	2	2	10
Planeación y programación	2	3	3	4	12
Mantenimiento correctivo	2	4	3	4	13
Mantenimiento preventivo	3	3	3	3	12
Mantenimiento predictivo	2	2	2	3	9
Desarrollo de competencias y capacitación continua	2	2	1	2	7
Control y evaluación	3	2	1	1	7
Sostenibilidad y eficiencia energética	1	1	1	1	4
Seguridad y salud ocupacional	3	3	2	3	11
Sistemas de información	3	3	2	2	10
Apoyo logístico	3	3	3	3	12

Fuente: Elaboración propia a partir de la ficha del manual.

Tabla 2. Resultados de la aplicación de la ficha de evaluación del manual propuesto.

Indicador de evaluación y desempeño	Puntaje
Puntaje total global (promedio de puntaje por área)	118
CVR de Lawshe para una determinado ítem (área de evaluación) del manual	0,67
Consistencia interna (α de Cronbach) de los cuatros dominios PHVA (observación = cada área)	0,827
Confiabilidad interevaluador (ICC [2,1]) entre dos evaluaciones (segunda evaluación sintética de demostración	0,939

Fuente: Elaboración propia a partir de la ficha del manual.

5.4.2 Lineamientos para la aplicación e interpretación de los indicadores de validación

Con el objetivo de asegurar la calidad técnica del instrumento y ofrecer pautas claras para su empleo en estudios piloto y auditorías internas, a continuación se describen los lineamientos para aplicar e interpretar los principales indicadores de validación: validez de contenido, consistencia interna y confiabilidad interevaluador. La selección de estos indicadores responde a su uso extendido en investigación aplicada y a su compatibilidad con la naturaleza del instrumento propuesto (ficha de evaluación por PHVA en 12 áreas), así como a las recomendaciones metodológicas ampliamente documentadas (Cronbach, 1951; Lawshe, 1975; Creswell, 2017; Hernández-Sampieri & Mendoza, 2018).

a. Validez de contenido (CVR de Lawshe). El propósito de este indicador es determinar si cada criterio o ítem del instrumento es esencial para valorar adecuadamente la función de mantenimiento. Este énfasis en la relevancia conceptual permite depurar el contenido antes de su uso operativo a gran escala.
   Para su aplicación se requiere un panel de expertos conformados entre 6 a 9 especialistas (en la medida conformado por un grupo heterogéneo entre 6 a 9 especialistas) con experiencia acreditada en mantenimiento, gestión de activos y auditoria. Cada experto emitirá un juicio clasificando cada área como esencial, útil o no necesaria en el sistema de mantenimiento de la empresa. Se recomienda mantener aquellas áreas que superan el umbral y revisar/rediseñar las que se encuentren por debajo (redefinición, mayor especificidad de evidencia, mejora de redacción).
   En el informe se debe reportar tamaño y perfil del panel, procedimiento de selección, confidencialidad del proceso, cálculo del CVR por ítem, porcentaje de ítems que superan el umbra, toma de decisiones (retención/eliminación) y justificaciones.
b. Consistencia interna (α de Cronbach). La intención de este indicador es estimar la homogeneidad de los ítems que componen una escala, es decir, si los dominios PHVA se comportan de forma coherente al medir un mismo constructo.
   Para su aplicación se deben considerar las 12 áreas como observaciones y los cuatro dominios PHVA como ítems. En el contexto de ingeniería y auditoria de mantenimiento, se consideran como referencias operativas: $\alpha \geq 0{,}70$ (consistencia buena) y $\alpha \geq 0{,}80$ (consistencia muy buena). Para aquellos ítems cuyos valores de α se encuentren por debajo de 0,70 requieren de la revisión por baja correlación interna (solapamientos, ambigüedad o divergencia conceptual) o el fortalecimiento de la guía de evidencias por áreas para estandarizar criterios de evaluación (Creswell, 2017; Hernández-Sampieri & Mendoza, 2018).
   En el informe se debe reportar el valor del α global de la escala PHVA (y por subescalas si aplica), número de observaciones (12 áreas), breve nota interpretativa (por ejemplo, “homogeneidad adecuada entre dominios” o “se detectaron dominios con contribución débil”).
c. Confiabilidad del interevaluador (Kappa/ICC). El objetivo de este indicador es verificar el grado de acuerdo entre dos o más evaluadores independientes al aplicar la ficha, es crítico en auditorias y *benchmarking* interno, donde la reproducibilidad del juicio es un requisito.
   Para su aplicación se debe tener en cuenta un par de criterios. En primer lugar, cuando la evidencia se registra como categórica (por ejemplo, presencia/ausencia de un documento o práctica), se recomienda usar kappa de Cohen u otro coeficiente afín; en cambio, si se trata de puntuaciones continuas (por ejemplo, totales por área), utilizar el coeficiente de correlación interclase (ICC). En segundo lugar, se debe tener en cuenta que en auditorias con evaluadores considerados aleatorios respecto de una población de posibles auditores, el modelo apropiado suele ser ICC [2,1] (dos vías aleatorio, medida individual). En este caso, se sugiere especificar el modelo, el número de evaluadores y el número de unidades (áreas/organizaciones) (Creswell, 2017).
   Para la interpretación de resultados, como guía práctica debe considerarse que un $ICC \geq 0{,}75$ indica un bien acuerdo; $ICC \geq 0{,}90$ se considera excelente. En variables categóricas, $kappa \geq 0{,}60$ suele interpretarse como moderado-bueno y si es mayor o igual a 0,80 como muy bueno. En todos los casos, conviene realizar sesiones calibración previas con ejemplos de evidencias para reducir la variabilidad entre auditores.
   En el informe debe reportarse cantidad de organizaciones a las cuales se le aplicaron la ficha de evaluación (se recomienda que sea mayor a dos organizaciones); registro de puntuaciones de nivel de madurez, tipo de coeficiente empleado (Kappa/ICC), modelo de ICC utilizado, tamaño muestral (unidades y evaluadores), valor del coeficiente con intervalo de confianza, y criterio interpretativo empleado.

La adopción sistemática de estos indicadores favorece la trazabilidad, comparabilidad y mejora continua del instrumento en contextos organizacionales diversos. En esta dase, los resultados *worked-out* incluidos en este artículo cumplen un fin demostrativo. En futuras aplicaciones empíricas, se recomienda sustituir las evidencias ilustrativas por datos reales de pilotaje y reportar los valores obtenidos con el mismo nivel de detalle, siguiendo los estándares de presentación recomendados **(**Cronbach, 1951; Lawshe, 1975; Creswell, 2017; Hernández-Sampieri & Mendoza, 2018).

5.5 Alineación con normas y tendencias internacionales

En un entorno industrial marcado por la aceleración tecnológica, la presión competitiva y los compromisos globales de sostenibilidad, la pertenencia de un manual de evaluación no solo depende de su solidez interna, sino también de su capacidad para integrarse y mantenerse coherente con estándares reconocidos y con las mejores prácticas emergentes. Por ello, además del sustento metodológico ya desarrollado, se presenta a continuación un análisis de alineación que sitúa la propuesta frente a marcos normativos y tendencias internacionales, con el doble propósito de potenciar su transferibilidad a diferentes contextos organizacionales y de garantizar su vigencia ante los desafíos de la industria 4.0 y de la agenda climática.

Esta alineación (*benchmark*) externa permite articular los hallazgos del desarrollo de manual con sistemas de gestión de activos y energía, con modelos de procesos y KPIs normalizados, con enfoques de ingeniería de mantenimiento a lo largo del ciclo de vida y con metodologías avanzadas (*RCM/TPM*) que escalan la mejora desde el diagnóstico hacia decisiones operacionales y estratégicas. Asimismo, habilita la trazabilidad de la evidencia (especialmente en datos, competencias y seguridad), fortalece la comparabilidad de resultados entre organizaciones y sectores, y ofrece un marco explícito para reportar contribuciones a los objetivos de desarrollo sostenible (ODS). De tal manera que el siguiente *benchmark* no altera el contenido del manual, sino que aporta directrices de adopción y referencias cruzadas con el fin de enriquecer su aplicación, facilitando la interoperabilidad con otros sistemas de gestión y elevando el impacto de las acciones de mejora que se derivan del proceso de evaluación.

- Gestión de activos y datos. La norma ISO 55001:2024 refuerza la toma de decisiones sobre activos (numeral 4.5) y la gestión de datos e información (numeral 7.7), y separa explícitamente riesgos y oportunidades dentro de la planificación, consolidando el enfoque de ciclo de vida y la creación de valor (alineada con la norma ISO 55000). En este sentido, la ficha y la matriz PHVA del manual soportan la trazabilidad de evidencias y el uso de datos para la decisión, mientras que el presente artículo recomienda complementar su aplicación con las guías recientemente publicadas en la norma ISO 55012:2024 (personas y competencias) e ISO 55013:2024 (gestión de datos) para robustecer la participación del personal y la calidad del dato en la gestión de activos.
- Procesos e índices clave de desempeños europeos. El manual ya incorpora procesos y *KPIs* típicos. Para asegurar compatibilidad internacional, se sugiere que la organización que aplique la ficha documente un mapa de correspondencia con la norma UNE-EN 17007:2018 (modelo de proceso e interrelaciones) y seleccione los *KPIs* normalizados de la norma UNE-EN 15341: 2020+A:2023 de acuerdo con prioridades y nivel de madurez.
- Ingeniería de mantenimiento en el ciclo de vida. Se propone vincular los planes de acción derivados de la evaluación con actividades de ingeniería de mantenimiento definidas en la norma UNE_EN 17666:2024 (etapas: conceptual, desarrollo, operación y retiro), incorporando criterios de mantenibilidad desde diseño, *RAMS* (Confiabilidad, Disponibilidad, Mantenibilidad y Seguridad) y costo total de propiedad (*TCO*) en las decisiones de mejora.
- Metodologías avanzadas. La evaluación con la ficha puede servir como disparador para iniciar mantenimiento centrado en confiabilidad (*RCM*) en activos críticos (norma IEC 60300-3-11) y, cuando proceda, para desplegar pilares de mantenimiento productivo total (*TPM*) en áreas con alto potencial de participación operativa. Se recomienda explicitar en el informe cómo las dificultades detectadas conducen a análisis de criticidad, modos de falla, consecuencias y tareas (*RCM*), o a iniciativas *TPM* de mejora continua.
- Industria 4.0/ Mantenimiento 4.0. El manual contempla mantenimiento predictivo (*PdM*) y gestión de mantenimiento asistida por computador (*CMMS*); y en el nivel 4 de madurez impulsa tecnologías como internet de las Cosas (*IoT*), gemelos digitales (*DT*) e inteligencia artificial. Se sugiere incorporar (en el informe o anexo) una tabla de evidencias tecnológicas por área (sensores, analítica de datos, *PdM*, estimación de la vida útil remanente (*RUL*), *dashboards*, integración *CMMS-DT*), fortaleciendo competitividad y sostenibilidad del mantenimiento.
- Energía y clima. Se recomienda que, al aplicar el área 9 del manual (sostenibilidad y eficiencia energética), la organización alineé su evaluación con la norma ISO 50001:2018 y la enmienda 1:2024, que introduce la consideración explicita del cambio climático en los sistemas de gestión (cláusulas 4.1 y 4.2). Esto refuerza el vínculo entre desempeño energético, riesgos climáticos y decisiones de mantenimiento.
- Alineación con los ODS de la Agenda 2030. La propuesta del manual se alinea con la Agenda 20230 en tres objetivos clave: el ODS 9 (industria, innovación e infraestructura), el ODS 12 (producción y consumo responsables) y el ODD 13 (acción por el clima). En particular, la meta 9.4 del ODS 9 impulsa la actualización sostenible de industrias, enfatizando la eficiencia en el uso de los recursos y la adopción de tecnologías limpias, mientras que los ODS 12 y 13 articulan la reducción de impactos ambientales y la integración del cambio climático en políticas y sistemas de gestión (energía, riesgo y resiliencia).

  Con el fin de operacionalizar esta alineación en auditorías y reportes, se sugiere desarrollar un mapeo explícito entre las 12 áreas de evaluación de manual y las metas pertinentes de los ODS citados. Este mapeo permite

que la empresa: identifique evidencias por áreas (políticas, KPIs, proyectos, registros); selecciones indicadores de apoyo (por ejemplo, huella del carbono, intensidad energética, tasas de residuos e incidentes de seguridad); y la vinculación con el plan de acción sugerido en el manual propuesto para el cumplimiento de los compromisos de sostenibilidad y clima en la organización.

6 Conclusión

En Este estudio abordó la necesidad de desarrollar un manual de evaluación de sistemas de mantenimiento industrial alineado con los estándares internacionales y las mejores prácticas vigentes. La metodología, sustentada en una revisión documental exhaustiva, análisis comparativos y el juicio de expertos, permitió identificar las áreas críticas de mejora e incorporar las tendencias tecnológicas más recientes. Al integrar el ciclo Deming (PHVA) y modelos de madurez organizacional, la herramienta no solo ofrece una estructura para la gestión proactiva y la mejora continua, sino que facilita la optimización de procesos y la reducción de costos operativos, fortaleciendo la competitividad en un entorno globalizado. En consecuencia, el diseño final del manual trasciende las referencias clásicas citadas al incorporar dimensiones contemporáneas como la sostenibilidad, la eficiencia energética y la transformación digital, asegurando una alineación estricta con los estándares internacionales ISO.

No obstante, en su fase actual de desarrollo, el manual debe considerarse una propuesta metodológica cuyo alcance está sujeto a validación empírica a gran escala. Esta limitación refleja un compromiso con el rigor científico y la necesidad de comprobar su eficacia, adaptabilidad y pertinencia en diversos contextos industriales. Con este fin, se elaboró un *benchmark* externo que vincula la aplicación del manual con normas y tendencias internacionales emergentes identificadas durante el proceso de investigación, con el objetivo de facilitar su adopción en entornos con estructuras múltiples. Se espera que este manual sea una herramienta valiosa para que las organizaciones enfrenten los desafíos y aprovechen las oportunidades del dinámico entorno industrial actual. En tal sentido, se recomienda que futuras investigaciones incluyan pruebas piloto y estudios de caso en diversos sectores industriales, a fin de validar, ajustar y consolidar la metodología. Estas etapas permitirán establecer una hoja de ruta para su evolución continua, asegurando su alineación con las realidades operativas y las exigencias tecnológicas emergentes.

Referencias

Asociación Española de Normalización y Certificación. (2004). *UNE 66178:2004 – Sistemas de gestión de la calidad. Guía para la gestión del proceso de mejora continua*.

Asociación Española de Normalización y Certificación. (2018a). *UNE-EN 13306:2018 – Mantenimiento, Terminología del mantenimiento*.

Asociación Española de Normalización y Certificación. (2018b). *UNE-EN ISO 19011:2018 - Directrices para la auditoría de los sistemas de gestión*. ISO

Cárdenas, R.; Díaz, J. y Zambrano, H. (2018). Estado de la gestión de mantenimiento en las ladrilleras de la zona metropolitana de Cúcuta (Colombia): Propuesta de uso de indicadores. *Revista Científica UNET*, 30(2), 351-360. https://www.researchgate.net/publication/329170912_ESTADO_DE_LA_GESTION_DE_MANTENIMIEN-TO_EN_LAS_LADRILLERAS_DE_LA_ZONA_METROPOLITANA_DE_CUCUTA_COLOMBIA_PROPUESTA_DE_USO_DE_INDICADORES_STATE_OF_MAINTENANCE_MANAGEMENT_IN_THE_METROPOLITAN_POTTERY_ZONE_OF

Castillo, T. (2011). Gestión de mantenimiento de la red hospitalaria del estado Anzoátegui, caso: Hospital Universitario ‘‘Dr. Luis Razetti’’. *CIENCIA ergo sum*, 18(2), 153-163. https://www.researchgate.net/publication/291957399_Gestion_de_mantenimiento_de_la_red_hospitala-ria_del_estado_Anzoategui_caso_Hospital_Universitario_"Dr_Luis_Razetti"

Comisión Venezolana de Normas Industriales. (1993a). *COVENIN 2500-93: Manual para evaluar sistemas de mantenimiento en la industria*. FONDONORMA.

Creswell, J. W. (2017). *Research Design: Qualitative, Quantitative, and Mixed Methods Approaches*. Sage Publications.

Cronbach, L. J. (1951). *Coefficient alpha and the internal structure of tests*. Psychometrika, 16(3), 297–334

Díaz. A.; Villar, L.; Rodríguez, A. y Tamayo, J. (2019). Methodology for maintenance management based on diagnostic criteria. *Revista DYNA*, 86(211). 208-214. http://doi.org/10.15446/dyna.v86n211.77704

ESingeniería. (s.f.). *Mantenimiento industrial 4.0: La revolución tecnológica*. https://esingenieria.net/mantenimiento-industrial-4-0-la-revolucion-tecnologica/

Hernández, R., Fernández, C., & Baptista, P. (2014). *Metodología de la investigación* (6ª ed.). McGraw-Hill.

Hernández-Sampieri, R., & Mendoza Torres, C. P. (2018). *Metodología de la investigación: Las rutas cuantitativa, cualitativa y mixta*. Ciudad de México: McGraw-Hill Interamericana Editores

IBM. (s.f.). *¿Qué es la Industria 4.0?* IBM.

https://www.ibm.com/es-es/think/topics/industry-4-0

Indestan. (s.f.). *Evolución de la Industria 4.0 en el mantenimiento industrial*. https://www.indestan.es/industria-4-0-mantenimiento-industrial/

International Organization for Standardization (2015a). *ISO 9001:2015 - Quality management systems: Requirements*. ISO.

International Organization for Standardization (2015b). *ISO 14001:2015 - Environmental management systems: Requirements with guidance for use*. ISO.

International Organization for Standardization (2018). *ISO 45001:2018 - Occupational health and safety management systems: Requirements with guidance for use*. ISO. International Organization for Standardization (2024).

ISO 55001:2024 - Asset management systems: Requirements. ISO.

Lawshe, C. H. (1975). *A quantitative approach to content validity*. Personnel Psychology, 28(4), 563–575

Márquez Contreras, V. C. (2024). *Revisión y actualización de procedimientos en la norma COVENIN 2500-93* [Trabajo de grado en proceso de publicación, Universidad de Los Andes (Venezuela)].

Mendoza, A. (2023). Plan de gestión de mantenimiento de equipos de la línea de producción en una planta productora de formaldehído. [Trabajo de grado, Universidad Tecnológica Indoamérica]. https://repositorio.uti.edu.ec/bitstream/123456789/5539/1/MENDOZA%20QUEZADA%20ARTURO%20ALEXANDER.pdf

Mora Gutiérrez, A. (2010). *Mantenimiento. Planeación, ejecución y control.* Alfaomega.

Morales, C. (2023). *Plan de mantenimiento preventivo para la línea de producción del triturado de plástico en la empresa de Proyecciones Plásticas Lirio del Campo, S.A.S.* [Trabajo de grado, Universidad Francisco de Paula Santander]. https://repositorio.ufps.edu.co/bitstream/handle/ufps/7131/TG_1121809%20.pdf?sequence=1&isAllowed=y

Mota, J. (2021). Evaluación del sistema de gestión de mantenimiento basado en la Norma ISO 9001:2015 de calidad y confiabilidad a la sección de electricidad de un complejo refinador de PDVSA. *Revista Ciencia e Ingeniería*, 42(3), 369-378. http://erevistas.saber.ula.ve/index.php/cienciaeingenieria/article/download/17280/21921928439

Olivo Moya, J. G. (2019). *Diseño del plan de mantenimiento preventivo para maquinaria pesada del gobierno autónomo descentralizado del cantón Baños de Agua Santa*. https://repositorio.uti.edu.ec/handle/123456789/1072

Olmos, J. y Morón, P. (2018). *Plan de mantenimiento preventivo para los montacargas de Cervecería Polar C.A., agencia Valera, siguiendo los lineamientos de las normas COVENIN 2500-93 y 3049-93* [Trabajo de grado, Universidad Valle del Momboy]. https://repositorio.uvm.edu.ve/items/cdd55e2d-dea8-499c-965c-f00b2eb48ecf

Ortiz, A.; Rodríguez, C. y Izquierdo, H. Gestión de mantenimiento en pymes industriales. *Revista Venezolana de Gerencia (RVG)*, 18 (61), 86- 104. https://www.researchgate.net/publication/337265327_Gestion_de_mantenimiento_en_pymes_industriales

Parida, A., Kumar, U. y Galar, D. (2015). Performance measurement and management for maintenance: a literature review. *Journal of Quality in Maintenance Engineering*, 21(1), 2-33. https://www.emerald.com/insight/content/doi/10.1108/jqme-10-2013-0067/full/html

Ruiz Olabuénaga, J.I. (2012). *Metodología de la investigación cualitativa* (5ª ed.). Universidad de Deusto. https://archive.org/details/ruiz-j.-i.-metodologia-de-la-investigacion-cualitativa-2012

Salas, P.; Barboza, J.; Díaz, A.; Gallo, R. y León, F. (2024). Gestión efectiva del mantenimiento industrial en las PYMEs: retos y soluciones. *Revista Ciencia e Ingeniería*, 45(1), 59-70. https://www.researchgate.net/publication/376170869_Gestion_efectiva_del_mantenimiento_industrial_en_las_PYMEs_retos_y_soluciones_Effective_management_of_industrial_maintenance_in_SMEs_challenges_and_solutions

Salas, P.; Márquez, V.; León, F. (2026). Sostenibilidad y eficiencia en la industria Metodología para evaluar sistemas de mantenimiento. Publicaciones del Vicerrectorado Académico. Universidad de Los Andes (Venezuela). http://bdigital2.ula.ve:8080/xmlui/654321/24086

Solano, A. (2020). *Diseño del modelo de gestión de mantenimiento para los equipos mineros La Chilena en Holcim Costa Rica.* [Trabajo de grado, Instituto Tecnológico de Costa Rica]. https://repositoriotec.tec.ac.cr/handle/2238/12299

Vargas, J. (2024). *Diseño e implementación de un plan de mantenimiento preventivo basado para incrementar la disponibilidad de los equipos críticos del bloque plano en una empresa de vidrio laminado automotriz* [Tesis de Maestría, Universidad Nacional de Ingeniería]. https://repositorio.uni.edu.pe/bitstream/20.500.14076/27733/1/vargas_cj.pdf

Recibido: *10 de enero de 2026*

Aceptado: *10 de marzo de 2026*

Márquez Contreras, Vanessa Caribay: *Ingeniero Mecánico, Universidad de Los Andes (Venezuela).*
Email: vanessacmc19@gmail.com
https://orcid.org/0009-0004-4031-5223

Salas Velázquez, Pedro Arístides: *Ingeniero Mecánico, Universidad Nacional Experimental del Táchira ((UNET, Venezuela). Magíster Scientiae en Ingeniería Mecánica, mención Diseño y Manufactura (ULA). Magíster Scientiae en Ingeniería de Mantenimiento (ULA). Profesor Agregado con dedicación exclusiva Universidad de Los Andes, Venezuela. Colaborador externo para la Universidad Internacional de Valencia (VIU), España. Candidato al grado de Doctor en Ciencias Aplicadas por la Universidad de los Andes, con investigación doctoral centrada en el desarrollo de modelos de mantenimiento predictivo para máquinas rotativas, asistidos por inteligencia artificial.*
https://orcid.org/0000-0003-2210-3046

León Oviedo, Francisco Manuel: *Ingeniero Mecánico, Universidad de Los Andes (ULA, Venezuela). Magíster Scientiae en Ingeniería de Mantenimiento (ULA). Magíster Scientiae (MSc) y Philosophiae Doctor (ph.D) en Ingeniería Mecánica, University of South Florida (USA). Profesor Titular con dedicación exclusiva Universidad de Los Andes, Venezuela.*
Email: fleon@ula.ve fleonovi@gmail.com
https://orcid.org/0000-0001-7706-5740

Artículo de Investigación. Revista Ciencia e Ingeniería. Vol. 47, No. 2 pp. 143-152, abril-julio, 2026.
ISSN 1316-7081. ISSN Elect. 2244-8780 Universidad de los Andes (ULA)

Synthesis and characterization of hydrogels of poly(acrylamide-*co*-itaconic acid) (AAm/IA) and poly(acrylamide-*co*-dimethoxyethyl itaconate) (AAm/DEI) semi interpenetrated with carboximethyl starch

Síntesis y caracterización de hidrogeles de poli(acrilamida-*co*-ácido itacónico) (AAm/IA) y poli(acrilamida-*co*-dimetoxietil itaconato) (AAm/DEI) semi interpenetrados con almidón carboximetilado

Luis José Rojas-Rojas, Amal El Halah, Gabriela Andarcia, Sandra Fajardo, María Solandreina Rondón and Francisco López-Carrasquero*
Grupo de Polímeros-ULA, Departamento de Química, Facultad de Ciencias, Universidad de Los Andes, Mérida, 5101-A, Venezuela
*flopezcarrasquero@gmail.com

Abstract

This study presents the synthesis and characterization of two series of semi-interpenetrating polymer network (semi-IPN) hydrogels based on acrylamide (AAm) combined with either itaconic acid (IA) or dimethoxyethyl itaconate (DEI) in a 70:30 molar ratio, incorporating carboxymethyl starch (CMS) in proportions of 0 to 20 wt%. Quantitative yields confirmed the total integration of CMS into the synthetic lattice. Swelling capacity was primarily governed by the nature of the comonomer: AAm/IA systems exhibited super-desiccant behavior, where swelling decreased upon CMS addition due to volume exclusion, whereas CMS enhanced the initial hydrophilicity of AAm/DEI systems. Kinetic analysis revealed anomalous (non-Fickian) transport in both series, with CMS acting as a modulator of diffusive flux. In 0.02 M $CuSO_4$ solutions, the AAm/IA series showed high adsorption efficiency, evidenced by a drastic network contraction and a shift toward a Fickian-controlled mechanism. Finally, 16-week compost biodegradation assays showed that AAm/DEI samples with 20% CMS lost a corresponding amount of mass, whereas control hydrogels remained intact. This demonstrates that CMS degrades selectively, leaving the polymer matrix intact; thus, CMS functions as a biodegradable 'jacket' or 'vest' for the hydrogel. Microorganisms selectively metabolize the polysaccharide component, enhancing the environmental vulnerability of the material while maintaining the structural integrity of the synthetic matrix during service.

Keywords: Semi-IPN Hydrogels, Carboxymethyl Starch (CMS), Swelling Kinetics, metal Ion Adsorption, Biodegradation.

Resumen

Este estudio presenta la síntesis y caracterización de dos series de hidrogeles de red polimérica semi-interpenetrada (semi-IPN) basados en acrilamida (AAm) combinada con ácido itacónico (IA) o itaconato de dimetoxietilo (DEI) en una relación molar 70:30, incorporando carboximetilalmidón (CMS) en proporciones del 0 al 20% en peso. Los rendimientos cuantitativos confirmaron la integración total del CMS en la red sintética. La capacidad de hinchamiento estuvo gobernada principalmente por la naturaleza del comonómero: los sistemas AAm/IA exhibieron un comportamiento superdesecante, donde el hinchamiento disminuyó al añadir CMS debido a la exclusión de volumen, mientras que el CMS mejoró la hidrofilicidad inicial de los sistemas AAm/DEI.El análisis cinético reveló un transporte anómalo (no Fickiano) en ambas series, con el CMS actuando como modulador del flujo difusivo. En soluciones de $CuSO_4$ 0,02 M, la serie AAm/IA mostró una alta eficiencia de adsorción, evidenciada por una contracción drástica de la red y un cambio hacia un mecanismo controlado por la difusión de Fick. Finalmente, los ensayos de biodegradación en compost durante 16 semanas mostraron que las muestras de AAm/DEI con un 20% de CMS perdieron una cantidad proporcional de su masa, mientras que los hidrogeles de control permanecieron intactos. Esto demuestra que el CMS se degrada selectivamente, dejando la matriz polimérica intacta; por lo tanto, el CMS funciona como una 'chaqueta' o 'chaleco' biodegradable para el hidrogel. Los microorganismos metabolizan selectivamente el componente de polisacárido, aumentando la vulnerabilidad ambiental del material mientras mantienen la integridad estructural de la matriz sintética durante su uso.

Palabras clave: Hidrogeles Semi-IPN, carboximetilalmidón (CMS), cinética de hinchamiento, adsorción de iones metálicos, biodegradación.

Introduction

In recent decades, hydrogels have emerged as state-of-the-art materials in polymer science due to their exceptional swelling capacity, biocompatibility (Zhang, et al, 2025), and stimuli-responsive behavior (El-Hamshary, 2007; González *et al.*, 2015; La Gatta *et al.*, 2021). These three-dimensional networks are pivotal in diverse fields, ranging from tissue engineering and controlled drug release (Suhail, et al, 2025) to environmental remediation via pollutant adsorption (Ahmadi *et al*., 2020; Zhou, *et al.*, 2026). Nevertheless, enhancing their mechanical integrity and functional tunability remains a significant challenge. A robust strategy to modulate these properties is the synthesis of semi-interpenetrating polymer networks (semi-IPN). In these systems, a crosslinked polymer network physically entangles a linear or branched polymer without covalent bonding between the phases (González *et al.*, 2013 and 2018). This architecture provides unique synergy, combining the structural stability of the crosslinked matrix with the specific functionalities of the guest polymer (An, *et al*. 2026). This study presents the development and characterization of semi-IPN hydrogels based on an acrylamide (AAm) and itaconic acid (IA) or dimethoxyethyl itaconate (DEI), (AAm/I) matrix integrated with carboxymethyl starch (CMS). The AAm/I combination yields a network with a high density of reactive functional groups; specifically, the carboxylic groups of itaconic acid confer pH-sensitivity and superior chelation capacity for metallic cations in aqueous solutions (El Halah, *et al*, 2015, 2019). The incorporation of CMS is a determining factor in the material design. As a cost-effective, biodegradable starch derivative, CMS enhances hydrophilicity through its carboxymethyl groups (Barrios, *et al*, 2012 y Balsamo, *et al*, 2011) and acts as a biodegradable phase that enmeshes with the synthetic matrix. Consequently, CMS would modulate physicochemical properties and facilitates material fragmentation post-service life, thereby reducing environmental persistence. The objective of this work is to synthesize and comprehensively characterize the morphology and swelling kinetics of AAm/IA and AAm/DEI semi-IPN hydrogels (70/30 molar ratio) with CMS loadings of 0, 5, 10, 15, and 20% w/w. Furthermore, AAm/IA/CMS Cu^{2+} adsorption capacity is evaluated as a preliminary study for effluent remediation, and AAm/DEI/CMS degradation susceptibility under composting conditions is analyzed to validate their eco-friendly nature.

Experimental

Materials

Itaconic acid (IA) (Aldrich), metoxiethanol (Aldrich) acrylamide (AAm) (Aldrich), ammonium persulfate (APS) Riel de Haën), and N,N´-methylene bis(acrylamide) (MBAm) (Ultrapure Bioreagent GT) were used without further purification. Double distilled water was used for the polymerization reactions and swelling studies. Other solvents were used as received. Cassava starch with an amylose content of about 17%, estimated according to the procedure of (McGrance, Cornell, and Rix, 1998), was kindly supplied by Agroindustriales Mandioca S.A., Venezuela. Other chemicals and solvents were of analytical grade and employed without further purification. Water used in the preparation of carboximethyl starch (CMS) was distilled and deionized before use.

The carboximethyl starch (CMS) were synthesized and characterized according to the procedures previous reported and all the details are described there (Barrios, *et al*, 2012 and Bálsamo, *et al*, 2011). In this work carboxymethyl starch was obtained with a degree of substitution of 0.11. Dimetoxyethyl itaconate (DEI) was prepared by the method previously described. (Rojas, *et al*, 2011, Katime, *et al*, 1989).

Synthesis of semi interpenetrated Hydrogels

The synthesis of semi-IPN hydrogels was carried out in aqueous solution using APS as the initiator and MBAM as the crosslinking agent, both at 1 mol% relative to the total moles of comonomers. The synthesis followed this procedure: a predetermined amount of comonomers, AAm with either IA or DEI in a 70:30 molar ratio, was dissolved in water in glass tube (A). In tube (B), the required amounts of initiator and crosslinking agent were dissolved in 2 mL of water. Both solutions were added to tube (C), which contained a previously stirred CMS aqueous solution thermostated at the reaction temperature to ensure complete dissolution.

The total water volume was 10 mL for the polymerization of DEI and 12 mL for IA. The reaction mixture was then placed in a thermostatic bath at 60 °C for 24 or 48 h. After polymerization, the hydrogels were recovered by breaking the glass tubes. The resulting fresh hydrogels, obtained in cylindrical shapes, were cut into fine pellets and washed several times with distilled water. Finally, the hydrogels were air-dried at room temperature for several days until reaching a constant weight. The chemical structure of the hydrogels was confirmed by FTIR spectroscopy.

In this study, several syntheses were performed to ensure sufficient quantities of hydrogel (HG) for swelling analyses. Tables 1 and 2 show the preparation conditions for one representative batch. Figure 1 schematically illustrates the synthesis procedure, and the idealized structure of the AAm/DEI/CMS semi-IPN HG, which may be consider representative for both series, is shown in **Scheme 1**.

Characterization

Infrared spectra (FTIR) of the HGs were recorded on a Perkin-Elmer 2000 instrument using KBr pellets prepared with xerogel samples. All spectra were acquired using 32 scans with a spectral resolution of ±4 cm^{-1}.

Swelling Measurements

The maximum swelling degree (%S) was measured using a conventional gravimetric procedure. Dry gel samples (xerogels) were immersed in double-distilled water and in a 0.02 M $CuSO_4$ solution at 25 °C until equilibrium was reached. Subsequently, the HGs were removed from the solution, gently wiped with filter paper to remove surface

water, and weighed on an electronic balance. The swelling ratio (%S) and equilibrium water content (EWC) were calculated using Equations 1 and 2 (Karadağ, *et al*, 2002):

$$\%S = [(W_t - W_0)/W_0] \times 100 \quad (1)$$

$$EWC = [(W_\infty - W_0)/W_\infty] \times 100 \quad (2)$$

Where W_t is the weight of swollen hydrogel at time t, and W_0 is the weight of the dry gel at time 0 and W_∞ is the weight of the sample swollen at equilibrium. All swelling measurements were done by triplicate.

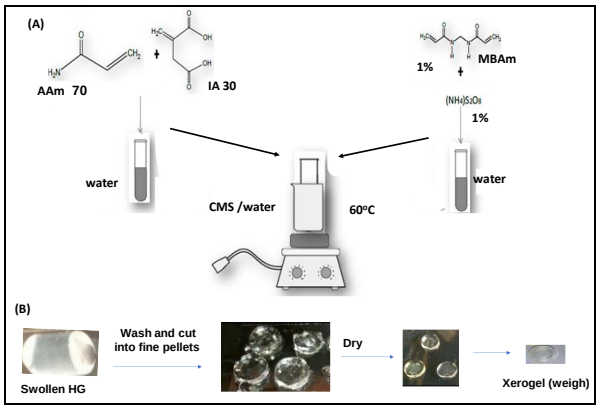

Fig. 1. (A) Synthesis protocol for semi-IPN hydrogels; (B) Post-synthesis processing to obtain dry xerogel pellets.

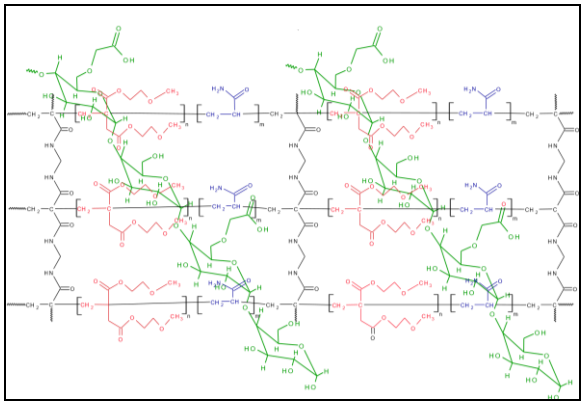

Scheme 1. Idealized structure of the semi-IPN of AAm/DEI/CMS.

Qualitative studies for Cu^{+2} ion absorption followed the same procedure as the swelling tests. Xerogel pellets (AAm/IA/CMS) of known mass were placed in beakers containing a 0.02 M copper sulfate pentahydrate solution.

Preliminary Biodegradation Studies

To study the degradation of the semi-IPN hydrogels, two systems were established using plastic boxes. One contained control gels (AAm/DEI without carboxymethyl starch) and the other contained AAm/DEI/CMS gels (with 20% CMS). Both boxes were filled with composted soil. Xerogel tablets of known mass were buried in rows of three at a depth of approximately 5 cm. Each sample location was identified with a wooden marker, as shown in Figure 2. The samples were kept moist by adding water weekly.

Fig.2. Experimental setup for preliminary biodegradation studies in composting soil.

Results and Discussion

Synthesis

Synthesis semi IPN hydrogels of AAm/IA, and AAm/DEI 70/30 (mol:mol) with CMS in weigh proportion of 0, 5, 10 15 and 20 % were prepared in water, with the aim to determine the effect of the CMS in their swelling properties. In all cases approximately 1 g of AAm was chosen for carry out all the reactions. For this amount of AAm, 10 mL of water for the synthesis used DEI and or 12 mL IA were adequate using all the proportions of CMS. When the amount of CMS was larger than 20%, CMS precipitated even when the volume of water was increased. At the end of the reactions, As can be seemed in Tables 1 and 2 In all cases, semi IPN hydrogels were obtained with quantitative conversions, for AAm/IDE yields were very close to 100% and for AAm/IA were above this value, this fact can be attributed to moisture retained in the network of all the AAm/IA/CMS, probably due to associate water. This behavior was also observed for AAm/IA HG which are more hydrophilic than AAm/DEI (El Halah, *et al*, 2015). AAm/DEI and AAm/IA free of CMS were colorless and transparent, but those with CMS were slightly opaque with light pink or amber colors.

Table 1. Synthesis parameters and feed composition for AAm/IA/CMS semi-IPN hydrogels and the obtained yield[(a)].

Sample	CMS [(b)] (%)	AAm (g)	IA (g)	CMS (g)	(APS) (g)	(MBAm) (g)	Yield[(c)] (%)
AAm/AI /0	0	0.9954	0.7807	-	0.0466	0.0309	115.7
AAm/AI /5	5	0.9962	0.7802	0.0893	0.0457	0.0311	113.1
AAm/AI /10	10	0.9965	0.7803	0.1775	0.0469	0.0310	109.9
AAm/AI /15	15	0.9964	0.7802	0.2671	0.0463	0.0308	111.5
AAm/AI /20	20	0.9952	0.7807	0.3552	0.0474	0.0313	111.5

[(a)]Carry out in 12 mL of water with 1% (mol:mol) of the initiator (APS) and crosslinker (MBAm) during 24h at 60 °C. [(b)] w:w referred to the mass of AAm and IA. [(c)] Based on the initial reactants mass.

Table 2. Synthesis parameters and feed composition for AAm/DEI/CMS semi-IPN hydrogels and the obtained yield [a].

Sample	CMS[b] (%)	AAm (g)	IDE (g)	CMS (g)	(APS) (g)	(MBAm) (g)	Yield[c] (%)
AAm/DEI /0	0	1.0001	0.6779	0.0000	0.0314	0.0214	99.84
AAm/DEI /5	5	1.0005	0.6770	0.0859	0.0315	0.0215	98.14
AAm/DEI /10	10	1.0002	0.6773	0.1708	0.0317	0.0215	98.47
AAm/DEI /15	15	1.0014	0.6772	0.2559	0.0319	0.0213	99.71
AAm/DEI /20	20	1.0006	0.6774	0.3417	0.0313	0.0218	98.51

[a]Carry out in 10 mL of water with 1% (mol:mol) of the initiator (APS) and crosslinker (NMBA) during 48h at 60 °C. [b] w:w referred to the mass of AAm and DEI. [c] Based on the initial reactants mass.

The structure of these materials was studied by FTIR spectroscopy. **Figure 3** displays the spectra of the series of AAm/DEI that could be consider representative of both series.

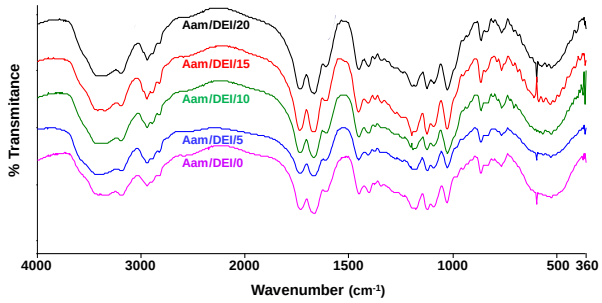

Fig. 3. FTIR spectra of the AAm/DEI/CMS semi-IPN HG with different proportions of CMS.

All de spectra are quite similar to the previous reported for the AAm/DEI hydrogels, showing all the signals of those (Halah, *et al* 2015]. There are noticeable the presence of the bands at 1672 cm^{-1} (Amide I,) and 1614 cm^{-1} (Amide II) characteristic of the AAm moiety and the stretching vibration of carbonyl group of DEI moiety at 1733 cm^{-1}. The characteristic CMS bands cannot be observed in the spectra because, in addition to being overlapping with those of the HG, the CMS is present in a smaller proportion. However, although CMS cannot be observed by IR spectroscopy, the quantitative yields and the formation of insoluble networks are sufficient evidence of the successful synthesis of semi-IPN hydrogels and the effective entrapment of CMS in the tridimensional lattice (**Scheme 1**).

These structural characteristics, along with the observed differences in water affinity between IA and DEI series, are expected to dictate the mass transport properties. Therefore, the following section examines the swelling kinetics to determine how CMS loading and chain relaxation govern the diffusion mechanisms in these matrices.

3.2. Swelling studies

After the HG were characterized, a swelling study in water was carried out and the results of this study indicated that the swelling ability of these hydrogel depends of the proportion of CMS in de semi-IPN HG. Hydrogels water absorption (%S) was followed as function of time until they reach equilibrium state and as may be seen in **Figures 4** and **5** all of them display typical swelling isotherms. In all cases the swelling behavior is reproducible after drying the samples and swell again. The equilibrium water content (EWC) was determined using the same methodology; although the corresponding kinetic plots are not shown, the results are summarized in **Table 3**.

The values of S_{eq} and EWC are given in the **Tables 3**. From there is clear that the swelling of semi-IPN AAm/I/CMS HG is influenced by the nature of the comonomer (IA or DEI), and the proportion of CMS used in the synthesis.

Regarding the AAm/IA/CMS semi-IPN hydrogel series, the swelling degree of all CMS-containing samples was lower than that of the pristine AAm/IA hydrogel. While CMS contents of 5, 10, and 15% resulted in a more or less similar reduction in swelling, the decrease became more pronounced at 20% (**Table 3** and **Figure 6**). This diminished absorption capacity upon CMS incorporation is attributed to the fact that, despite its hydrophilic nature, CMS is significantly less hydrophilic than the AAm/IA matrix. Consequently, water uptake is predominantly governed by the latter. Furthermore, CMS occupies a substantial portion of the network's free volume, imposing a physical constraint on water ingress. Thus, the volume exclusion effect of the starch overrides its inherent absorption capacity, leading to a reduction in swelling proportional to the CMS loading.

In contrast, the AAm/DEI/CMS hydrogels exhibit a distinct behavior. The base AAm/IDE hydrogel reaches a maximum swelling degree (%S) of only 4.124, as IDE is considerably less hydrophilic than IA. However, the incorporation of CMS initially enhances the swelling capacity, peaking at a 10 wt% starch content; beyond this threshold, swelling progressively declines (**Figure 6**). This phenomenon stems from the low hydrophilicity of IDE (El Halah, *et al*, 2015, 2019). Since the absorption capacity of CMS is comparable to or exceeds that of the AAm/IDE matrix, its initial addition improves the overall hydrophilicity of the system. Nevertheless, as CMS concentration surpasses 10%, the free volume occupied by the starch begins to physically restrict the network—a volume exclusion effect analogous to that observed in the previous series. Notably, even at 20% CMS, the swelling degree remains superior to that of the starch-free control.

Finally, using equation 2, the percentage of water by weight of the hydrogels was determined, and their classification according to their capacity to absorb water was established. These results are summarized in Table 3.

The diffusion of small molecules into a hydrogel depends on the network's physical properties and segment-molecule interactions. According to Fick's second law, the water transport mechanism can be determined using the power law equation (3):

$$F = W_t / W_\infty = Kt^n \qquad (3)$$

Where F is the fractional swelling W_t and W_∞ are the water uptake at time t and at equilibrium, respectively; K is a structural constant, and n is the swelling exponent that characterizes the transport mechanism.

The value of n depends on the relative rates of water diffusion and polymer chain relaxation (Franson and Peppas

1983):
n ≈ 0.50 (Case I / Fickian): Diffusion is much slower than relaxation.
0.50 < n < 1.00 (Anomalous / Non-Fickian): Diffusion and relaxation occur at comparable rates.
n = 1.00 (Case II): Diffusion is much faster than relaxation.
n < 0.50 (Less Fickian): Water penetration is significantly slower than the relaxation rate.

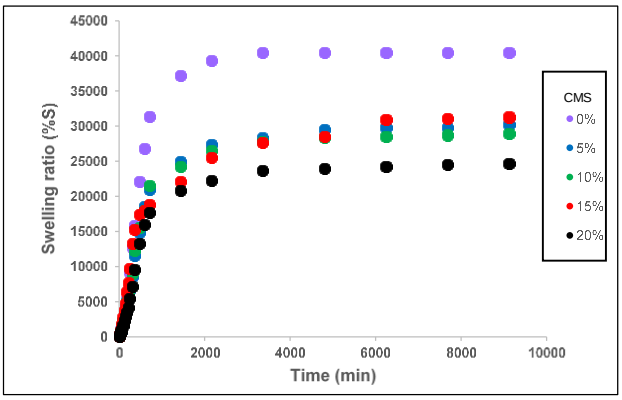

Fig. 4. Swelling isotherms of semi-IPN AAm/IA (70/30) hydrogels in distilled water at 25°C.

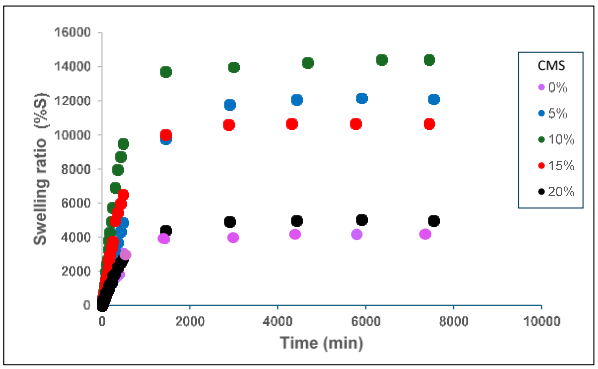

Fig. 5. Swelling isotherms of semi-IPN AAm/DEI (70/30) hydrogels in distilled water at 25°C.

Table 3. Values of swelling of semi-IPN HG of AAm/IA/CMS, and AAm/DEI/CMS[a].

	AAm/IA (70/30)[b]		**AAm/IDE (70/30) [c]**	
Sample	**S_{eq}[d] (%)**	**EWC[e] (%)**	**S_{eq}[d] (%)**	**EWC[e] (%)**
AAM/I/0	40,485	99.75	4,124	97.63
AAM/I/5	30,182	99.67	12,104	99.18
AAM/I/10	28,881	99.65	14,414	99.31
AAM/I/15	31,301	99.68	10,682	99.07
AAM/I/20	24,692	99.60	5,030	98.05

[a)]Synthesized at 60ºC for 24h for AAm/AI/CMS and 48h for AAm/DEI/CMS, using AMS as initiator (1% molar) and MBAm as crosslinking agent (1% molar) [b)] All of them classify as Superdesiccant. [c)] All of them classify as High swelling.

The parameters n and K were determined from the slope and intercept of the plot of $\ln W_t / W_\infty$ vs. $\ln t$ for the initial swelling stage (F < 0.6).

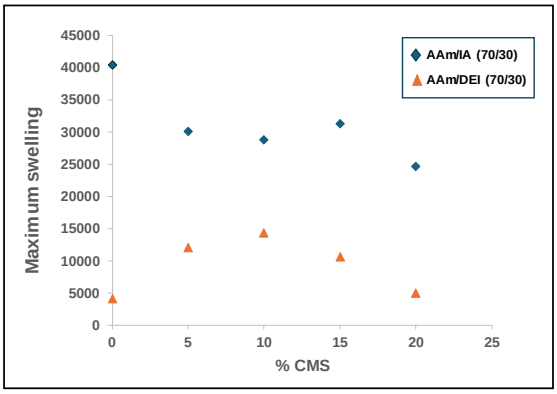

Fig. 6. Maximum swelling degree (%S) vs. CMS content for AAm/IA/CMS and (AAm/DEI/CMS series.

The curves of both series (not showed) also indicate that the swelling process follows a zero-order behavior and the parameters n and K obtained from them, are listed in **Table 4.**

Table 4. Diffusion exponents (n) and swelling rate constants k determined for the semi-IPN AAm/IA/CMS and AAm/DEI/CMS hydrogel series as a function of CMS content.

	AAm/IA/CMS		**AAm/DEI/CMS**	
Sample	**n**	**$k*10^3$ (min-1)**	**n**	**$k*10^3$ (min-1)**
AAm/I/0	0,95	0.76	0.62	8.39
AAm/I/5	0,93	0.89	0.76	2.71
AAm/I/10	0.91	1.17	0.89	2.38
AAm/I/15	0.89	1.53	0.81	3.26
AAm/I/20	0.92	1.03	0.69	6.31

Parameters n and k were calculated from the power law $F = kt^n$ using the initial swelling data (F < 0.6). Values represent the mean of three independent measurements (n=3). Correlation coefficients (R^2) for all samples ranged between 0.966 and 0.992.

Kinetic parameters in **Table 4** indicate that the transport mechanism for both hydrogel series follows anomalous (non-Fickian) behavior, arising from the simultaneous contribution of solvent diffusion and viscoelastic polymer chain relaxation (Kim *et al*, 2003, El-Hamshary, 2007). For the AAm/IA/CMS system, n values ranging from 0.90 to 0.95 suggest that diffusive flux predominates over matrix relaxation. This is attributed to the carboxylic groups of itaconic acid (IA), which enhance charge density and network hydrophilicity, thereby promoting osmotic water diffusion.

Notably, carboxymethyl starch (CMS) acts as a synergistic transport modulator; its incorporation into the AAm/DEI matrix increases n from 0.62 to values near or above 0.80. This shift demonstrates that the hydrophilic nature of CMS compensates for the hydrophobic character of DEI, driving a transition toward a predominantly

diffusion-controlled regime.

Table 4 reveals higher kinetic constants (k) for the AAm/DEI series compared to AAm/IA. Although AAm/IA possesses superior absorption capacity, its swelling rate is restricted by the slow chain relaxation required to accommodate large solvent volumes (Case II transport). Conversely, the less hydrophilic AAm/DEI reaches equilibrium faster through a diffusion-dominated process with minimal structural reconfiguration. Essentially, "*AAm/IA behaves like a large balloon—offering high capacity but filling slowly as the material must stretch—whereas AAm/DEI acts like a small vessel, reaching its limited capacity almost instantly.*"

Preliminary study of the adsorption of Cu^{+2} in aqueous solutions 0.02 M

Acrylamide-based (AAm) hydrogels are well-established materials for the removal of heavy metal ions from aqueous solutions (El Halah, *et al*, 2018). Previous comparative studies between AAm/IA and AAm/DEI matrices revealed that IA-containing systems exhibit significantly higher adsorption efficiencies than DEI and other reported hydrogels (El Halah, *et al*, 2019; García-Manzano and, Alvarez-Igarzabal, 2010; Orzay *et al*, 2009). This enhanced performance is linked to the high chelating potential of itaconic acid moieties. Building upon these findings, this study investigates semi-IPN AAm/IA/CMS hydrogels to evaluate the specific role of carboxymethyl starch (CMS) in Cu^{+2} adsorption.

Figure 7 illustrates swelling kinetics in Cu^{2+} solution exhibited an initial maximum followed by a contraction toward equilibrium. This profile suggests a competitive mechanism where rapid water diffusion initially expands the network, followed by displacement by Cu^{2+} ions. The formation of metal-carboxylate complexes increases the effective crosslinking density, leading to network collapse and stabilization at a lower equilibrium swelling capacity. As observed in **Table 5**, the equilibrium swelling ratio (%S) in the copper solution decreased drastically (from ~40,000 to < 250) compared to distilled water. This massive network contraction is attributed to the screening of electrostatic repulsions between carboxylate groups upon complexation with Cu^{2+}.

Experiments conducted by adding 20 mg of CMS to 30 mL of either pure water or $CuSO_4$ solution did not significantly alter the final pH or the xerogel mass increment. The lack of chromatic changes in isolated CMS–copper solutions suggests that the modified starch acts primarily as a structural matrix modifier rather than participating directly in the coordination of copper ions within this semi-IPN system.

Finally, upon reaching physicochemical equilibrium in 0.02 M $CuSO_4$, the hydrogels were removed and dried at room temperature to a constant weight. Gravimetric analysis revealed a uniform mass increase of approximately 6% AAm/IA semi-IPN xerogels, regardless of the CMS content indicating that Cu is incorporated in to the HG like a complex with de carboxylic groups of the itaconic acid moiety structure similar to de previous reported for Cooper complex with IA (El Halah *et al*, 2020). The formation of this complex is further supported by the HG's transition from colorless to blue, a property that persists upon dehydration (**Figure 8**).

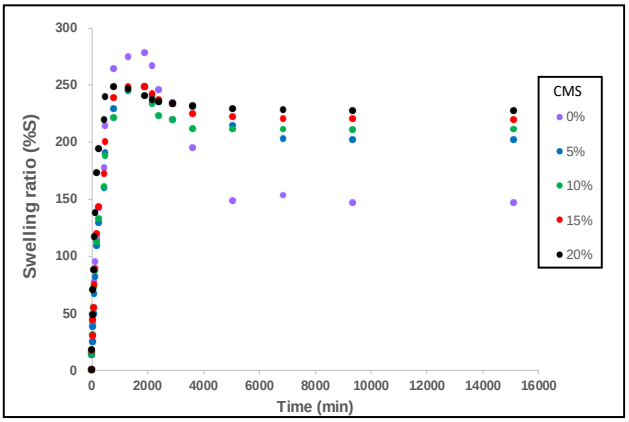

Fig. 7. Swelling kinetics of AAm/IA/CMS hydrogels in 0.02 M $CuSO_4$ solution.

Table 5. Maximum swelling indices (%S) and maximum weight water percentages (EWC) of semi-IPN AAm/IA hydrogels in [$CuSO_4$] = 0.02 M, according to % of CMA; as well as their classification.

Sample	Seq in Cu^{2+} (%)	EWC$^{(e)}$ (%)	Clasification
AAm/IA/0	147.44	59.59	Medium swelling
AAm/IA/5	202.87	66.98	Medium swelling
AAm/IA/10	211.21	67.87	Medium swelling
AAm/IA/15	220.52	68.80	Medium swelling
AAm/IA/20	227.80	69.49	Medium swelling

Copper solution transport mechanisms in hydrogels

To analyze the initial swelling kinetic process in a 0.02M CuSO4 solution, the corresponding plots were constructed using the transport equations (Eq. 3). The results, obtained in quadruplicate to ensure repeatability, indicate that the swelling process follows zero-order kinetics.

As shown in Table 6, an increase in the CMA content within the semi-IPN hydrogels leads to a decrease in the diffusion coefficient, characterizing a non-Fickian transport mechanism. This behavior contrasts significantly with that observed in pure water, where n values near 0.9 reflect a process primarily controlled by polymer chain relaxation (Case II transport).

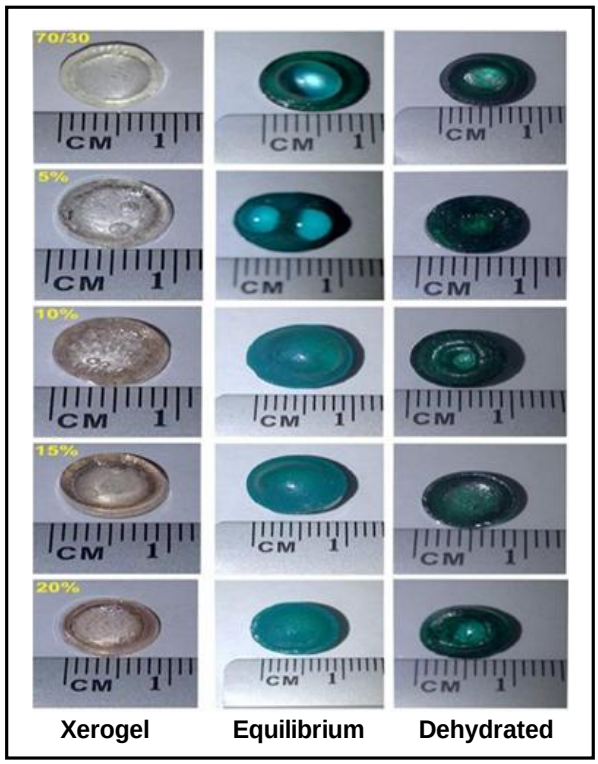

Fig. 8. Color change of HGs before, in the equilibrium and after be dried.

As shown in **Table 6**, an increase in the CMA content within the semi-IPN hydrogels leads to a decrease in the diffusion coefficient, characterizing a non-Fickian transport mechanism. This behavior contrasts significantly with that observed in pure water, where n values near 0.9 reflect a process primarily controlled by polymer chain relaxation (Case II transport).

In the metallic solution, the shift of n toward values approaching 0.5 suggests that Cu^{2+} ions establish coordination interactions with the functional groups of the polymer network, acting as ionic cross-linking points. This interaction restricts segmental mobility and hinders structural relaxation; consequently, the Fickian diffusion mechanism becomes predominant over chain relaxation in the overall swelling kinetics.

Preliminary biodegradation study of AAm/DEI/CMS

A preliminary biodegradation study was conducted under composting conditions to evaluate the role of carboxymethyl starch (CMS) in the environmental degradation of semi-IPN hydrogels. The process was monitored over 16 weeks via weight loss (gravimetry) and surface morphological analysis.

The hydrogels initially exhibited a smooth, white surface. Following compost exposure, samples developed surface irregularities and significant discoloration, shifting from white to brown, with black spots appearing specifically in CMS-containing samples (**Figure 9**). These changes are attributed to microbial colonization and the diffusion of minerals from the compost into the polymer matrix during the swelling phase.

Table 6. Diffusion exponents n and swelling rate constants (k) determined for AAm/AI/CMS semi-IPN hydrogels according to CMA content in a 0.02M Cu^{2+} ion solution.

Sample	n	$K*10^2$ (min-1)
AAm/I/0	0.61	2.10
AAm/I/5	0.57	1.85
AAm/I/10	0.53	2.29
AAm/I/15	0.54	2.25
AAm/I/20	0.51	3.48

Parameters n and k were calculated from the power law $F = kt^n$ using the initial swelling data ($F < 0.6$). Values represent the mean of three independent measurements (n=3). Correlation coefficients (R^2) for all samples ranged between 0.966 and 0.992.

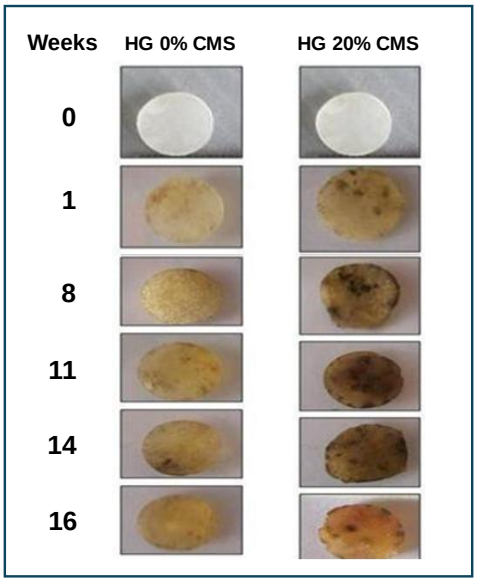

Fig. 9. Appearance of the samples taken from the compost at different treatment times.

As shown in **Figure 10**, weight retention results indicate that control hydrogels (0% CMS) underwent negligible degradation. Conversely, semi-IPN hydrogels with 20% CMS showed consistent weight loss starting from the first week.

Although data dispersion was observed due to compost heterogeneity and moisture gradients within the experimental setup, samples located in the high-moisture central zone exhibited weight losses between 15% and 20%. These values, which correlate closely with the initial CMS content, suggest a selective degradation mechanism. In this process, microorganisms specifically metabolize the starch component without inducing significant cleavage or fracture of the synthetic tridimensional network. Consequently, while the polysaccharide is bioassimilated, the primary hydrogel structure remains largely intact under the studied conditions.

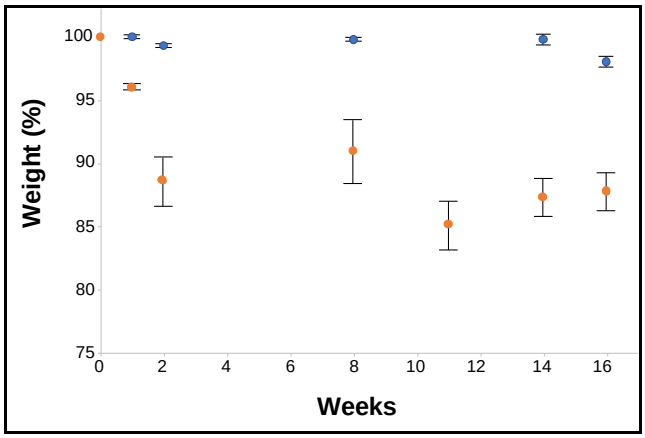

Fig.10. Mass loss percentage as a function of composting time for control (0% CMS) (Blue dots) and semi-IPN (20% CMS) (Yellow dots dots) hydrogels.

Conclusions

Semi-interpenetrating polymer network (semi-IPN) hydrogels based on AAm/IA and AAm/DEI were successfully synthesized with quantitative yields. The insolubility of the resulting networks confirms the effective physical entrapment of carboxymethyl starch (CMS) within the three-dimensional lattice, ensuring structural stability.

The water absorption capacity is primarily governed by the chemical nature of the itaconate comonomer. Due to its high hydrophilicity, the AAm/IA system functions as a super-desiccant material, whereas the AAm/DEI system exhibits a lower, yet significant, swelling capacity, categorizing it as a high-swelling hydrogel.

CMS acts as a critical transport modulator. In highly hydrophilic networks (AAm/IA), its incorporation reduces swelling through a volume exclusion effect. Conversely, in less hydrophilic systems (AAm/DEI), CMS enhances the initial absorption capacity by introducing additional carboxymethyl functional groups into the matrix.

Kinetic analysis revealed anomalous (non-Fickian) behavior for both series. In the AAm/IA system, the process is predominantly controlled by polymer chain relaxation (Case II transport), while in the AAm/DEI system, the incorporation of CMS shifts the mechanism toward a diffusion-controlled regime, compensating for the inherent rigidity of the synthetic matrix**.**

AAm/IA-based hydrogels exhibited high affinity for Cu^{2+} ions, undergoing a drastic network contraction upon the formation of coordination complexes. This ionic self-crosslinking phenomenon shifts the transport mechanism toward Fickian behavior, validating the potential of these materials for wastewater remediation.

Composting assays revealed that CMS undergoes preferential degradation without altering the structural integrity of the synthetic polymeric matrix. In this regard, the CMS acts as a biodegradable "jacket" or "vest" that envelops and protects the hydrogel during its service life; upon degradation, it facilitates the eventual fragmentation and mass loss of the material in the environment.

The incorporation of up to 20% CMS enables the development of materials with tunable functional properties and a reduced environmental footprint. The observed mass loss (up to 20% over 16 weeks) confirms that the inclusion of biopolymers is an effective strategy to increase the biological vulnerability of otherwise persistent acrylic polymers.

References

Ahmadi, S., Pourebrahimi, S., Malloum, A., Pirooz, M., Osagie, C., Ghosh, S., Zafar, M. y Dehghani, M. (2024). Hydrogel-based materials as antibacterial agents and super adsorbents for the remediation of emerging pollutants: A comprehensive review. *Emerging Contaminants*, 10 (3), 100336. https://doi.org/10.1016/j.emcon.2024.100336

An, S., Huang, S., Perumal, R. K., et al. (2026). Fabrication of starch-based hydrogels as drug controlled release carriers: Characterization, anti-bacterial, and cytotoxicity assessment. *International Journal of Biological Macromolecules*, 337 (Part 2), 149568. https://doi.org 10.1016/j.ijbiomac.2025.149568.

Araque, J., Martín, M. y Fygueroa, S. (2006). Estudio de la combustión en un motor de gasolina. *Ciencia e Ingeniería*, 27 (3), 119-127. http://erevistas.saber.ula.ve/index.php/cienciaeingenieria/article/view/308/327

Arredondo Peñaranda, A. y Londoño López, M. (2009). Hidrogeles. Potenciales biomateriales para la liberación controlada de medicamentos. Rev. ing. biomed., 3 (5), 21-30. ISSN 1909-9762

Balsamo, V., López-Carrasquero, F., Laredo, E., Contó, K., Contreras, J. y Feijoo, J. (2011). Preparation and Thermal Stability of Carboxymethyl Starch/Quaternary Ammonium Salts Complexes. *Carbohydrate Polymers*, 8 (4), 1680-1689. https://doi.org/10.1016/j.carbpol.2010.10.025

Barrios, S., Contreras, J., López-Carrasquero, F. y Müller, A. (2012). Chemical modification of cassava starch by carboxymethylation reactions using sodium monochloro acetate as modifying agent. *Revista de la Facultad de Ingeniería UCV*, 27 (2), 97-105. ISSN 0798-4065.

El Halah, A., Contreras, J., Rojas-Rojas, L., Rivas, M., Romero, M. y López-Carrasquero, F. (2015). New superabsorbent hydrogels synthesized by copolymerization of acrylamide and N-2-hydroxyethyl acrylamide with itaconic acid or itaconates containing ethylene oxide units in the side chain. *J Polym Res*, 22 (233), 1-13. https://doi.org/10.1007/s10965-015-0876-2

El Halah, A., López-Carrasquero, F. y Contreras, J. (2018). Applications of hydrogels in the adsorption of metallic ions. *Ciencia e Ingeniería*, 39 (1), 57-69. http://www.redalyc.org/articulo.oa?id=507555109006. ISSN: 2244-8780

El-Halah, A., Machado, D., González, N., Contreras, J. López-Carrasquero, F. (2019). Use of super absorbent hydrogels derivative from acrylamide with itaconic acid and itaconates to remove metal ions from

aqueous solutions. *Journal of Applied Polymer Science*, 136 (4), 46999. https://doi.org/10.1002/app.46999

El-Halah, A., Boide-Trujillo, V., Erder-Concordia, M., Vizcaya, M., Delgado, G., Lopez-Carrasquero F. (2020) Synthesis and characterization of Cu(II), Zn(II) and Sm(III) metal complexes with itaconic acid. Avances en Química, 15(2), 49-56. https://doi.org 10.35207/avances.v15i2.314

El-Hamshary, H. (2007). Synthesis and water sorption studies of pH sensitive poly(acrylamide-co-itaconic acid) hydrogels. *European Polymer Journal*, 43, 4830-4838. https://doi.org/10.1016/j.eurpolymj.2007.08.018

Franson, N. and Peppas, N. (1983). Influence of copolymer composition on non-Fickian water transport through glassy copolymers. *Journal of Applied Polymer Science*, 28, 1299–1310. https://doi.org/10.1002/app.1983.070280404

García-Manzano MF, Alvarez-Igarzabal CI (2010) Síntesis de hidrogeles de N-[3-(dimetilamino) propil] metacrilamida para la retención de metales. Revista Iberoamericana de Polímeros 11(7):428-441. ISSN 1988- 4206.

González, N., Contreras, J., López Carrasquero, F., El Halah, A., Torres, C., Prin, J., Benítez, J. y Rojas de Gáscue, B. (2013). Estudio de la síntesis y caracterización de hidrogeles semi-ipn obtenidos a partir de poliacrilamida y el biopolímero poli(hidroxibutirato-co-hidroxivalerato). *Interciencia*, 38 (6), 430-436. ISSN: 0378-1844 http://www.redalyc.org/articulo.oa?id=33928571003

González, N., El-Halah, A., Contreras, J. y Rojas de Gascue, B. (2018). Estudio de la capacidad de absorción en hidrogeles semi-interpenetrados de poliacrilamida/poli(hidroxibutirato-co-hidroxivalirato). *Rev. Colomb. Quim.*, 47 (3), 19-27. https://doi.org/10.15446/rev.colomb.quim.v47n3.69280

Karadağ, E., Üzüm, Ö. y Saraydın, D. (2002). Swelling equilibria and dye adsorption studies of chemically-crosslinked superabsorbent acrylamide/maleic acid hydrogels. *Eur. Polym J.*, 38, 2133-2141. https://doi.org/10.1016/s0014-3057(02)00117-9

Katime, I., Palomares, F., Lesteros, L., Laborra, C. y Domínguez, E. (1989). Non-classical free-radical polymerization Part 2. The polymerization of mono-2-methoxyethyl and mono-2-ethoxyethyl itaconate. *Thermochim. Acta*, 142, 317-328. https://doi.org/10.1016/0040-6031(89)85028-2

Kim, B., La Flamme, K. y Peppas, N. (2003). Dynamic swelling behavior of pH sensitive anionic hydrogels used for protein delivery. *Journal of Applied Polymer Science*, 89, 1606–1613. https://doi.org/10.1002/app.12337

La Gatta, A., Schiraldi, C., Esposito, A., D'Agostino, A. y De Rosa, A. (2009). Novel poly(HEMA-co-METAC)/alginate semi-interpenetrating hydrogels for biomedical applications: Synthesis and characterization. *J of biomedical Materials Research*, 90A (1), 292-302. https://doi.org/10.1002/jbm.a.32094

Laya, J., Marfisi, S., López, G., Pastrana, J., de Sousa, M., Peña, G. y Rojas de Gascue, B. (2017). Hidrogeles semi-interpenetrados de poliacrilamida/poli (vinil alcohol): estudio de su estructura, capacidad de absorción y propiedades mecánicas. *Avances en Química*, 12 (2-3), 37-40. http://www.redalyc.org/articulo.oa?id=93357608003

Masaro, L. y Zhu, X. (1999). Physical models of diffusion of polymer solutions gel and solids. *Prog Polym Sci*, 24, 731-775. https://doi.org/10.1016/S0079-6700(99)00016-7

McGrance, S., Cornell, H. y Rix, C. (1998). A Simple and Rapid Colorimetric Method for the Determination of Amylose in Starch Products. *Starch/Stärke*, 50 (4), 158–163. https://doi.org/10.1002/%28SICI%291521-379X%28199804%2950%3A4%3C158%3A%3AAID-STAR158%3E3.0.CO%3B2-7

Ozay O, Ekici S, Baran Y, Aktas N, Sahiner, N (2009) Removal of toxic metal ions with magnetic hydrogels. Water Research 43:4403-4411. https://doi.org/10.1016/j.watres.2009.06.058

Rojas, L., El Halah, A., Contreras, J., Romero, M., Rangel, E. y López-Carrasquero, F. (2011). Estudio preliminar de la copolimerización de acrilamida con el itaconato de mono y dimetoxietilo. A*vances en Química*, 6 (2), 21-28. www.saber.ula.ve/avancesenquimica, https://doi.org/10.53766/AVANQUIM

Suhail, M., An S., Kiran, B., Huang, S., Abdul Wahab, A., Yang S., Kong, X., Iqbal, M. Z., Wu, P-C. (2025). Formulation, characterization, anti-bacterial, anti-inflammatory, anti-cancer, and cytotoxicity assessment of collagen/gelatin-based hydrogels as controlled drug release agents. International Journal of Biological Macromolecules,328, Part 2,147653. https://doi.org/10.1016/j.ijbiomac.2025.147653.

Zhang, B-G., Liu Q., Ma, T., Liu J-J., Zhang, Y., Liu, F., Wen, X -M., Wang, D-X., Jiang, Wei., An W-B. (2025). Mechanism and application of injectable hydrogel as carrier system in the treatment of osteoarthritis. Frontiers in Bioengineering and Biotechnology 13, 1-22 https://doi.org/10.3389/fbioe.2025.1636518

Zhao, J., Zhao, X., Guo, B. y Ma, P. (2014). Multifunctional Interpenetrating Polymer Network Hydrogels Based on Methacrylated Alginate for the Delivery of Small Molecule Drugs and Sustained Release of Protein. *Biomacromolecules*, 15 (9), 3246–3252. https://doi.org/10.1021/bm5006257

Zhou Z-X, Zheng, W-X., Tan,Y-Z., Wang,Y., Guo,Y-R., Pan Q-J. (2026). Fabrication of chitosan-magnesium hydroxide hydrogels for efficient removal of copper ions. International Journal of Biological Macromolecules, 340, Part 2, 150081. https://doi.org/10.1016/j.ijbiomac.2026.150081.

Received: *December 30, 2025*

Accepted: *March 24, 2026*

Luis J. Rojas Rojas Licenciado en Química ULA, MSc en Quimica aplicada. Profesor asociado Grupo de Polímeros-ULA, Departamento de Química, Facultad de Ciencias, Universidad de Los Andes, Mérida, 5101-A, Venezuela. ljrojas2021@gmail.com
https://orcid.org/ 0009-0009-1494-7098

Amal El Halah Licenciada en Química ULA, Dra. en Química aplicada Universidad de los Andes. Fue Profesora Asistente del Grupo de Polímeros-ULA, Departamento de Química, Facultad de Ciencias, Universidad de Los Andes, Mérida, 5101-A, Venezuela. aelhalah@gmail.com
https://orcid.org/ 0000-0002-75584-5221

Gabriela Andarcia Licenciada en Química ULA. Departamento de Química, Facultad de Ciencias, Universidad de Los Andes, Mérida, 5101-A, Venezuela.
https://orcid.org/0009-0008-6793-8155

Sandra Fajardo Licenciada en Química ULA. Departamento de Química, Facultad de Ciencias, Universidad de Los Andes, Mérida, 5101-A, Venezuela.

https://orcid.org/0009-0000-8675-8143

María Solandreina Rondón Licenciada en Química ULA, MSc en Química aplicada ULA. Profesora del Grupo de Polímeros-ULA, Departamento de Química, Facultad de Ciencias, Universidad de Los Andes, Mérida, 5101-A, Venezuela.
mariasrondons1@gmail.com
https://orcid.org/ 0009-0007-3839-8017

Francisco López-Carrasquero Licenciado en Química USB, Dr. en Ciencias Químicas Universidad Politécnica de Cataluña. Profesor Titular y Coordinador del Grupo de Polímeros-ULA, Departamento de Química, Facultad de Ciencias, Universidad de Los Andes, Mérida, 5101-A, Venezuela.
https://orcid.org/ 0000-0002-0012-2839

Artículo de Investigación. Revista Ciencia e Ingeniería. Vol. 47, No.2 pp. 153-164, abril-julio, 2026.
ISSN 1316-7081. ISSN Elect. 2244-8780 Universidad de los Andes (ULA)

Synthesis of activated carbons from natural sources for the removal of trace methane in specialized environments

Síntesis de carbones activados a partir de fuentes naturales para la eliminación de trazas de metano en ambientes especiales.

Lugo, Claudio[1]*; Marín Astorga, Karina[1†]; Pérez, Patricia[2]; Vizcaya, Marietta[2]; Rondón, Jairo[3]; Rodríguez, Pedro[1]

[1]Laboratorio de Cinética y Catálisis, Departamento de Química, Facultad de Ciencias, Universidad de Los Andes, Mérida, Venezuela.
[2]Laboratorio de Polímeros, Departamento de Química, Facultad de Ciencias, Universidad de Los Andes, Mérida, Venezuela.
[3]Biomedical Engineering Department, Universidad Politécnica de Puerto Rico, San Juan, Puerto Rico, USA.

**claudiolugo@ula.ve*

Abstract

Activated carbons (ACs) were synthesized from natural precursors (coconut shells and peach pits) via carbonization in a muffle furnace at 700 °C, followed by activation with nitric acid (HNO_3). The materials were characterized using Fourier Transform Infrared Spectroscopy (FTIR), X-ray Diffraction (XRD), Scanning Electron Microscopy (SEM), and Brunauer–Emmett–Teller (BET) analysis to determine the specific surface area (N_2 physisorption). XRD patterns revealed a highly disordered and/or amorphous structure, in which carbon layers are interconnected and intertwined, forming voids associated with porosity. BET surface area analysis showed that nitrogen adsorption increased after nitric acid activation; in all cases, Type I isotherms were observed according to the BDDT classification. SEM analysis indicated that non-activated coconut shell particles were smaller compared to those derived from peach pits. Finally, the CH_4 adsorption capacity of both non-activated and activated carbons was evaluated, showing that nitric acid–activated carbons exhibit enhanced adsorption capacity at low temperatures (40 °C).

Keywords: *Activated carbons, methane, greenhouse gases.*

Resumen

Se sintetizaron Carbones Activados (CAs) a partir del método de carbonización de la materia prima (cáscaras de coco y semillas de durazno) en una mufla a 700 °C y activación con ácido nítrico (HNO_3). Estos materiales se caracterizaron a partir distintas técnicas como la Espectroscopia infrarroja con transformada de Fourier, FTIR, la Difracción de rayos x, DRX, la Microscopia Electrónica de Barrido (MEB) y por Analizador B.E.T. para determinar el Área superficial (adsorción física de N_2). Los DRX obtenidos de las muestras presentan una estructura altamente desordenada y/o amorfa en las cuales las láminas de carbón se conectan y se entrelazan unas con otras, con espacios vacíos que corresponden a la porosidad. En los análisis de área superficial BET, las isotermas muestran que la cantidad adsorbida de nitrógeno es mayor después que el carbón es activado con ácido nítrico, en todos los casos se observó isotermas del tipo I de la clasificación de B.D.D.T. En el análisis por MEB se determinó que las partículas de las cáscaras de coco sin activar son de menor tamaño, respecto a los carbones de las semillas de duraznos. Finalmente se estudió la capacidad de adsorción de CH_4 de los carbones sin activar y activados, lo cual dio como resultado que los carbones activados con ácido nítrico presentan una mejor capacidad de adsorción a bajas temperaturas (40 ºC).

Palabras clave*: Carbones activados, metano, gases de invernadero.*

1 Introducción

Activated carbon is an amorphous form of carbon with a microcrystalline structure like graphite. This broad definition encompasses a wide variety of materials with diverse properties and applications (Mattson et al., 1971).

Under the term activated carbon, a range of products is grouped that differ in physical properties and composition; however, they all share a high degree of porosity and, therefore, a high adsorption capacity, with carbon as their main constituent. The term "activated" refers to the development of extensive porosity and specific surface area associated with the activation process, which ultimately determines the final characteristics of the material. Due to their high adsorption capacity, these carbons are widely used as adsorbents for various substances in both liquid and solid phases (Da Costa et al., 2015).

Adsorption is the change in concentration of a component at the surface of an adsorbent. The most relevant aspects of adsorption phenomena include (Parida, 2006): (i) interfacial characteristics, where adsorption represents the enrichment (positive adsorption) or depletion (negative adsorption) of one or more components at a surface; (ii) adsorption isotherms, which describe the mathematical relationship between the mass of adsorbed solute and its equilibrium concentration in solution; (iii) adsorption thermodynamics, based on equilibrium concepts and the Gibbs dividing surface model; and (iv) adsorbate–adsorbent interactions, which may be physical or chemical. Physical adsorption arises from weak interactions, such as van der Waals forces, and is associated with adsorption heats typically below 80 kJ/mol.

For adsorption processes, materials of greatest interest are those with high surface area, such as microporous and mesoporous solids, or materials combining micro-, meso-, and macroporosity, as in activated carbons (Haynes, 1988; Armatas et al., 2005; Ferreira et al., 2006). Industrial adsorbents and some activated carbons can reach surface areas of 1000-1500 m²/g (Nijhuis et al., 1999; Araújo et al., 2008).

Activated carbon can be produced from carbonaceous materials (e.g., coconut shells or fruit seeds) that are pyrolyzed and subsequently subjected to physical or chemical activation processes (Yalcin et al., 2002). Depending on the intended industrial application, activated carbon may be commercialized as: (1) granular carbon, with lower surface area and smaller pore diameter due to the binders used, or (2) powdered carbon, with higher surface area and larger pore size. To be considered an effective adsorbent, activated carbon must meet certain criteria: (i) high surface area, (ii) microporous structure, and (iii) high reactivity. Typically, industrial activated carbons exhibit surface areas of 800–1500 m²/g.

Activated carbons are also commonly used as support for adsorbing hydrocarbons derived from industrial processes. In 2005, Lee et al. investigated the adsorption capacity of these materials by modifying synthesis conditions, demonstrating significant adsorption performance with carbon tetrachloride (CCl_4) and ammonia (NH_3) over a relative pressure (P/P_0) range of 10^{-4} to 0.8 (Lee et al., 2005).

Currently, novel methodologies allow precise control over porosity and surface chemistry in molecular sieves and advanced carbon materials for catalytic applications. These include carbon molecular sieves, activated carbons, activated carbon fibers, carbon nanotubes, and graphite nanofibers (Parida, 2006). However, the potential application of the adsorption properties of these carbonaceous materials remains insufficiently explored. Activated carbons exhibit unique surface properties compared to other adsorbents, due to their slightly polar or nonpolar surfaces. This characteristic provides several advantages: (a) they are the only commercial adsorbents capable of performing separation and purification processes without requiring moisture removal, such as in air purification; (b) they effectively adsorb a wide range of nonpolar and weakly polar organic molecules due to their extensive internal surface area and large pore volume; and (c) their adsorption heat or bonding strength is generally lower than that of other adsorbents, facilitating easier desorption and regeneration through simple thermal treatment.

In processes involving mixtures of humid gases or aqueous solutions, the use of activated carbons is essential, as adsorption of nonpolar or weakly polar organic compounds is stronger under these conditions.

In this work, activated carbons were synthesized via carbonization, followed by chemical activation using concentrated nitric acid (HNO_3). The carbonaceous materials were characterized using Fourier Transform Infrared Spectroscopy (FTIR), X-ray Diffraction (XRD), Scanning Electron Microscopy (SEM), and BET surface area analysis. Adsorption tests were performed using a gas chromatograph (GC) coupled to the adsorption system to evaluate the adsorption capacity of the activated carbons toward greenhouse gases, particularly methane (CH_4).

2. Experimental Procedure

2.1 Synthesis of Activated Carbons

Activated carbons (ACs) were prepared from: (1) peach pits and (2) coconut shells using a modified impregnation method described by Kim and Ahn (Kim y Ahn, 2010) and validated at the Kinetics and Catalysis Laboratory of the Universidad de Los Andes by Marín (Marín, 2015) and Prado (Prado, 2018). This synthesis consists of two main stages:

2.1.1 Preparation of Carbonaceous Materials

The raw materials (peach pits and coconut shells) were treated via a carbonization process (Kim and Ahn, 2010), which allowed the production of the desired carbon materials.

2.1.1.1 Carbons from Peach Pits

Initially, the collected peach pit samples were washed with distilled water to remove pulp residues. They were then dried in an oven at 100 °C for 5 h, followed by further drying at 200 °C for 12 h prior to thermal treatment.

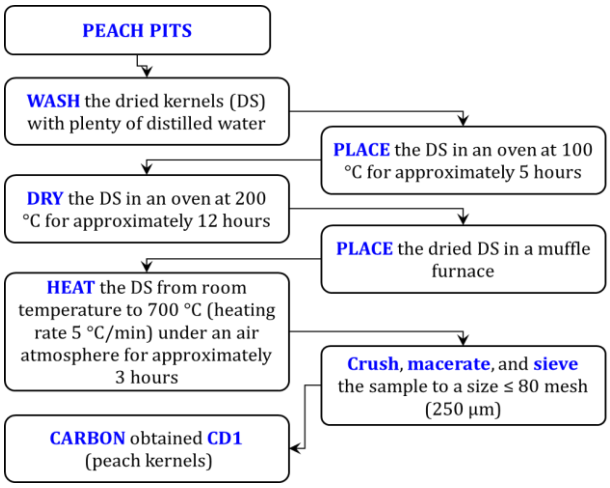

Fig. 1. Scheme of synthesis of Carbon obtained (CD1) from Peach seeds.

The carbonization process was carried out in a muffle furnace (with precise control of temperature ramp and time). The dried samples (~6.0 ± 0.1 kg) were heated from room temperature to 700 °C at a heating rate of 5 °C/min under an air atmosphere and maintained at 700 °C for approximately 3 h. The resulting solid (492.1 ± 0.1 g) was ground, crushed, and sieved to obtain particles ≤ 80 mesh (250 µm) (Kim and Ahn, 2010). The synthesis scheme is shown in Fig. 1.

2.1.1.2 Carbons from Coconut Shells

The collected coconut shells were sanded, washed, and boiled in distilled water at 100 °C for 5 h to remove residual organic matter. The cleaned shells were then dried at 200 °C for 12 h prior to thermal treatment.

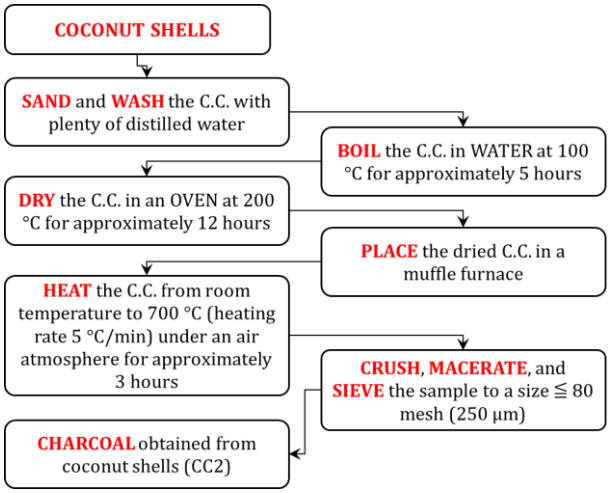

Fig. 2. Scheme of synthesis of Carbon obtained (CD1) from Coconut shells.

Carbonization was performed in a muffle furnace under controlled temperature and time conditions. The dried samples (~5.0 ± 0.1 kg) were heated from room temperature to 700 °C at 5 °C/min under an air atmosphere and held at 700 °C for approximately 3 h. The resulting solid (421.7 ± 0.1 g) was ground, crushed, and sieved to a particle size ≤ 80 mesh (250 µm) (Kim and Ahn, 2010). The synthesis scheme is shown in Figure 2.

2.1.2 Activation of Carbons

Chemical activation of the prepared carbons (from peach pits, CD1, and coconut shells, CC2) was carried out in a reflux system using nitric acid (HNO_3, 65 wt.%, Merck). First, ~400 mL of nitric acid was placed in a three-neck round-bottom flask. Subsequently, 4.0 g of carbon was slowly added under constant stirring (1000 rpm). The mixture was maintained at 75 °C under reflux for 16 h.

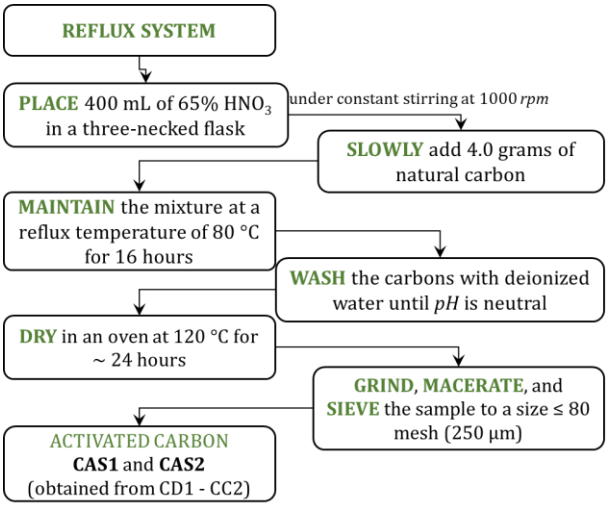

Fig. 3. Activation scheme of Activated Carbons (CAD1 and CAC2).

After chemical activation, the resulting activated carbons were washed with abundant deionized water until the pH reached neutrality. Finally, the activated carbons (CAD1 and CAC2) were dried in an oven at 120 °C for 24 h. The procedure is illustrated in Fig. 3.

2.2 Synthesized Materials

The activated carbons obtained from different natural sources (peach pits (SD1) and coconut shells (CC2)) are summarized in Table 1.

Table 1. Activated Carbons from different types of raw materials (SD1 and CC2) synthesized via SCS.

Material	Method	Code
Carbon (SD)	Impregnation	CD1
Carbon (CC)	Impregnation	CC2
Activated carbon (SD)	—	CAs1
Activated carbon (CC)	—	CAs2

SD: peach pits; CC: coconut shells

2.3 Characterization

The synthesized materials were characterized using the following techniques:

1. **Fourier Transform Infrared Spectroscopy (FTIR)** using a PerkinElmer Frontier spectrophotometer (Kinetics and Catalysis Laboratory, Universidad de Los Andes).
2. **X-ray Diffraction (XRD)** (powder method) using a Rigaku Geiger flex diffractometer (Metal Catalysis Laboratory, Universidad de Concepción, Chile), employing Cu Kα radiation at 40 kV and 2 mA. Operating conditions included continuous scan mode at 1°/min over a 2θ range of 1–90°.
3. **Scanning Electron Microscopy (SEM)** using a JEOL JEM 100-CX II microscope (Universidad de Concepción, Chile).
4. **BET Surface Area Analysis** using a Micromeritics ASAP 2020 analyzer (Johnson Matthey Inc., Sevierville, TN, USA) to determine specific surface area via N_2 physisorption.

All analyses were performed on both activated and non-activated samples.

3. Results and Discussion

3.1 Fourier Transform Infrared Spectroscopy (FTIR)

The infrared spectra of non-activated carbons obtained from peach pits and coconut shells (CD1–CC2) are shown in Fig. 4. Table 2 summarizes the FTIR band assignments for the non-activated carbons.

The broad band observed in the range 3700–3300 cm^{-1} is attributed to O–H stretching vibrations, indicating the presence of moisture in the synthesized samples (non-activated carbons) (Primera et al., 2011). Peaks between 2925.2 and 2856 cm^{-1} correspond to symmetric and asymmetric stretching vibrations of aliphatic C–H bonds (–CH_3 and –CH_2) (Rosquete, n.d.).

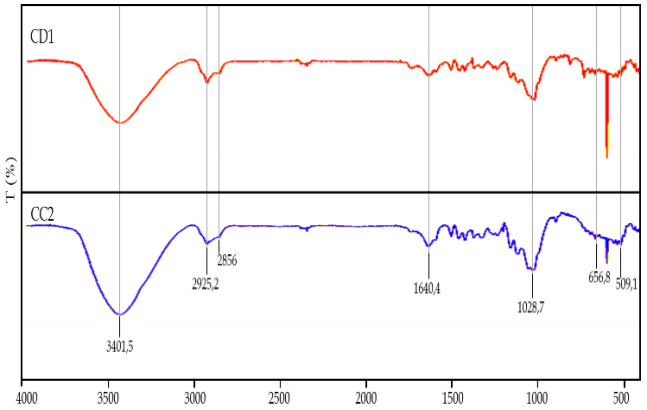

Fig. 4. FTIR spectra of non-activated carbons obtained from coconut shells (CC2) and peach pits (CD1).

The signal around 1640.4 cm^{-1} is associated with C=C stretching vibrations characteristic of aromatic compounds (Primera et al., 2011). Absorption bands near 959 cm^{-1} are attributed to in-plane bending vibrations of C–H bonds (Primera et al., 2011). Peaks around 656.8 cm^{-1} and 509.1 cm^{-1} correspond to out-of-plane bending vibrations of aromatic structures (Yin et al., 2009).

Table 2. FTIR band assignments for non-activated carbons synthesized from different raw materials (SD1 and CC2).

$\nu_{(ref.)}$ (cm^{-1})	ν (cm^{-1})	Bond	Assignment
3700–3300	3428.6	O–H	Symmetric and asymmetric O–H stretching
2950–2845	2925.2–2856	C–H	Symmetric and asymmetric stretching (aliphatic –CH_2 – CH_3)
1650–1600	1640.4	C=C	Aromatic C=C stretching
1440–880	1400–1028	C–H	In-plane bending vibrations
650	~656.8	H–C=C	Out-of-plane aromatic bending
455	~509.1	H–C=C	Out-of-plane aromatic bending

The FTIR spectra of activated carbons (CAs1–CAs2) are shown in Fig. 5, and their band assignments are presented in Table 3.

The broad band at ~3405 cm^{-1} corresponds to O–H stretching vibrations, indicating the presence of moisture in the activated samples (Primera et al., 2011). Weak bands between 2928 and 2855.5 cm^{-1} are associated with aliphatic C–H stretching vibrations (Rosquete, n.d.). The signal at ~1717.8 cm^{-1} is attributed to C=O stretching from functional groups such as ketones, aldehydes, lactones, or carboxylic acids (Rosquete, n.d.).

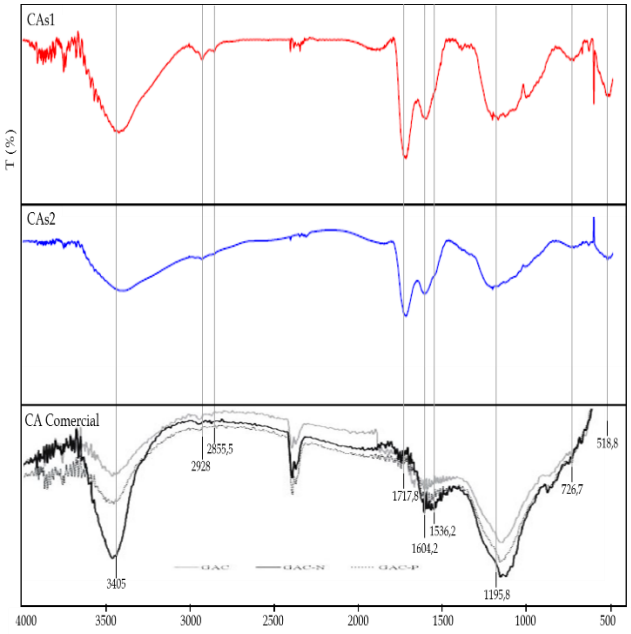

Fig. 5. FTIR spectra of activated carbons (HNO_3-treated) obtained from coconut shells (CAs2) and peach pits (CAs1).

Table 3. FTIR band assignments for activated carbons (CAs1 and CAs2).

$\nu_{(ref.)}$ (cm^{-1})	ν (cm^{-1})	Bond	Assignment
3700–3300	3405	O–H	Symmetric and asymmetric O–H stretching
2950–2845	2928–2855.5	C–H	Aliphatic C–H stretching
1765–1645	~1717.8	C=O	Carbonyl stretching (ketones, aldehydes, lactones, carboxylic acids)
1650–1600	1604.2–1536.2	C=C	Aromatic C=C stretching
1260–1180	~1195.8	C–O	Ester C–O stretching
790–650	~726.7	H–C=C	Out-of-plane aromatic bending
455	~518.8	H–C=C	Out-of-plane aromatic bending

Bands at 1604.2 and 1536.2 cm^{-1} correspond to aromatic C=C stretching vibrations (Primera et al., 2011). The peak at ~1195.8 cm^{-1} is assigned to C–O stretching in esters (Primera et al., 2011). Bands near 726.7 cm^{-1} and 518.8 cm^{-1} correspond to out-of-plane bending vibrations of aromatic structures (Yin et al., 2009).

3.2 X-ray Diffraction (XRD)

Figure 6 shows the diffraction patterns of non-activated (CD1–CC2) and activated carbons (CAs1–CAs2).

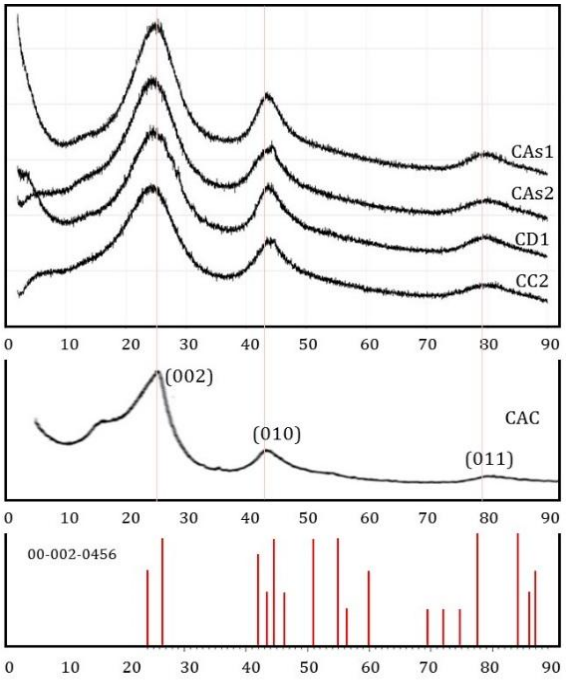

Fig. 6. XRD patterns of carbons obtained from peach pits and coconut shells (non-activated and activated). Activated carbon pyrolyzed at 800 ºC (Yin y col., 2009). File: 00-002-0456 (Graphite, carbon).

Phase identification was carried out using X'Pert HighScore Plus software with the PDF2-2004 ICDD database, revealing a hexagonal graphitic carbon phase (space group: *P63mc*), identified by card 01-088-0638 (Harcourt et al., 1942), and confirmed by comparison with literature (Yin et al., 2009; Liu et al., 2014).

The diffraction peaks correspond to the (002), (010), and (111) planes. The (002) reflection is associated with stacked aromatic layers, whereas the (010) and (111) reflections correspond to less ordered aromatic structures (Yin et al., 2009). Furthermore, the activated carbon synthesized in this study shows a diffraction pattern identical to that obtained for a commercial activated carbon studied by Liu et alia in 2014 (Liu et al., 2014).

The most intense peak near 25° is attributed to graphitic plate formation, indicating the development of a carbon–pore structure. Increasing the calcination temperature reduces the interlayer spacing and increases the crystallite size, promoting a transition from amorphous to semicrystalline carbon structures (Rampe et al., 2011).

3.3 Nitrogen Adsorption Isotherms

Figures 7 and 8 show nitrogen adsorption isotherms at 77 K for non-activated and activated carbons. Nitrogen adsorption increases after nitric acid activation, indicating enhanced micro- and mesoporosity.

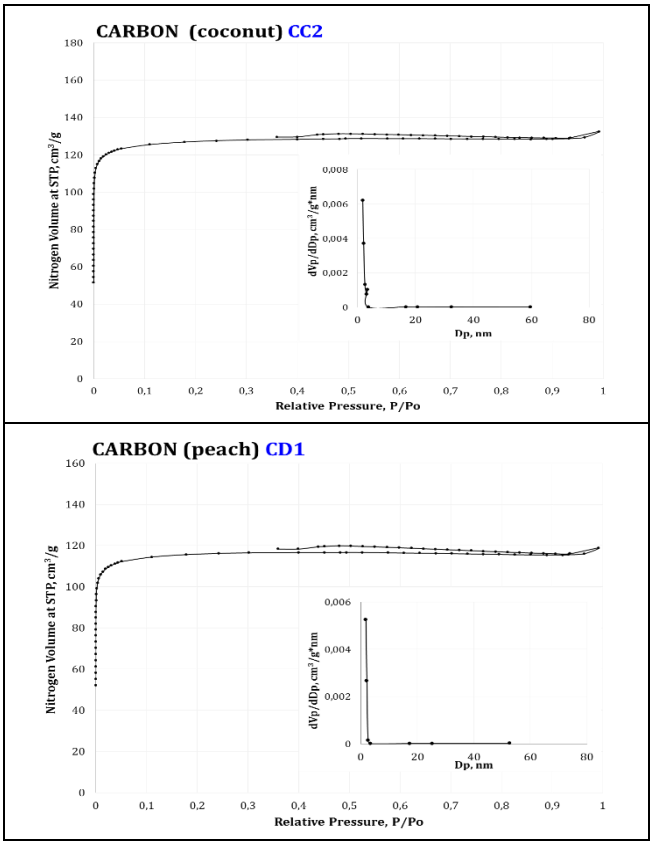

Fig. 7. N_2 adsorption isotherms (77 K) for non-activated carbons (CD1, CC2).

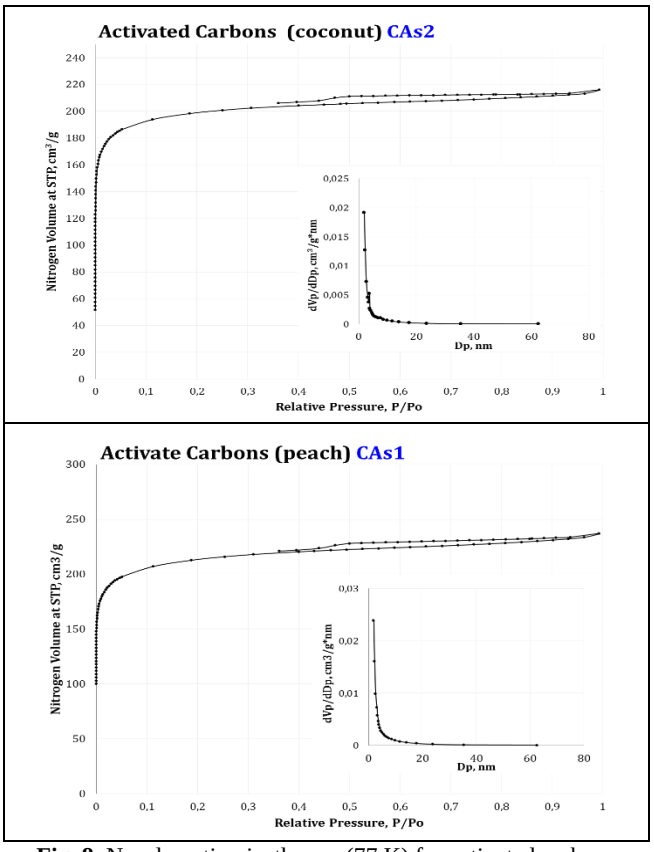

Fig. 8. N_2 adsorption isotherms (77 K) for activated carbons (CAs1, CAs2).

All samples exhibit Type I isotherms according to the Brunauer–Deming–Deming–Teller (BDDT) classification, confirming the predominance of microporosity.

Non-activated carbons show pore radii between 1 and 5 nm, while activated carbons exhibit increased pore diameters (~5–10 nm). BET results (Table 4) indicate increased surface area and pore volume after activation.

Table 4. Textural properties of synthesized carbons (from coconut shells and peach seeds).

Solid	Code	A_{BET} (m^2/g)	Report *t*-plot		V_{PORE}* (cm^3/g)	D_{PORE}* (nm)
			A_{MICRO} (m^2/g)	A_{EXT} (m^2/g)		
Carbon (coconut)	CC2	350 ± 2	326.0	21.0	0.18	4.42
Carbon (peach)	CD1	380 ± 2	343.7	36.2	0.20	4.62
Activated carbon (coconut)	CAs2	600 ± 3	-----	-----	0.33	3.81
Activated carbon (peach)	CAs1	694 ± 5	538.0	116.8	0.37	3.94

* *measured by BJH adsorption.*

3.4 Scanning Electron Microscopy (SEM)

SEM micrographs (Fig. 9) of non-activated carbons show heterogeneous particles (1–20 µm), irregular shapes, sharp edges, and cracks that contribute to surface area. Coconut-derived carbons exhibit higher heterogeneity than

peach-derived carbons.

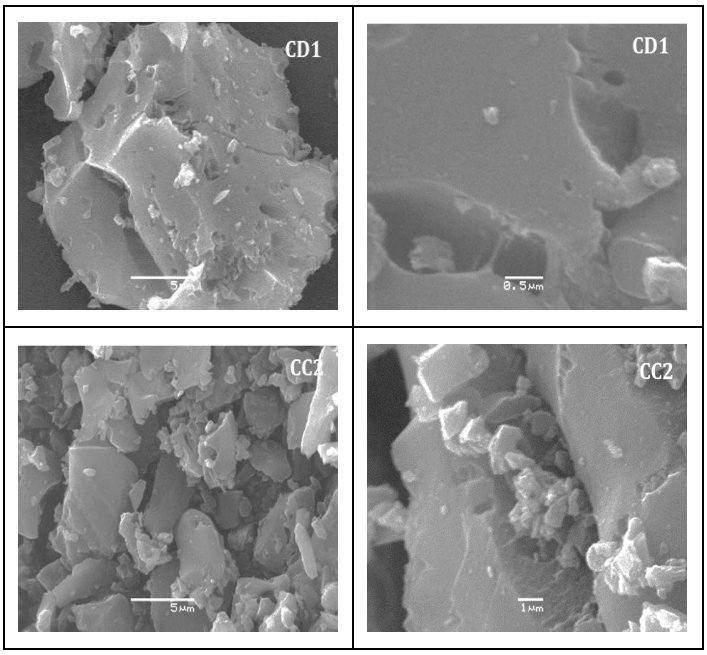

Fig. 9. SEM images of non-activated carbons (CD1, CC2).

After activation (Fig. 10), coconut carbons show minor morphological changes, while peach-derived carbons exhibit reduced particle size and increased surface roughness and porosity (36,2 to 116,8 m^2*g^{-1}).

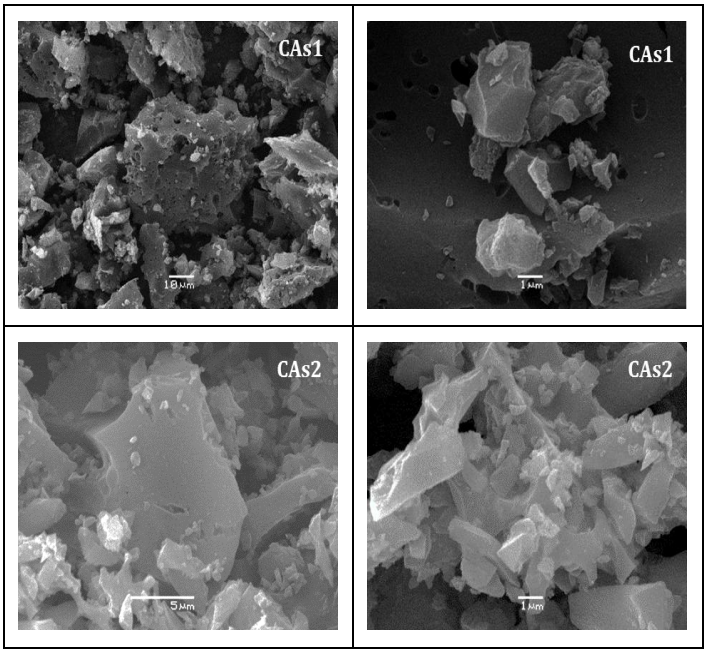

Fig. 10. SEM images of activated carbons (Cas1, CAs2).

In general, carbons obtained from coconut shells have fewer surface irregularities compared to carbons obtained from peach seeds; in addition, chemical treatment allows for a decrease in the particle size of peach seed carbons, leading to a more pronounced increase in the surface area of peach seed carbons than in the case of coconut shells.

3.5 Methane Adsorption Tests

3.5.1 Instrumental Response

A Hewlett-Packard 6890 Plus gas chromatograph equipped with a thermal conductivity detector (TCD) was used, with nitrogen as carrier gas (30 *mL*/min).

3.5.2 Pretreatment

About 200 mg of activated carbon (from coconut or peach) was placed inside a U-shaped steel reactor and the solid was pretreated by circulating ~30 mL/min of gaseous nitrogen, N_2(g), through the reactor from room temperature to 120 ºC, where it remained for 90 minutes.

3.5.3 Calibration (CGases)

Parameters such as mass, hydrocarbon flow rate, temperature range, and space velocity were calibrated. The ideal conditions for studying methane adsorption on activated carbons are shown in Table 5 below.

3.5.4 Adsorption Conditions

After the sample pretreatment was completed, 103 mL/min of a CH_4/N_2 (3/100) mixture was passed through the reactor. The adsorbent (CAs) was subjected to a temperature ramp from room temperature to the adsorption temperature of 40°C and 60°C, where it remained for a little over 1 hour (~100 minutes). The adsorption scheme is shown in Figure 11.

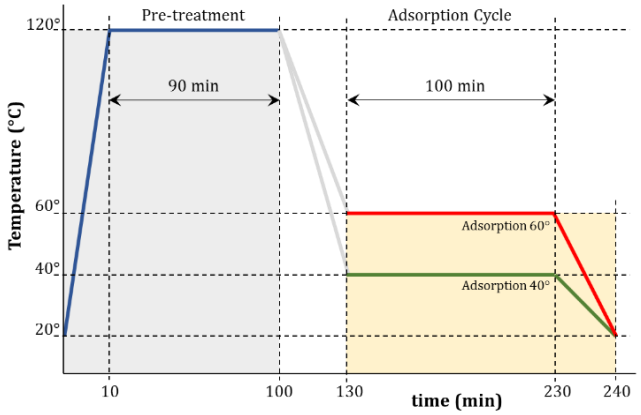

Fig. 11. Schematic of methane adsorption on activated carbons (coconut shells and peach seeds).

Table 5. Actual conditions for *CGases* analysis.

Parameter	Value
Total flow rate (*mL/min*)	~ 30
Temperature range (°C)	40-60
Activated carbon mass (*mg*)	≥ 0,030
Space velocity range x10^{-3} (*mL/g.h*)	120-240

3.5.5 Adsorption Tests of methane

Figure 12 (Table 6) shows the methane adsorption capacity during the studied cycle, which contains non-activated carbons (CC2-CD1) and activated carbons with nitric acid (CAs2-CAs1), prepared from different raw materials (coconut shells and peach pits), at temperatures between 60 and 40 °C. In this graph (Fig. 12), a linear behavior of methane (conductimetric response with respect to CGases) is observed before passing through the reactor, that is, at times below 25 minutes.

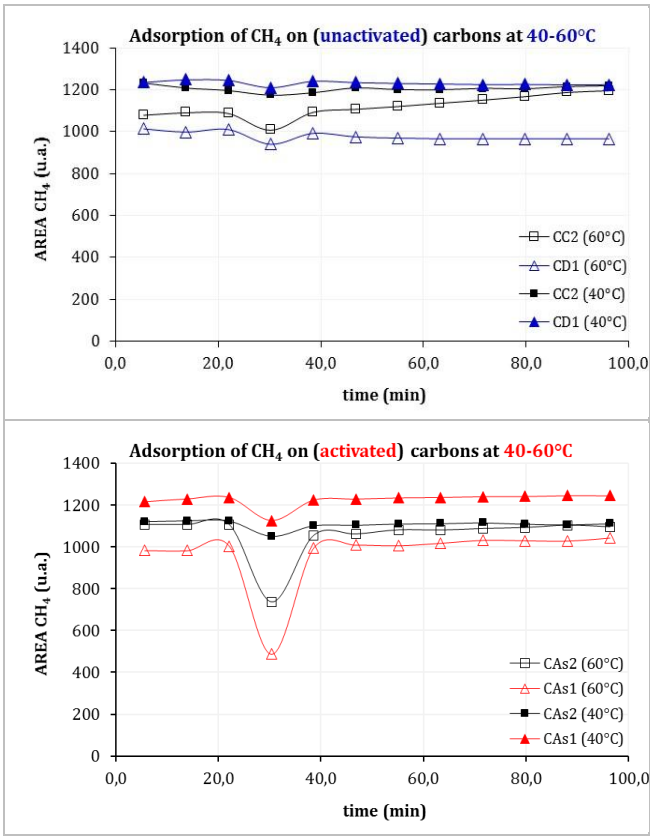

Fig. 12. Adsorption of methane on non-activated carbons (CC2 and CD1) and activated carbons (CAs2 and CAs1) at different temperatures, 40 and 60 °C.

Once the hydrocarbon enters the reactor, it can be determined that the amount of methane adsorbed onto

activated carbons (ACs) increases compared to non-activated carbons at different adsorption temperatures, 60 and 40°C. After the adsorbent is saturated, the initial methane concentration is recovered. This increase in the adsorptive capacity of activated carbons (ACs2-ACs1) compared to non-activated carbons (CC2-CD1) is due to the fact that the smaller the mesopore size and the height of the crosslinking of the polyaromatic molecules that compose it, the better the activation process, resulting in products with medium-sized pores; in addition, there is a significant increase in the porosity and volume of the micropores.

Table 6. Percentage Adsorption Data of methane on non-activated (CC2-CD1) and activated carbons (CAs2-CAs1) at 40 and 60 °C.

Adsorbent	time (min)	Area methane (u.a.)	Adsorption (%)
60 °C			
CAs2	30,4	735	**33,47**
CAs1	30,4	487	**50,79**
CC2	30,3	1010	**7,16**
CD1	30,2	940	**6,81**
40 °C			
CAs2	30,4	1052	**6,42**
CAs1	30,4	1126	**8,27**
CC2	30,3	1175	**3,04**
CD1	30,4	1210	**2,78**

These "new" properties give activated carbons a high degree of hydrocarbon adsorption (Martínez et al., 2013). Based on these results, it is possible to indicate that the adsorption capacity of activated carbons increases due to the modification of their surface, which, after activation, exhibits chemical species that change its acidity, making it more reactive to the molecules of the hydrocarbon studied (methane).

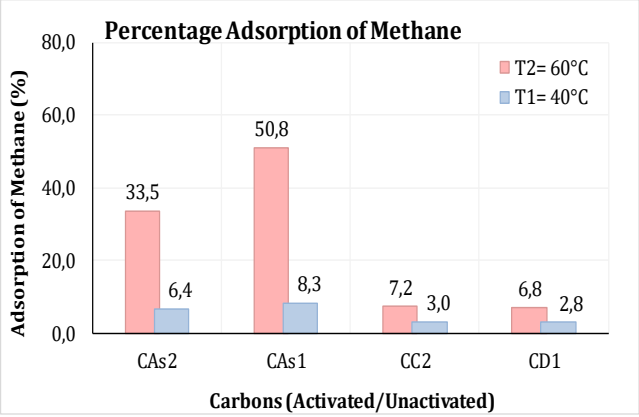

Fig. 13. Percentage Adsorption of methane on non-activated carbons (CC2-CD1) and activated carbons (CAs2-CAs1) at different temperatures 40 and 60 °C.

Due to 1) the nonpolar nature of activated carbons and 2) the type of forces involved in the different adsorption processes, they have the capacity to preferentially retain nonpolar molecules of high molecular weight (long-chain hydrocarbons, phenols, dyes, among others); while substances such as CH_4, CO_2, H_2, N_2, O_2, and H_2O are practically not retained by the carbon at room temperature.

This would explain the experimental results obtained: at 60 °C, the highest methane adsorption capacities are observed, with adsorption percentages between 33.5 and 50.8%, compared to the same activated carbons (CAs2-CAs1) tested at 40 °C, whose adsorption percentages are between 6.4 and 8.3 %, that is, below 10 % (Fig. 13, Table 6). Furthermore, the organic species studied (methane) that is expected to adsorb onto activated carbons has a low molecular weight and is highly diluted in high amounts of nitrogen (N_2/CH_4 100/3 mL); in this case, retention at room temperature by the carbon is only effective if it is impregnated with specific reagents or if the catalytic properties of the carbon are taken advantage of.

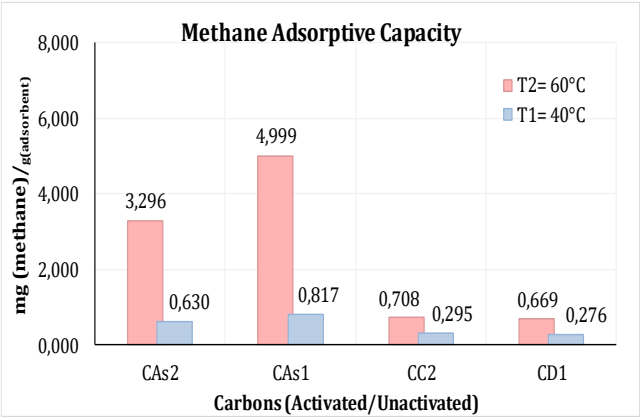

Fig. 14. Adsorptive Capacity of methane on non-activated carbons (CC2-CD1) and activated carbons (CAs2-CAs1) at different temperatures 40 and 60 °C.

Figure 14 shows the methane adsorption capacity for different activated (CAs2-CAs1) and non-activated (CC2-CD1) carbons at different working temperatures of 60 and 40 °C. In all cases, the interaction or adsorption force of the adsorbate (methane) with the surface of the adsorbent (carbonaceous species) is weak, favoring physisorption (Van Der Waals forces); in other words, high energies are not needed for the adsorption of the hydrocarbon to occur on the surface of the carbonaceous adsorbent (Droguett, 1983).

The activated carbon obtained from peach seeds, CAs1, at 60 °C (which showed the highest percentage adsorption of all the synthesized carbons 50.79%), shows an adsorptive capacity ~ 1,001 mg of CH_4 for every 1,968 mg of CH_4 injected into the total 103 *mL* that circulate through the system stream (Table 7).

Table 7. Adsorptive Capacity Data of methane on non-activated (CC2-CD1) and activated carbons (CAs2-CAs1) at 40 and 60 °C.

Adsorbent	ppm (CH_4) adsorbent	mg (CH_4) adsorbent	Cap. Adsorptive mg/g(adsorbent)
60°C			
CAs2	5188,40	0,659	3,296
CAs1	**7867,79**	**1,001**	**4,999**
CC2	1115,12	0,142	0,708
CD1	1053,13	0,134	0,669
40°C			
CAs2	991,22	0,126	0,630
CAs1	**1285,48**	**0,163**	**0,817**
CC2	464,63	0,059	0,295
CD1	433,66	0,055	0,276

grams $_{(adsorbent)}$ = 0,200
mg (CH_4) $_{(initials)}$ = 1,968

This allows us to determine that the adsorptive capacity of this solid is 4,999 mg of methane per 200 mg of initial adsorbent (~ 24,994 mg of methane per gram of activated carbon). A good CA-type adsorbent should have an adsorptive capacity between 20 and 50% of its own mass, which means that between 0.2 and 0.5 g of methane should be adsorbed per gram of activated carbon (Álvarez, 2016). The adsorption capacity for the other adsorbents is shown in Table 7.

Conclusions

Fourier Transform Infrared (FTIR) spectroscopy revealed the characteristic bands of carbonaceous materials and their transformation after treatment with nitric acid. The infrared spectra of the activated carbons exhibit typical functional groups of carbon materials, along with nitrate-related species that remain after washing the carbonized product with deionized water.

X-ray diffraction (XRD) patterns showed broad diffraction peaks, indicating the predominantly amorphous nature of the synthesized solids, with nanometric crystalline domains ($\lesssim$ 100 nm). A predominant hexagonal graphitic carbon phase (space group: $P6_3mc$) was identified using the PDF2-2004 ICDD database (card 01-088-0638) and confirmed through comparison with literature reports.

BET surface area analysis demonstrated that nitrogen adsorption increases significantly after activation with nitric acid. In all cases, Type I isotherms according to the Brunauer–Deming–Deming–Teller (BDDT) classification were observed, confirming the predominance of microporosity and relatively moderate surface areas. These results indicate that the synthesized materials contain a higher fraction of micropores compared to mesopores.

Textural analysis using SEM micrographs provided insight into the morphology of the prepared carbons. Non-activated coconut shell carbons exhibited smaller particle sizes compared to those derived from peach pits. The presence of cracks and openings in the peach pit-derived carbon (CD1) facilitates access to its internal structure, resulting in a higher surface area than in coconut-derived carbon (CC2), in agreement with BET results.

For activated carbon, the morphology of coconut-derived carbon (CAs2) showed minimal changes after nitric acid treatment, although a slight increase in particle dispersion was observed, thereby increasing surface area. In contrast, peach pit-derived activated carbon (CAs1) exhibited significant morphological changes, including reduced particle size and a pronounced increase in surface area, highlighting the stronger effect of HNO_3 activation.

Methane adsorption tests using gas chromatography demonstrated that nitric acid-activated carbons exhibit higher methane uptake compared to non-activated carbons, particularly at higher temperatures (60 °C vs. 40 °C). After saturation of the adsorbent, the initial methane concentration was recovered in all cases.

Temperature plays a crucial role in the adsorption process. At 60 °C, activated carbons showed the highest adsorption capacities, with methane adsorption percentages ranging from 6.8% to 50.8%, compared to values between 2.8% and 8.3% at 40 °C. The activated carbon derived from peach pits (CAs1) evaluated at 60 °C exhibited the highest adsorption capacity among all synthesized materials, reaching approximately 1.001 mg of CH_4 adsorbed per 1.968 mg of methane injected into the 103 mL gas stream.

4 References

Álvarez N., (**2016**), Capture from biogas streams adsorption processes for CO_2, Programa de Doctorado en Ingeniería Energética, Universidad de Oviedo, España, 50-51.

Araújo R., Azevedo D., Cavalcante C., Jiménez A., Rodríguez E., (**2008**), Adsorption properties of natural Cu(II), Zn(II) and Ag(I) exchanged Cuban mordenites, *Microporous and Mesoporous Materials*, Vol. 108 (1-3), pp. 213-222.

Armatas G., Petrakis D., Pomonis P., (**2005**), Estimation of diffusion parameters in functionalized silica's with modulated porosity: Part I: Chromatographic studies, *Journal of Chromatography Analysis*, Vol. 1074(1-2), pp. 53-59.

Da Costa A., De Carvalho S., Barros D., De Alcántara R., Oliveira M., (**2015**), Surface Modification of Commercial Activated Carbon (CAG) for the Adsorption of Benzene and Toluene, *American Journal of Analytical Chemistry*, Vol. 6(6), pp. 528-538.

Droguett S.E., (**1983**), *Elementos de Catálisis Heterogénea*, Serie de Química: Monografía, OEA. Programa Regional de Desarrollo Científico y Tecnológico,

Número 26 de Serie de química, Universidad de Texas, USA, 43-46.

Ferreira A., Mittelmeijer-Hazeleger M., Bliek A, (**2006**), Adsorption of normal and iso-butane on zeolite MFI, *Microporous and Mesoporous Materials*, Vol. 91(1-3), pp. 47-52.

Harcourt G.A., (**1942**), Tables for the identification of ore minerals by X-ray powder patterns, *The American Mineralogist*, Vol 27, 63-113.

Haynes H., (**1988**), The Experimental Evaluation of Catalyst Effective Diffusivity, *Catalysis Review Science Engineering*, Vol. 30(4), pp. 563-627.

Kim K-J., Ahn H-G., (**2010**), The adsorption and desorption characteristics of a binary component system of toluene and methylethylketone on activated carbon modified with phosphoric acid, *Carbon*, Vol. 48(8), pp. 2198-2202.

Lee W., Park J., Sok J., Reucroft P., (**2005**), Effects of pore structure and surface state on the adsorption properties of nano-porous carbon materials in low and high relative pressures, *Applied. Surface Science*, Vol. 246(1-3), pp. 77-81.

Liu B., Wang W., Wang N., Tong Au C., (**2014**), Preparation of activated carbon with high surface area for high-capacity methane storage, *Journal of Energy Chemistry*, vol. 23(5), pp.662-668.

Mattson J., Mark H., (**1971**), Activated Carbon: Surface Chemistry and Adsorption from Solution, Marcel Dekker, Inc New York, pp. 238-239.

Marín-Astorga† K., (**2015**), *Síntesis y caracterización de adsorbentes del tipo carbonáceos para trazas de metano*, Trabajo Especial de Grado (Lic. en Química), Laboratorio de Cinética y Catálisis, Departamento de Química, Facultad de Ciencias, Universidad de Los Andes, Mérida-Venezuela, pp. 1-84.

Martínez M., Molina M., Rodríguez F., (**2013**), *Preparación de carbones activados con KOH a partir de residuos de petróleo*. Adsorción de hidrógeno, Departamento de química inorgánica, Universidad de Alicante, España.

Nijhuis T., van den Broeke L., Linders M., van de Graaf J., Kapteijn F., Makkee M., Moulijn J., (**1999**), Measurement and modeling of the transient adsorption, desorption and diffusion processes in microporous materials, *Chemical Engineering Science*, Vol. 54(20), pp. 4423-4436.

Parida, S., (**2006**), Adsorption of organic molecules on silica surface Advances in Colloid and Interface, *Science*, Vol. 121, pp. 77-110.

Prado J., (**2018**), *Síntesis y caracterización de carbón activado obtenido a partir de residuos lignocelulósicos de la caña de azúcar, cáscara de coco y semillas de durazno y su empleo como adsorbente de CO_2, H_2 y CH_4*, Trabajo Especial de Grado (Lic. en Química), Laboratorio de Cinética y Catálisis, Departamento de Química, Facultad de Ciencias, Universidad de Los Andes, Mérida-Venezuela, pp. 1-122.

Primera O., Colpas F., Meza E., Fernández R., (**2011**), Carbones activados a partir de bagazo de caña de azúcar y zuro de maíz para la adsorción de cadmio y plomo. *Revista de la Academia colombiana de ciencias exactas físicas y naturales*, Vol. 35(136), 387-396.

Rampe J., Setiaji B., Trisunaryanti W., Triyono I., (**2011**), Fabrication and Characterization of carbon composite from coconut shell carbon, *Indian Journal Chemistry*, Vol. 11 (2), pp.124-130.

Rosquete C., S/A. Análisis orgánico (tablas). Laboratorio de Productos Naturales, Facultad de Ciencias, Departamento de química, Universidad de los Andes.

Yin Y., Zhang J., Sheng C., (**2009**), Effect of pyrolysis temperature on the char micro-structure and reactivity of NO reduction, *Korean Journal Chemistry Engineering*, Vol. 26(3), pp. 895-901.

Yalcin M., Arol A., (**2002**), Gold cyanide adsorption characteristics of activated carbon of non- coconut shell origin, *Hydrometallurgy*, Vol. 63(2), pp. 201-206.

Received: *november 22, 2025*

Accepted: *february 22,2026*

Lugo González, Claudio Antonio: *Ph.D. in Applied Chemistry, mention Materials Studies, 2017, Universidad de Los Andes; Professor of Chemistry Department (Kinetics and Catalysis Laboratory), at the Faculty of Sciences, ULA. Mérida, Venezuela.*

https://orcid.org/0000-0001-8003-0354

Marín Astorga, Karina†: *Bachelor's Degree in Chemistry, 2015, Chemistry Department (Kinetics and Catalysis Laboratory) at the Faculty of Sciences, Universidad de Los Andes, Mérida. karinasolangemarinastorga@gmail.com*

Pérez Dávila, Patricia: *Ph.D. in Drug Chemistry, 2017, Scientific Research Institute, Faculty of Pharmacy and Bioanalysis, Universidad de Los Andes; Professor of Polymer Laboratory at the Faculty of Sciences, ULA. Mérida, Venezuela. Email: perezdpatricia@gmail.com*

https://orcid.org/0000-0003-0591-2351

Vizcaya, Marietta: *Ph.D. in Drug Chemistry, 2014, Scientific Research Institute, Faculty of Pharmacy and Bioanalysis, Universidad de Los Andes; Professor of Polymer Laboratory at the Faculty of Sciences, ULA. Mérida, Venezuela. Email: marietta@ula.ve*

https://orcid.org/ 0000-0002-2064-4175

Rondón Contreras, Jairo: *Ph.D. in Applied Chemistry, mention Materials Study, 2015, Universidad de Los Andes; Professor of Biomedical & Chemical Engineering Departments, at the Polytechnic University of Puerto Rico, San Juan, PR-USA. Email: jrondon@pupr.edu*

https://orcid.org/0000-0002-9738-966X

Rodríguez Sulbarán, Pedro: *Doctor of Science in Chemistry, 2025, Universidad de Concepción, Chile; Ph.D. in Applied Chemistry, mention Materials Studies, 2015, Universidad de Los Andes; Professor of Chemistry Department (Kinetics and Catalysis Laboratory), at the Faculty of Sciences, ULA. Mérida, Venezuela. Correo electrónico: pedrojrs@gmail.com*

https://orcid.org/0000-0002-1309-8532

Artículo de Investigación. Revista Ciencia e Ingeniería. Vol. 47, No. 2 pp. 165-180, abril-julio, 2026.
ISSN 1316-7081. ISSN Elect. 2244-8780 Universidad de los Andes (ULA)

Study of *Sardinella aurita* mortality in Las Piedras Bay

Estudio de la mortandad de *Sardinella aurita* en la bahía de Las Piedras

De Lima, Aída[1]*; Veroes, Carlos[2]; Méndez, Karelys[3]; Muñoz, Alexandra[4]; Sánchez, María[5]
[1] Laboratory of Physical Chemistry and Environmental Microbiology, School of Chemical Engineering, Faculty of Engineering, Universidad de los Andes (ULA), Mérida, Venezuela.
[2] Department of Fisheries Sciences, Universidad Nacional Experimental Francisco de Miranda (UNEFM), Falcón, Venezuela.
[3,4] Department of Chemistry, Universidad Nacional Experimental Francisco de Miranda (UNEFM), Falcón, Venezuela.
[5] Master's Degree in Agricultural Development, Universidad de los Andes, Mérida, Venezuela
*aidajdl@gmail.com

Abstract

Las Piedras is a coastal town on the Paraguaná Peninsula in Falcón State, where a high mortality rate of Sardinella aurita occurred in its bay during October 2009. This event triggered a series of environmental problems that prompted an investigation into the causes of the species' deaths. The research design was non-experimental, field-based, and explanatory. The study examined the physicochemical, environmental, and biological variables of Las Piedras Bay during the period of the phenomenon. The results were analyzed using a one-way analysis of variance with Tukey and Duncan's post-hoc tests. The findings determined that the fish died due to a synergistic effect of oxygen deficiency at night, feeding failure, and thermal stress, resulting from possible stratification of water masses caused by altered environmental conditions in the area due to the El Niño phenomenon.

Keywords: *Bahía de las Piedras, fish mortality, Sardinella aurita.*

Resumen

Las Piedras es un pueblo costero de la Península de Paraguaná del Estado Falcón, en el que durante el mes de Octubre de año 2009 se presentó una elevada mortandad de Sardinella aurita en su Bahía, desencadenando una serie de problemas ambientales que despertaron el interés por determinar las causas de la muerte de esta especie en la bahía de Las Piedras. El diseño de la investigación es no experimental, tipo de campo y nivel explicativo. En esta se estudiaron las variables físicoquímicas, ambientales y biológicas de la Bahía de Las Piedras durante los días del fenómeno. Los resultados obtenidos se analizaron mediante un análisis de varianza de un solo factor con pruebas a posteriori de HDS Tukey y Duncan, determinándose que las especies murieron por un efecto sinérgico entre déficit de oxígeno durante la noche, fallas de alimentación y estrés térmico, a consecuencia de una posible estratificación de las masas de agua debido alteración en las condiciones ambientales de la zona, causadas por la presencia del fenómeno El Niño.

Palabras claves: Bahía de las Piedras, mortandad de peces, Sardinella aurita.

1. Introduction

Venezuela is an important fishing country in the Caribbean. Across its vast territory, the country possesses fishery resources in both its marine and riverine environments, characterized by their high diversity and growing potential (FAO, 2025). The *Sardinella aurita* stands out as Venezuela's most important hydrobiological resource, being the most accessible source of animal protein for the population (Gómez, 2022).

The Venezuelan coastline stretches for 2,830 km and has a continental shelf of 90,000 km². With the creation of the new Maritime Legal Regime, national jurisdiction was extended to 200 nautical miles (Organic Law of Aquatic Spaces, 2014), establishing an extensive exclusive economic zone of approximately 640,000 km². This represents a

significant opportunity to expand and develop fishing activity through the comprehensive utilization of marine resources.

Las Piedras is a coastal town on the Paraguaná Peninsula, located in the North Parish of the Carirubana Municipality in Falcón State, Venezuela. Its economy is based primarily on artisanal fishing and shrimp farming, making it a town of great importance to the fishing industry (García, 2023).

The inhabitants of this community reported that at the end of the second week of October 2009, a high mortality rate of *Sardinella aurita* began to occur in the bay. This worsened in the third week of October with an increase in the biomass of dead fish, triggering a series of environmental problems. This prompted their interest in understanding the causes of this situation.

Given this problem, and in order to find answers to this question, document the facts, and lay the groundwork for future studies on this or similar events, the present investigation was undertaken. Its objective was to determine the causes of the *Sardinella aurita* mortality in Las Piedras Bay, Carirubana Municipality, Falcón State.

The study was carried out as part of an extension project developed in the community of the Las Piedras sector of the North parish, Carirubana municipality of the Falcón state by an interdisciplinary team from UNEFM and ULA, during 9 months, in the period between the end of October 2009 and July 2010, time during which the project was developed and the actions undertaken by the community were monitored.

2. Theoretical Framework

2.1 Background on Aquatic Species

The Pan American Health Organization (PAHO, 2009) reported the most significant and recent mortality event of aquatic species in the Caribbean Sea, occurring between July and September 1999, due to the number of countries affected almost simultaneously. This phenomenon affected numerous waters of the countries of the Caribbean Community and Common Market (CARICOM), including Grenada, Saint Vincent and the Grenadines, Barbados, and Tobago. Other affected countries were Guyana in July and Venezuela in August; no other CARICOM country reported fish mortality. The study did not provide definitive evidence to link the fish deaths to a single factor; these incidents were more likely due to the action and interaction of several physicochemical and biological environmental factors (PAHO, 2009).

Pomares (2004), in his study on the mass mortality of bivalve mollusks in Amuay Bay, Venezuela, concluded that the mollusk mortality was due to the deposition of contaminated and previously suspended sediments from the southern part of the bay (with historical pollution patterns) onto the mollusk beds to the north (with little or no pollution), which suffocated and impregnated the species. Globally, many causes have led to the mortality of aquatic species, both marine and freshwater. In 2009 alone, the following events occurred: On February 17, Herrera (2009) published an article on fish mortality in Santa Marta Bay, Colombia. The results of the investigations, provided by the José Benito Vives de Andréis Institute of Marine and Coastal Research (INVEMAR, 2009), revealed that the convergence of several factors, including the influx of wastewater, limited water circulation in the area, and a massive presence of fish, caused the oxygen levels to drop to anoxic levels, resulting in the mass death of the fish by asphyxiation.

According to information published by Bionero (2009), in May of that year, approximately nine tons of dead fish of various species appeared in the Laguna del Carpintero in the city of Tampico, Mexico. These included snook, tilapia, carp, shad, silver catfish, catfish, mullet, and crab, some weighing up to 3 kilograms. The investigation concluded that the cause of death was oxygen deficiency in the water.

The environmental magazine Catorce 6 (2009) from Cartagena, Colombia, published an article entitled: "Temperature change would be responsible for another fish kill in Cartagena," this event occurred in August in the Chambacú lagoon, where the conclusion was that the death of species occurred due to an increase in the temperature of the lagoon water.

2.2 The Sardine (*Sardinella aurita*)

His is a coastal pelagic species that forms very compact schools. It is distributed from the United States to Brazil and has also been reported in the Mediterranean Sea and the western Pacific. In Venezuela, it is found mainly in the eastern part of the country and is associated with the highly productive coastal zone due to upwelling (Castillo et al., 2012; Mendoza et al., 2021; González et al., 2021).

The continental shelf off northeastern Venezuela represents the most important fishing area in the Caribbean Sea. This is largely attributed to the upwelling event produced by local winds, which establishes high biological productivity reflected primarily in the increase in the biomass of planktonic organisms, which, through filter feeding, constitute the main food source for sardines (Castillo et al., 2012; Gómez, 2022; González et al., 2021; Mendoza et al., 2021).

In Venezuela, sardines are considered a strategic resource because they represent a low-cost protein source and support the country's most socio-economically important artisanal fishery, due to the large catch volumes and the numerous jobs generated by their extraction. However, since 2005, the sardine fishery has suffered a significant collapse, possibly due to a combination of environmental factors and overfishing (Castillo et al., 2012; Gómez, 2022).

2.3 Self-purification in water

Zaror (2000) explains that living activity gives a body of water a certain capacity for self-purification, since the organic compounds that are discharged into it are consumed by heterotrophic microorganisms. As a result of metabolic activity, the dissolved organic compounds are transformed into cellular biomass, CO_2 and other simple inorganic compounds.

The same author states that the capacity for self-purification is highly dependent on the availability of dissolved oxygen in the water. This element is the essential reactant in aerobic systems. When aerobic organisms metabolize, organic nutrients simultaneously consume dissolved oxygen. The high metabolic requirements of the gas are offset by its low solubility in water (in the range of 7-10 g/m3). If the rate of oxygen transfer from the air into the water is less than the rate of its metabolic consumption, its concentration in the water will gradually decrease, eventually becoming a limiting reactant in intracellular oxidation reactions.

The reduction in oxygen availability will primarily affect the higher organisms in the food chain. This will cause an imbalance in the population equilibrium, leading to a rapid increase in the number of microorganisms in the water body. As a consequence, oxygen consumption increases, eventually creating an anoxic aquatic environment (Zaror, 2000).

2.4 Biological Parameters of Water Quality

Water is a medium where thousands of biological species live and carry out their life cycle. According to Arellano (2002), the range of aquatic species in size and diversity extends from unicellular organisms to the largest fish, and these are, in a sense, parameters of water quality, since their presence or absence can indicate the condition of a body of water. If it contains a wide variety of species in a balanced proportion, it can be considered a healthy system.

2.5 *Physicochemical Parameters of Seawater*

These are variables that allow us to understand the behavior of aquatic ecosystems over a specific period of time. They can be useful for identifying the possible causes of abnormal events in these ecosystems. Some of the most important parameters are:

2.5.1 Sea Surface Temperature (SST)

SST is one of the most widely used oceanographic variables as an environmental indicator because it is related to physical aspects such as ocean currents, surface wind intensity, mixed layer dynamics, precipitation, solar radiation intensity, upwelling, and sea level changes. Furthermore, it is related to life cycles, metabolism, population factors, organism stress, and, in general, all biological variability (Bernal et al., 2006).

In the oceans, temperature limits are between 2 and 30 °C. Increased temperature intensifies respiration; in some zooplankton, respiratory activity doubles when the water temperature rises from 10 to 20 °C. An increase in this parameter implies an increase in metabolism and greater gill permeability. Fish are poikilothermic, meaning they cannot regulate their body temperature. There is a direct relationship between water temperature and their metabolic rate; increases in temperature cause hyperventilation, loss of appetite, lethargy, and even death. According to Seoanez (2000), temperature can influence the mortality rate of various species and is crucial for the survival of juvenile sardines. It also affects the amount of dissolved oxygen. Water at 15°C can contain 10 mg/L of oxygen, while at 30°C it can only contain 1 mg/L.

2.5.2 Oxygen

Oxygen is a non-conservative gas and, like other gases, is dissolved in seawater. The solubility of oxygen in water depends on the partial pressure of the gas, the temperature, and the salinity of the water; it increases with the first and decreases with the latter two. According to SHOA (2007), dissolved oxygen in seawater comes from the atmosphere and is a product of photosynthesis.

Dissolved oxygen unsaturation is often observed in waters where its consumption through the decomposition of organic matter is high and its renewal through water circulation is low. Extreme situations of unsaturation have also been observed in very isolated areas with very low circulation and large inputs of organic matter, whether natural or deposited by humans, where dissolved oxygen becomes depleted, producing an anoxic condition that prevents the development of aerobic organisms. Fish need high oxygen levels of at least 5 mg/l, invertebrates need lower levels, and bacteria need the lowest levels (SHOA, 2007; Seoanez, 2000).

2.5.3 Phosphates, Nitrates, and Silicates

These are important nutrient salts whose depletion in water limits organic production. The amounts of these elements in a location indicate its potential fertility and the biological processes that have occurred or are occurring there. Nutrient pollution, especially from nitrogen and phosphorus, has consistently been identified as a major cause of degradation in some U.S. waters for over a decade. Excess nitrogen and phosphorus lead to significant water quality problems, including harmful algal blooms, hypoxia, and the decline of wildlife and wildlife habitat (Ager et al., 1974).

2.5.4 Salinity

This is the most commonly used measure of seawater salinity and is defined as the total number of grams of inorganic salts dissolved in 1 kg of seawater (S‰). The average salinity of seawater is 35‰, which is equivalent to 35 g of salts in 1 kg of seawater. According to SHOA (2007), salinity changes are important in pollution phenomena, since

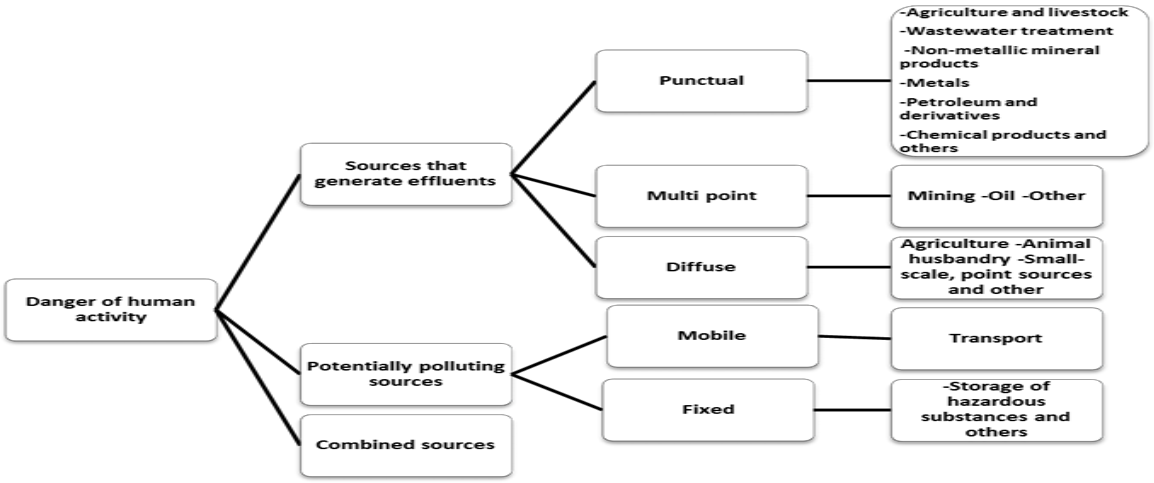

Figure 1. Types of water pollution sources according to the method of effluent production. Source: (INVEMAR, 2009).

lower salinity increases the toxicity of certain heavy metals such as mercury, copper, and cadmium, among others. Seoanez (2000) states that salinity variations far from the coast are relatively small, but are considerable in coastal areas due to changes in runoff, which influence the osmotic balance of fish and the buoyancy of pelagic eggs.

2.5.5 Hydronium Ion Potential (pH)

In a body of water, pH is a parameter to consider when determining the solubility of various organic and inorganic substances in water. It is an abiotic factor that regulates enzyme-mediated biological processes (photosynthesis, respiration), as well as the availability of essential nutrients that limit microbial growth in many ecosystems (NH_4^+, PO_4^{-3}, and Mg^{+2}), the mobility of heavy metals such as copper, which is toxic to many microorganisms, and also affects or regulates the structure and function of macromolecules and organelles such as nucleic acids, structural proteins, and cell wall and membrane systems. Variations in pH can therefore have marked effects on each level of organization of living matter, from the cellular level to the ecosystem level (Seoanez, 2000).

2.5.6 Heavy Metals

Heavy metal pollution is one of the major pollution problems in the coastal marine environment. The main problem with these elements in the marine environment is that they are not degraded by microbial activity; on the contrary, they can be enriched by organisms that sometimes form organometallic complexes; others, when present in concentrations that exceed natural levels, cause serious ecological problems as a result of bioaccumulation and biomagnification processes through the food chain (Ansari, et al., 2004).

2.5.7 Thermocline

This is defined as the "layer of marine or lacustrine water whose temperature decreases rapidly with depth." It is the zone of the ocean's surface layer where the seawater temperature decreases rapidly vertically, with little increase in depth. It constitutes a thin layer of water located between the warmer surface and the colder bottom (Trujillo and Thurman, 2016; Wetzel, 2001; Garrison and Ellis, 2016).

2.5.8 Terrestrial Sources of Pollution

The risk and hazard of pollution sources are related to the environment's capacity to assimilate, process, disperse, dilute, or filter the waste or effluents that enter the physical environment, transporting them to locations where the impacts are of low or moderate severity, keeping them below the levels permitted by current legislation or acceptable standards (Fernández, 2006).

The external factors that give rise to a risk situation represent the hazard; therefore, they can be called the "source of risk," whether natural or induced by human activity, with the potential to cause damage.

Water pollution sources can be natural, usually very dispersed and not causing high concentrations of pollution, except in some very specific locations, or anthropogenic (human activities), which present some type of hazard to the quality of the water resource, as shown in Figure 1.

2.6. National and international standards

2.6.1 Main laws

The Constitution of the Bolivarian Republic of Venezuela (1999), in Articles 127, 128, and 129, establishes environmental rights and the State's obligation to protect water resources. Within this framework, the fundamental pillar is the Water Law (2007), which establishes provisions for the integrated management of water as an essential element for life and sustainable development. Likewise, the Environmental Criminal Law (2012) criminalizes actions that degrade, pollute, or poison water sources.

2.6.2 Technical Standards (Official Gazettes)

Decree 883 (Extraordinary Official Gazette No. 5,021, 1995), which establishes the "Standards for the Classification and Quality Control of Water Bodies and Liquid Discharges." Article 12 of this decree establishes the maximum permissible concentration levels of metals in discharges into the marine environment. The criteria established by the international EPA standard (2002), which has allowed for the evaluation of the environmental quality of coastal and estuarine ecosystems, were also used as a reference for the assessment.

3. Experimental Procedure

This study used a non-experimental, field-based, and explanatory research design. To carry out the research, the mortality of the species was characterized in situ using an adaptation of the instrument "*Monitoring and Advisory Program for Cases of Fish Mortality in Aquatic Environments of the Province of Buenos Aires*" (MAA, 2007).

Water samples were collected randomly in five (5) stations of the bay at the surface, in accordance with the General Plan for Global Research on Marine Pollution and Guidelines for Basic Studies (UNESCO, 1976), In the lab, dissolved oxygen, nitrogen, phosphorus, and the heavy metals lead, copper, cadmium, and zinc, were determinated according to Standard Methods (APHA, 1995).

Species sampling consisted of collecting 15 specimens of (Sardinella aurita). Necropsies of collected species were performed according to the necropsy protocol for aquatic specimens at the "laboratorio de Ciencias Biológicas del Programa de Ingeniería Pesquera de la UNEFM". Temperature and salinity were measured at surface in each station using a YSI multiparameter probe (Yellow Springs Instruments), and pH with a digital pH meter.

Sea Surface Temperature (SST) and Chlorophylla concentrations in the area were evaluated using information from the Cariaco Project of the "Instituto de Tecnología y Ciencias Marinas" (2009) at Simón Bolívar University. Information regarding wind speed and direction was also requested from the National Institute of Civil Aeronautics (2009), located in the control tower of the Josefa Camejo Airport in Punto Fijo. Statistical analyses include one-way analysis of variance (ANOVA) and Tukey and Duncan post-hoc tests.

Figure 2. Bahía de Las Piedras, October 30, 2009 (during the *Sardinella aurita* mortality)

4. Results and Discussion

4.1 In situ characterization of species mortality

On October 30, 2009, the Las Piedras Bay pier was visited to gather details about the species mortality reported by affected residents. It was observed that there was indeed a large number of dead fish on the bay shores and floating on the water's surface, primarily the Sardinella aurita species. An iridescent surface film with a diesel odor was also observed. Therefore, information was collected from community members, yielding the following results:

4.1.1 General Data on the Phenomenon

Community members reported that the phenomenon began on October 16, 2009, between approximately 2:00 am and 3:00 am, when they observed fish rising to the surface and exhibiting erratic swimming. This situation lasted only a few minutes; afterward, the fish would die, floating to the surface and piling up along the shore. Despite this, the community members stated they hadn't paid much attention to the situation, assuming they were simply fish caught in the fishing nets (seines) set in the area, which were released when the catch was hauled in.

However, by Thursday, October 29, 2009, the situation had gradually worsened with the continued accumulation of dead marine life on the beach, causing foul odors, a proliferation of flies, and the potential outbreak of disease. They also stated that this situation had never before occurred on the shores of the bay.

4.1.2 Data Regarding the Fish.

Regarding the species involved, it was determined through information from local residents (mostly fishermen), as well as through direct observation and subsequent taxonomic classification, that the most affected species was the Sardine *(Sardinella aurita),* followed in much smaller quantities by the Corocoro (*Haemulon plumieri*). The size was relatively uniform, with most fish being small, and the approximate quantity exceeded 1000 kg. Most of the fish found on the banks were in a state of decomposition, while those observed in the water were either dying or dead. No external abnormalities were observed in the dead specimens in the water, and those on the banks exhibited characteristics consistent with decomposition (swelling of the ventral area and a putrid odor). The fish kill was progressive. It was also observed that dead fish were present on nearby beaches such as Villa Marina, Punta Cardón, Amuay, and Los Taques, carried to the shore by the surface currents of the bay

4.1.3 Data Regarding the Body of Water

The environment where the fish kill occurred is a bay with open access to both the Caribbean Sea and the Atlantic Ocean. Its location is at 11° 42' 23.99" N latitude and 070° 12' 55.65" W longitude. The surface area is approximately 225 hectares, the bottom is sandy, and the predominant vegetation is floating.

4.1.4 Observations Regarding the Last Week

The community reported that the most noticeable change was the formation of a shiny, iridescent film on the water's surface, with a strong, characteristic diesel odor and abnormal behavior in the area's birds, which were not feeding as they normally did on the species found in the bay. They also reported the gradual appearance of dead fish, mainly sardines.

4.1.5 Climatic Data from the Days Prior to the Phenomenon

The residents of Las Piedras reported that in the days prior, there was an almost total absence of wind in the area, with completely clear skies and no rain, as well as abnormally high water and air temperatures.

Table 1. Average concentration in ppm of heavy metals in the water of Las Piedras Bay.

Date (ppm)	*CCM	30/10/2009	05/11/2009	24/11/2009
Cadmium	40	0,2667±0,0033[a]	0,2629±0,0052[a]	0,5677±0,0044[b]
Copper	4,8	0,1100±0,0000[a]	0,0943±0.0037[a]	0,1485±0,0036[b]
Lead	210	1,1167±0,0088[a]	1,0571±0,0187[a]	1,9362±0,0760[b]
Zinc	90	0,1067±0,0328[a]	0,0671±0,0061[a]	0,0969±0,0072[b]
Nickel	74	0,7067±0,0240[a]	0,7129±0,0151[a]	1,5577±0,0151[b]

[a,b] The mean metal concentrations for each sample with different superscripts are significantly different.
CCM, maximum permissible concentration for saline surface waters in ppm, according to EPA regulations (2002).

4.1.6 Human Activity Surrounding the Body of Water

At the time of the event, the Las Piedras sector had a population of 1,504 people. In some cases, due to sewage pipe collapses, waste ends up in the bay's waters. There are various industries that can affect the beach's water quality, including PDVSA, the military pier of the Naval Base, the fishing pier for the local artisanal boats, and the Las Piedras pier, where industrial trawlers have been anchored since March 2009, awaiting conversion or scrapping. There are also restaurants, inns, fish markets, and other businesses that, according to information provided by the community, occasionally discharge their waste directly into the sea. In addition, there is constant jet skiing activity, as well as artisanal and industrial boats. The predominant construction materials are fiberglass, naval steel, and wood. There is no direct presence of agricultural, forestry, or aquaculture activity in the area.

4.2 Physicochemical Variables of the Water in Las Piedras Bay

4.2.1 Metals

Table 1 shows that the concentrations of cadmium, copper, lead, zinc, and nickel (in ppm) in the bay water sampled on days within the mortality period were below the levels specified in national (Decree 883) and international EPA (2002) standards. Specifically, the EPA values were lower than the maximum concentration limits at which the marine ecosystem is affected. However, an increase in the presence of these contaminants was observed on November 24th, although the recorded values did not exceed the levels considered hazardous.

The one-way analysis of variance shown in Table 1 demonstrates that in 2009, the metal concentrations for October 30 and November 5 differed significantly ($p < 0.05$) from the sample taken on November 24 of the same year. This could indicate that the concentrations obtained in the water on that day reflect the effects of specific events that can change over short periods. This phenomenon may be influenced by changes caused by water discharges and variations in the suspended solids load, which are ultimately deposited in the sediments through various physicochemical processes.

4.2.2 Temperature.

Table 2 shows the monthly variation in sea surface temperature (SST) from 2004 to 2009. The observed pattern coincides with that described by Arteaga (2009) for the years 1995 to 2005, characterized by low SSTs at the beginning of the year, between January and March, and the highest temperatures during September and October.

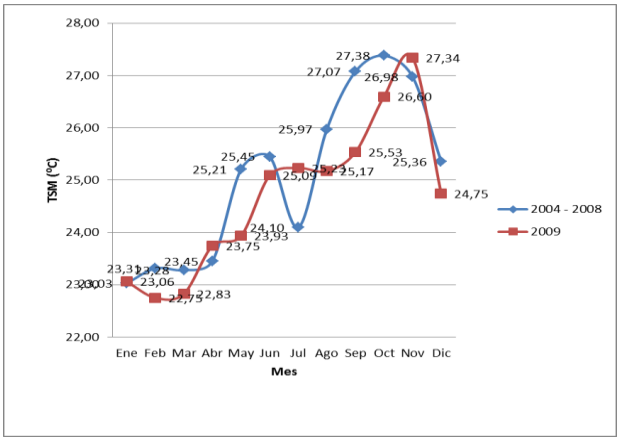

Figure 3. Variación de las medias de TSM para el promedio del periodo 2004 al 2008 comparado con el año 2009.

Table 2. Average Monthly Sea Surface Temperature (SST) in °C, per Year

Year / Month	2004	2005	2006	2007	2008	2009
January	22,47±1,18	23,65±1,43[a]	23,55±0,76	22,52±1,25[b]	22,94±0,99	23,06±1,05
February	24,37±0,77[a]	24,73±1,14[a]	22,86±1,23[b]	22,25±1,12[b]	22,36±0,80[b]	22,75±0,63[b]
March	23,09±0,86[a,c]	25,06±1,06[b]	23,36±1,17[a]	22,61±0,54[a]	22,27±0,90[c]	22,83±0,62[a]
April	23,74±2,13	23,74±1,19	23,48±1,99	23,86±1,64[a]	22,45±1,10[b]	23,75±1,05[a]
May	24,21±1,97[a,c]	25,62±2,49[a]	25,59±0,85	26,24±1,41[b]	24,38±1,33	23,93±1,47[c]
June	23,70±1,27	26,37±1,74	26,07±0,93	25,68±1,95	25,43±0,88	25,09±1,15
July	23,23±1,25[a]	25,32±1,56[b]	24,37±1,40	23,47±1,64[a]	24,11±1,06[a]	25,23±1,00[b]
August	25,36±2,43[a]	25,45±2,17[a]	24,97±1,01[a]	28,02±1,32[b]	26,05±1,88[a]	25,17±0,78[a]
September	27,02±2,00[a,b,c]	26,35±1,60[a]	26,87±1,15[a]	27,76±1,19[b]	29,39±1,27[d]	26,00±1,19[c]
October	27,55±1,79	28,55±0,77[a]	27,83±1,00[a]	28,53±1,05[a]	28,27±1,46[a]	26,60±1,20[b]
November	26,05±1,38[a]	26,87±1,74	27,23±1,12	27,56±1,21[b]	27,18±1,21	27,34±1,20[b]
December	24,80±1,16[a]	25,17±1,56	25,72±1,17	25,16±1,64	25,94±0,75[b]	24,75±1,08[a]

[a,b,c] The average monthly temperatures for each year with different superscripts are significantly different ($p < 0.05$).

Figure 3 shows an increasing trend in SST averages from 2004 to 2008, from January to October. This contrasts with the monthly averages for 2009, where the increasing trend begins in February and ends in November. This observation is corroborated in Table 2 by the analysis of variance, which demonstrated significant differences in monthly sea surface temperatures (SSTs) for the years 2004 to 2008 compared to 2009. The analysis showed that 2009 differed from the other years primarily in the month of October, while the other months did not show significant differences. This suggests that the increase in temperature is one of the possible variables involved in the mortality of *Sardinella aurita.*

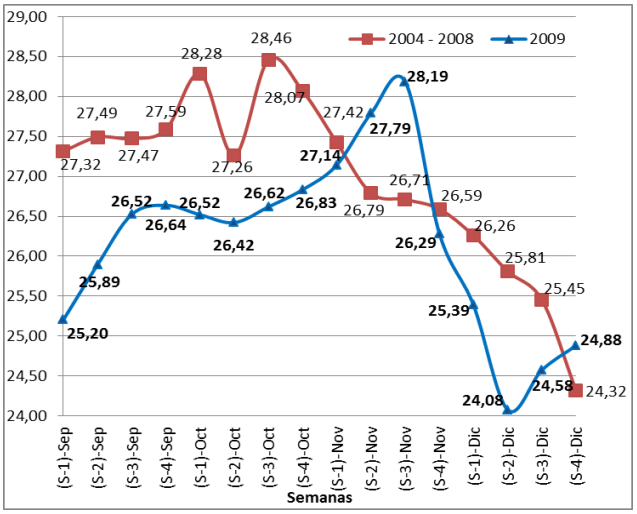

Figure 4. Average weekly variation of the SST during the months of September to December in the years 2004 – 2008 and 2009.

In order to observe the behavior of the SST in detail, Figure 4 shows the average weekly variation of the temperature, during the months of September to November for the years 2004 to 2008 in contrast to 2009. It can be seen that in the latter, there is a completely different behavior to the average of the years 2004 to 2008, showing a tendency to increase the temperature from the fourth week of October, when according to the behavior of the years 2004 to 2008 the temperature should have decreased.

During the last weeks of October 2009, significant daily temperature variations were observed, as shown in Figure 5, with differences of up to 3°C on some days. This abnormal temperature behavior coincided with the beginning of the die-off of species in Las Piedras Bay, as reported by local residents.

The prolonged period of high temperatures in 2009 is

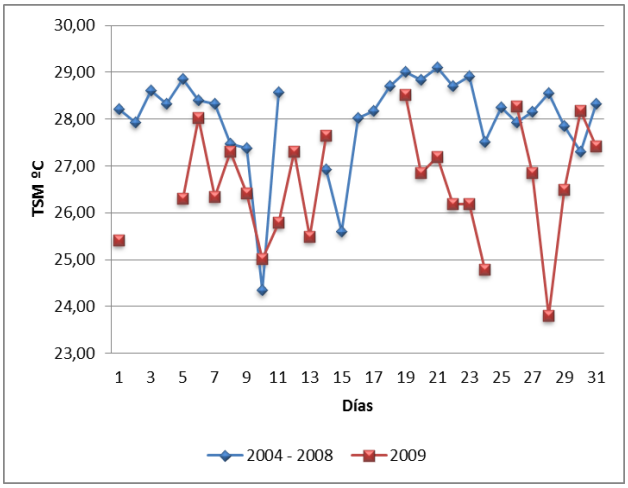

Figure 5. Daily variation of the SST during the month of October of the years 2004 – 2008 and 2009.

Table 3. ANOVA of Average Fortnightly Temperatures in °C for the Month of October from the Years 2004 to 2009.

Year Fortnight	2004	2005	2006	2007	2008	2009
1st	27,02±2,35	28,73±0,51	27,59±0,66	28,51±1,31	28,19±2,38	26,46±1,05
2nd	28,09±0,94[a]	28,09±0,94[a]	28,49±0,61[a]	28,01±1,18[a]	28,55±0,59[a]	26,73±0,40[b]

The average fortnightly temperatures for each year with different superscripts (a,b,c) are significantly different .

related to the El Niño phenomenon detected by NOAA (2009), which reported abnormal temperature increases in the tropical Atlantic Ocean starting in October of that year, along with a decrease in winds and convection currents. These conditions hindered the mixing processes that promote primary productivity and, consequently, the production and dissolution of oxygen in the water, which could be fatal for the species found there.

On the other hand, Gonzales et al. (2007) report a negative correlation between sea surface temperature (SST) and the distribution of *Sardinella aurita*, implying that this species is severely affected by increased temperatures. Similarly, Hernández (2009) states that sardines are organisms that are stressed by temperature changes; specifically, the species *Sardinops sagax* exhibits a thermal preference in the range of 17°C to 20°C with a maximum critical temperature of 26°C to 32°C. The same author obtained mortality rates of 40% for temperature increases from 18°C to 23°C, and also noted that at a constant temperature between 15°C and 27°C, mortality exceeded 70% at the highest temperature.

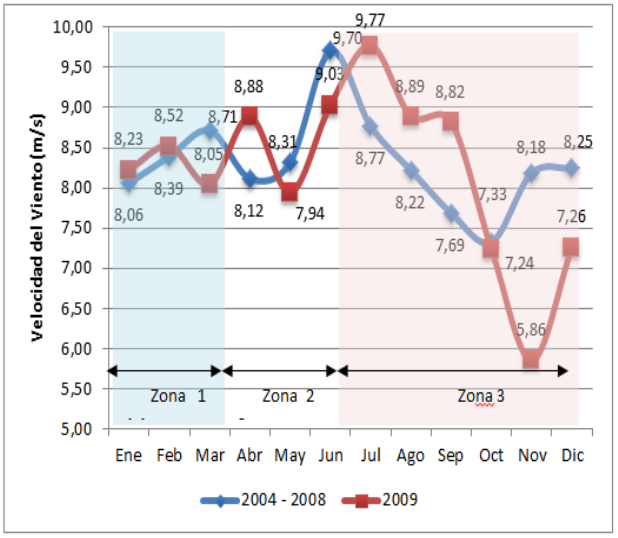

Figure 6. Monthly variation of wind speed for the years 2004–2008 and 2009.

Table 3 below presents the results of the one-way analysis of variance (ANOVA) applied to the bi-weekly average temperatures for the years 2004 to 2009. The results showed significant differences ($p < 0.05$) in sea surface temperatures (SSTs) for the last two weeks of October from 2004 to 2009. Duncan's post-hoc test and Tukey's HSD test for the bi-weekly averages showed that 2009 differed from the other years only in the last weeks of the month, while the other weeks showed no significant discrepancies. This supports the hypothesis that temperature variation may have contributed to the mortality.

However, in Figure 5 we can also observe that for the average of the years 2004 to 2008, temperatures were higher than those reported in 2009, without any species mortality occurring, which is indicative that although the variation of the SST affected the species, it could not by itself generate the phenomenon, so it is inferred that other factors could also have influenced as possible causes of the mortality.

4.3 Meteorological Variables

4.3.1 Wind Direction and Speed

Table 4 shows the analysis of variance for wind speed from 2004 to 2009. This analysis demonstrated significant differences ($p < 0.05$) in wind speed between these years.

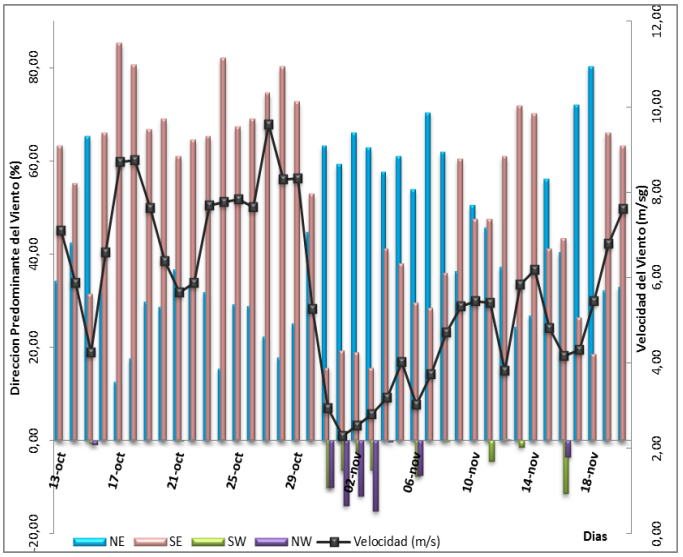

Figure 7. Wind speed and direction from the second half of October to the first half of November

Duncan's post-hoc test and Tukey's HSD test for monthly averages showed that wind speed in 2009 differed significantly from the other years in November, while the other months showed no significant differences.

and October (7.69 m/s and 7.33 m/s respectively). In the figure, three zones are also distinguished in which the average speed of the years 2004-2008 increases to a maximum point and then decreases.

Table 4. *Monthly Average Wind Speed in m/s for the Years 2004 to 2009.*

Year / Month	2004	2005	2006	2007	2008	2009
January	8,12±1,55	7,88±2,00	7,62±1,79	8,53±1,40	8,19±1,71	8,10±1,82
February	8,64±1,44	8,49±1,40	8,39±1,06	8,00±2,17	8,45±2,11	8,52±1,89
March	8,94±1,99	9,00±1,89	8,65±1,26	8,64±1,43	8,23±1,37	8,04±1'40
April	8,26±2,46	8.44±2,81	7,60±2,42	8,04±1,91	8,27±2,18	8,88±1,68
May	8,52±2,33	7,77±2,38	8,17±2,14	8,13±1,78	9,00±1,60	7,94±2,24
June	10,54±1,27[a]	8,37±2,47[b]	9,55±1,85	10,44±1,83[a,c]	9,63±1,14	9,03±1,82[b,c]
July	8,71±1,69	8,41±2,35	9,46±2,41	8,58±2,04	8,64±1,80	9,76±1,37
August	9,49±2,09[a]	7,88±2,01	8,41±1,78[a]	8,62±2,24[a]	6,53±2,62[b]	8,89±1,80[a]
September	6,56±2,26	8,01±2,30	8,18±2,14	8,21±2,66	7,48±2,78	8,62±1,50
October	7,31±1,81	6,59±2,58	8,49±3,24	6,43±2,29	7,91±3,00	7,24±1,58
November	8,18±2,41[a]	7,90±2,57[a]	8,31±1,17[a]	8,91±2,02[a]	7,65±1,51[a]	5,86±2,21[b]
December	7,33± 1,65[a]	8,83± 1,93 [b,c]	9,28±1,53 [b]	7,90± 1,74[a,c]	7,90±1,28 [a,c]	7,26± 1,37[a]

The average wind speeds for each year with different superscripts (a,b,c) are significantly different.

Figure 6 illustrates the average wind speed behavior from 2004 to 2008. For most of the year, wind speeds were above 8 m/s, while the lowest speeds occurred in September

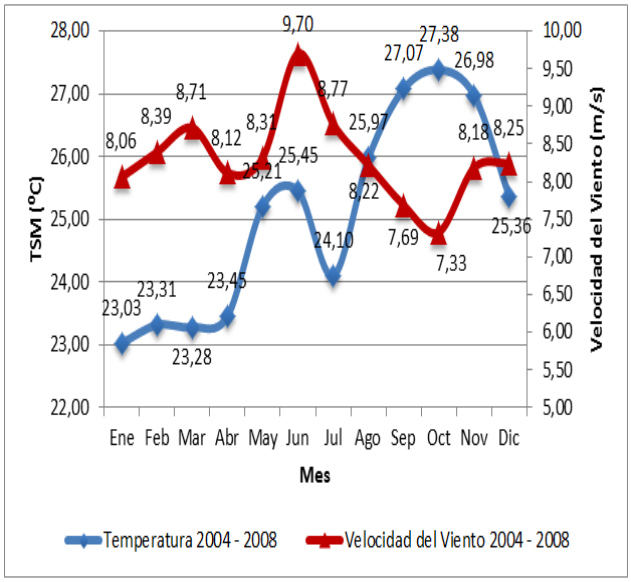

Figure 8. Average monthly variation of SST and wind speed between the years 2004 – 2008.

In 2009, a delay in the wind speed curve was observed, with peak wind speeds occurring in months later than the historical average for 2004-2008. Specifically, in November, the wind should have reached higher speeds, but instead, it continued to decrease. This abnormal wind speed behavior coincided with the days of highest mortality among species in Las Piedras Bay, as reported by localresidents. Regarding wind direction in the area, it is noteworthy that, for most of the year, winds predominantly come from the southeast and northeast, according to historical data provided by the "Dirección de Hidrografía y Navegación, Estación Meteorológica Punto Fijo".

Figure 7 shows the wind speed and direction patterns during October and November 2009. A key observation is that wind speed coincides with the prevailing southeasterly wind direction, and it is noted that when the frequency of this direction decreases, so does the wind speed. This figure also illustrates the sharp decrease in wind speed on October 13-15, October 18-21, and October 27-November 1. During these periods, the frequency of northwesterly winds increased relative to the frequency of southeasterly winds, and there was an atypical presence of winds from the northwest and southwest.

This behavior again coincides with the period during which species mortality was observed in the bay. According to Pomares et al. (2004), these decreases in wind speed and changes in wind direction bring about changes in the dynamics of water currents, since these are a function of the tangential stress of the wind and the action of the tides, leading to negative consequences for the organisms that inhabit them.

Figure 8 shows the average monthly variation of sea surface temperature (SST) and wind speed between 2004 and 2008, in which it can be observed that these variables have an inversely proportional relationship: while the wind speed tends to decrease until reaching a minimum in October, the SST increases to a maximum in the same month.

Figure 9 shows the average monthly variation of sea surface temperature (SST) and wind speed for 2009. This figure shows a similar pattern to that of 2004-2008, but unlike those years, November saw the lowest wind speed and the highest SST.

According to Quintero and Terejova (2008), these changes tend to decrease the amount of water flowing out of the bay, even leading to calm conditions. This, combined

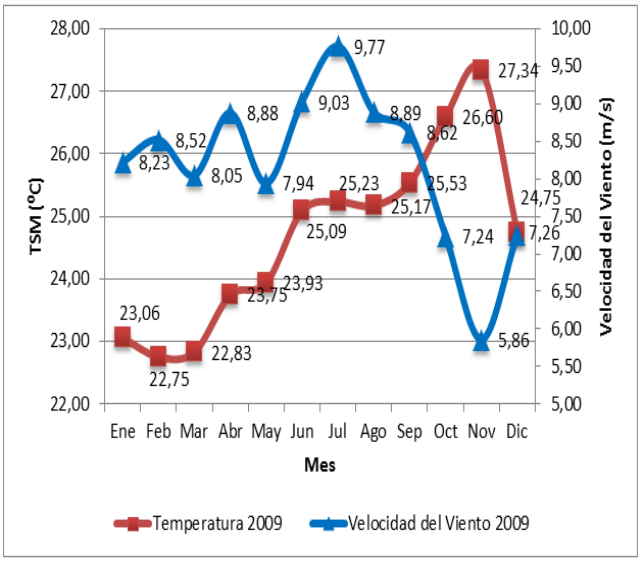

Figure 9. Average monthly variation of SST and wind speed for the year 2009.

with high SST, results in stratification of the water column, with a corresponding impact on the primary productivity of ecosystems and a decrease in oxygen levels. This is similar to what was reported by NOAA (2009) for the Central Pacific Ocean, where temperature anomalies of +1 to +5 °C were observed at the end of October 2009, as well as changes in wind direction, indicating a strengthening of the El Niño phenomenon.

The conditions observed from October 15, 2009, through the first week of November suggest increased thermal stratification (thermocline depression) in the water masses of Las Piedras Bay. This was caused by atmospheric disturbances, possibly due to the El Niño phenomenon in the Pacific, which led to lower wind speeds and changes in wind direction. The thermocline separates the water body into two distinct layers based on their physical properties: an upper layer with low density due to high temperatures resulting from solar radiation on the water's surface, and a

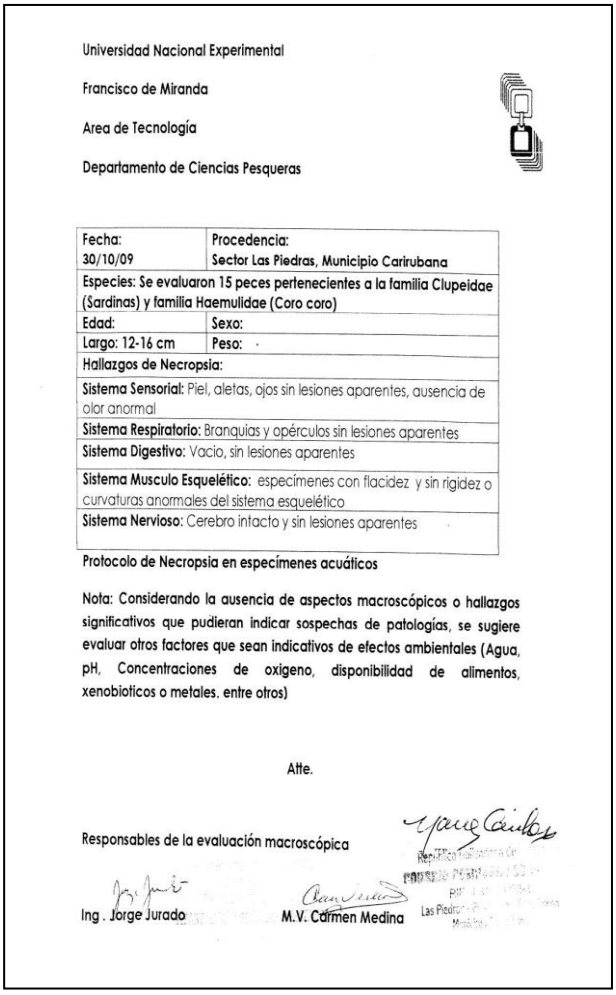

Universidad Nacional Experimental
Francisco de Miranda
Area de Tecnología
Departamento de Ciencias Pesqueras

Fecha: 30/10/09	Procedencia: Sector Las Piedras, Municipio Carirubana
Especies: Se evaluaron 15 peces pertenecientes a la familia Clupeidae (Sardinas) y familia Haemulidae (Coro coro)	
Edad:	Sexo:
Largo: 12-16 cm	Peso:
Hallazgos de Necropsia:	
Sistema Sensorial: Piel, aletas, ojos sin lesiones aparentes, ausencia de olor anormal	
Sistema Respiratorio: Branquias y opérculos sin lesiones aparentes	
Sistema Digestivo: Vacio, sin lesiones aparentes	
Sistema Musculo Esquelético: especímenes con flacidez y sin rigidez o curvaturas anormales del sistema esquelético	
Sistema Nervioso: Cerebro intacto y sin lesiones aparentes	

Protocolo de Necropsia en especímenes acuáticos

Nota: Considerando la ausencia de aspectos macroscópicos o hallazgos significativos que pudieran indicar sospechas de patologías, se sugiere evaluar otros factores que sean indicativos de efectos ambientales (Agua, pH, Concentraciones de oxigeno, disponibilidad de alimentos, xenobioticos o metales. entre otros)

Atte.

Responsables de la evaluación macroscópica

Ing. Jorge Jurado
M.V. Carmen Medina

Figure 10. Necropsy of species belonging to the Clupeidae family

deeper layer with greater density due to lower temperatures. This condition prevents the upper and lower layers from mixing, negatively impacting the species inhabiting these ecosystems.

When the depth of the thermocline increases, there is a decrease in the transfer of heat and oxygen from surface to deep waters. Similarly, the transport of nutrients from deep to surface waters is impeded, affecting primary productivity. Consequently, organisms at higher trophic levels (phytoplankton and zooplankton) are affected in their survival, reproduction, and distribution, causing marine organisms to die or fail to reproduce due to lack of food (Snet, 2010; Trasviña et al., 2009).

According to Freón and Mendoza (1998), the species *Sardinella aurita*, with its omnivorous diet preferring zooplankton, filter-feeding habits, low selectivity, and predominantly opportunistic nature, is affected by a decrease in zooplankton volume. This is corroborated by the results of the necropsy of the *Sardinella aurita* species collected in the bay of Las Piedras at the time of mortality (figure 10), which showed no stomach contents, this being an indication of a feeding deficit.

4.4 Physicochemical Parameters Measured in the Waters of Las Piedras Bay.

Table 5 shows the average values obtained from the surface physicochemical variables measured in Las Piedras Bay. These values were taken on November 5, 2009, in the afternoon (between 2:00 pm and 3:00 pm) and at midnight (between 11:00 pm and 12:00 am) when marine life was still observed in the bay. It is important to note the decrease in oxygen levels that occurred that day, dropping from 6.04 mg/L in the afternoon to 2.87 mg/L at night. According to Freon and Mendoza (2003), the vertical distribution of tem perature and dissolved oxygen shows greater stratification and critical decreases in oxygen in the deep layers of water in the month of October, with concentrations lower than 3mg/l from 50 meters, which is an indication that the month of October can become critical for the sardine if the environmental conditions alter the critical limits.

A subsequent sampling was carried out on November 24, 2009, when conditions had apparently returned to normal, as no dead or dying species were observed. The temperature, pH, and oxygen values taken on the afternoons of November 5 and 24, 2009, were found to coincide with those reported by Chirinos (2002) and Pomares et al. (2004). Average salinity values of 39.42 ± 0.46 ‰ and 39.56 ± 0.07 ‰ were observed, higher than those reported by Chirinos (2002) (31.82 ‰), Pomares et al. (2004) (34.39 ‰), and Freon and Mendoza (2003) (37 ‰).

It is important to note that although the temperature values found during the sampling on November 5th coincide with those reported by other authors, they are slightly above the maximum temperature values to which the Sardinella aurita is acclimatized, as reported by Freon and Mendoza (2003) (28°C), who studied the physicochemical characteristics of the Sardinella aurita habitat in eastern Venezuela, indicating that the temperature to which they are acclimatized has a minimum during the first quarter of the year, varying between 25°C and 26°C, and a maximum between September and October of 27°C and 28°C, a period during which they begin to migrate to western Venezuela.

The average total nitrogen concentration was 120.96 ± 32.77 µg/L (see Table 7), exceeding the values considered safe by the EPA (2002). High nitrogen concentrations in the water result in critically low oxygen levels due to the decomposition of organic matter by bacteria (EPA, 1997). Regarding total hydrocarbons and oils and greases measured on November 5, 2009, the values obtained were 8.4 and 8.3 ppm, respectively. These values are below the permissible levels established by Venezuelan regulations (Decree 883) and are not indicative of species mortality. The analysis of variance showed significant differences ($p < 0.05$) in oxygen concentration and temperature between the day and night of the November 5 sampling. Salinity and pH did not show significant differences.

The distribution of dissolved oxygen in the water column is characterized by a saturated surface layer in equilibrium with the atmosphere. Oxygen production by photosynthetic organisms during the day causes supersaturation above the thermocline. The greatest oxygen unsaturations are found below the thermocline. The reasons for this are strong density stratification, which inhibits vertical mixing between the surface and subsurface layers, isolating the latter from atmospheric oxygen and even from the oxygen

Table 5. Physicochemical Parameter Values in Water Samples Taken from Las Piedras Bay

Date / Variable	05/11/2009		24/11/2009	
	Afternoon	**Night**	**Afternoon**	**Night**
Temperature (°C)	28,94 ± 0,46	27,58 ± 0,46	27,44 ± 0,25	-
Salinity (‰)	39,42 ± 0,46	39,40 ± 0,05	39,56 ± 0,07	-
Oxygen (mg/L)	6,04 ± 0,27	2,87 ± 0,09	4,00 ± 0,32	-
pH	8,30 ± 0,05	8,31 ± 0,03	8,33 ± 0,00	-
Total Nitrogen (µg/L)	120,96 ± 32,77	-	-	-
Oils and Fats	8,3	-	-	-
Total Hydrocarbons	8,4	-	-	-

produced in the surface layers during the day (SHOA, 2007). Conversely, the amount of particulate organic matter in the thermocline zone is greater than in the deeper zone, so the demand for dissolved oxygen for its decomposition is greater. This becomes critical at night, when photosynthesis ceases and plant respiration begins, which can dramatically lower oxygen levels to hypoxic or anoxic concentrations.

Table 6. Average annual chlorophyll concentrations from 2004 to 2009.

Year	Chlorophyll mg/m3
2004	0,65±0,41a
2005	0,48±0,27a
2006	0,72±0,52a
2007	1,62±1,88b
2008	0,68±0,62a
2009	0,68±0,50a

a,b,c The average chlorophyll values for each year with different superscripts are significantly different.

The conditions described above, along with high SSTs, increase the likelihood of stress in most aquatic species, which are unable to regulate their temperature to tolerate changes in the water (poikilotherms). This, in turn, leads to an increase in metabolism and, consequently, a greater demand for oxygen. If this demand is not met by the environmental conditions, it can trigger mortality, especially in species that move in schools, such as *Sardinella aurita* (Wheaton, 1982). This coincides with what was described

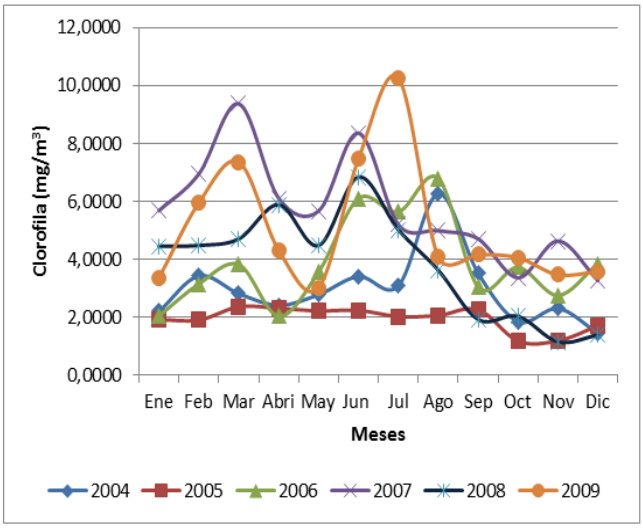

Figure 11. Variation in chlorophyll concentration during the years 2004 to 2009.

by the inhabitants of the community, who stated that the species began to die from approximately 3 a.m. onwards, and then throughout the rest of the morning they gradually accumulated on the shores of the bay.

4.5 Biological Variables

4.5.1 Chlorophyll

Analysis of variance using one-way ANOVA showed significant differences ($p < 0.05$) in chlorophyll levels between 2004 and 2009, as shown in Table 6. Duncan's post-hoc test and Tukey's HSD test for the annual averages showed that 2009 belongs to the homogeneous group containing all years except 2007. 2009 showed no relevant differences compared to 2004-2006 and 2008.

Figure 11 shows the variation in chlorophyll concentration from 2004 to 2009. It can be observed that the months with the highest chlorophyll concentrations are March, June, and August, while the months with the lowest concentrations correspond to the last quarter of the year, with a marked downward trend after the month of highest concentration. This suggests that, due to the relationship between chlorophyll levels and oxygen levels, there is a tendency for oxygen levels to decrease after June. This, combined with the previously described temperature increase, would result in lower amounts of oxygen available to the species during the last quarter of the year.

5 Conclusions

The most probable cause of death of S. aurita was the oxygen deficits during the night, as a consequence of a possible stratification of water masses due to the decrease in wind speed and changes in its direction. That could have been caused by the presence of the “El Niño” phenomenon; ruling out the influence of mortality due to heavy metals, hydrocarbons or their derivatives.

References

Agger, P., Bagge, O., Hansen, O., Hoffman, E., Holden, M., Kesteven, G., Knudsen, H., Raitt D., Saville, A. and Williams T. (1974). Methods for Investigating Resources and Their Application. In Manual of Fisheries Science Part 2 - . Series title: FAO Fisheries Technical Papers - T115Rev.1 1974 255 pp.

APHA. (1995). American Public Health Association. Standard Methods for the Examination of Water and Wastewater (19th ed.). A. D. Eaton, L. S. Clesceri, & A. E. Greenberg (Eds.). Washington, DC.

Ansari, T., Marr, L., & Tarid, N. (2004). Heavy metals in marine pollution: A mini-review. Journal of Applied Sciences, 4(1), 1-20.

Arellano D, J. (2002). Introduction to Environmental Engineering. Mexico: Alfaomega Publishers. 127 pp.

Arteaga-Sogamoso, E. (2009). Monthly variation of sea surface temperature in the Colombian Caribbean

(1995-2005). Journal of the Colombian Academy of Exact, Physical and Natural Sciences, 33(128), 415-425.

Bernal, G., Poveda, G., Roldán, P., & Andrade, C. (2006). Variability patterns of sea surface temperatures on the Colombian Caribbean coast. Revista de la Academia Colombiana de las Ciencias, 30(115), 195-208. ISSN 0370-3908.

Bionero, S. (2009). Seeking causes of fish mortality in lagoon. http://www.bionero.org/ecologia/buscan-causas-de-mortandad-de-peces-en-laguna/discussion_reply_form#discussion

Castillo, S., & Castillo, J. (2012). Marine biodiversity of Miranda State. http://biodiversidadmiranda.cbm.usb.ve/organism/553/

Catorce 6. (2009). Temperature change could be responsible for another fish kill in Cartagena. http://www.catorce6.com/797/cambio-de-temperatura-seria-responsable-de-otra-mortandad-de-peces-en-cartagena/

Chirinos, A. (2002). Evaluation of coastal areas with aquaculture potential in the Paraguaná Peninsula, Falcón State. Unpublished undergraduate thesis. Francisco de Miranda National Experimental University. Punto Fijo.

Constitution of the Bolivarian Republic of Venezuela. (1999). Official Gazette of the Bolivarian Republic of Venezuela (No. 36,860). December 30, 1999.

EPA (1997). Protecting Coastal Waters from Nonpoint Source Pollution. In: U.S. Environmental Protection Agency. Washington, D.C., USA. 841-F-96-

FAO (2025). "A snapshot of the sustainability of global marine fisheries resources: The context of Area 31 (Venezuela and the Caribbean)." Food and Agriculture Organization of the United Nations.

Fernández, N. (2006). "Effluent hazard index. Water and soil quality component." Irrigation and drainage program of the province of Mendoza PROSAP – DGI – OEI. 48 p.

Freón, P., & Mendoza, J. J. (1998). The sardine (Sardinella aurita): Its environment and exploitation in eastern Venezuela. In P. Freón & J. J. Mendoza (Eds.), Fisheries resources of northeastern Venezuela: Sardines (pp. 13-36). Spanish Institute of Oceanography.

Fréon, P., & Mendoza, J. J. (2003). The Cariaco Basin System: Physical and Biological Dynamics. In P. Fréon & J. J. Mendoza (Eds.), The Cariaco Basin System: Physical and Biological Dynamics (pp. 1-25). IRD Éditions.

García, A. (2023). Historical and social evolution of fishing ports in Falcón State: Identity and resistance. Memorias de Venezuela, (65), 112-128.

Garrison, T., & Ellis, R. (2016). Oceanography: An Invitation to Marine Science (9th ed.). Cengage Learning.

Gómez, A. (2022). Nine decades of exploitation of Sardinella aurita sardine in Venezuela: A critical review. Boletín de Investigaciones Marinas y Costeras, 51(1), 171-192. https://doi.org/10.21272/boletin.v51i1.1102

González, L. W., Eslava, N., & Troccoli, L. (2007). Relationship between sea surface temperature and the capture of sardine (Sardinella aurita) in the State of Nueva Esparta, Venezuela. Memoirs of the LIX Congress of the Society of Marine Sciences of Venezuela. Margarita, Venezuela.

González, L. W., Núñez, E., Eslava, N., & Guevara, F. (2021). Population dynamics of the sardine (Sardinella aurita) in the state of Nueva Esparta, Venezuela. Bulletin of the Peruvian Marine Institute, 35(1), 127-133. https://revistas.imarpe.gob.pe/index.php/boletin/article/view/296

Hernández Miranda, R. J. (2009). Physiological responses of the Monterey sardine Sardinops sagax (Jenyns, 1842) subjected to thermal and captive stress [Doctoral dissertation, Northwest Biological Research Center, S.C.]. CIBNOR Institutional Repository.

Herrera, L. (2009). Fish mortality in Santa Marta Bay may have been caused by lack of oxygen. http://www.eltiempo.com/colombia/caribe/mortandad-de-peces-en-la-bahia-de-santa-marta-habria-sido-causada-por-falta-de-oxigeno_4820282-1]

Institute of Technology and Marine Sciences. (2009). "CARIACO Project". Caracas: Simón Bolívar University; [cited December 7, 2009]. http://www.cariaco.org

National Institute of Civil Aeronautics. (2009). Meteorological Records: Wind Speed and Direction at Josefa Camejo Airport. Punto Fijo Control Tower.

INVEMAR. (2009). Laboratory Results on Fish Deaths in Santa Marta Bay [Available at: www.invemar.org.co

Water Law. (2007). Official Gazette of the Bolivarian Republic of Venezuela, No. 38,595, January 2, 2007.

Organic Law of Aquatic Spaces. (2014). Decree with the Rank, Value, and Force of Organic Law No. 1,446, published in Extraordinary Official Gazette No. 6,153, dated November 18, 2014.

Environmental Criminal Law. (2012). Official Gazette of the Bolivarian Republic of Venezuela, 39,913 (Extraordinary), May 2, 2012.

Mendoza, J., Larez, A., Marcano, J., & Heredia, J. (2021). Assessment of fishery resources on the northeastern shelf of Venezuela: Trends and challenges in a climate change scenario. Bulletin of the Oceanographic Institute of Venezuela, 60(1), 12-25.

Ministry of Agrarian Affairs of the Government of the Province of Buenos Aires (MAA) (2007). Immediate Action Guidelines.

NOAA (2009). El Niño/Southern Oscillation Diagnostic Discussion (November 5). http://www.cpc.noaa.gov/products/analysis_monitoring/enso_disc_nov2009/ensodisc_sp.pdf

Pan American Health Organization (PAHO). (2009). Fish Mortality in Southeast Caribbean Countries. Epidemiological Bulletin, 21 (2). http://www.paho.org/Spanish/SHA/be_v21n2-peces.htm

Pomares, O., Leal I., Rengel J., Morán H., and Jurado J. (2004). Evaluation of the causes of a mass mortality event of bivalve mollusks in Amuay Bay. Proceedings of the VII Research Conference within the framework of the 30th anniversary of UNEFM. http://investigacion.unefm.edu.ve/memorias2007/memoriasunefm2007/2.amb.recnatorales.pdf

Presidency of the Republic (1995). Regulations on the Control of the Generation and Management of Hazardous Waste. Decree No. 883, October 11, 1995. Official Gazette of the Republic of Venezuela No. 5,021 (Extraordinary), December 18, 1995.

Quintero, A., and Terrejova, G. (2008). Influence of ocean currents on sediment transport at the mouth of the Gulf of Coro, Venezuela. Bulletin of the Oceanographic Institute of Venezuela, 47 (1): 77-87.

Seoanez, M. (2000). Manual of marine pollution and coastal restoration. http://books.google.co.ve/books?id=g_KtvFFCJcoC&printsec=frontcover&dq=manual+de+contaminacion+marina&source=bl&ots=Y0zR359WBd&sig=sm2JQXkK1shkXYBwzPk4ad3JdnQ&hl=es&ei=GEqYS8a4G8mztgfA2uHkAQ&sa=X&oi=book_result&ct=result&resnum=2&ved=0CAkQ6AEwAQ.

SHOA. (2007). The Ocean. [Online Book]. http://mardechile.cl/educacion/index.php?option=com_content&task=view&id=379&Itemid=66. [Accessed: 09/12/07]

Snet (2010). The coastal-marine zone of El Salvador: http://www.snet.gob.sv/ver/oceanografia/oceanografia+en+e.s./zona+costero-marina/]

Trasviña, A., Lluch, D., Filonov, A. and Gallegos, A. (2009). Oceanography and El Niño. http://www.atmosfera.unam.mx/editorial/libros/el_nino/cap3.pdf

Trujillo, A. P., & Thurman, H. V. (2016). Essentials of Oceanography (12th ed.). Pearson.

UNESCO (1976). General Plan for Global Marine Pollution Research and Guidelines for Basic Studies (IOC Guides and Manuals Series No. 5). United Nations Educational, Scientific and Cultural Organization.

United States Environmental Protection Agency. (2002). Methods for evaluating wetland condition: Coastal pathways and environmental indicators (EPA-822-R-02-024). Office of Water. https://www.epa.gov/sites/production/files/2015-09/documents/wetlands_13coastal.pdf

Wetzel, R. G. (2001). Limnology: Lake and River Ecosystems (3rd ed.). Academic Press. Wheaton, F. (1982). Aquaculture: Design and Construction of Systems. Mexico: A. G. T. Editor, s.a. 704 pp.

Zaror Z, Claudio A. (2000). Introduction to Environmental Engineering for the Process Industry. Chile: University of Concepción. 500 pp.

Agger, P., Bagge, O., Hansen, O., Hoffman, E., Holden, M., Kesteven, G., Knudsen, H., Raitt, D., Saville, A., and Williams, T. (1974). Methods for Investigating Resources and Their Application. In Manual of Fisheries Science, Part 2. Series Title: FAO Fisheries Technical Papers - T115 Rev. 1, 1974. 255 pp.

Recibido: *13 de noviembre de 2025*

Aceptado: *15 de febrero de 2026*

De Lima, Aída: *MSc in Chemical Engineering, ULA. Associate Professor, attached to the Department of Industrial and Applied Chemistry,* ***School*** *of Chemical Engineering, ULA; Laboratory of Physical Chemistry and Environmental Microbiology.*
https://orcid.org/0009-0003-3850-0019

Veroes, Carlos: *PhD in Oceanography, UDEC (Chile); MSc in Hydrography, UMBV; Fisheries Engineer, UNEFM. Associate Professor in the Fisheries Engineering Program, Technology Area, Francisco de Miranda National Experimental University. Email: carlosve-roes@hotmail.com*
https://orcid.org/0009-0003-0090-9484

Méndez, Karelys: *Chemical Engineer, UNEFM; Associate Professor, Department of Chemistry, Technology Area, Francisco de Miranda National Experimental University. Email: karelyta@gmail.com*
https://orcid.org/0009-0005-8093-5673

Muñoz, Alexandra: *Chemical Engineer, UNEFM; MSc in Environmental Engineering, LUZ. Associate Professor, Department of Chemistry, Technology Area, Francisco de Miranda National Experimental University. Email: alexandram11@hotmail.com*
https://orcid.org/0009-0003-3850-0019

Maria, Sanchez: *Lawyer, ULA. Master's student in Agricultural Development, University of the Andes, Mérida, Venezuela. Email address: abgmaricamensanhez@gmal.com*
https://orcid.org/0009-0006-7225-0502

Artículo de Investigación. Revista Ciencia e Ingeniería. Vol. 47, No. 2 pp. 181-190, abril-julio, 2026
ISSN 1316-7081. ISSN Elect. 2244-8780 Universidad de los Andes (ULA)

Hepatitis C: Análisis estadístico de los factores de riesgo y creación de modelos predictivos mediante Machine Learning

Hepatitis C: Statistical analysis of risk factors and creation of predictive models using Machine Learning

Segovia, José de la Trinidad.
Departamento de Ingeniería Aeronáutica,
Universidad Nacional Experimental Politécnica de la Fuerza Armada, Núcleo Aragua, Sede Maracay 2101, Venezuela.
jdltsm@gmail.com

Resumen

En este trabajo de investigación se desarrollaron modelos predictivos de aprendizaje automático (Machine Learning) orientados a la detección temprana de la hepatitis C, dada su capacidad de generar daño hepático irreversible. La metodología abarcó la construcción y categorización binaria de un conjunto de datos, seguida de un riguroso preprocesamiento que incluyó la verificación de integridad, imputación de valores faltantes, codificación de variables categóricas y escalado numérico. Tras un análisis estadístico de los factores de riesgo, se entrenaron y compararon tres modelos de aprendizaje supervisado: XGBoost, Máquinas de Vectores de Soporte (SVM) y Random Forest. La evaluación de estas herramientas computacionales evidenció un alto rendimiento general, con una precisión, basada en el Área Bajo la Curva (AUC), superior al 99%. El análisis de las diversas métricas demostró que los tres algoritmos son altamente eficientes para identificar a potenciales portadores de la patología, destacándose SVM y Random Forest por exhibir el mejor desempeño predictivo global.

Palabras clave: Hepatitis C, aprendizaje automático, modelos predictivos, detección temprana, aprendizaje supervisado.

Abstract.

In this research work, predictive machine learning models were developed for the early detection of hepatitis C, given its potential to cause irreversible liver damage. The methodology encompassed the construction and binary categorization of a dataset, followed by rigorous preprocessing that included integrity verification, imputation of missing values, encoding of categorical variables, and numerical scaling. Following a statistical analysis of risk factors, three supervised learning models were trained and compared: XGBoost, Support Vector Machines (SVM), and Random Forest. The evaluation of these computational tools revealed high overall performance, achieving an accuracy based on the Area Under the Curve (AUC) greater than 99%. The analysis of various metrics demonstrated that all three algorithms are highly efficient in identifying potential carriers of the pathology, with SVM and Random Forest standing out for exhibiting the best global predictive performance.

Key words: *Hepatitis C, machine learning, predictive models, early detection, supervised learning.*

1 Introducción

La hepatitis es un término médico que abarca una variedad de trastornos marcados por la inflamación del hígado, siendo las infecciones virales las causas predominantes a nivel global. En particular, la hepatitis C es una enfermedad contagiosa causada por un virus de ARN (VHC) que ocasiona un daño hepático progresivo. Su infección crónica desencadena procesos inflamatorios que pueden derivar en complicaciones severas como fibrosis hepática, cirrosis, carcinoma hepatocelular e incluso la muerte. A nivel mundial, decenas de millones de individuos sufren de esta infección crónica, convirtiendo a esta afección en la principal razón para realizar trasplantes de hígado en diversas regiones del planeta.

Para el manejo clínico de esta patología, el diagnóstico se apoya tradicionalmente en pruebas de función hepática. Estas evaluaciones se realizan mediante análisis sanguíneos rutinarios que miden los niveles de enzimas y otras sustan-

cias clave, tales como la alanina aminotransferasa (ALT), la aspartato aminotransferasa (AST), la fosfatasa alcalina (ALP), la bilirrubina y la albúmina. Con el monitoreo de estos marcadores, los especialistas buscan detectar anomalías estructurales o daños en los tejidos para establecer un tratamiento adecuado, el cual puede ir desde fármacos antivirales hasta modificaciones en el estilo de vida.

No obstante que en la medicina moderna se toman en cuenta estos indicadores para el diagnóstico, la hepatitis C a menudo se presenta como una infección silenciosa que puede persistir durante décadas sin causar síntomas evidentes en el paciente. Debido a esta naturaleza asintomática en sus etapas tempranas y a la gran magnitud del perjuicio que genera el virus una vez que avanza, resulta una necesidad imperativa descubrir nuevas formas de analizar los datos clínicos. Los diagnósticos convencionales pueden requerir apoyo adicional para identificar interacciones complejas entre múltiples factores de riesgo (como la edad, el género y diversas métricas sanguíneas) que intervienen en el desarrollo de la enfermedad.

En este sentido, el Aprendizaje Automático (Machine Learning), como componente de la Inteligencia Artificial, ha surgido como un recurso tecnológico sumamente útil en el campo médico. Esta tecnología emplea algoritmos avanzados que le permiten a la computadora aprender de la experiencia, analizar bases de datos complejas, detectar patrones ocultos y realizar predicciones sin necesidad de ser programada explícitamente para cada regla. Su aplicación abre la puerta a un pronóstico mucho más exacto sobre la evolución de las enfermedades hepáticas y la identificación temprana de biomarcadores relevantes.

Un caso particular de gran interés es la evaluación del riesgo de infección a través de bases de datos de donadores de sangre y pacientes. Por ello, en el presente trabajo de investigación se planteó el uso de datos serológicos y demográficos para desarrollar tres modelos predictivos de aprendizaje supervisado: XGBoost, Máquinas de Vectores de Soporte (SVM) y Random Forest. El objetivo de este estudio es predecir de manera temprana qué individuos son posibles infectados o portadores de la enfermedad de la hepatitis C y, paralelamente, determinar cuál de estos modelos computacionales resulta ser el más eficiente para dicha tarea.).

2 Procedimiento experimental

Para el desarrollo de esta investigación, se empleó el entorno de programación Python en su versión 3.11, operando a través de la plataforma en línea Google Colab. La elección de este lenguaje se fundamentó en su extensa disponibilidad de bibliotecas especializadas en ciencia de datos y aprendizaje automático. Específicamente se integraron herramientas analíticas como pandas, matplotlib, numpy, scipy, seaborn y sklearn. Esta última biblioteca fue de vital importancia, ya que provee una amplia gama de algoritmos de aprendizaje supervisado junto con utilidades prácticas para la preparación y evaluación de los datos.

La información base se obtuvo a partir de los registros referenciados en investigaciones previas centradas en la aplicación de técnicas de minería de datos y enfoques explicables de aprendizaje automático para el diagnóstico de infecciones virales. A partir de estas fuentes, se generó un archivo consolidado en formato CSV. Este documento agrupó los registros clínicos de 615 individuos evaluados. Durante la revisión inicial, se identificaron 533 pacientes completamente saludables y 7 clasificados como sospechosos. Por otro lado, se contabilizaron 24 personas diagnosticadas con la patología central del estudio junto a 21 pacientes con fibrosis y 30 con cirrosis hepática.

Con la finalidad de enfocar el modelo predictivo hacia la detección binaria de la afección, se procedió a agrupar a los individuos en dos categorías principales. La primera categoría englobó a las personas sanas y a los casos sospechosos. La segunda categoría agrupó a los pacientes confirmados con la enfermedad junto a aquellos con complicaciones clínicas derivadas. Posteriormente, se llevó a cabo una fase de exploración para comprender la estructura general y verificar la integridad de la información médica.

En esta etapa, se ejecutó un análisis descriptivo que permitió obtener detalles básicos sobre la distribución de las variables y sus posibles interconexiones biológicas. Luego, se aplicó un preprocesamiento riguroso donde se identificaron los valores ausentes para proceder a su eliminación o imputación según correspondiera. Las variables categóricas presentes fueron codificadas a formatos numéricos para viabilizar su procesamiento computacional. Asimismo, las variables numéricas resultantes fueron escaladas para garantizar que todas mantuvieran una proporción uniforme y así facilitar el entrenamiento de los algoritmos.

Una vez estructurados los datos, se realizó un análisis estadístico profundo orientado a identificar los factores de riesgo más influyentes. Se emplearon pruebas de normalidad de Shapiro Wilk y coeficientes de correlación de rango de Spearman para evaluar las relaciones lineales entre las distintas métricas serológicas. También se aplicaron herramientas inferenciales como la prueba U de Mann Whitney para investigar las conexiones precisas entre los resultados de los exámenes de sangre y la condición de salud del paciente.

Para la fase predictiva, se definieron las mediciones de los exámenes sanguíneos como variables predictoras y la categoría binaria como la variable objetivo. El conjunto de datos total se dividió aleatoriamente asignando el 80 por ciento de los registros para el entrenamiento del sistema y el 20 por ciento restante para la fase de comprobación. Sobre esta base, se entrenaron tres algoritmos distintos de aprendizaje supervisado. El primero fue el Extreme Gradient Boosting o XGBoost el cual se fundamenta en la creación progresiva de árboles de decisión. El segundo consistió en las Máquinas de Vectores de Soporte diseñadas

para encontrar el hiperplano óptimo de separación espacial. El tercero fue el Random Forest que emplea múltiples árboles de decisión completamente independientes. El rendimiento de cada modelo se midió y comparó utilizando métricas estandarizadas como la exactitud, la sensibilidad, la especificidad y el Área Bajo la Curva ROC. La interpretación integral de estos resultados permitió evaluar el impacto individual de cada factor clínico en la predicción global de la enfermedad.

3 Resultados y análisis

3.1 Características demográficas de la población de estudio

En primer lugar, se realizó un análisis descriptivo exhaustivo de las características demográficas de los pacientes que conformaron el conjunto de datos de la investigación. Se evaluaron los registros de 615 donadores de sangre, cuyas edades oscilaron entre los 19 y 77 años, observándose una mayor concentración de individuos que rondaban los 50 años de edad, tal como se ilustra en la Fig. 1. Diversas investigaciones señalan que la cohorte más grande de personas que conviven con la infección crónica se ubica, precisamente, en el rango de 40 a 59 años (Balter et al., 2014). Asimismo, en la Fig. 2 se evidencia que la mayoría de los pacientes evaluados pertenecían al sexo masculino, lo cual coincide con la literatura médica que sugiere una mayor prevalencia de infecciones virales hepáticas en hombres, debido a diversos factores de riesgo ocupacionales y de estilo de vida. En cuanto a la clasificación general del estado de salud, plasmada en la Fig. 3, se determinó que la gran mayoría de los individuos se encontraban completamente sanos, mientras que una pequeña proporción representaba a los pacientes enfermos o sospechosos de portar el virus.

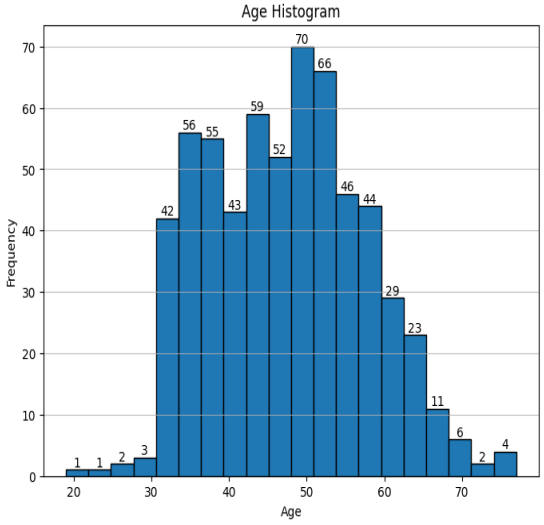

Fig. 1. Histograma de la frecuencia de personas según su edad

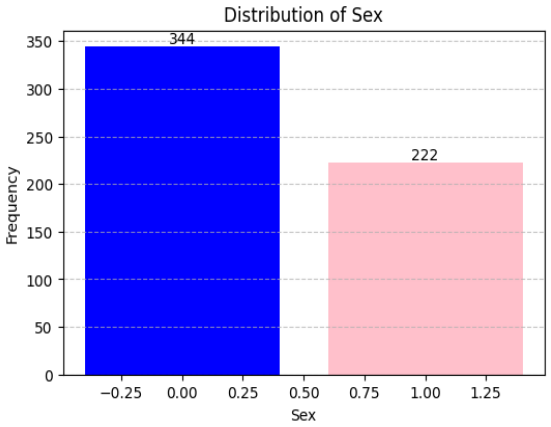

Fig. 2. Histograma de la frecuencia de los pacientes según su sexo, masculino (azul) y femenino (rosado).

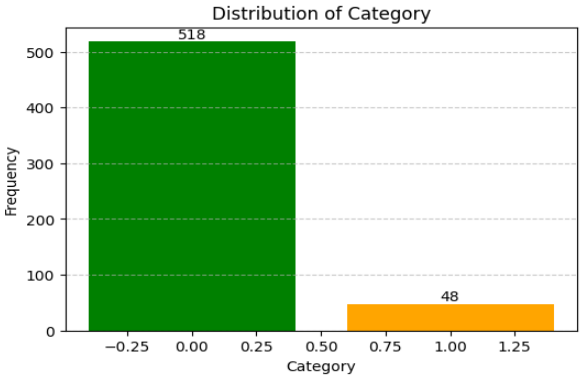

Fig. 3. Histograma de la frecuencia de pacientes según la categoría a la que pertenece, verde (pacientes saludables) y naranja (pacientes enfermos)

3.2 Evaluación de las pruebas de función hepática.

Para comprender el estado de la función hepática de los individuos, se analizaron a profundidad los niveles de diversas enzimas y proteínas séricas. Al evaluar la prueba de albúmina, cuya distribución se muestra en la Fig. 4, se evidenció que una gran cantidad de los donadores presentaron niveles superiores a 36 gramos por litro, lo cual indica, de manera preliminar, la ausencia de daño hepático significativo. Estudios médicos previos han identificado que un nivel sérico de albúmina inferior o igual a 3.6 decilitros por gramo representa un factor de riesgo considerable para la recurrencia de carcinoma en personas con hepatitis C (Nojiri et al., 2011). En cuanto a la fosfatasa alcalina (Fig. 5), la mayoría de los pacientes registraron valores por debajo de los umbrales asociados con patologías hepáticas crónicas.

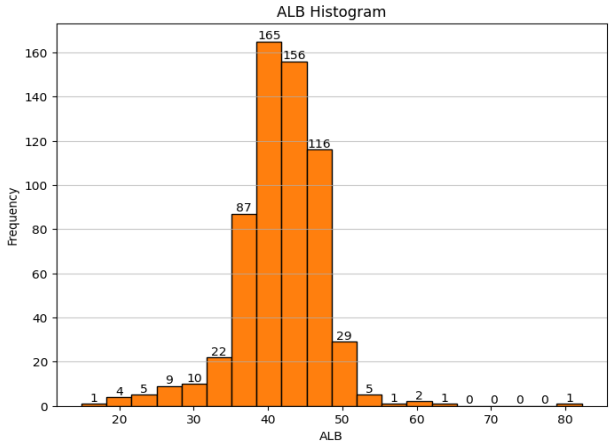

Fig. 4. Histograma de la frecuencia de personas según sus valores en la prueba de albúmina

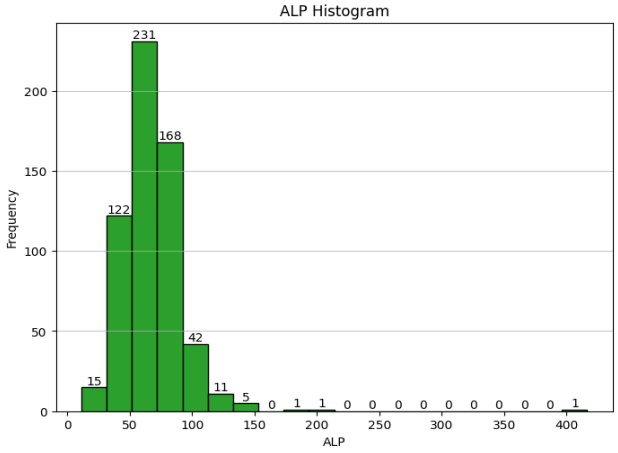

Fig. 5. Histograma de la frecuencia de personas según sus valores en la prueba de fosfatasa alcalina

Por otro lado, investigaciones previas indican un incremento significativo en las concentraciones de esta enzima en pacientes con la enfermedad crónica, sugiriendo una fuerte correlación clínica (Haq et al., 2019). Por su parte, los valores de alanina aminotransferasa (Fig. 6) resultaron críticos para el análisis. Tradicionalmente, se considera que el límite máximo normal es de 40 unidades internacionales por litro (Lee et al., 2010). En el conjunto de datos analizado, aproximadamente 561 pacientes mostraron valores por debajo de 50 unidades internacionales por litro, indicando un estado de salud favorable en su mayoría

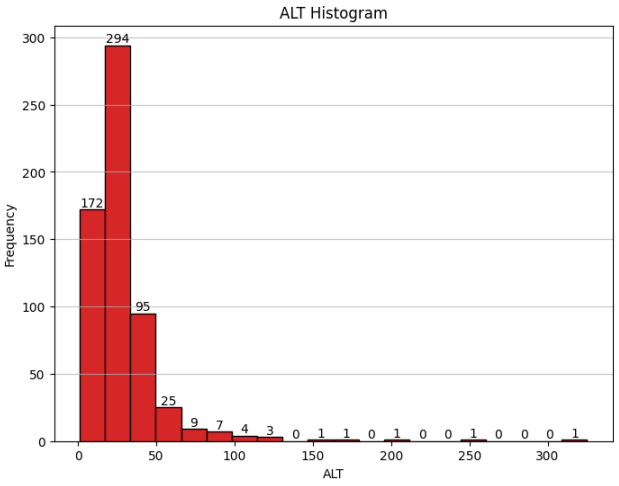

Fig. 6. Histograma de la frecuencia de personas según sus valores en la prueba de alanina aminotransferasa

Al revisar minuciosamente los niveles de aspartato aminotransferasa en la Fig. 7, se observó que gran parte de los valores se ubicaron dentro del intervalo normal establecido para adultos sanos. Sin embargo, se sabe que los pacientes con hepatitis C crónica suelen presentar altas concentraciones de dicha enzima, con niveles basales medios que superan las 59 unidades por litro (Nadeem et al., 2010). De manera complementaria, los niveles de bilirrubina sérica (Fig. 8) se mantuvieron predominantemente por debajo de los 25 micromoles por litro en la población sana del estudio. La literatura comprueba que niveles superiores a ciertos umbrales son indicativos de disfunción hepática severa, e incluso se asocian con cuadros de fibrosis en pacientes infectados (Kopterides et al., 2011). Adicionalmente, se evaluaron los parámetros de colinesterasa y colesterol. Los niveles de colinesterasa se encontraron mayoritariamente en el rango normal de 3 a 9 unidades por litro (Yue et al., 2022).

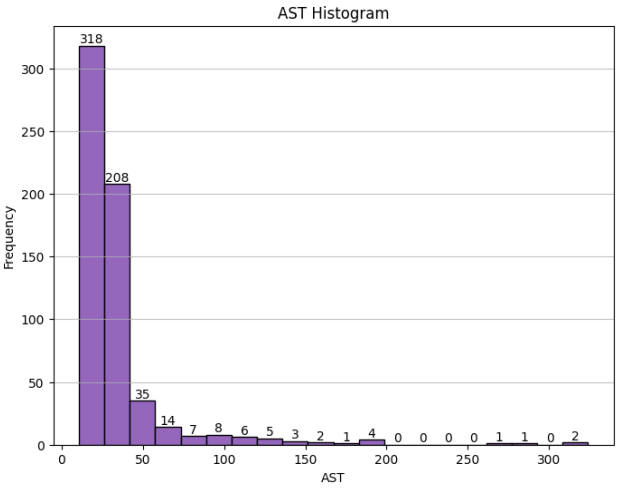

Fig. 7. Histograma de la frecuencia de personas según sus valores en la prueba de aspartato aminotransferasa

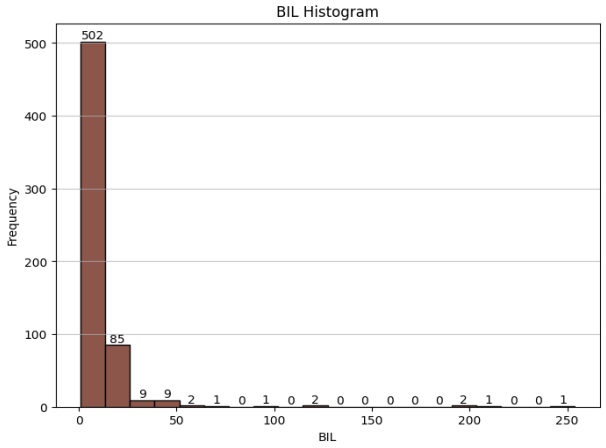

Fig. 8. Histograma de la frecuencia de personas según sus valores en la prueba de bilirrubina

Respecto al colesterol, se conoce que la infección crónica ha estado consistentemente asociada con alteraciones en los perfiles lipídicos, generando valores reducidos de colesterol total (Corey et al., 2009). Las mediciones de creatinina, gamma glutamil transferasa y proteínas totales también respaldaron la tendencia general de un conjunto de datos dominado por individuos sanos, aunque se identificaron pacientes específicos con valores atípicos que superaban los umbrales normales, lo cual es un claro indicativo de padecer alguna alteración estructural en el hígado

3.3 Dispersión estadística y correlación de variables

Para visualizar la dispersión estadística y la presencia de valores atípicos, se elaboraron diagramas de cajas para cada uno de los exámenes de laboratorio, los cuales se presentan en la Fig. 9. Las mediciones de proteína y albúmina resultaron ser las menos variables, manteniendo una consistencia notable entre la mayoría de los individuos. En marcado contraste, los valores de alanina aminotransferasa, aspartato aminotransferasa y gamma glutamil transferasa presentaron la mayor cantidad de valores atípicos, probablemente vinculados a la progresión de la enfermedad en los casos positivos o a variaciones biológicas extremas.

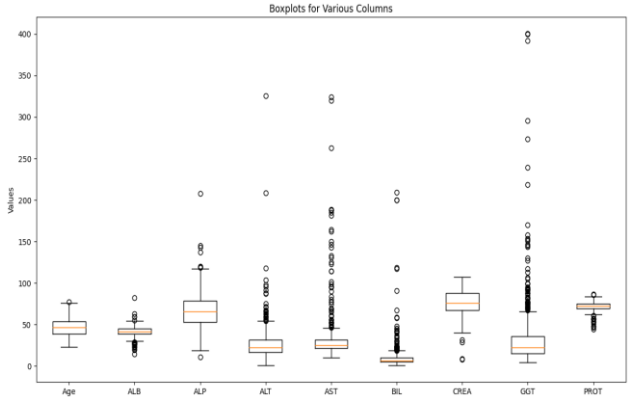

Fig. 9. Diagrama de cajas de las diferentes pruebas serológicas

Asimismo, al evaluar las relaciones entre estas variables mediante una matriz de correlación de Spearman (Fig. 10), se detectaron asociaciones directamente proporcionales y ligeramente significativas entre el colesterol y la colinesterasa, así como entre la albúmina y la colinesterasa. Destaca especialmente una correlación positiva y moderadamente significativa entre la aspartato aminotransferasa y la gamma glutamil transferasa, lo cual responde de manera lógica a su naturaleza biológica compartida como enzimas con alta concentración en los tejidos hepáticos The

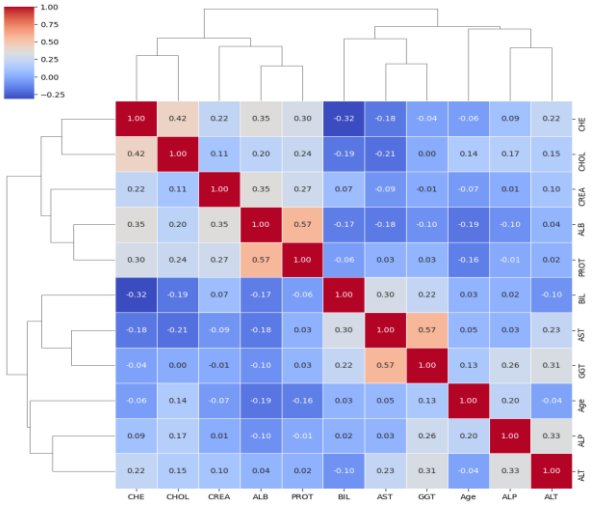

Fig. 10. Matriz de correlación entre las diferentes pruebas serológicas

3.4 Pruebas de significancia y comparación de medianas

Para validar estadísticamente la distribución de estos hallazgos, se aplicó la prueba de normalidad de Shapiro Wilk, la cual demostró de forma concluyente que todas las variables evaluadas poseían una distribución estadísticamente significativa, alejándose de la normalidad perfecta. Acto seguido, se implementó la prueba U de Mann Whitney para contrastar las medianas de los exámenes de laboratorio frente a la categoría binaria que definía el estado general de los pacientes. Los resultados arrojados por esta prueba, detallados en la Tabla 1, rechazaron categóricamente la hipótesis nula, evidenciando que existe una diferencia sustancial y comprobable en las medianas de variables como la alanina aminotransferasa, la albúmina, la bilirrubina y el colesterol, al comparar individuos completamente sanos frente a individuos portadores de la enfermedad.

Tabla 1. Resultados de prueba Mann Whitney U

	Variable	U Statistic	P-Value	Result
0	ALT	18807.0	4.073421e-09	Reject H0
1	ALB	14941.0	2.064296e-02	Reject H0
2	BIL	4012.5	7.983212e-15	Reject H0
3	CHOL	18605.0	1.234999e-08	Reject H0

3.5 Desempeño y validación de los modelos predictivos de Machine Learning.

Con la validación estadística completamente confirmada y los factores de riesgo identificados, se procedió a la evaluación analítica de los sistemas de aprendizaje automático. Las curvas de aprendizaje generadas permitieron observar el comportamiento dinámico de los modelos durante su fase de entrenamiento y posterior validación cruzada. En la Fig. 11, se aprecia que el modelo predictivo XGBoost presentó una precisión de entrenamiento con valores cercanos a la unidad, mientras que su respectiva curva de validación se mantuvo en un rango aceptable, oscilando entre 0.97 y 0.995, lo que demuestra una excelente capacidad de generalización sin incurrir en alteraciones de memoria o sesgo computacional.

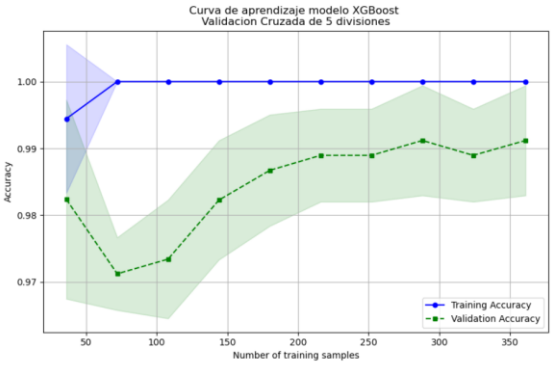

Fig. 11. Curva de aprendizaje del modelo XGBoost

Por su parte, la evaluación analítica de las Máquinas de Vectores de Soporte (Fig. 12) reflejó una dinámica de aprendizaje bastante similar y robusta. La precisión del entrenamiento de este algoritmo se consolidó en un rango superior entre 0.99 y 1, con una curva de validación paralela que alcanzó niveles estables de 0.98 a 0.99, evidenciando así un modelo sumamente confiable para la clasificación médica en escenarios de alta dimensionalidad de datos. Finalmente, la Fig. 13 muestra que el algoritmo Random Forest exhibió un desempeño excepcional y superior al lograr un valor perfecto de precisión estadística en la fase inicial de entrenamiento, manteniendo paralelamente una curva de validación sumamente estable y elevada que descartó cualquier problema de sobreajuste limitante.

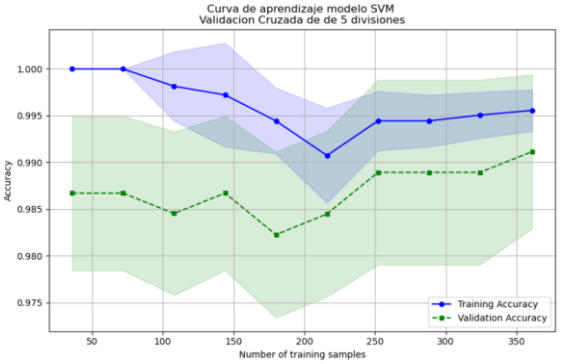

Fig. 12. Curva de aprendizaje del modelo SVM

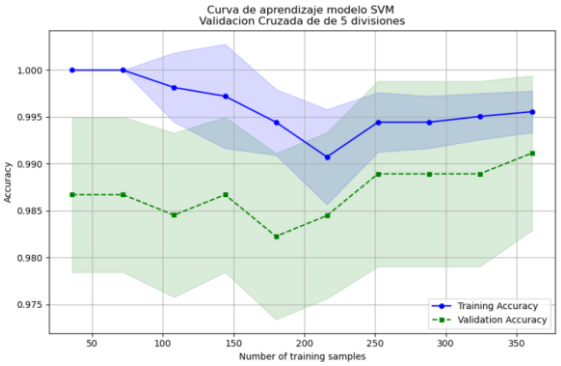

Fig. 13. Curva de aprendizaje del modelo Random Forest

El análisis definitivo y concluyente del desempeño operativo de estas herramientas computacionales se fundamentó en la Curva de Características Operativas del Receptor, conocida como curva ROC, ilustrada en la Fig. 14. Esta métrica visual y cuantitativa es fundamental en el campo médico para comprender con exactitud qué tan bien los modelos desarrollados pueden distinguir entre la clase de pacientes sanos y la clase de pacientes enfermos. El área bajo la curva calculada confirmó el altísimo rendimiento global de todos los sistemas predictivos ensayados en esta investigación.

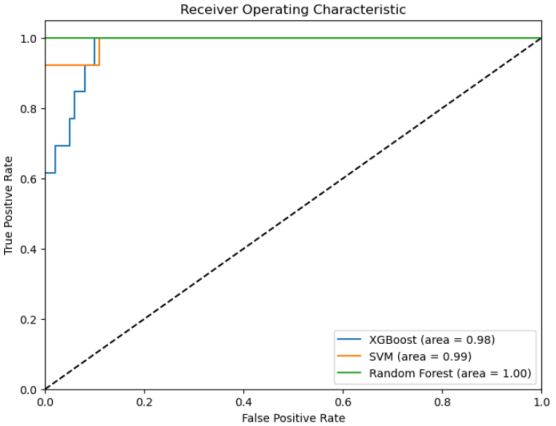

Fig. 14. Curva ROC de los modelos de Machine Learning

El modelo computacional Random Forest alcanzó una perfección teórica impecable con un valor consolidado de 1, indicando una capacidad absoluta y sin margen de error aparente para predecir la variable categórica clínica en este conjunto de datos específico. Le siguieron muy de cerca el modelo basado en Máquinas de Vectores de Soporte con un destacable valor de 0.99 y el algoritmo de refuerzo de gradiente XGBoost con un valor de 0.98. Todos estos resultados globales validan de manera contundente y científica la eficacia superior del aprendizaje automático en el reconocimiento de patrones clínicos complejos y en la detección temprana de patologías irreversibles

4 Discusión

El propósito central de esta investigación se enfocó en desarrollar y evaluar modelos computacionales para predecir la infección por hepatitis C a partir de pruebas sanguíneas y datos demográficos (Alam, 2023). Los resultados obtenidos demostraron que las herramientas de aprendizaje automático poseen una capacidad predictiva excepcional para distinguir entre individuos sanos y portadores de la patología (Yarasuri et al., 2019). Al evaluar el rendimiento global mediante la métrica del Área Bajo la Curva, se evidenció que el algoritmo Random Forest alcanzó una precisión perfecta con un valor de 1 (Ali et al., 2023). Le siguieron muy de cerca las Máquinas de Vectores de Soporte con un valor de 0.99 y el modelo XGBoost con 0.98. Esta superioridad predictiva en los resultados confirma, de manera contundente, que las tecnologías de inteligencia artificial son sumamente eficientes para el reconocimiento de patrones clínicos complejos.

Al analizar las variables serológicas involucradas, se comprobó estadísticamente la relevancia de los marcadores hepáticos tradicionales en la predicción de esta enfermedad. La prueba de Mann Whitney U demostró que existen diferencias sustanciales y comprobables en las medianas de la alanina aminotransferasa, la albúmina, la bilirrubina y el colesterol, al comparar a los pacientes sanos frente a los enfermos. Adicionalmente, el análisis de correlación de Spearman reveló asociaciones directamente proporcionales entre diversas enzimas, como la aspartato aminotransferasa y la gamma glutamil transferasa (Cross et al., 2008). Esta relación enzimática particular resulta lógica desde el punto de vista biológico y subraya su gran utilidad como indicador clave en la detección de alteraciones estructurales en el tejido hepático (Nadeem et al., 2010). Todo esto reafirma el alto valor diagnóstico de los exámenes de sangre rutinarios cuando son procesados mediante algoritmos avanzados.

La alta precisión alcanzada por estos modelos computacionales tiene implicaciones profundamente positivas para la práctica médica y la salud pública. La hepatitis C es una enfermedad silenciosa que, al ser detectada en etapas avanzadas, genera daños irreversibles como la cirrosis o el carcinoma (Bardají, 2020). La integración de estos modelos predictivos en los centros de salud facilitaría la evaluación temprana de los donadores de sangre y de los pacientes sospechosos. Al identificar anticipadamente a los individuos en riesgo, los especialistas pueden implementar estrategias preventivas y terapéuticas totalmente personalizadas. Esto no solo optimiza los recursos sanitarios, sino que incrementa de manera significativa la probabilidad de recuperación y la calidad de vida de las personas afectadas.
En síntesis, el presente estudio contribuye sustancialmente a la modernización de los métodos de diagnóstico clínico para afecciones virales. Queda demostrada la pertinencia de incorporar el aprendizaje supervisado como una herramienta de apoyo primario en la toma de decisiones médicas. Estos excelentes resultados respaldan la necesidad de continuar investigando y perfeccionando este tipo de tecnologías para combatir eficazmente las patologías hepáticas a escala global.

5 Comprobación estadística de las variables predictoras

Para validar matemáticamente la idoneidad de los datos empleados en el estudio, se ejecutaron pruebas de hipótesis rigurosas sobre los exámenes de laboratorio. Inicialmente, se aplicó la prueba de Shapiro Wilk para cada una de las variables serológicas, con el propósito estricto de evaluar si la información clínica presentaba una distribución normal. Los resultados de este análisis demostraron que todas las variables evaluadas son estadísticamente significativas, confirmando así la naturaleza específica de su distribución poblacional.

Tabla 2. Resultados de la prueba Shapiro Wilk

	Variable	P-Value	Significance
0	Age	0.000	Significant
1	ALB	0.000	Significant
2	ALP	0.000	Significant
3	ALT	0.000	Significant
4	AST	0.000	Significant
5	BIL	0.000	Significant
6	CHE	0.000	Significant
7	CHOL	0.000	Significant
8	CREA	0.000	Significant
9	GGT	0.000	Significant
10	PROT	0.000	Significant

Posteriormente, se llevó a cabo el test de correlación de rango de Spearman, el cual estuvo enfocado en pares específicos de variables para comprobar la significancia matemática de sus interacciones. Al analizar los parámetros de fosfatasa alcalina y aspartato aminotransferasa, la evaluación determinó un valor de probabilidad superior a 0.05. Por otro lado, al estudiar el par conformado por la proteína y la creatinina, los resultados arrojaron un valor de probabilidad inferior a 0.05, lo que indica de manera concluyente que existe una relación matemáticamente significativa entre estas dos métricas de laboratorio.

Tabla 3. Resultados del rango de correlación de Spearman.

Pair	Spearman Rank Correlation	P-value
PROT and CREA	0.178885	0.000019
ALP and AST	0.058177	0.166914

6 Conclusión

Tras analizar de manera exhaustiva los datos clínicos y aplicar diversas técnicas de validación estadística, se comprobó concluyentemente la existencia de correlaciones significativas entre las variables serológicas estudiadas. Esto sugiere, de forma clara y evidente, la presencia de factores de riesgo sumamente relevantes para el diagnóstico de la hepatitis C. Resulta de especial importancia destacar la correlación positiva y moderadamente significativa que se encontró entre las enzimas aspartato aminotransferasa y gamma glutamil transferasa, un hallazgo biológico que se perfila como un indicador clínico clave para la detección temprana de esta enfermedad.

Por otro lado, los modelos predictivos de aprendizaje automático desarrollados durante el estudio, que incluyen los algoritmos XGBoost, Máquinas de Vectores de Soporte y Random Forest, demostraron ser altamente eficaces para la identificación precisa de potenciales portadores del virus. En este sentido, es sumamente relevante resaltar el rendimiento superior y perfecto del modelo Random Forest, el cual alcanzó un Área Bajo la Curva de valor unitario, siendo seguido muy de cerca por las Máquinas de Vectores de Soporte con un valor de 0.99 y el modelo XGBoost con un 0.98. Estos excelentes resultados respaldan, desde una perspectiva tanto científica como tecnológica, la inmensa utilidad que tiene la aplicación de la inteligencia artificial para la predicción de enfermedades hepáticas de alta complejidad.

Adicionalmente, la interpretación profunda de estos resultados métricos ha permitido identificar con total claridad cuáles son los factores de riesgo y los marcadores sanguíneos más influyentes al momento de realizar la predicción médica. Este conocimiento resulta verdaderamente fundamental para diseñar e implementar estrategias preventivas y terapéuticas que sean mucho más precisas y totalmente personalizadas para cada paciente. La capacidad de detectar la infección de forma temprana en individuos que se encuentran en situación de riesgo, facilitada enormemente por estos modelos computacionales, tiene el potencial real de conducir a una mejora significativa en los pronósticos clínicos y, por consiguiente, en la calidad de vida integral de las personas afectadas.

En síntesis, este trabajo de investigación ha contribuido de manera sustancial y directa al avance de las metodologías orientadas a la detección precoz y al tratamiento oportuno de la hepatitis C. Queda demostrada, con evidencia matemática y estadística sólida, la gran importancia y pertinencia que tiene la incorporación de los sistemas de aprendizaje supervisado dentro de la práctica clínica diaria. Todos estos hallazgos respaldan de forma contundente la necesidad imperativa de continuar apoyando, investigando y desarrollando nuevas herramientas predictivas de vanguardia, con el firme propósito de combatir de manera eficaz esta grave afección hepática y elevar los estándares de la salud pública a nivel global.

Referencias

Alam, A. (2023). What is machine learning? Zenodo. https://doi.org/10.5281/zenodo.8231580

Ali, A. M., Hassan, M. R., Aburub, F., Alauthman, M., Aldweesh, A., Al-Qerem, A., Jebreen, I., & Nabot, A. (2023). Explainable Machine Learning Approach for Hepatitis C Diagnosis Using SFS Feature Selection. Machines, 11(3), 391. https://doi.org/10.3390/machines11030391

Balter, S., Stark, J. H., Kennedy, J., Bornschlegel, K., & Konty, K. (2014). Estimating the prevalence of hepatitis C infection in New York City using surveillance data. Epidemiology and Infection, 142(2), 262–269. https://doi.org/10.1017/S0950268813000952

Bardají, M. (2020). Utilidad de un sistema de análisis masivo de datos (Big Data) insertado en la historia clínica electrónica, en la búsqueda activa de pacientes con hepatitis C (Trabajo de Grado). Universidad de Valladolid UVaDOC. https://uvadoc.uva.es/handle/10324/41390

Chen, T., & Guestrin, C. (2016). XGBoost. Proceedings of the 22nd ACM SIGKDD International Conference on Knowledge Discovery and Data Mining, 785–794. https://doi.org/10.1145/2939672.2939785

Corey, K. E., Kane, E., Munroe, C., Barlow, L. L., Zheng, H., & Chung, R. T. (2009). Hepatitis C virus infection and its clearance alter circulating lipids: Implications for long-term follow-up. Hepatology, 50(4), 1030–1037. https://doi.org/10.1002/hep.23219

Cross, T., Antoniades, C., & Harrison, P. (2008). Non-invasive markers for the prediction of fibrosis in chronic hepatitis C infection. Hepatology Research, 38(8), 762–769. https://doi.org/10.1111/j.1872-034X.2008.00364.x

Cutler, A., Cutler, D. R., & Stevens, J. R. (2012). Random Forests. En Ensemble Machine Learning (pp. 157–175). Springer New York. https://doi.org/10.1007/978-1-4419-9326-7_5

Haq, M., Salman, F., Haq, M., Obaid, S., Gul, A., & Khan, A. M. K. (2019). Correlation of serum vitamin D levels with serum levels of alkaline phosphatase. The Professional Medical Journal.

Kecman, V. (2005). Support Vector Machines – An Introduction (pp. 1–47). https://doi.org/10.1007/10984697_1

Kopterides, P., Liberopoulos, P., Ilias, I., Anthi, A., Pragkastis, D., Tsangaris, I., Tsaknis, G., Armaganidis, A., & Dimopoulou, I. (2011). General Prognostic Scores in Outcome Prediction for Cancer Patients Admitted to the Intensive Care Unit. American Journal of Critical Care, 20(1), 56–66. https://doi.org/10.4037/ajcc2011763

Lee, J. K., Shim, J. H., Lee, H. C., Lee, S. H., Kim, K. M., Lim, Y.-S., Chung, Y.-H., Lee, Y. S., & Suh, D. J. (2010). Estimation of the healthy upper limits for serum alanine aminotransferase in Asian populations with normal liver histology. Hepatology, 51(5), 1577–1583. https://doi.org/10.1002/hep.23505

Nadeem, A., Mazhar, M., & Aslam, M. (2010). Correlation of serum alanine aminotransferase and aspartate aminotransferase levels to liver histology in chronic hepatitis C. J Coll Physicians Surg Pak.

Nojiri, S., Kusakabe, A., Shinkai, N., Matsuura, K., Iio, E., Miyaki, T., & Joh, T. (2011). Factors influencing distant recurrence of hepatocellular carcinoma following combined radiofrequency ablation and transarterial chemoembolization therapy in patients with hepatitis C. Cancer Management and Research, 3, 267–272. https://doi.org/10.2147/CMR.S22073

Yap, C. Y., & Aw, T. C. (2010). Liver Function Tests (LFTs). Proceedings of Singapore Healthcare, 19(1), 80–82. https://doi.org/10.1177/201010581001900113

Yarasuri, V. K., Indukuri, G. K., & Nair, A. K. (2019). Prediction of Hepatitis Disease Using Machine Learning Technique. 2019 Third International Conference on I-SMAC (IoT in Social, Mobile, Analytics and Cloud) (I-SMAC), 265–269. https://doi.org/10.1109/I-SMAC47947.2019.9032585

Yue, C., Zhang, C., Ying, C., & Jiang, H. (2022). Reduced serum cholinesterase is an independent risk factor for all-cause mortality in the pediatric intensive care unit. Frontiers in Nutrition, 9. https://doi.org/10.3389/fnut.2022.809449

Recibido: *19 de diciembre de 2025*

Aceptado: *10 de marzo de 2026*

Segovia, José T.: *Ingeniero Aeronáutico y Licenciado en Ciencias y Artes Militares, con estudios de Máster en Bioinformática y Bioestadística, y en Ingeniería de Software e Inteligencia Artificial. Posee más de 20 años de experiencia en gerencia de operaciones, ingeniería y proyectos. Actualmente se desempeña como Gerente General de Certificación de Productos Aeronáuticos (EANSA) y es especialista en el uso de metodologías ágiles e inteligencia artificial.*
https://orcid.org/0009-0004-3187-2335

Artículo de Investigación. Revista Ciencia e Ingeniería. Vol. 47, No. 2 pp. 191−198, abril-julio, 2026
ISSN 1316-7081. ISSN Elect. 2244-8780 Universidad de los Andes (ULA)

Efecto de la composición química sobre la aceptabilidad general de una mayonesa.

Effect of chemical composition on the general acceptability of a mayonnaise.

Zambrano, Lorena[1*]; López, Juan[1,2,3]; Celis, María Teresa[4]
[1] Escuela Básica de Ingeniería, Facultad de Ingeniería, Universidad de Los Andes, Mérida, Venezuela.
[2] Centro de Investigaciones y Proyectos en Matemática Aplicada, CIMA.
[3] Lab. Química Experimental Aplicada, QUEXA.
[4] Laboratorio de Polímeros y Coloides, POLYCOL.
*lczambranorivas@gmail.com

Resumen

En este trabajo se estudió el efecto de la composición química sobre la aceptabilidad general de una mayonesa. Se corrieron dos diseños experimentales factoriales 2^2, cuatro composiciones químicas, dos réplicas, ocho mayonesas por experimento. En el primer experimento se variaron las concentraciones de un extracto oleoso de orégano y de sal de mesa. En el segundo, se modificaron la cantidad de aceite y yemas de huevo. La idea final era conocer mediante un evento de cata el efecto de las variables de control sobre el grado de aceptabilidad y mejorar la formulación para lograr una mayonesa de alta aceptación. El extracto oleoso se obtuvo por maceración de hojas molidas de orégano puestas en contacto con aceite de soya. Las fases aceite y acuosa se prepararon mezclando el extracto oleoso de orégano con aceite de soya y la acuosa mezclando huevo, sal, azúcar, vinagre, mostaza y pimienta para lograr las concentraciones extracto de orégano y sal, respectivamente, de acuerdo al diseño experimental. La mayonesa se preparó añadiendo la fase aceite en formato de hilo a la fase acuosa. Se realizaron dos catas, una para cada experimento, para el primero se presentaron 20 personas con poco conocimiento profesional del arte culinario; para el segundo, se contó con 10 expertos. Los resultados sugieren de manera contundente que los efectos de las concentraciones de orégano y de sal, así como el de su interacción sobre el nivel de aceptación general muestran ser estadísticamente altamente significativos. El segundo experimento, muestra que las mayonesas gustaron en un nivel alto, promedio global de 7.66/9; los efectos evaluados no mostraron evidencias estadísticas significativas sobre el nivel de aceptación. Vale mencionar, sin embargo, que a los profesionales de la cocina se mostraron más afín a las mayonesas con bajo contenido de yemas de huevo y alto contenido de aceite.

Palabras clave: Cata de mayonesas, emulsiones alimenticias, efecto de la composición química, experimento factorial.

Abstract

This study examined the effect of chemical composition on the overall acceptability of mayonnaise. 2^2-factorial experimental designs were run, with four chemical compositions, two replicates, and eight mayonnaises per experiment. In the first experiment, the concentrations of an oregano oil extract and table salt were varied. In the second, the amount of oil and egg yolks was modified. The final idea was to use a tasting event to determine the effect of the control variables on the degree of acceptability and improve the formulation to achieve a highly acceptable mayonnaise. The oil extract was obtained by macerating ground oregano leaves in soybean oil. The oil and aqueous phases were prepared by mixing the oregano oil extract with soybean oil and the aqueous phase by mixing egg, salt, sugar, vinegar, mustard, and pepper to achieve the oregano extract and salt concentrations, respectively, according to the experimental design. The mayonnaise was prepared by adding the oil phase in a thin stream to the aqueous phase. Two tasting events were conducted, one for each experiment. For the first, 20 people with little professional knowledge of the culinary arts participated; for the second, 10 experts participated. The results strongly suggest that the effects of oregano and salt concentrations, as well as that of their interaction on the level of overall acceptance, are statistically highly significant. The second experiment showed that the mayonnaises were rated at a high level, global average off 7.66/9; the effects evaluated did not show statistically significant evidence regarding the level of acceptance. It is worth mentioning, however, that culinary professionals showed a preference for mayonnaises with low egg yolk and high oil content.

Keywords: *Mayonnaise tasting, food emulsions, effect of chemical composition, factorial experiments.*

1 Introducción

Hoy en día la experimentación es una parte fundamental en todos los campos de la investigación y desarrollo científico-tecnológico. El objetivo de la experimentación es obtener información de calidad que permita validar y formular teorías y leyes que expliquen el comportamiento de la naturaleza, así como también ayudar en el desarrollo de nuevos y mejores productos, procesos y servicios (Montgomery, 2002).

El diseño de experimento puede definirse como un procedimiento que en resumen busca establecer relación entre los efectos de las variables de control y las respuestas; para ello se plantear con claridad los pasos a seguir y su orden de ejecución para obtener datos significativos que permitan un análisis confiable del sistema que conduzca a una síntesis que exprese la información relevante sobre características y comportamiento, relación entre las variables de control y las respuestas del sistema; conocer los efectos de dichas variables y el de sus interacciones sobre las distintas respuestas que pueda presentar el sistema en estudio (Gutiérrez Pulido & De la Vara Salazar, 2012).

La planificación de los experimentos es vital; muchas veces, en particular en las industrias, se hacen experimentos muy costosos y al final se tiene una colección de datos de muy poco valor. Su objetivo es el de obtener el máximo de información requerida por el experimento con el mínimo coste (menor tiempo, número de corridas experimentales y uso de recursos humanos, materiales y tecnológicos) sin prescindir de una alta eficiencia (Antony, 2014). El diseño estadístico factorial a k variables y 2 niveles uno de los más sencillos, efectivos y económicos de emplear.

Estudiar un sistema complejo, como la mayonesa, cuyo comportamiento depende de muchos factores que interactúan, que se pueden variar a muchos niveles, lo cual implica un costo alto, muchos experimentos, cientos e incluso miles, para conocer quizás un poquito del mismo. En tal sentido, el diseño estadístico de experimento factorial a dos niveles puede ser de gran utilidad y eficacia para determinar los efectos de k variables y el de sus interacciones sobre el nivel de aceptación general que ayude a formular una mayonesa de gran calidad y alto agrado que satisfaga las demandas de la población.

Esto resulta de gran interés, dado que, desde el punto de vista comercial, la mayonesa es el aderezo más consumido a nivel mundial. La misma es un alimento emulsionado que se obtiene mezclando de manera adecuada aceites vegetales comestibles, yema de huevo líquido o su equivalente en cualquiera de sus formas, vinagre, adicionado o no de jugo de limón, sal, edulcorantes nutritivos, acidulantes permitidos, mostaza, paprica y otras especies o extractos y aceites esenciales de las mismas con excepción de azafrán y cúrcuma. Una mayonesa debe tener un contenido de aceite de, al menos, 65%, y 4% mínimo de yema de huevo; además de un pH entre 3.9 y 4.1, esto, según la Comisión Venezolana de Normas Industriales (COVENIN), específicamente bajo la norma COVENIN 90:2020.

Desde la perspectiva de la fisicoquímica, una mayonesa se define como una emulsión de aceite en agua (O/W); esto es, un sistema termodinámicamente inestable y estabilizado cinéticamente por la acción de un agente con acción interfacial; en este caso, la lecitina, una molécula fosfolípida presente de manera abundante en la yema de huevo, cumple este rol adsorbiéndose sobre la superficie de aceite facilitando la formación de gotas diminutas y creando una interfase robusta que atenúa considerablemente en la cinética de los fenómenos de la coalescencia y floculación de éstas (McClements, 2015).

La industria actual evoluciona continuamente para mejorar y optimar los productos que satisfagan las demandas exigentes de las sociedades modernas; para ello, se enriquecen los conceptos tradicionales; así, por ejemplo, las nuevas mayonesas buscan cumplir estándares que aporten a la salud y sostenibilidad sin sacrificar la palatabilidad (el "mouthfeel") (McClements, 2015). El orégano, por ejemplo, es una hierba aromática, producto natural, cuyos aceites esenciales presentan un paquete de propiedades, con funciones específicas, que aportan a las propiedades organolépticas de cualquier producto alimenticio; pero que también pueden reemplazar parcial o total el uso de antioxidantes sintéticos como el EDTA, permitido por la norma COVENIN 910:2016; los aceites esenciales del orégano pueden actuar como antimicótico y bactericida contra microorganismos patógenos como *Salmonella typhimurium*, *Escherichia coli*, *Staphylococcus aureus*, *Staphylococcus epidermidis*, *hongo Cándida*, entre otros, (Arcila-Lozano et al., 2004; López-Pedrouso et al., 2022; Nurzyńska-Wierdak & Walasek-Janusz, 2025). Esto pone de manifiesto que las características del orégano aportar gran valor a distintos productos de la industria alimentaria mejorando sus propiedades organolépticas y favoreciendo también funciones relacionadas con la inocuidad, estabilidad física y química, como las alteraciones lipídicas (López-Pedrouso et al., 2022). Existen, además, algunos trabajos que reportan el efecto antimutagénico y anticarcinogénico del orégano sugiriendo que representan una alternativa para el tratamiento y/o prevención de trastornos crónicos como el cáncer, sinusitis, migraña, etc (Balusamy et al.,2018). Finalmente, en el contexto de un sistema coloidal (O/W), estos compuestos actúan como secuestrantes de radicales libres, interrum-

piendo la cadena de autooxidación de los lípidos.

Es importante mencionar que, la ciencia de las emulsiones ha entendido que las mayonesas, emulsiones alimenticias, aunque pudieran ser tratadas desde el punto de vista de la fisicoquímica igual que las otras emulsiones también se debe tomar en cuenta que entran en juego otros aspectos por parte del consumidor; algunos de naturaleza psicológicos, otros endocrinos, perceptivos e incluso culturales. En tal sentido, se acostumbra a emplear una tabla hedónica como instrumento de medición para apoyar las pruebas sensoriales que se llevan a cabo, para medir de alguna manera "numérica" las valoraciones que un panel de cata tenga sobre productos alimenticios, como una mayonesa. Así, el instrumento hedónico, transforma una propiedad cualitativa en un valor numérico que permite análisis estadístico.

En este trabajo, para estudiar el efecto de factores controlables como las concentraciones de sal, extracto oleoso de orégano, aceite y yema de huevo, sobre la respuesta aceptabilidad general de unas mayonesas por un panel de catadores, se realizaron dos diseños de experimentos 2^2 factorial. La información del primer experimento se usó para formular una mayonesa de mayor aceptabilidad. El segundo confirmó lo útil del diseño experimental en la formulación de un producto alimenticio complejo como la mayonesa.

2 Materiales, Instrumentos y Métodos

Materiales.

La mayonesa es una emulsión alimenticia del tipo "aceite" en "agua" (O/W); en este estudio, la fase acuosa se constituyó con huevo, vinagre, sal, azúcar; y se aderezó con pimienta y mostaza; mientras que, la fase oleosa por aceite comestible de soya, Portumesa, aderezado con extracto oleoso de orégano.

Equipos e instrumentos

Para pesar los ingredientes requeridos para la preparación de las distintas mayonesas se usó una balanza analítica de la serie PCLE-LS (^{M} clase II) con precisión de 0.01 gramos y rango de pesado de 0 a 500 gramos; para mezclar los ingredientes de la fase acuosa e integrar el aceite para la elaboración de las mayonesas se usó un recipiente de acero inoxidable de un litro y medio, un mezclador manual de cocina. Posteriormente, se usó un mezclador manual marca Press y una licuadora de inmersión marca Guttlem. Finalmente, las mayonesas preparadas se almacenaron en recipientes de plástico con tapa de 250 ml en un refrigerador a la temperatura de 4ºC.

Métodos

- **Extracto oleoso de orégano**

Para la obtención del extracto oleoso de orégano, las hojas deshidratadas de dicha especie se sometieron a un proceso de maceración, poniéndolas en contacto con aceite de soya, Portumesa, en una proporción 1:4, respectivamente, durante 7 días. Vale mencionar que, primero, las hojas de orégano deshidratadas se molieron en una licuadora Oster para aumentar la superficie de contacto y hacer más eficiente el proceso de maceración. Posteriormente, mediante un proceso de doble filtrado se obtuvo el extracto oleoso de orégano, con sus aceites esenciales disueltos en el aceite de soya. El primer proceso de filtrado tuvo como objetivo separar la mayor cantidad de sólidos de una manera rápida; el mismo se llevó a cabo a través de un trozo de Dopiovelo, tela de poros grandes; el segundo filtrado se llevó a cabo a través de un trozo de Tafeta Bahamas, tela de poros finos, para obtener una separación casi completa, resultando en un extracto oleoso rico en aroma a orégano con un color verde oliva intenso y sin sólidos visibles. Finalmente, la mezcla resultante se envasó y preservó en recipientes limpios y secos, previamente rotulados.

- **Pasteurización de los huevos**

Para reducir la posibilidad de contagio con *Salmonella*, de los participantes en las dos catas, pruebas sensoriales, se procedió a pasteurizar los huevos empleados en la elaboración de las mayonesas. Las *Salmonellas* pueden estar presentes tanto en las cáscaras como en el interior de los huevos, generalmente, por la infección de los oviductos de las gallinas ponedoras. El proceso de pasteurización garantiza una eliminación casi total de dichas bacterias; el mismo se lleva a cabo sin que el huevo se llegue a cocinar. Los huevos se lavaron para quitar todo tipo de suciedad, que pudieran traer, de sus superficies; luego, se colocaron en agua a temperatura de 65°C durante 12 minutos; inmediatamente después, se enfriaron poniendo los recipientes en contacto con agua fría y, luego, colocándolos en el refrigerador a cuatro grados centígrados por una hora. Por simple inspección, se pudo apreciar que luego de la pasteurización los huevos mantuvieron un aspecto natural, esto es, no se vio transformación alguna que sugiriese que sus proteínas se hayan desnaturalizado o cocido.

- **Preparación de la fase acuosa**

Para el primer experimento se prepararon dos fases acuosas constituidas por huevo, vinagre, sal y azúcar; además, se le agregaron mostaza y pimienta como aderezos. La primera se preparó con 205 gramos de huevo (144 gramos de yema y el resto de clara), luego se le agregó 10 gramos de azúcar, 5 gramos de pimienta y **25 gramos de sal de mesa**, 30 gramos de vinagre y 30 gramos de mostaza. La segunda, se preparó igual a la primera, pero se le agregaron solo **10 gramos de sal de mesa**, en lugar de 25. Luego, los ingredientes se integraron con un mezclador de mano y ambas

fases acuosas se preservaron en recipientes previamente rotulados.

Para el segundo experimento también se prepararon dos fases acuosas de manera similar a como se hizo en el primer experimento ambas con 10 gramos de sal, pero esta vez se modificó la relación entre yema y clara de huevo. Una fase acuosa se preparó con 144 gramos de yema y el resto de clara de huevo hasta llegar a 205 gramos; mientras que en el segundo se añadieron 69 gramos de yema de huevo y el resto de clara hasta llegar a 205 gramos. Las mezclas resultantes se preservaron en recipientes rotulados para el momento de la emulsificación.

- **Elaboración de la mayonesa**

Para ambos experimentos se elaboración ocho mayonesas mediante dos experimentos factoriales 2^2, dos variables a dos niveles cada una, cuatro condiciones de experimentación y dos réplicas lo que resultó en ocho corridas. Dos días después, las ocho mayonesas se sometieron a una valoración por un panel de catadores. Para el primer experimento, el panel de catadores se constituyó por 20 personas no expertas en temas culinarios, para conocer el nivel de aceptación general que dicho panel percibía sobre las mismas; el panel evaluó mediante una escala hedónica de nueve puntos (Tabla 1). Para el segundo experimento, el panel de catadores se constituyó por 10 integrantes, expertos en el tema culinario, entre profesores y estudiantes avanzados del Centro Gastronómico de Alta Cocina, la Escuela del Chef Jesús Sánchez, de la ciudad de Mérida, Venezuela. Para el segundo experimento se tomó en cuenta la información del primero y, apuntó a obtener un producto de alta aceptación; además, se modificó en dos niveles los contenidos de yema de huevo y aceite.

Tabla 1: Escala hedónica de nueve puntos

Puntaje	Categoría	Puntaje	Categoría
1	Me digusta muchísimo	6	Me gusta poco
2	Me disguta mucho	7	Me gusta bastante
3	Me disgusta bastante	8	Me gusta mucho
4	Me disgusta poco	9	Me gusta muchísimo
5	No me gusta ni me disgusta		

Para el primer experimento factorial, el proceso, propiamente dicho, de elaboración de las mayonesas comenzó por batir, con un mezclador manual, marca Press, 58 o 61 gramos de fase acuosa, según las condiciones de operación (alto o bajo contenido de sal), en un recipiente de acero inoxidable, Para el segundo experimento factorial, se empleó siempre 58 gramos de fase acuosa. Luego, para todos los casos, se agregó la fase aceite en forma de hilo sin dejar de mezclar; a medida que se va incorporando la fase aceite, por simple inspección, se observó que la viscosidad del sistema se incrementó progresivamente. La mezcla resultante se trasvasó al recipiente de la licuadora de inmersión y se sometió a un proceso de mezclado (molienda) más intenso derivando en un sistema emulsionado (mayonesa) mucho más viscoso. Finalmente, las mayonesas se trasvasaron a vasos plásticos con tapa, previamente rotulados, y se llevó a refrigeración manteniéndose allí hasta la prueba de valoración sensorial, cata respectiva.

- **Experimentos factoriales 2^2**

La Tabla 2 sintetiza de manera representativa los dos diseños estadísticos experimentales factoriales 2^2 que se realizaron en esta investigación; en ella se muestran la matriz de diseño, las observaciones promedio para cada réplica y la matriz de los efectos. Para el primer experimento, "**A"** y "B" representan las concentraciones de sal de mesa y de extracto oleoso de orégano, respectivamente, a dos niveles. Los signos "**-**" y "**+**" representan los niveles bajo y alto, respectivamente, de las concentraciones. De manera similar, para el segundo experimento factorial 2^2, "A" y "B" representan las cantidades de yema de huevo y fase aceite, respectivamente. Los signos "**-**" y "**+**" representan los dos niveles bajo y alto, respectivamente, de las cantidades de yema y fase aceite. Los resultados de ambos experimentos se representan mediante el promedio de las observaciones de los participantes en las pruebas sensoriales sobre la aceptabilidad general de las mayonesas por parte de éstos teniendo en cuenta la escala hedónica de nueve puntos, Tabla 1. Los efectos principales y de interacción se calculan, teniendo en cuenta los signos de la matriz de efectos, como la diferencia de los promedios positivos y negativos de las respuestas, esto es: Efecto de A= ($\bar{y}_+ - \bar{y}_-$); así que, para el efecto de "**A**" sobre el grado de aceptabilidad general, el promedio $\bar{y}_+$ viene a ser (1/4)*($y_{12} + y_{14+} y_{22} + y_{24}$); mientras que $\bar{y}_-$ viene a ser (1/4) *($y_{11} + y_{13} + y_{11} + y_{13}$). El proceso de estimación de los efectos restantes, principal B y de interacción AB, sobre el grado de aceptabilidad general es similar.

Tabla 2: Diseño factorial 2^2

Matriz de Diseño		Observaciones Promedios		Matriz de Efectos		
A	B	y_1	y_2	A	B	AB
-	-	y_{11}	y_{21}	-	-	+
+	-	y_{12}	y_{22}	+	-	-
-	+	y_{13}	y_{23}	-	+	-
+	+	y_{14}	y_{24}	+	+	+

- **Valoración sensorial (cata) de las mayonesas**

La cata de las mayonesas se llevó a cabo en dos ambientes; la primera se hizo con un grupo de no expertos culinarios, en las residencias Terrazas del Sol, Mérida, Venezuela. La segunda se llevó a cabo en el Centro Gastronómico de Alta Cocina, Escuela del Chef Jesús Sánchez. Con la idea de disminuir el ruido de la secuencia en la que se prueban las mayonesas se hizo primero un sorteo que condujo en asignarles un número a cada participante de la cata; luego, con la función ALEATORIO de Excel se aleatorizó, para cada participante, el orden en que se debían probar las ocho preparaciones de mayonesa. El proceso de valoración sensorial,

cata, consistió en degustar cada mayonesa sobre una rodajita de pan, que cada uno de los participantes tomaba de una bandeja y la untaba con la mayonesa, indicada según la aleatorización, la comía y reportaba una opinión de acuerdo a la escala hedónica de nueve puntos, Tabla 1. Inmediatamente después, los participantes apuntaban su valoración y limpiaban el paladar con agua y galletas de soda y después de varios minutos proseguían con la siguiente muestra. Al culminar con las ocho muestras, cada participante entregó su planilla de valoración.

- **Medición de tamaño de gota**

Existen diferentes métodos para la determinación del diámetro promedio de gotas y la distribución del tamaño de gotas de una emulsión. En este trabajo se empleó el equipo Malvern Mastersizer, el cual se fundamenta en la técnica de difracción de luz láser. Después de cada medida se genera un reporte que presenta: el diámetro d[4,3] o d_{43} y diámetro d[3,2] o d_{32} que corresponden al promedio aritmético de la distribución en volumen y en área, respectivamente. Se tomó como valor promedio de gotas el diámetro de Sauter (d_{32}), porque ha sido usado frecuentemente en los estudios de correlaciones reportados en la literatura (Rounsley, 1982; Eckert *et al.*, 1985; Briceño *et al.*, 2002).

3 Resultados y Discusión

El primer experimento factorial 2^2 se presenta de manera sintética en la tabla 3a y su análisis de varianza en la Tabla 3b. En la Tabla 3a se presentan de manera sintetizada el diseño experimental, las cuatro condiciones de operación, las observaciones promedio de cada una de las cuatro condiciones de operación para las dos réplicas y la matriz de efectos, que facilita estimar los efectos. La Tabla 3b, se presenta el análisis de varianza; primero se muestran los tres efectos, dos de cada una de las variables (A y B) y el de su interacción (AB) sobre el nivel de aceptación general de las ocho mayonesas. Por simple inspección de los valores de los efectos presentados en dicha tabla se ve que son significativos por su valor, luego el análisis de varianza y el factor "p" lo confirman; se muestra que hay evidencias estadísticas altamente significativas de que el efecto de las concentraciones de sal (variable A), y extracto oleoso de orégano (variable B) y el de su interacción tienen efectos altamente significativos estadísticamente sobre la respuesta nivel de aceptación general de parte de los participantes. La tabla muestra que el efecto de la concentración de sal es el más importante. Vale mencionar que los tres efectos (los dos principales y el de interacción) operan de forma sinérgica sugiriendo que un producto con mayor aceptación se podría conseguir a menores concentraciones de sal y del extracto oleoso de orégano. Así, este resultado dio pistas para diseñar el segundo experimento factorial el cual se valoró por profesionales del Centro Gastronómico de Alta Cocina, la Escuela del Chef Jesús Sánchez, de la ciudad de Mérida, Venezuela.

Tabla 3: Primer experimento factorial 2^2; A: concentración de sal; B concentración de extracto de orégano

Matriz de Diseño		Observaciones Promedios		Matriz de Efectos		
A	B	y_1	y_2	A	B	AB
-	-	8,3	7,8	-	-	+
+	-	5,1	4,7	+	-	-
-	+	5,5	6,1	-	+	-
+	+	4,3	4,5	+	+	+

Fuente	Efectos	SS	GL	MS	Fo	F_{crit}	p
A	-2,28	10,35	1	10,35	102,23	7,71	5,4,E-04
B	-1,38	3,78	1	3,78	37,35	7,71	3,6,E-03
AB	0,88	1,53	1	1,53	15,12	7,71	1,8,E-02
Error		0,40	4	0,10			
Total		16,07	7				

a) Corrida experimental y su réplica; **b)** Efectos y análisis de varianza

Las Tablas 4a y 4b presentan, de manera similar al caso del primer experimento factorial, los resultados del segundo experimento factorial. En este caso, sin embargo, se muestra que no hay evidencias altamente significativas de que las cantidades de yema y aceite, entre los valores estudiados, tengan efectos importantes sobre la aceptabilidad general de las mayonesas por parte de los participantes. Sin embargo, tomando en cuenta que dicha cata la tomaron profesionales del arte de preparar alimentos, que valoraron la aceptabilidad general con un 7.66 de promedio global en la escala hedónica de nueve puntos y que expresaron abiertamente que casi todas las mayonesas les habían gustado mucho, aunque mostraron preferencias por las mayonesas preparadas de acuerdo a las condiciones de operación del diseño 3, - +, esto es menos yemas, más clara, y más fase aceite. Así que, se puede decir que los resultados del primer experimento estuvieron muy acertado al sugerir menores concentraciones de sal y del extracto oleoso de orégano. También se puede decir que modificar la variación en la cantidad de yema de huevo y de fase aceite no modificaron (disminuir o aumentar) de manera importante el grado de aceptación general.

Tabla 4: Segundo experimento factorial 2^2; A: Cantidad de yema; B Cantidad de fase aceite.

Matriz de Diseño		Observaciones Promedios		Matriz de Efectos		
A	B	y_1	y_2	A	B	AB
-	-	8,0	8,0	-	-	+
+	-	6,4	7,0	+	-	-
-	+	7,4	8,6	-	+	-
+	+	7,9	8,0	+	+	+

Fuente	Efectos	SS	GL	MS	Fo	F_{crit}	p
A	-0,68	0,91	1	0,91	4,03	7,71	1,2,E-01
B	0,63	0,78	1	0,78	3,45	7,71	1,4,E-01
AB	0,63	0,78	1	0,78	3,45	7,71	1,4,E-01
Error		0,91	4	0,23			
Total		3,38	7				

a) Corrida experimental y su réplica; **b)** Efectos y análisis de varianza

El tamaño y distribución de tamaño de gota de una emulsión da cuenta de su textura y viscosidad; por simple inspección, se observó que las viscosidades de las distintas mayonesas se incrementaron progresivamente al ir incorporando el aceite de manera manual; luego, se observó que dichas mayonesas sufrieron un incremento mucho mayor en su viscosidad al someterlas al proceso de alta cizalla mediante la licuadora de inmersión para obtener la mayonesa final. Posiblemente, esto se deba a dos causas provocadas por la acción de la licuadora de inmersión: la primera, la disminución de tamaño de gota y la segunda una distribución de tamaño de gotas más estrecha, (McClements, 2015). La licuadora de inmersión incorpora mucho más energía y cizalla que la que pueda aportar un agitador manual por muy buen diseño que este último tenga. A las mayonesas finales del primer experimento se les midió la distribución

del tamaño de gotas, resultando que todas presentaron una distribución bimodal como la que se muestra en la **Fig.1.**

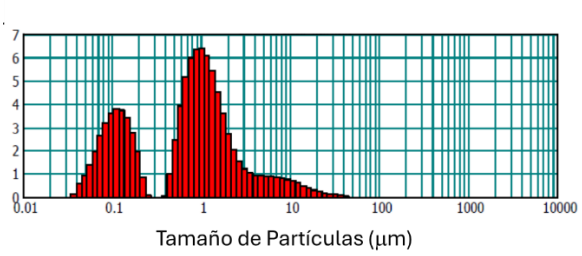

Fig.1.: Distribución de tamaño de gota de la mayonesa con condiciones de experimentación "- -", ver Tabla 3a.

El comportamiento bimodal en la distribución de tamaño de gotas sugiere dos mecanismos de molienda o una restricción que separe el sistema en una zona una de baja y otra de alta cizalla, en los que se produzcan gotas grandes y pequeñas, respectivamente. Esto último tiene sentido, puesto que una vez que el sistema se pasó por la licuadora de inmersión el sistema se puso tan viscoso que era muy difícil hacer que todo el sistema pasara por la zona de alta cizalla, cercana a las cuchillas de la licuadora.

Finalmente, vale mencionar que hoy en día se ha puesto de moda en la formulación de alimentos industriales y artesanales agregarles algunos componentes con cualidades funcionales específicas a los alimentos emulsionados, de modo que aparte de coadyuvar a incrementar la aceptabilidad de un producto en el mercado, afectando su sabor, aroma, textura o estabilidad, cumplan otra función. Así, se encuentra en la literatura que, el orégano es muy utilizado en la cocina mundial para potenciar las cualidades organolépticas de las comidas y aderezos. Pero, además, se menciona en la introducción, el orégano, sus aceites esenciales, presenta un paquete increíble de propiedades de naturaleza clínica como germicida, fungicida, antiparasítico, alta capacidad antigenotóxica, etc. y como antioxidante natural. Esto es, los aceites esenciales del orégano pueden ayudar a combatir afecciones como la sinusitis y la migraña, enfermedades ligadas al hongo Candida; así como también, coadyuvar a atenuar la dificultad para bajar de peso, frecuentemente relacionada al desequilibrio de la biota intestinal. Por todo lo anterior, el orégano se postula como un fuerte candidato para aportar a cualquier producto emulsionado alimenticio, además de mejorar propiedades organolépticas, múltiples funciones que le darían a dichos productos un verdadero plus a sus demandas de consumo global. Una mayonesa preparada a base de extracto oleoso de orégano no sólo podría ser un excelente producto alimenticio, sino que también podría presentar propiedades curativas.

4 Conclusiones

Las variables concentraciones de sal y extracto oleoso de orégano, así como su interacción muestran tener gran efecto sobre el grado de aceptación general de una mayonesa, lo cual es de gran importancia a la hora de formular una mayonesa de gran aceptabilidad general. La cantidad de aceite y huevo parecen no ser determinantes, en los niveles estudiados, sobre el nivel de aceptación general de una mayonesa; sin embargo, vale mencionar que, no parecen influir de manera negativa sobre el nivel de aceptación en sistemas en los que las concentraciones de sal y de extracto oleoso de orégano se establecen a las condiciones para producir mayonesas de gran aceptación general.

Todas las mayonesas del primer experimento presentaron un comportamiento bimodal sugiriendo dos mecanismos de molienda, dos zonas de cizalla, una asociada a gotas pequeñas y la otra a gotas grandes.

Agradecimientos

Los autores reconocen y agradecen el gran apoyo del laboratorio FIRP por la determinación de la distribución de tamaño de gotas de las distintas mayonesas elaboradas en este trabajo, en especial, al profesor Johnny Bullón, por haber concedido la autorización para llevar a cabo los ensayos y a la licenciada Francis Véjar, quien coordinó las pruebas de laboratorio. De igual manera, se agradece el apoyo de los laboratorios POLYCOL, QUEXA y al Centro de Investigaciones y Proyectos en Matemática Aplicada, CIMA. También, se agradecen el apoyo del Centro de Gastronómico de Alta Cocina, la Escuela del Chef Jesús Sánchez; por su disposición para realizar la segunda cata; y, finalmente, a cada uno de los integrantes de las dos catas por su indispensable aporte, sin el cual este trabajo no se hubiese podido llevar a cabo.

Referencias

Antony, J. (2014). Design of experiments for engineers and scientists (2.ª ed.). Elsevier.

Arcila-Lozano, C. C., Loarca-Piña, G., Lecona-Uribe, S., y González de Mejía, E. (2004). El orégano: propiedades, composición y actividad biológica de sus componentes. *Archivos Latinoamericanos de Nutrición*, *54*(1),100-111. https://ve.scielo.org/scielo.php?script=sci_arttext&pid=S0004-06222004000100015

Balusamy, S. R., Perumalsamy, H., Huq, M. A., & Balasubramanian, B. (2018). Anti-proliferative activity of *Origanum vulgare* inhibited lipogenesis and induced

mitochondrial mediated apoptosis in human stomach cancer cell lines. *Biomedicine & Pharmacotherapy*, *108*,1835-1844. https://doi.org/10.1016/j.biopha.2018.10.028

Briceño, M. I., Solórzano, Y., Bertrand, J., y Salager, J. L. (2002). Emulsification of concentrated O/W emulsions in controlled hydrodynamic conditions: How formulation and mixing efficiency are linked. En *Proceedings of the 3rd World Congress on Emulsion* (Paper 145). Lyon, Francia.

Eckert, R. E., McLaughlin, C. M., y Rushton, J. H. (1985). Liquid-liquid interfacial areas formed by turbine impellers in baffled, cylindrical mixing tanks. *AIChE Journal*,*31*(11),1811-1819. https://doi.org/10.1002/aic.690311107

FONDONORMA. (2016). *Aditivos alimentarios (3ra. Revisión)* (COVENIN 910:2016). Caracas, Venezuela: Fondo para la Normalización y Certificación de la Calidad.

FONDONORMA. (2020). *Mayonesa (5ta. Revisión)* (COVENIN 90:2020). Caracas, Venezuela: Fondo para la Normalización y Certificación de la Calidad.

Gutiérrez Pulido, H., & De la Vara Salazar, R. (2012). *Análisis y diseño de experimentos*. México: McGraw-Hill.

López-Pedrouso, M., Lorenzo, J. M., y Franco, D. J. (2022). Advances in Natural Antioxidants for Food Improvement. *Antioxidants*, *11*(9), 1825. https://doi.org/10.3390/antiox11091825

McClements, D. J. (2015). *Food emulsions: Principles, practices, and techniques* (3.ª ed.). CRC Press. https://doi.org/10.1201/b18868

Montgomery, D. C. (2002). *Diseño y análisis de experimentos* (2.ª ed.). Limusa Wiley.

Nurzyńska-Wierdak, R., y Walasek-Janusz, M. (2025). Chemical composition, biological activity, and potential uses of oregano (*Origanum vulgare* L.) and oregano essential oil. *Pharmaceuticals*, *18*(2), 267. https://doi.org/10.3390/ph18020267

Rounsley, R. R. (1983). Oil dispersion with a turbine mixer. *AIChE Journal*, *29*(4), 597-603. https://doi.org/10.1002/aic.690290412

***Recibido**: 10 de enero de 2026*

***Aceptado:** 26 de marzo de 2026*

***Zambrano, Lorena:** Ingeniero Químico, Profesora del Departamento de Cálculo de la Escuela Básica, Facultad de Ingeniería, Universidad de Los Andes, Mérida, Venezuela.*
https://orcid.org/0009-0009-0092-7571

***López, Juan:** Profesor Titular de la Escuela Básica, Facultad de Ingeniería, Universidad de Los Andes PhD, Universidad de Florida.. MSc, Universidad de Los Andes.*
Correo electrónico:quexajc@gmail.com.
https://orcid.org/0009-0006-4109-624X.

***Celis, María-Teresa**: Ingeniero Químico Universidad de Los Andes (ULA), Mérida, Venezuela-1981; Master en Ingeniería Química, 1997, University of South Florida (USF), USA; Ph.D. en Ingeniería Química 2000, USF, USA; Post. Doc. (Water-based, Natural Polymer Surfactants: Implications for Deepwater Horizon Oil Spill Dispersions and Cleanup Opera-tions), 2012, USF, USA; Directora Laboratorio de Polímeros y Coloides, Facultad de Ingeniería (ULA), Coordiandora tecnica Laboratorio FIRP, Facultad de Ingeniería (ULA), Profesora Titular, Facultad de Ingeniería ULA. Investigadora y experta en el área de polímeros, emulsiones y caracterización de sistemas dispersos usando espectroscopia, Miembro correspondiente estadal de la Academia de Mérida.*
Correo electrónico: celismt@ula.ve.
https://orcid.org/0000-0003-3618-3569

Artículo de Investigación. Revista Ciencia e Ingeniería. Vol. 47, No. 2 pp. 199-212, abril-julio, 2026.
ISSN 1316-7081. ISSN Elect. 2244-8780 Universidad de los Andes (ULA)

Evaluation of plasma-induced surface modification in PLA-alginate biocomposites and their dielectric response: a review

Evaluación de la modificación superficial inducida por plasma en biocompuestos de PLA- alginato y su respuesta dielectrica: una revisión

Rivera, Victoria[1]*; Resto, Joymar[1]; Rondón, Jairo[2]; Lugo Claudio[3]
[1] Biomedical Engineering Department, Universidad Politécnica de Puerto Rico, San Juan, PR 00918, USA
[2] Chemical Engineering Department, Universidad Politécnica de Puerto Rico, San Juan, PR 00918, USA
[3]Laboratorio de Cinética y Catálisis, Departamento de Química, Facultad de Ciencias, Universidad de Los Andes, Mérida, Venezuela.
*rivera_133187@students.pupr.edu

Abstract

Surface engineering is fundamental for advancing biomaterials in regenerative medicine. Biocomposites fabricated from polylactic acid (PLA) and alginate combine the mechanical strength of PLA with the hydrophilic and crosslinkable properties of alginate. However, their intrinsic hydrophobicity limits early tissue integration. Plasma modification offers a selective and non-destructive method to improve surface chemistry, wettability, and biological response through nanolayer surface functionalization. This research examines plasma-induced modifications in PLA–alginate biocomposites and their dielectric behavior, focusing on hydration, ionic mobility, and interfacial polarization. Non-thermal plasma introduces oxygen- and nitrogen-based functional groups (e.g., hydroxyl, carboxyl, carbonyl), increases surface energy, and generates nanoscale roughness, thereby enhancing protein adsorption, fibroblast adhesion, and osteogenic activity. Dielectric spectroscopy measures these changes through parameters such as relative permittivity (ε'), dielectric loss (ε"), loss tangent (tan δ), AC conductivity (σ_ac), and Maxwell–Wagner–Sillars (MWS) relaxation, which reflect water uptake and interfacial behavior. This review consolidates findings on plasma-functionalized biomedical scaffolds and plasma activation of PLA.

Keywords: polylactic acid, alginate, non-thermal plasma, dielectric spectroscopy, tissue engineering, biomaterial

Resumen

La ingeniería de superficies es fundamental para el avance de los biomateriales en la medicina regenerativa. Los biocompuestos fabricados con ácido poliláctico (PLA) y alginato combinan la resistencia mecánica del PLA con las propiedades hidrófilas y reticulables del alginato. Sin embargo, su hidrofobicidad intrínseca limita su integración temprana en los tejidos. La modificación por plasma ofrece un método selectivo y no destructivo para mejorar la química superficial, la humectabilidad y la respuesta biológica mediante la funcionalización de la nanocapa superficial. Esta investigación estudia las modificaciones inducidas por plasma en los biocompuestos PLA-alginato y su comportamiento dieléctrico, centrándose en la hidratación, la movilidad iónica y la polarización interfacial. El plasma no térmico introduce grupos funcionales basados en oxígeno y nitrógeno (p. ej., hidroxilo, carboxilo, carbonilo), aumenta la energía superficial y genera rugosidad a nanoescala, mejorando así la adsorción de proteínas, la adhesión de fibroblastos y la actividad osteogénica. La espectroscopia dieléctrica mide los cambios mediante parámetros como la permitividad relativa (ε'), la pérdida dieléctrica (ε"), la tangente delta (tan δ), la conductividad de CA (σac) y la relajación de Maxwell-Wagner-Sillars (MWS), que reflejan la absorción de agua y el comportamiento interfacial. Esta revisión consolida los hallazgos sobre los andamios biomédicos funcionalizados con plasma y la activación del PLA mediante plasma.

Palabra clave: ácido poliláctico, alginato, plasma no térmico, espectroscopia dieléctrica, ingeniería de tejidos, biomaterial

1 Introducción

Over the past years, we have observed the growing concern of having the loss of tissue or end-stage organ failure, living with the demand of not having enough donors to prioritize the patient's life (Velázquez et al., 2025). Re-

search into biocompatible and biodegradable polymers, both natural and synthetic, has emerged as a vital area for biomedical applications, tissue engineering, and environmental sustainability (Rondón et al., 2023). Furthermore, these materials have been evolving, focusing on replacing or restoring the function of human tissues and organs that have been damaged or lost (Abdulsalam et al., 2025).

PLA is a biodegradable polymer, used as a biomaterial for biomedical applications, tissue engineering, scaffolds, and bone fixation devices (Abdulsalam et al., 2025). The physical properties of PLA vary with molecular weight. Therefore, it degrades through simple hydrolysis of ester bonds; the degradation rate can be influenced by the isomer ratio, oxygen, and temperature of hydrolysis, pH, burial time, humidity, and shape and sample size. Unfortunately, PLA applications are limited due to several disadvantages, such as excessive brittleness, poor osteointegration, low cell adhesion, and biological inertness. In fact, depending on the PLA applications, it has a low degradation rate (Velázquez et al., 2025).

Poly(lactic acid)- based systems have been developed to deliver a variety of payloads, from small drug molecules to nucleic acids and large proteins, in a sustained-release manner. Usually, the polymer is blended with another biodegradable polymer or agent to avoid disadvantages. Furthermore, PLA can be combined with alginate, once combined forms PLA-Alginate. Alginate is a natural anionic linear biopolymer commonly obtained from brown algae and certain bacteria. However, there are challenges related to reproducibility and standards, as it varies across species, seasons, and geographic origins. It has poor mechanical properties; it may be improved by crosslinking with multivalent cations. The degradation rate is fast at high temperatures, and a key limitation is the difficulty of customization. The combination of PLA and Alginate is highly beneficial, as it increases surface wettability and hydrophilicity, thereby promoting cell adhesion and biocompatibility. Due to its high moisture-absorbance capacity, the alginate-chitosan composite is typically developed to reduce moisture permeability (Bodaghi et al., 2019). Additionally, it provides antimicrobial activity and improves mechanical properties (Abdulsalam et al., 2025; Popelka et al., 2020). The NTP (non-thermal plasma) promotes the controlled incorporation of polar functional groups, increases surface energy, modifies dielectric behavior, and generates micro-roughness (Rondón et al., 2025; Rajasekar et al., 2025).

However, there are challenges due to reproductive and standard variations, as they vary across species, seasons, and geographic origins. It has poor mechanical properties; these may be improved by crosslinking with multivalent cations. The degradation rate is fast at high temperatures, and a key limitation is the difficulty of customization. Even alginate exhibits beneficial properties, including biodegradability, non-toxicity, and high water absorption, for various biomedical applications (Hurtado-Fernández et al., 2026). The combination of PLA and alginate is highly beneficial, as it increases surface wettability and hydrophilicity, thereby promoting cell adhesion and biocompatibility. Due to the high moisture absorbance capacity, an alginate/chitosan composite is typically developed not only to reduce moisture permeability but also to bestow it with additional antimicrobial and enhanced mechanical properties (Yadav et al., 2025). The NTP (non-thermal plasma) promotes the controlled incorporation of polar functional groups, increases surface energy, modifies dielectric behavior, and generates micro roughness (Walden et al., 2024; Nayak et al., 2023).

2 Methodology

The methodology used in this research will be document- exploratory following the PRISMA guidelines (Page et al., 2021; Moher et al., 2009), based on:

a. Data search strategy and compilation: A comprehensive literature search was conducted across academic databases including PubMed, MDPI, Scopus, Web of Science, Science Direct and Research Gate. The search will be limited to the period from 2010-2026.
b. Information Selection and refinement: To organize the information, it was performed by the bibliographic manager Mendeley. Organizing into 6 databases: types of plasma and parameters, surface physicochemical changes, effects on wettability, adhesion, and degradation in SBF, dielectric properties/impedance, and their relationship to interface chemistry and implications for tissue engineering (cell adhesion /proliferation), characterization guidelines, and future applications. Relevant research articles and reviews will be prioritized.

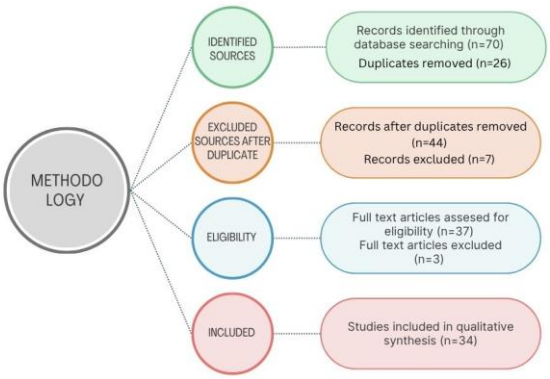

Figure 1. Study selection methodology flowchart for the research.

c. Subtopic Selection: The subtopic obtained information is analyzed to identify properties and physicochemical advances and their relevance to the growing field of regenerative medicine and tissue engineering.
d. Analysis of Results: The analysis performed of results

leads to organizing information into a structured analysis review, highlighting its relevance to tissue engineering applications and future advances.

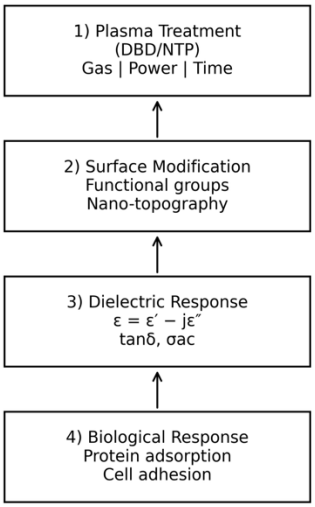

Figure 2. Plasma–surface–dielectric–biological interaction framework. Plasma treatment modifies surface chemistry and nano-topography, altering complex permittivity ($\varepsilon = \varepsilon' - j\varepsilon''$), dielectric loss ($\tan\delta$), and AC conductivity ($\sigma_{ac}$), which subsequently influence protein adsorption and cellular response.

3 Results and Discussions

3.1 Types of plasma and parameters

The plasmas generated under low pressure or atmospheric pressure conditions enables the cleavage of surface bonds, the introduction of oxidative functional groups, and the formation of micro-roughness factors that collectively increase surface free energy and enhance cell material interactions (Rondón et al., 2025; Yehia, 2024). As a matter of fact, non-thermal plasmas can reconfigure surface chemistry through the incorporation of polar functional groups and the generation of micro-roughness. As if these two mechanisms significantly enhance wettability and interfacial compatibility (Kamalov et al., 2022).

Recent literature on polymer surface modification has established plasma treatment as one of the most versatile and effective strategies for improving adhesion in thermoplastics, thermosetting, and elastomeric materials (Rajasekar et al., 2025; Walden et al., 2024; Nayak et al., 2023; Yadav et al., 2025). In addition, a comparative analysis of various experimental works consistently reported notable reductions in water contact angles and increases in surface energy, directly indicating improved adhesion and chemical anchoring (Rondón et al., 2025). These physicochemical transformations are recognized as optimizing the bonding of coatings, adhesives, and functional layers, extending the impact of plasma treatment to diverse biomedical engineering, tissue engineering, and microelectronics (Rondón et al., 2025; Rajasekar et al., 2025). The DBD dielectric barrier discharge plasma consists mostly of two parallel plates, and they are characterized by presence of the dielectric layer covering at least the internal surface of one the two discharge electrodes or both (Yehia, 2024). In Addition, the system operates only on high-voltage AC power supplies. It can be used to form non–thermal plasma under different operating conditions. Furthermore, the DBD has unprecedented flexibility with respect to operating conditions. It is possible to generate different electrode systems, each with dielectric layers made from materials such as glass, ceramic, epoxy, and others. This system can be operated at high voltage and fed with different gases and mixtures at high flow rates at atmospheric pressure and room temperature (Yehia, 2024; Gershman et al., 2021). Ensuring effectiveness of plasma surface modification strongly depends on both the operating parameters and the plasma type. Following the parameters ensures effective enhancement of cell adhesion and hydrophilicity promoting an effective biomedical application (Jacobs et al., 2013; Rondón et al., 2025; Fernandes et al., 2026).

3.2 Surface physicochemical changes

Bioactive scaffolds represent an evolution from purely structural support toward dynamically instructive biomaterials. In fact, they are engineered to modulate cell adhesion, proliferation, differentiation, and ECM deposition through tailored surface chemistry, nano/micro architecture, and controlled presentation of biochemical signals. Furthermore, scaffolds can be designed from natural and synthetic polymers, ceramics, and composite systems, increasing attention to the interplay between material composition, degradation behavior, and host responses. A key strategy for scaffold-enhanced performance is functionalization, involving deliberate modifications of the scaffold's bulk or surface to introduce specific physicochemical, biological, and topographical features that promote the desired cellular response (Aponte-López et al., 2025).

Polylactic acid (PLA) is among the most promising materials for tissue engineering due to its favorable biocompatibility and biodegradability. On the other hand, its relatively long degradation time of 2 to 5.5 years limits its suitability for applications. PLA is degraded by enzymatic activity or hydrolysis, forming lactic acid, which is usually present in the body. In this way, inflammatory reactions are prevented, and the by-products are expelled through normal cell activity and urine. Copolymers of PLA and polyglycol-

ic acid (PGA) offer a more adaptable degradation profile based on their composition ratios, with opportunities to develop resorbable membranes capable of supporting complex bone regeneration scenarios (Zernitckaia et al., 2025).

Another critical step is the sterilization of PLA for clinical use. Due to PLA's thermal sensitivity, autoclaving is not suitable; it is possible to deform the material and alter its properties, potentially affecting both degradation behavior and osteoinductive potential (Pérez-Dávila et al., 2021) Besides, gamma irradiation is widely employed for sterilizing PLA-based materials with doses up to 25kGy that have been shown to be effective without compromising material safety or performance (Zernitckaia et al., 2025; Pérez-Dávila et al., 2021). This sterilization method is considered optimal for thermally sensitive medical devices that require both internal and surface sterility. The biodegradable plates were analyzed using Fourier-transform infrared spectroscopy on a Shimadzu IRTracer –100 spectrometer, *the spectra* recorded range of 500-400cm^-1 for the evaluation of structural changes in the materials resulting from both biodegradation and sterilization processes. Indeed, the irradiation performance was a linear pulsed electron accelerator (Ee=10MeV), there are studies that have shown that this dose of ionizing radiation does not damage the structural integrity of PLA and its composites, preserving their mechanical and physicochemical properties. At 25kGy, the composites such as hydroxyapatite/PLLA remain structurally stable. However, at higher doses, surface damage has been observed, negatively affecting performance, substantially reducing tensile strength and elongation at break in PLA concerns over excessive irradiation (Zernitckaia et al., 2025; Pérez-Dávila et al., 2021). In addition, changes were found indicating degradation on PLA by irradiations, such as a decrease in molecular weight, other changes in mechanical, thermal, and permeability properties (Pérez-Dávila et al., 2021). UV irradiation affects the diblock copolymer of Me.PEG-PLA, at different radiation times (0,2,5,10 and 25h). In two hours, it was observed that irradiation required properties nor the cell adhesion was altered, compared with the control. However, once the radiation time was further increased, the copolymer surface changes occurred affecting cell/protein-polymer interactions. The hydrogen peroxide plasma, which has shown electro spun biodegradable matrices without altering their chemical composition or surface morphology. In addition, the electron beam parameters are gaining traction due to its efficiency, speed, and compatibility with thermally sensitive materials (Pérez-Dávila et al., 2021). As with gamma radiation, the morphology and alignment of the fibers were not affected, nor the mechanical or thermal properties; only a slight increase in wettability was observed, and like gamma radiation, the membranes had a good cellular response (Zernitckaia et al., 2025; Pérez-Dávila et al., 2021).

The clinical potential of biodegradable polymers lies in their ability to serve as customized, resorbable scaffolds. PLA, PLGA and its copolymers have been explored for applications ranging from jawbone reconstruction to tendon repair, biocompatibility and long-term in vivo safety remain key focus areas for ongoing investigations (Aponte-López et al., 2025). In surgical applications, the mechanical performance of bioresorbable materials is as critical as their biocompatibility. For instance, adequate strength, stiffness, and controlled degradation are essential for maintaining implant stability through the healing process. To continue, the potential of PLA and copolymers is reliable biodegradable membrane materials for clinical and medical use. The analysis of physicochemical and biodegradation properties revealed material specific differences in stability (Zernitckaia et al., 2025).

3.3 Effects on Wettability, Adhesion, and Degradation in SBF

3.3.1 Impact of Plasma Treatment on Surface Wettability

The surface properties of PLA-based biomaterials undergo substantial changes upon non-thermal plasma surface modification using a dielectric barrier discharge (DBD), thereby affecting their wettability. PLA surfaces treated with plasma become more water-absorbing as their contact angles decrease from above 80° to 50°-70° (Rondón & Gonzalez-Lizardo, 2025; Hergelová et al., 2015). This change results from the addition of polar oxygen- and nitrogen-containing functional groups (such as hydroxyl, carbonyl, and carboxyl groups) and from nanoscale surface irregularities induced by plasma treatment (Hergelová et al., 2015; Pillai & Mohan, 2025).

The PLA–alginate system benefits from plasma-induced wettability enhancement due to the hydrophilic and ionic properties of alginate. Alginate domains enable water absorption and ion exchange, strengthening plasma activation results and producing a water-rich surface that promotes biological responses (Sun & Tan, 2013). This method has shown equivalent wettability enhancements in various polymeric biomaterials for orthopedic, dental, and cardiovascular applications (Pillai & Mohan, 2025; Ferreira et al., 2023).

3.3.2 Cell Adhesion and Biological Interactions

Surface wettability significantly influences cell attachment because it controls protein binding to material surfaces. Plasma treatment of PLA and PLA-based composites enhances protein adsorption, particularly extracellular ma-

trix proteins like fibronectin and vitronectin, which facilitate cell attachment through integrin receptors (Rondón & Gonzalez-Lizardo, 2025; Krutty et al., 2016). Plasma-modified surfaces yield better fibroblast cell spreading, stronger focal adhesions, and improved cytoskeletal structure compared to untreated surfaces (Rondón & Gonzalez-Lizardo, 2025; Hergelová et al., 2015). This is crucial in tissue engineering, as early cell attachment determines the success of regenerative procedures.

Moreover, plasma surface activation combined with bioactive components enhances cell-material interactions. PLA functionalization and bioactive scaffold studies show that plasma treatment facilitates the attachment of biomolecules or nanoparticles, promoting cell attachment, growth, and tissue formation (Abdulsalam et al., 2025; Świerczyńska et al., 2024; Aponte-López et al., 2025). The ionic bonds between PLA and alginate in these composites create bioactive interfaces, maintaining stable focal adhesions and functional signaling pathways essential for tissue healing (Lopes et al., 2012).

3.3.3 Dielectric Properties and Their Role in Biomaterial Functionality

The dielectric properties of plasma-treated surfaces are influenced by their water-attracting properties and their ability to form bonds with other materials. Dielectric spectroscopy studies reveal that plasma treatment increases relative permittivity (ε′), dielectric losses, and Maxwell–Wagner–Sillars (MWS) polarization effects in PLA materials and composites (Spinelli et al., 2020; Dichtl et al., 2017; Kremer & Tress, 2025; Walker et al., 2019). These dielectric signatures reflect elevated water levels and enhanced ionic movement at the interface, supporting nutrient transport, metabolic processes, and overall cellular function. Dielectric parameters serve as secondary indicators of how plasma treatment affects surface bioactivation and biological performance (Abdelhamid, 2022).

3.3.4 Degradation Patterns in Simulated Body Fluid (SBF)

Plasma modification alters the degradation pattern of PLA-based biomaterials during exposure to simulated body fluid. Increased surface hydrophilicity allows water to penetrate the top polymer layers, accelerating surface hydrolysis without compromising the material's core structural strength (Abdulsalam et al., 2025; Kurowiak et al., 2023; Zernitckaia et al., 2025). Studies on PLA membranes and composites immersed in SBF show that improved membrane wettability enhances ionic bonding with calcium and phosphate ions, promoting bioactivity and the formation of apatite-like minerals for bone tissue engineering (Castro et al., 2022; Kudzin et al., 2021; Zernitckaia et al., 2025). The PLA–alginate system gains additional benefits from ionically active alginate, which supports Ca^{2+}-mediated crosslinking and surface mineralization (Sun & Tan, 2013).

3.3.5 Advantages of Dielectric Barrier Discharge (DBD) Plasma Treatment

The DBD plasma treatment process mitigates the risks of uncontrolled material breakdown and thermal damage. The dielectric barrier limits energy transfer, preventing overheating and confining plasma-induced surface modifications to the top nanolayers without harming the internal structure (Yehia, 2024; Subedi et al., 2017). This combination of surface reactivity and structural stability is critical for developing biomaterials that degrade in a controlled manner while maintaining long-term functionality.

3.4 Dielectric properties/impedance and their relationship to interface chemistry

Plasma-induced surface modification of polylactic acid (PLA)–alginate biocomposites results in pronounced changes in dielectric behavior and impedance response, directly linked to alterations in interfacial chemistry. In heterogeneous biodegradable polymer systems, dielectric spectroscopy and electrical impedance spectroscopy (EIS) provide sensitive probes of interfacial polarization, ionic mobility, and hydration phenomena, all of which are governed by surface functionalization and interphase structure (Kremer & Tress, 2025; Abdelhamid, 2022).

3.4.1 Interface Chemistry Induced by Plasma Treatment

Non-thermal plasma treatments, particularly dielectric barrier discharge (DBD), introduce polar oxygen- and nitrogen-containing functional groups (e.g., –OH, –COOH, –C=O) onto PLA surfaces without affecting bulk properties (Hergelová et al., 2015; Rondón et al., 2025). These chemical modifications increase surface energy, reduce hydrophobicity, and promote interfacial compatibility with hydrophilic and ionically active biopolymers such as alginate (Sun & Tan, 2013; Kudzin et al., 2021).

The efficiency of plasma-induced functionalization is strongly dependent on discharge energetics and thermal losses, as Yehia (2024) described, underscoring the importance of controlling plasma parameters to achieve stable surface activation. Reviews on polymer functionalization further highlight that plasma-generated interfaces are dynamic and susceptible to aging effects, which can influence long-term dielectric stability (Abdulsalam et al., 2025; Pillai & Mohan, 2025).

3.4.2 Dielectric Permittivity and Interfacial Polarization Mechanisms

Across PLA-based composites and nanocomposites, plasma-induced changes in interface chemistry are consistently reflected in the real part of the dielectric permittivity (ε′), particularly in the low-frequency region. Studies on PLA reinforced with carbon-based particles, cellulose nanofibrils, nanobioglass, and alginate report increased ε′ values associated with enhanced interfacial polarization (Spinelli et al., 2020; Ranakoti et al., 2022; Castro et al., 2022; Kudzin et al., 2021).

This behavior is commonly attributed to Maxwell–Wagner–Sillars (MWS) polarization, which arises from charge accumulation at interfaces between phases of differing conductivity and permittivity (Walker et al., 2019). Plasma functionalization intensifies this effect by increasing dipole density and enabling stronger coupling between the PLA surface and the alginate-rich interphase. Dielectric spectroscopy theory confirms that such interfacial contributions dominate the dielectric response of heterogeneous polymers at low frequencies (Kremer & Tress, 2025).

Dielectric Losses, Conductivity, and Ionic Mobility

The imaginary component of permittivity (ε″) and dielectric loss tangent (tan δ) provide insight into energy dissipation mechanisms linked to dipolar relaxation and ionic conduction. Plasma-treated PLA systems exhibit increased dielectric losses due to enhanced molecular mobility and water uptake within the modified interphase (Dichtl et al., 2017; Abdelhamid, 2022). In PLA–alginate composites, alginate's ionic character further amplifies these effects by facilitating ion hopping and polarization under alternating electric fields (Sun & Tan, 2013).

The observed increase in AC conductivity (σ_ac) following plasma treatment reflects improved ionic displacement and interfacial charge transport. These findings align with reports on biodegradable polymer nanocomposites, where surface chemistry and interphase hydration strongly influence electrical conductivity and dielectric relaxation behavior (Spinelli et al., 2020; Abdelhamid, 2022).

3.4.3 Impedance Spectroscopy and Interfacial Resistance

Electrical impedance spectroscopy complements dielectric measurements by quantifying resistive and capacitive elements associated with the polymer interphase. Plasma-treated PLA-based biomaterials consistently exhibit reduced impedance magnitude and lower interfacial resistance, as evidenced by smaller semicircle diameters in Nyquist plots and increased interfacial capacitance (Kudzin et al., 2021; Ferreira et al., 2023).

In PLA–alginate systems, plasma activation of the PLA surface promotes stronger physicochemical interactions at the interface, enabling more efficient ionic continuity across phases. Equivalent circuit analyses reported in polymer electrolyte and hydrogel systems suggest that these changes correspond to the formation of a more hydrated, polar, and charge-supportive interphase (Abdelhamid, 2022; Walker et al., 2019).

3.4.4 Biological and Functional Implications

The strong correlation between dielectric response and interface chemistry has direct implications for biomedical applications. Plasma-induced increases in dielectric permittivity and reductions in impedance are consistently associated with enhanced protein adsorption, fibroblast adhesion, and biocompatibility in PLA-based scaffolds and films (Rondón et al., 2025; Rondón & Gonzalez-Lizardo, 2025; Krutty et al., 2016). These effects are particularly relevant for PLA–alginate constructs used in bone and soft tissue regeneration, where interfacial hydration and ionic signaling play critical roles (Sun & Tan, 2013; Kudzin et al., 2021; Aponte-López et al., 2025).

Furthermore, dielectric and impedance measurements offer a powerful means of monitoring the stability of plasma-induced modifications during sterilization, aging, and biodegradation processes (Pérez-Dávila et al., 2021; Zernitckaia et al., 2025). As such, dielectric spectroscopy emerges as both a diagnostic and predictive tool for evaluating interface-driven performance in plasma-modified PLA–alginate biomaterials (Table 1).

3.5. Implications for tissue engineering (cell adhesion/proliferation) and characterization of guidelines.

3.5.1 Tissue Engineering

Tissue Engineering aims to review native tissue or organ function and identify replacements when damaged or diseased tissues and organs are present. It is composed of living cells, scaffolds, and signals. The scaffolds used are widely diverse, including synthetic and natural polymers (Velázquez et al., 2025). Therefore, scaffolds must provide a favorable environment for cell growth, proliferation, infiltration, differentiation, and migration, and they must have properties such as biocompatibility, good mechanical properties, degradability, and a porous morphology (Parangusan et al., 2025). However, the emergence of scaffold-free processes has expanded the field's capabilities. For instance, it has been successfully used in engineering musculoskeletal, cardiovascular, metabolic, and corneal tissues. Supporting this, scaffold-free approaches, has two primary, thermodynamically driven modalities of self-organization and self-

assembly. Although the preparation methods for synthetic and biologically active scaffolds with the capacity to induce regenerative healing are three-dimensional printing, bioprinting, and electrospinning (Velázquez et al., 2025).

3.5.2 Strategies to replace damaged organs or tissues

All tisues in the human body are integrated by animal cells, which are grouped and organized to work in spectacular precision to form organs in the body. Similarly, all cells in the body are components of four tissues, such as connective tissue, epithelial tissue, nervous tissue, and muscle tissue. Therefore, strategies to replace damaged organ or tissue involve a cyclic process beginning with the donor or patient, followed by incorporating cells and growth factors into biomaterials to construct a functional graft (Velázquez et al., 2025).

Table 1. Summary of Plasma Types, Dielectric Effects, and Biological Responses Reported in Included Studies

Plasma type	Key parameters	Dielectric effects	Biological response
Dielectric barrier discharge (DBD)	Atmospheric pressure; AC high voltage (kV); air, O_2, N_2 or Ar; short exposure times	Increase in ε′ and tan δ at low frequencies; enhanced Maxwell–Wagner–Sillars polarization due to a hydrated interphase	Enhanced protein adsorption; improved fibroblast and osteoblast adhesion and proliferation
Atmospheric pressure plasma jet (APPJ)	Moderate voltage; controlled gas flow; room-temperature operation	Increase in AC conductivity (σ_ac) and interfacial permittivity due to higher ionic mobility	Improved cell spreading and early cell–material interactions
Low-pressure RF plasma	Vacuum environment; longer treatment times; uniform energy distribution	More homogeneous dielectric response with reduced interfacial variability	Highly reproducible cell adhesion and stable surface activation
Oxidative plasma (O_2/air)	High density of reactive oxygen species	Higher dielectric losses due to increased surface dipole density	Significant improvement in wettability and overall surface bioaffinity

3.5.3 Poly (lactic acid) Production for tissue engineering applications.

Polylactic acid is one of the most promising polymers due to its being obtained from nontoxic monomers obtained from renewables. The monomer employed in the production of PLA is the lactic acid (2-hydroxypropinic acid), a chiral molecule, which exists in two enantiomers, L-lactic acid an L-lactic acid, this acid can be produced by fermentative or chemical synthesis.

On the other hand, PLA is the reference of a family of polymers: poly (L-lactic acid) (PLLA), poly (D-lactic acid) (PDLA), and poly (D, L-lactic acid) (PDLLA). However, the stereoisomers PLLA and PDLA have similar physicochemical properties, PDLLA has different characteristics due to its structure. Additionally, PLA can be prepared through different polymerization techniques from lactid acid by indirect processes such as polycondensation, ring-opening polymerization and direct method such as azotropic dehydration and enzymatic polymerization. Among this, enzymatic polymerization and ROP are the most used techniques.

Ring-opening polymerization (ROP) is the method used to produce PLA with controlled molecular weight. This consists of three main steps: polycondensation, depolymerization, and ring-opening polymerization. However, this process requires purification of products, causing elevation of costs. Furthermore, degradation of PLA mechanisms mare hydrolytic, oxidative, thermal, microbial, enzymatic, photo-degradative, and chemical processes (Velázquez et al., 2025).

3.5.4 PLA for Skin Tissue Engineering

Skin is the largest organ in the human body, and when it is damaged, a series of complex physicochemical and biological processes are activated to restore tissue integrity (Abdelhakim & Ogawa, 2025). The development of materials that promote tissue regeneration has emerged as an innovative alternative for the treatment of skin injuries and wound healing (Mamun et al., 2024). Furthermore, Xu et al. (2023) fabricated a three-layer bandage composed of a MXene coating (top), a PLA/polyvinyl pyrrolidone (PLA/PVP) Kirigami structure (middle), and an integrated f-sensor (bottom), capable of sensing microenvironmental changes caused by wound infection in real time. This system demonstrated high extensibility (up to 831% increase over the original structure), flexibility, and biocompatibility. Similarly, recent advances in smart wound dressings enable the creation of adaptive, comfortable environments for wounds in dynamic body regions while enabling continuous monitoring and effective treatment of infections (Xue et al., 2021).

Moreover, recent studies have reported the development of nanofibrous scaffolds incorporating metal-based nanoparticles with good biocompatibility and suitable mechanical properties for wound healing applications. Electrospun nanofiber scaffolds loaded with nanoparticles such as ZnO exhibit antibacterial, anti-inflammatory, and regenerative capabilities, making them promising candidates for tissue engineering (Dang et al., 2024). In particular, the incorporation of ZnO nanoparticles enhances antibacterial activity, improves cell viability, and accelerates wound healing processes (Athamneh et al., 2025). Additionally, nanofibrous aerogel scaffolds with interconnected porous structures facilitate wound exudate absorption, air exchange, and nutrient transport, while supporting cell proliferation and migration (Mao et al., 2021). Furthermore, ZnO-containing systems have been shown to promote angiogenesis, further enhancing tissue regeneration.

3.5.5 Cartilage Regeneration

Cartilage is a specialized connective tissue responsible for supporting the body and transmitting mechanical stress. The most common types found in the human body are hyaline cartilage and fibrocartilage, each with distinct structural and functional properties (Sophia Fox et al., 2009). In recent years, innovative strategies have focused on the development of bilayer composite scaffolds that mimic the hierarchical structure of native cartilage. For instance, bilayer systems combining a hydrogel layer, such as gelatin methacrylate (GelMA), with a fibrous scaffold layer based on polymers like PLA and silk fibroin have demonstrated promising results in cartilage tissue engineering (Huang et al., 2022). These scaffolds exhibit high porosity (around 90%), suitable mechanical properties in the MPa range, and excellent cell viability. Furthermore, ex vivo studies using mesenchymal stem cells, chondrocytes, and meniscal cells suggest their strong potential for cartilage regeneration and implantation.

However, recent advances in 3D bioprinting have enabled the fabrication of polymer-based scaffolds, including PLA-based systems, for cartilage tissue engineering. These scaffolds have been extensively evaluated for their ability to support cell growth, viability, and tissue formation. In particular, 3D-printed porous scaffolds with large pore sizes (in the range of hundreds of micrometers, e.g., ~500–700 μm) have demonstrated enhanced cell infiltration, proliferation, and chondrogenic differentiation (Zhang Y et al., 2022). Furthermore, bioprinted constructs have shown high cell viability and the ability to promote extracellular matrix deposition, including proteoglycans and type II collagen, which are key components of cartilage tissue (Jang et al., 2017; Li et al., 2022; Zhang et al., 2022). These findings highlight the potential of 3D-printed scaffolds with adequate mechanical stability and controlled porosity for cartilage regeneration.

3.5.6 Bone Tissue

Bone tissue can regenerate and repair itself when experiencing minor damage, it is not sufficient repairing large defects caused by trauma, cancer, osteoporosis and congelital disorders, which significantly impart the life quality and very often require clinical interventions (Akderya et al., 2025). Furthermore, in bone tissue regeneration PLA is a biopolymer exceptional for bone applications because there is no need of other surgeries. Eventhough, it can promote a foreign body reaction, hence PLA implant is eventually encapsulated by fibrous tissues. However, the osseointegration is not reached and PLA implant failure (Velázquez et al., 2025).

Currently, clinical procedures such as autografts, allografts, and xenografts are widely used to repair large-scale bone defects; however, they present significant limitations and risks, including donor shortage, immune rejection, infection, and variability in biological performance (Grayson et al., 2022). As an alternative, the combination of polylactic acid (PLA) with bioactive ceramic materials such as hydroxyapatite, calcium phosphates, and other apatite-based compounds has been extensively explored to improve the bioactivity and osteoconductivity of implants (Zhang et al., 2019). In particular, PLA/hydroxyapatite composite scaffolds have demonstrated promising results for bone regeneration, exhibiting enhanced mechanical properties, cell proliferation, and osteogenic potential (Shuai et al., 2025). Moreover, the development of advanced scaffolds fabricated through 3D printing technologies allows precise control of pore architecture and mechanical performance, making them suitable candidates for the treatment of large bone defects (Zhang et al., 2021).

Eventhough, PLA has a poor cellular adhesion on its surface and brittleness that limits its use, mixing it with other biomaterials has benefits that provide solutions to these disadvantages. With surface modification on the hydrophobic surface of PLA, can achive to make it hydrophylic adjusting production techniques and incorporating other biomaterials. Also, the lactic acid byproduct resulting form PLA degradation, is metabolized in vivo without cytotoxic effects on living tissues. Despite the inadequacies in PLA's mechanical strength, being. Reinforced or coated by biomaterials, enhance a better durability (Akderya et al., 2025).

3.5.7 Fenugreek-enriched electrospun PLA scaffold

Electrospun nanofibrous scaffolds have been under

analysis and have presented great potential as materials for tissue regeneration. The use of medicinal plant components for biomedical and wound-healing applications promotes improved performance and enhances shared positive outcomes. In addition, the electrospinning technique for fabricating fenugreek-incorporated PLA scaffolds was analysed using X-ray diffraction, Fourier transform infrared spectroscopy, mechanical testing, contact angle measurement, swelling measurement, and weight loss assessment. Moreover, the MTT aasay evaluated the scaffold's in vitro cell viability and biocompatibility using NIH/3 T3 fibroblast cells. Furthermore, the properties of polymeric based materials are determined by their cristalinity. The pure PLA and PLA/fenugreek scaffolds had a smooth, bead-free, randomly arranged surface, and, because of their porous nanostructure and surface area, they can mimic the native extracellular matrix and provide an ideal environment for cell attachment and growth (Parangusan et al., 2025).

The mechanical properties of pure PLA and PLA/fenugreek composites analyzed showed higher tensile stress in PLA/Fenugreek than in PLA scaffolds. However, swelling behavior of PLA/Fenugreek scaffolds obtained a higher water absorption rate than pure PLA. Equally important, cell attachment to tissue engineering is directly modified by surface wettability. Comparing pure PLA exhibited a higher contact angle, being that said, the Fenugreek incorportation resulted in a decrease of contact angle, which indicates an enhanced surface wettability. This MTT cell viability and in-vitro wound healing assay demonstrated that fenugreek could enhance cell migration and wound repair combining it with PLA, promoting skin cells proliferation. Another point to consider, is their excellent properties, good biocompatibility and ability to accelerate wound healing, promoting excellent candidates for tissue engineering implementation (Parangusan et al., 2025).

3.5.8 Future applications on Tissue Engineering

Tissue engineering is a constant emerging area of innovation, which looks forward to next-generation regener ative platforms which relys on the emerging technologies such as 4D bioprinting, gene-activated scaffolds, bioelectronic interfaces and AI- guided material designs. Furthermore, these innovations compromise to deliver more dynamic, adaptive and patient-specific developments that can respond to physiological stimuli promoting robust functional tissue regeneration (Aponte-López et al., 2025) (Table 2).

Table 2. PLA for skin tissue engineering and wound healing

Studies	Composites	Potential applications	Key Properties
In vitro cellular experiment performed on the back of a rat	Mxene/PLA/PVP bandage	Surgical Wound Care	Satisfactory stretching, bending and biocompatibility properites
In vivo studies that promote skin infection' wound healing and enhance angiogenesis	PLA/Gelatin/ZnO nanofibrous aerogel	Wound healing	Adequate antibacterial properties, biocompatibility absorption and permeability.
In vitro experiment proving biocompatibility of material, while in vivo experiment demonstrated good healing enhance of wound healing and no signs of infection.	PCL/PLA/gelatic biomimedic 3D scaffold	Skin Regeneration	Elevated surface area to volume ratio to cell adhesion, stronger mechanical properties and good hydrophilicity.
In vivo and in vitro biocompatibility 3T3-PMS/PLA interaction	PMS/PLA nanofibrous scaffolds	Skin tissue engineering	Excelent elasticity, stiffness and strength, as well as degradation rate is appropriate for soft tissues.

4 Conclusion

This study established a structured relationship between plasma surface modification, dielectric behavior, and biological response through a systematic PRISMA-based analysis of the literature. Evidence indicates that plasma treatment (DBD/NTP) induces controlled changes in sur-

face chemistry and nano-topography, resulting in increased surface energy and altered interfacial charge distribution. These modifications directly affect the complex permittivity ($\varepsilon = \varepsilon' - j\varepsilon''$), dielectric loss ($\tan\delta$), and AC conductivity ($\sigma\_ac$), reflecting changes in polarization mechanisms at the material–environment interface.

The reviewed studies consistently demonstrate that dielectric properties correlate with protein adsorption dynamics and subsequent cellular adhesion behavior. Interfacial polarization effects appear to mediate electrostatic interactions that influence early biological events at the biomaterial surface, suggesting that dielectric characterization may serve as a quantitative engineering parameter for predicting biological performance. Additionally, surface aging and biofouling were identified as variables that can modulate dielectric stability, highlighting the importance of time-dependent characterization under physiologically relevant conditions.

A primary limitation of this review is the heterogeneity in plasma parameters, dielectric measurement protocols, and biological assay methodologies across studies, which restricts direct quantitative comparison and limits the potential for meta-analytic standardization.

Overall, the proposed plasma–surface–dielectric–biological framework provides an engineering-based approach for biomaterial optimization. Integrating dielectric spectroscopy with surface functionalization strategies may enhance predictive control over biological outcomes and support the rational design of next-generation biomedical materials.

PLA applications in tissue engineering make it one of the most versatile biopolymers due to its biocompatibility and biodegradability. Several studies have demonstrated its good interaction with other biopolymers, even fusing with natural plants to create beneficial possibilities. It demonstrates its ability to emulate key functions as extracellular matrix, cell behaviour and physicochemical processes which ensure an excellent ability for wound healing acceleration and skin cell proliferation. Some of the analyses included in vitro, in vivo, and 3D electrospinning techniques, relying on and looking forward to next-generation regenerative technologies.

References

Abdelhakim, M., & Ogawa, R. (2025). Emerging Therapies in Chronic Wound Healing: Advances in Stem Cell Therapy, Growth Factor Modulation, Mechanical Strategies and Adjuvant Interventions. *Dermatology and Therapy*, *15*(12), 3533-3545. https://doi.org/10.1007/s13555-025-01564-2

Abdelhamid, H. N. (2022). Dielectric, thermal, and electrical conductivity properties of biodegradable polymer nanocomposites. Research Square. https://doi.org/10.21203/rs.3.rs-2003331/v1

Abdulsalam, L., Abubakar, S., Permatasari, I., Lawal, A. A., Uddin, S., Ullah, S., & Ahmad, I. (2025). Advanced biocompatible and biodegradable polymers: A review of functionalization, smart systems, and sustainable applications. *Polymers*, *17*(21), 2901. https://doi.org/10.3390/polym17212901

Akderya, T., İncesu, R., Gök, C., Bilir, C., Tabakoğlu, G., & Kaplan, A. (2025). The use of poly (lactic acid)(PLA) in bone tissue engineering. *Open Journal of Nano*, *10*(1), 1-13. https://doi.org/10.56171/ojn.1611817

Aponte-López, N., Rondón, J., Gonzalez-Lizardo, Á., & Lugo, C. (2025). *A review on bioactive scaffolds in biomedical engineering: Functionalization with nanoparticles and biomolecules*. Revista Ciencia e Ingeniería, 47(1), 75–84. https://doi.org/10.5281/zenodo.18508255

Athamneh, T., Abuawad, A., Odat, T., Alshweiat, A., Obaidat, R., Bani Yaseen, F., ... & Gurikov, P. (2025). Investigation of the antibacterial activity of ZnO-loaded alginate/hyaluronic acid aerogels for wound dressing applications. *Polymers*, *17*(4), 506. https://doi.org/10.3390/polym17040506

Bodaghi, M., Damanpack, A. R., & Liao, W. (2019). Dielectric properties of PLA, PGA, chitosan, and hydroxyapatite composites. Journal of Materials Science: Materials in Electronics, 30(3), 2253–2263. https://www.researchgate.net/publication/330259092

Castro, J. I., Valencia Llano, C. H., Tenorio, D. L., Saavedra, M., Zapata, P., Navia-Porras, D. P., ... & Grande-Tovar, C. D. (2022). Biocompatibility assessment of polylactic acid (PLA) and nanobioglass (n-BG) nanocomposites for biomedical applications. *Molecules*, *27*(11), 3640. https://doi.org/10.3390/molecules27113640

Dang, Z., Ma, X., Yang, Z., Wen, X., & Zhao, P. (2023). Electrospun nanofiber scaffolds loaded with metal-based nanoparticles for wound healing. *Polymers*, *16*(1), 24. https://doi.org/10.3390/polym16010024

Dichtl, C., Sippel, P., & Krohns, S. (2017). Dielectric properties of 3D printed polylactic acid. Advances in Materials Science and Engineering, 2017, Article 6913835. https://doi.org/10.1155/2017/6913835

Fernandes, A. C., Lima, L. B. S., Krol, M. F., Oliveira, M. H. L., Karnopp, J., Sagás, J. C., & Becker, D. (2026). Surface modification of 3D-printed PLA using an integrated remote plasma JET: in situ enhancement of wettability and functionalization without post-processing. *Progress in Additive Manufacturing*, *11*(2), 2123-2139. https://doi.org/10.1007/s40964-025-01461-2

Ferreira, I., Lopes, C., Rodrigues, M. S., Rodrigues, P. V.,

Castro, C., Braga, A. C., ... & Martín-Biedma, B. (2023). Functionalization of gutta-percha surfaces with argon and oxygen plasma treatments to enhance adhesiveness. *Scientific Reports*, *13*(1), 12303.. https://doi.org/10.1038/s41598-023-37372-x

Gershman, S., Harreguy, M. B., Yatom, S., Raitses, Y., Efthimion, P., & Haspel, G. (2021). A low power flexible dielectric barrier discharge disinfects surfaces and improves the action of hydrogen peroxide. *Scientific reports*, *11*(1), 4626. https://doi.org/10.1038/s41598-021-84086-z

Grayson, W. L., Bunnell, B. A., Martin, E., Frazier, T., Hung, B. P., & Gimble, J. M. (2015). Stromal cells and stem cells in clinical bone regeneration. *Nature Reviews Endocrinology*, *11*(3), 140-150. https://doi.org/10.1038/nrendo.2014.234

Hergelová, B., Zahoranová, A., Kováčik, D., Stupavská, M., & Černák, M. (2015). Polylactic acid surface activation by atmospheric pressure dielectric barrier discharge plasma. Open Chemistry, 13(1), 564–569. https://doi.org/10.1515/chem-2015-0067

Huang, J., Liu, F., Su, H., Xiong, J., Yang, L., Xia, J., & Liang, Y. (2022). Advanced nanocomposite hydrogels for cartilage tissue engineering. *Gels*, *8*(2), 138. https://doi.org/10.3390/gels8020138

Hurtado-Fernández, E., Trujillo-Cayado, LA, Álvarez-Mateos, P., & Santos, J. (2026). Extracción, Caracterización y Aplicaciones de Biopolímeros de Fuentes Sostenibles. *Polímeros* , *18* (5), 581. https://doi.org/10.3390/polym18050581

Jacobs, T., Declercq, H., De Geyter, N., Cornelissen, R., Dubruel, P., Leys, C., ... & Morent, R. (2013). Plasma surface modification of polylactic acid to promote interaction with fibroblasts. *Journal of Materials Science: Materials in Medicine*, *24*(2), 469-478. https://www.researchgate.net/publication/232813112

Jang, J., Park, H. J., Kim, S. W., Kim, H., Park, J. Y., Na, S. J., ... & Cho, D. W. (2017). 3D printed complex tissue construct using stem cell-laden decellularized extracellular matrix bioinks for cardiac repair. *Biomaterials*, *112*, 264-274. https://doi.org/10.1016/j.biomaterials.2016.10.026

Kamalov, A. M., Kolbe, K. A., Pavlov, A. A., Borisova, M. E., & Yudin, V. E. (2022). Activation of polylactide films by cold plasma dielectric barrier discharge to improve the interaction of fibroblasts. *Научно-технические ведомости Санкт-Петербургского государственного политехнического университета. Физико-математические науки*, *15*(S3. 2), 257-262. https://doi.org/10.18721/JPM.153.247

Kremer, F., & Tress, M. (2025). Dielectric spectroscopy: Yesterday, today and tomorrow. Applied Sciences, 15(13), Article 6954. https://doi.org/10.3390/app15136954

Krutty, J. D., Schmitt, S. K., Gopalan, P., & Murphy, W. L. (2016). Surface functionalization and dynamics of polymeric cell culture substrates. Current Opinion in Biotechnology, 40, 164–169. https://doi.org/10.1016/j.copbio.2016.05.006

Kudzin, M. H., Giełdowska, M., Mrozińska, Z., & Boguń, M. (2021). Poly (lactic acid)/zinc/alginate complex material: Preparation and antimicrobial properties. Antibiotics, 10(11), Article 1327. https://doi.org/10.3390/antibiotics10111327

Kurowiak, J., Klekiel, T., & Będziński, R. (2023). Biodegradable polymers in biomedical applications: a review—developments, perspectives and future challenges. *International journal of molecular sciences*, *24*(23), 16952. https://doi.org/10.3390/ijms242316952

Li, M., Sun, D., Zhang, J., Wang, Y., Wei, Q., & Wang, Y. (2022). Application and development of 3D bioprinting in cartilage tissue engineering. *Biomaterials science*, *10*(19), 5430-5458. https://doi.org/10.1039/D2BM00709F

Lopes, M. S., Jardini, A. L., & Maciel Filho, R. (2012). Poly(lactic acid) production for tissue engineering applications. In Procedia Engineering (pp. 1402–1413). Elsevier. https://doi.org/10.1016/j.proeng.2012.07.534

Mamun, A. A., Shao, C., Geng, P., Wang, S., & Xiao, J. (2024). Recent advances in molecular mechanisms of skin wound healing and its treatments. *Frontiers in immunology*, *15*, 1395479. https://doi.org/10.3389/fimmu.2024.1395479

Mao, Z., Bai, J., Jin, X., Mao, W., & Dong, Y. (2021). Construction of a multifunctional 3D nanofiber aerogel loaded with ZnO for wound healing. *Colloids and Surfaces B: Biointerfaces*, *208*, 112070. https://doi.org/10.1016/j.colsurfb.2021.112070

Moher, D., Liberati, A., Tetzlaff, J., & Altman, D. G. (2009). Preferred reporting items for systematic reviews and meta-analyses: the PRISMA statement. *Bmj*, *339*. https://doi.org/10.1371/journal.pmed.1000097

Nayak, V. V., Mirsky, N. A., Slavin, B. V., Witek, L., Coelho, P. G., & Tovar, N. (2023). Non-Thermal Plasma Treatment of Poly (tetrafluoroethylene) Dental Membranes and Its Effects on Cellular Adhesion. *Materials*, *16*(20), 6633. https://doi.org/10.3390/ma16206633

Page, M. J., McKenzie, J. E., Bossuyt, P. M., Boutron, I., Hoffmann, T. C., Mulrow, C. D., Shamseer, L., Tetzlaff, J. M., Akl, E. A., Brennan, S. E., Chou, R., Glanville, J., Grimshaw, J. M., Hróbjartsson, A., Lalu, M. M., Li, T., Loder, E. W., Mayo-Wilson, E., McDonald, S., McGuinness, L. A., Stewart, L. A., Thomas, J., Tricco, A. C., Welch, V. A., Whiting, P. & Moher, D. (2021). The PRISMA 2020 statement: an updated guideline for reporting systematic reviews. *BMJ*, 372, pp. n71. https://doi.org/10.1136/bmj.n71

Parangusan, H., Karuppasamy, K., & Bhadra, J. (2025).

Fenugreek-enriched electrospun PLA scaffold: revolutionizing tissue engineering solutions. *Journal of Polymer Research*, *32*(5), 175. https://doi.org/10.1007/s10965-025-04373-5

Pérez-Dávila, S., González-Rodríguez, L., Chiussi, S., Serra, J., & González, P. (2021). How to sterilize polylactic acid-based medical devices. Polymers, 13(13), Article 2115. https://doi.org/10.3390/polym13132115

Pillai, R. R., & Mohan, L. (2025). Plasma surface modification of biomedical implants and devices: Emphasis on orthopedic, dental, and cardiovascular applications. Prosthesis, 7(6), Article 143. https://doi.org/10.3390/prosthesis7060143

Popelka, A., Abdulkareem, A., Mahmoud, A. A., Nassr, M. G., Al-Ruweidi, M. K. A., Mohamoud, K. J., ... & Kasak, P. (2020). Antimicrobial modification of PLA scaffolds with ascorbic and fumaric acids via plasma treatment. *Surface and Coatings Technology*, *400*, 126216. https://doi.org/10.1016/j.surfcoat.2020.126216

Rajasekar, P., Swetha, P., Suwathi, S., & Rishikesavan, S. (2025). 9 Biomateriales y modificaciones de superficies. *Biotribología: Fricción, desgaste y lubricación en sistemas biológicos* , 209.

Ranakoti, L., Gangil, B., Mishra, S. K., Singh, T., Sharma, S., Ilyas, R. A., & El-Khatib, S. (2022). Critical review on polylactic acid: properties, structure, processing, biocomposites, and nanocomposites. *Materials*, *15*(12), 4312. https://doi.org/10.3390/ma15124312

Rondón, J., & Gonzalez-Lizardo, A. (2025). Plasma-treated polymeric biomaterials for improved surface and cell adhesion. arXiv. http://arxiv.org/abs/2504.03883

Rondón, J., Urrutia, G., & Gonzalez-Lizardo, A. (2025). Activation of polylactic acid and polycarbonate surfaces with non-thermal plasma. arXiv. http://arxiv.org/abs/2512.09205

Rondón, J., Vázquez, J., & Lugo, C. (2023). Biomateriales utilizados en ingeniería de tejidos para la fabricación de andamios Biomaterials used in tissue engineering for the manufacture of scaffolds. *Revista Ciencia e Ingeniería. Vol*, *44*(3).

Shuai, C., Yu, Z., Qi, F., Yang, M., Shuai, X., & He, T. (2025). Thermal post-processing driven surface smoothing of 3D-printed PLA-Hydroxyapatite scaffolds for bone tissue engineering. *Journal of Materials Research and Technology*. https://doi.org/10.1016/j.jmrt.2025.08.262

Sophia Fox, A. J., Bedi, A., & Rodeo, S. A. (2009). The basic science of articular cartilage: structure, composition, and function. *Sports health*, *1*(6), 461-468. https://doi.org/10.1177/1941738109350438

Spinelli, G., Kotsilkova, R., Ivanov, E., Georgiev, V., Ivanova, R., Naddeo, C., & Romano, V. (2020). Dielectric spectroscopy and thermal properties of poly (lactic) acid reinforced with carbon-based particles: Experimental study and design theory. *Polymers*, *12*(10), 2414. https://doi.org/10.3390/polym12102414

Subedi, D. P., Joshi, U. M., & Wong, C. S. (2017). Dielectric barrier discharge (DBD) plasmas and their applications. In *Plasma science and technology for emerging economies: an AAAPT experience* (pp. 693-737). Singapore: Springer Singapore. https://doi.org/10.1007/978-981-10-4217-1_13

Sun, J., & Tan, H. (2013). Alginate-based biomaterials for regenerative medicine applications. Materials, 6(4), 1285–1309. https://doi.org/10.3390/ma6041285

Świerczyńska, M., Kudzin, M. H., & Chruściel, J. J. (2024). Poly(lactide)-based materials modified with biomolecules: A review. Materials, 17(21), Article 5184. https://doi.org/10.3390/ma17215184

Velázquez, A., Ruvalcaba- Paredes, E.K., Estrada-Villegas, M. G., Fabela-Sanchez, O.F., & Fonseca-García, A. (2025). Poly(Lactic acid) Production for Tissue Engineering Applications. Interdisciplinary Biotechnological Advances, 67-99. Springer Nature. https://doi.org/10.1007/978-981-95-0094-9_3

Walker, E., et al. (2019). Maxwell–Wagner–Sillars dynamics and enhanced radio-frequency elastomechanical susceptibility in PNIPAm hydrogel–KF-doped barium titanate nanoparticle composites. Nanoscale Research Letters, 14(1), Article 317. https://doi.org/10.1186/s11671-019-3171-z

Walden, R., Goswami, A., Scally, L., McGranaghan, G., Cullen, P. J., & Pillai, S. C. (2024). Nonthermal plasma technologies for advanced functional material processing and current applications: Opportunities and challenges. *Journal of Environmental Chemical Engineering*, *12*(5), 113541. https://doi.org/10.1016/j.jece.2024.113541

Xu, L., Ding, L., Sun, Y., Zhang, T., Zhu, Y., Yan, B., ... & Long, Y. Z. (2023). Stretchable, flexible and breathable polylactic acid/polyvinyl pyrrolidone bandage based on Kirigami for wounds monitoring and treatment. *International Journal of Biological Macromolecules*, *237*, 124204. https://doi.org/10.1016/j.ijbiomac.2023.124204

Xue, K., Wang, F., Suwardi, A., Han, M. Y., Teo, P., Wang, P., ... & Loh, X. J. (2021). Biomaterials by design: Harnessing data for future development. *Materials Today Bio*, *12*, 100165. https://doi.org/10.1016/j.mtbio.2021.100165

Yadav, J., Chahal, S., Kumar, P., & Kumar, C. (2025). Thermo-Responsive Smart Hydrogels: Molecular Engineering, Dynamic Cross-Linking Strategies, and Therapeutics Applications. *Gels*, *12*(1), 12. https://doi.org/10.3390/gels12010012

Yehia, A. (2024). The thermal energy loss in the dielectric barrier discharge plasma. International Journal of Plasma Environmental Science and Technology, 18(3), Article e03002.

https://doi.org/10.34343/ijpest.2024.18.e03002

Zernitckaia, E. A., Lozada, J. L., Yaremenko, A. I., Reutova, A. P., Markova, M. A., & Lyutova, Z. B. (2025). In vitro analysis of biodegradation properties and sterilization stability of PLA membranes for bone regeneration. Journal of Maxillofacial and Oral Surgery. https://doi.org/10.1007/s12663-025-02751-6

Zhang, B., Wang, L., Song, P., Pei, X., Sun, H., Wu, L., ... & Zhang, X. (2021). 3D printed bone tissue regenerative PLA/HA scaffolds with comprehensive performance optimizations. *Materials & Design*, *201*, 109490. https://doi.org/10.1016/j.matdes.2021.109490

Zhang, L., Yang, G., Johnson, B. N., & Jia, X. (2019). Three-dimensional (3D) printed scaffold and material selection for bone repair. *Acta biomaterialia*, *84*, 16-33. https://doi.org/10.1016/j.actbio.2018.11.039

Zhang, P., Xu, L., Gao, J., Xu, G., Song, Y., Li, G., ... & Yang, H. (2022). 3D collagen matrices modulate the transcriptional trajectory of bone marrow hematopoietic progenitors into macrophage lineage commitment. *Bioactive Materials*, *10*, 255-268. https://doi.org/10.1016/j.bioactmat.2021.08.032

Zhang, Y., Sun, N., Zhu, M., Qiu, Q., Zhao, P., Zheng, C., ... & Lu, T. (2022). The contribution of pore size and porosity of 3D printed porous titanium scaffolds to osteogenesis. *Biomaterials Advances*, *133*, 112651. https://doi.org/10.1016/j.msec.2022.112651

Received: *January 13th, 2026*

Accepted: *March 24th, 2026*

Rivera, Victoria*: BSc. in Biomedical Engineering, 2027, Polytechnic University of Puerto Rico. San Juan, PR-USA.*
https://orcid.org/0009-0005-9778-1214

Resto, Joymar*: BSc. in Biomedical Engineering, 2027, Polytechnic University of Puerto Rico. San Juan, PR-USA. Email: resto_137016@students.pupr.edu*
https://orcid.org/0009-0005-1667-3183

Rondón Contreras, Jairo: *Ph.D. in Applied Chemistry, mention: Materials Study, 2015, Universidad de Los Andes.Professor of Biomedical & Chemical Engineering Departments, at the Polytechnic University of Puerto Rico. San Juan, PR-USA. Email: jrondon@pupr.edu*
https://orcid.org/0000-0002-9738-966X

Lugo Claudio, *Doctor in Chemistry in Applied Chemistry, Materials Study, 2017. (ULA). Professor at the University of the Andes, Faculty of Sciences, Kinetics and Catalysis Laboratory. Email: claudiolugo@ula.ve*
https://orcid.org/ 0000-0001-8003-0354